VISIBILITY IMPROVEMENTS THROUGH INFORMATION PROVISION REGARDING SUN GLARE:
A Case Study in Cape Town

University of Cape Town, Department of Civil Engineering
Centre for Transport Studies

DISSERTATION to obtain a Master's Degree

Compiled and Written by:
Nothando Khumalo (KHMNOT001)

Supervised by:
Associate Professor Marianne Vanderschuren

August 2014

Dedication

This thesis is dedicated to my mother, Phyllis Miranda (nee Dlamini). I could never ask for a better mother. You sacrificed so much for me to be able to do my Master's. I will forever carry you in my heart.

Acknowledgements

First and foremost, I would like to extend my sincere gratitude to my supervisor, Associate Professor Marianne Vanderschuren, for all her support and guidance in the two years of my Master's. Her valuable suggestions and comments always served to be a source of inspiration and encouragement.

My special thanks go to Associate Professor Mark Zuidgeest who took the time to help me understand the scope of my thesis and which direction to take. I also extend a special token of appreciation to Mpafane Deyi, PhD candidate in the Department of Civil Engineering at the University of Cape Town, who graciously showed me support and kindness that went beyond his responsibilities. His advice and research resources provided clarity and direction. I also extend much gratitude to Melusi Mavuso and Kumbirai Gundani for selflessly taking time from their busy schedule to proof read my work; and to Nomzamo Bukani for pushing me through the sleepless late nights.

Many thanks go to my friends and family for their constant encouragement, support and faith in me. I would also like to, especially, thank my dear friend Rene Nsanzubuhoro who was a constant source of reassurance and acted as my "substitute shrink" throughout the course of the past two years and the duration of this thesis.

Last but not least, I would like to thank Thomas Slingsby and Nicholas Lindenberg in the UCT GIS Laboratory, who have gone over and above their line of duty to help me with ArcGIS and understanding the work that I was doing and what had to be done. This thesis would not have been possible without them. I am forever grateful.

Plagiarism Declaration

Name:	Nothando Khumalo
Student Number:	KHMNOT001
Course:	Civil Engineering Thesis (CIV4044S)
Institution:	University of Cape Town
Date:	August 2014

Plagiarism Declaration

1. I know that plagiarism is wrong. Plagiarism is to use another's work and to pretend that it is one's own.
2. I have used the Harvard Convention for citation and referencing. Each significant contribution to and quotation in this report form the work or works of other people has been attributed and has been cited and referenced.
3. This report is my own work
4. I have not allowed and will not allow anyone to copy my work with the intension of passing it as his or her own work.

Student Number: _____ **Signature:** _____

Abstract

Vision is inarguably a fundamental component of safe driving. Any obscurity in a driver's vision can impose a threat to roadway safety due to interference with the driving task. Sun Glare is a hazard that few people anticipate. The sun is most potent to drivers when it is low in the sky on the horizon, particularly an hour or so after sunrise (dawn) and before sunset (dusk). The position of the sun and the angle of the rays during this period may render sun visors useless. This increases the risk of an accident as a result of interference with a driver's ability to see the road ahead. The primary purpose of this study was to develop a method which will determine which areas in the City of Cape Town road network are exposed to direct sunlight, thus, making them vulnerable to road accident risk as a result of impaired vision. Additional objectives included the validation of the methodology by comparing field investigation outcomes with those of the established methodology.

Considering the need for a tool with the ability to combine spatial data and sun position data, the ArcGIS software, which contains the hillshade tool, was selected for use in the study. The study was conducted for the City of Cape Town road network. The data used in the investigation included a Digital Elevation Model (DEM) and road network data of the study area. The DEM and road network data were both derived from a 10m topographical map. Sun position data (azimuth and altitude) was obtained from the Astronomical Applications Department of the U.S. Naval Observatory server. The sun position data obtained was for the morning and afternoon period of four days chosen for usage in the development of the model: Autumnal Equinox (AE), Spring Equinox (SE), Summer Solstice (SS) and Winter Solstice (WS). A 19º-25º altitude sun cone and a ±15º threshold (azimuth sun cone) were adopted for the filtering of road segment azimuth and slope. The field investigation carried out to validate the model was executed using a Road Eye JS-300 camera.

The results revealed that the AE and SE both have approximately 14.7% of the total length of the road network exposed to direct sunlight, while the SS and WS have about 12.2% and 15.2%, respectively. Statistical analysis of the output data confirmed that the AE and SE have the most

sunlight exposure, while the WS has the least exposure. In addition, with the exception of the WS, the analysis also revealed a significant difference in the amount of sunlight exposure between the morning and afternoon time periods in the other three days. According to this statistical analysis, the AE and SE have more sunlight in the morning compared to the afternoon, while the SS and WS have more sunlight in the afternoon compared to the morning.

The validation of the proposed model through the comparison of the field investigation outcomes and model outcomes revealed a satisfactory level of concurrence between the results. It was, therefore, concluded that the model is valid. Any differences observed between the two outcomes were a result of the assumptions and limitations of the study, which are informants that relate to whether increased exposure entails increased risk of accidents. Such assumptions include the absence of atmospheric effects (cloud cover, rainfall etc.) and the absence of special on site conditions (buildings, line of trees etc.) affecting direct sunlight.

In summary, results from this methodology can be an informative dimension to consider when evaluating existing roads or different layout and alignment alternatives for new roads. Apart from mitigation measures such as visual barriers, Intelligent Transport Systems such as automated real time warning systems can be implemented to provide real-time sun glare risk information to drivers. The incorporation of GIS technology with GPS technology could enable the development of such systems.

Table of Contents

List of Tables

List of Figures

Abbreviations

AE:	Autumnal Equinox
AM:	Morning
ANOVA:	Analysis of Variance
CIE:	Commission Internationale de l'Èclairage
CBD:	Central Business District
CoCT:	City of Cape Town
DEM:	Digital Elevation Model
FHWA:	U.S. Federal Highway Administration
GIS:	Geographic Information System
GMST:	Greenwich Mean Sidereal Time
HID:	High-Intensity Discharge
HRE:	Head/Rear End
ITS:	Intelligent Transport System
JD:	Julian Day
JDE:	Ephemeris Julian Day
LMST:	Local Mean Sidereal Time
MADB:	Metropolitan Accident Database
MRC:	Medical Research Council
NASS-GES:	National Automotive Sampling System-General Estimates System
NE:	Northeast
NIMSS:	National Information Management and Support Systems

NTSB:	National Transportation Safety Board
NW:	Northwest
OECD:	Organisation for Economic Co-operation and Development
PM:	Afternoon
PSA:	Plataforma Solar de Almerýa
Rd/RD:	Road
RTA:	Road Traffic Accidents
SAPS:	South African Police Services
SE:	Southeast
SE:	Spring Equinox
SPA:	Solar Position Algorithm
SS:	Summer Solstice
SSD:	Sideswipe-Same Direction
St:	Street
SW:	Southwest
TRRL:	Transport and Road Research Laboratory
TT:	Terrestrial Time
UT:	Universal Time
WHO:	World Health Organisation
WS:	Winter Solstice
WSRT:	Wilcoxon Signed-Rank Test

Definition of Terms

ArcGIS – a Geographic Information System, produced by ESRI, which allows people to collect, organise, manage, analyse, communicate, and distribute geographic information.

Autumnal Equinox – the equinox in autumn.

Azimuth – sun's relative positions along the horizon, and is expressed in positive degrees ranging from 0 to 360, measured clockwise from north.

Altitude – sun's angle of elevation above the horizon, and is expressed in positive degrees ranging from 0 to 90˚; with 0° at the horizon and 90° directly overhead.

Dazzle – temporarily blinding brightness

Digital Elevation Model – presentation of continuous elevation values over topographic surface by a regular array of z-values, referenced to a common datum; DEMs are typically used to represent terrain relief.

Direct sunlight exposure – a situation when a driver is facing the sun.

Equinox – astronomical days when the sun is in its zenith over the equator and the Earth experiences day and night of generally equal length.

Hillshade – shaded relief technique, which mimics the sun's effects – illumination, shading and shadows – on hills and canyons; thus, obtaining hypothetical illumination of a surface by determining illumination values for each cell in a raster.

Luminance – intensity of light emitted from a surface per unit area in a given direction.

Road segment – (also segment) multiple straight lines, with constant direction, that make up a form/form part of a road.

Road Visibility – state of [a driver] being able to see the road and surrounding environment ahead.

Scenario – (also time snapshot or snapshot) the different data sets produced for each of the four days, which totals up to 16 as seen in Table 5-1. For example, the autumnal equinox is one day which has the morning and afternoon periods modelled, which in turn each have two data sets: one for the 19° angle one for the 25° angle, thus making it a total of four scenarios in one day.

Solstice - two recurring periods of the year at which the sun is farthest distant north or south from the equator, which mark midsummer and midwinter; also applied to the two points in the ecliptic which the sun appears to reach on these two dates.

Spring Equinox – the equinox in spring.

Summer Solstice – longest day of the year in the Southern Hemisphere, when the Southern Hemisphere is tilted toward the sun.

Sunlight Exposure – (also insulation, radiation and illumination)

Sun glare – the dazzling sensation of relatively bright light from the sun which produces unpleasantness, discomfort or interferes with optimal vision.

Sun glare risk – the vulnerability to accidents occurrence as a result of visibility impairment due to sun glare.

Winter Solstice – shortest day of the year in the Southern Hemisphere, when the Northern Hemisphere is tilted toward the sun.

1 Introduction

1.1 Background

Around 1.2 million people are killed in road traffic accidents globally each year, and between 20 and 50 million suffer non-fatal injuries (World Health Organisation, 2009). Without increased efforts and new initiatives, in 2004 WHO forecasted a 65% increase in road accidents between the years 2000 and 2020. The provision of countermeasures to drastically reduce the number and rate of road traffic accidents can, therefore, not be over emphasised. Previous studies have shown that accident rates are higher during night-time than during daytime (Hargroves, 1983; Jun, 2010; Liu, 2007). A variety of factors can be attributed to this conclusion, and key among these factors is decreased visibility. Although the risk of decreased visibility is greater at night, other visibility conditions during daytime, such as fog and sun glare, also present a much greater risk. Visibility in this study refers to the state of being able to see the road and surrounding environment ahead.

Visibility is one of the basic requirements for safe driving, as it gives drivers a preview of roadway information. Any obscurity in a driver's vision can impose a threat to roadway safety as a result of the interference with the driving task (Choi and Singh, 2005). Reduction in sight distance as a result of vision-impairing weather conditions affects driver behaviour, which ultimately affects traffic flow; ergo the increased accident risk under these conditions. A study by the US Federal Highway Administration (FHWA) concluded that approximately 15% of congestion experienced by travellers is attributable to non-recurrent weather-related causes (FHWA, 2005). Moreover, a number of studies have concluded that adverse weather conditions such as rain, snow and fog highly influence traffic operations and overall road safety (Andrey et al., 2001; Hermans et al. 2002).

Literature on weather-related traffic accidents typically focuses on weather conditions considered to be the most fatal to road safety: rain, snow or fog. There is a great deal of literature on the impact of these weather conditions on road safety. There is, however, little research on the effects of direct sunlight reflection (sun glare) on road safety (Auffray et al., 2008). Glare is a

temporary dazzling sensation produced by an unwanted source of luminance, within a visual field that is significantly greater than that to which the eyes are adapted to (Knott, 1983). Among other reasons, the scarcity of literature on sun glare effects on road safety may be attributed to sun glare not being considered a highly significant factor in road safety – regardless of the countless accidents that have occurred due to blind spots created by sun glare. Glare resulting from direct sunlight exposure can be painful to the eye of the observer and potentially very distracting to the driver in terms of visibility (Auffray, 2007). Consequently, this distraction to the driver has well understood adverse effects, not only on the safety of the driver but on adjacent drivers as well.

The aim of this study was to present a methodology, which can model direct sunlight exposure for the Cape Town road network through the use of the ArcGIS software program. Based on the assumptions and limitations, the outcome of this study gives an overview of the vulnerability of the road network to accidents as a result of sun glare.

1.2 Problem Statement

Trends and patterns of road accidents resulting from glare show that sun glare indeed has a strong influence on crash occurrence (Mitra, 2008). Auffray (2007) found that glare from the sun is found to be one of the significant causal factors of vision obstruction and threat to safe driving, contributing to degraded traffic operations and crashes. According to the NHTSA of the U.S. Department of Transportation, sun glare is the official cause of only a fraction of fatal crashes across the country, which is 195 in 56 793 (0.34%) (Hastings, 2012). Data compiled by the Abu Dhabi Traffic Department showed that sun glare was blamed for 22 minor crashes in the capital during the first eight months of the year 2010 (Salama, 2010).

Mitra et al. (2007) pointed out that sun glare is most problematic during the early or late hours of the day, presumably within an hour after sunrise and before sunset, when the sun is low in the sky on the immediate horizon – and little protection is offered by a car's sun visor. Unfortunately, these times coincide perfectly with rush hour, making accidents even more likely. Mitra also highlights that in Tucson, Arizona, sun glare is especially bad in early spring and early fall when the sun rises almost exactly east and sets almost exactly west. As a result of

geographical variations, these observations may not apply to all places; more especially in most African regions where there is more sunlight in a year.

Regardless of how common sun-related events may be, there is still very little research towards understanding its effects on road safety. Lastly, because of the limited infestation of sun glare effects, there are very few existing options for the mitigation of sun glare related problems on roadways.

1.3 Research Objectives

Literature does provide proof that sun glare is a hazard that increases the road safety risk, and that the danger of the sun is even more potent at dusk and dawn, an hour or so after sunrise and before sunset. The principal aim of this dissertation is to identify a method that can quantify, geographically, where and when sun glare risk occurs on a road network. Essentially, the method determines which areas in a geographic setting's road network, i.e. city, are exposed to direct sunlight, thus making them vulnerable to road accident risk as a result of impaired vision. The City of Cape Town was used as case study to prove and validate the method.

1.4 Research Questions

In addressing the principal aim stated in the preceding section, several research questions (which double as research objectives) had to be answered. These were formatted as follows:

i. Is sun glare a road safety issue (chapter 3)?
ii. What are the key factors that influence sun glare conditions (chapter 3)?
iii. For an arbitrary position on a roadway alignment, how can the times of the year or day be determined that drivers on that roadway could be faced with the risk of vision impairment as a result of sun glare (chapters 2 and 4)?
iv. What tools need to be available to develop and execute the proposed methodology for the City of Cape Town road network (chapter 4)?
v. What data needs to be available to develop and execute the proposed methodology for the City of Cape Town road network (chapter 4)?
vi. Using the chosen methodology, is it possible to identify which road networks are vulnerable to sun glare conditions in the City of Cape Town road network (chapter 5)?

vii. Does the proposed methodology produce valid results (chapter 5)?

viii. In the event of accidents which occurred as a result of sun glare in the City of Cape Town, would it have been possible to warn drivers of this risk through the provision of real time information provided by the methodology (chapter 5)?

ix. With regards to mitigation and implementation, how can this methodology benefit the City of Cape Town (Recommendations)?

1.5 Research Significance

The purpose of this research was to verify if sun glare is actually a problem for drivers in the City of Cape Town. As already pointed out in the problem statement, the majority of studies reported in literature on the effects of weather conditions on road safety focused on other weather conditions considered to be the most fatal. This study, therefore, aimed at contributing to the general knowledge of the effects of sun glare on road safety by way of considering factors, such as the angle of the sun, the time of day, the geography, the geometric design of the road and the physical environment in the evaluation of sun glare risk. In doing so, the study is expected to bridge a gap in literature by establishing a database for sun glare risk spots in the study area (Cape Town).

Furthermore, the research also aimed to lessen the inconvenience of hazardous sun glare effects by identifying potential mitigation measures well suited to the study area. Aside from the obvious influence on road safety, the outcomes of this study are expected to be an informative dimension to consider in the design process of roadways. Awareness of sun glare high risk areas will allow the implementation of mitigation measures in the planning and design phases of roadways, thus yielding designs that are less susceptible to sun glare effects.

1.6 Assumptions and Limitations

This research was born out of the obvious interference of direct sunlight exposure on drivers in the road. This research was limited in scope to the City of Cape Town (CoCT). To validate the results produced by the proposed methodology, a field investigation was carried out to verify if the methodology actually produces credible results. The following assumptions, and limitations, were made in the study:

- The identification of a sun cone ranging between 19º and 25º altitude,
- The adoption of an azimuth sun cone, which is in the form of a ±15º threshold for azimuth and slope filtering of road segments,
- The model assumes an absence of atmospheric effects (cloud, rainfall etc.), and
- The absence of special on site conditions, such as buildings or a line of trees, affecting the direct sunlight is also assumed.

1.7 Thesis Structure and Content

The breakdown of chapters of this document is outlined as follows:

Chapter 1: Introduction

This chapter provides a background to the study. It highlights the research problem, outlines the objectives of the study, and also discusses the significance of the research work.

Chapter 2: Methodology

This chapter presents an overview of the research approach and research process.

Chapter 3: Literature Review

This chapter presents discussions of the background studies carried out in defining the research approach and process.

Chapter 4: Tool and Study Area Selection

This chapter consists of a comprehensive description and discussion of the study area and tool for the study. It is basically an account of the proposed methodology in Chapter 2.

Chapter 5: Results: Analysis and Findings

This chapter comprises an analysis of the model results, validation of the model and an application of the model to Cape Town accident data.

Chapter 6: Conclusions and Recommendations

This chapter consists of concluding remarks and recommendations based on the research objectives, which were phased as research questions.

Bibliography: Includes a list of articles, books, websites, reports etc. cited and used in the study.

Appendices: This section gives supplementary information on the topics explored in the contents of the text.

2 Methodology

2.1 Background

Sun glare conditions have a strong influence on the road safety risk. However, there is an observed scarcity in the availability of literature/research work on the impacts of sun glare on road safety. Regardless of how common sun glare related accidents may be, this weather condition is not considered to be as hazardous as other weather conditions, such as precipitation, fog and snow, ergo the literature scarcity.

The purpose of this chapter is to give an overview of the methodology, which entails the research approach and research process. An in-depth discussion of the research process is presented in Chapter 4.

2.2 Research Approach

Literature research carried out in this study has shown that a number of factors influence the occurrence of sun glare conditions. However, three factors have been identified in this study to be key influences in sun glare occurrence. As seen in the research framework in Figure 2-1, these are: the geometric design of the road network; the physical environment, which comprises topography, geographic location and terrain profile; and the solar position, which consists of the azimuth and altitude angles. Ultimately, the wrong combination of these factors could result in hazardous conditions, due to increased sun glare risk which is actually, to a larger extent, a road safety risk, among other risks.

Literature study on sun glare and other subject matters that relate to it, such as visibility and weather effects on road safety, steered the formulation of this research process. Subsequently, this led to the identification of the appropriate instrumentation plan to execute this study. The following section gives an elaborate discussion of the research process and its components.

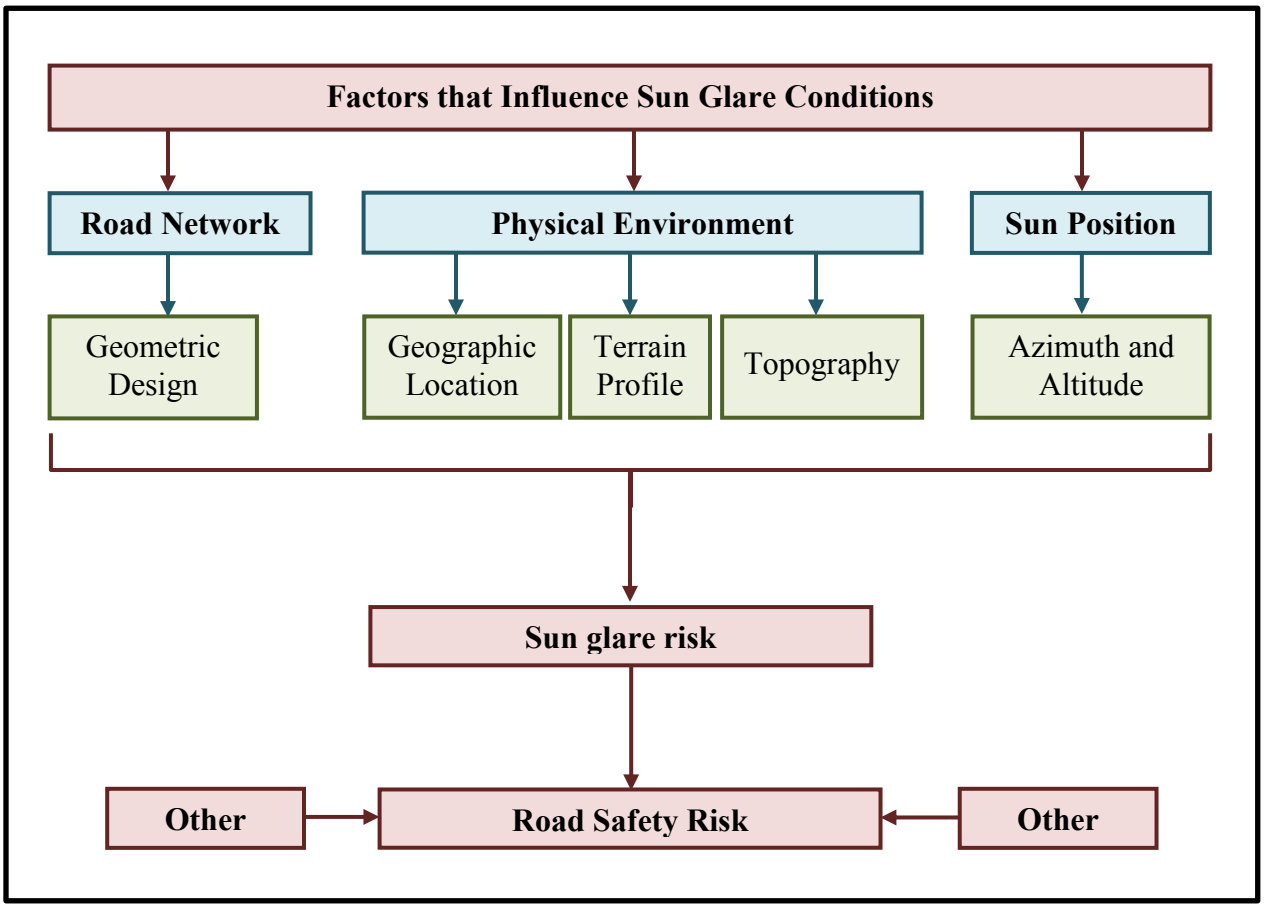

Figure 2-1: Research Framework

2.3 Research Process

The research process is a simple means of effectively locating information for a research project, be it a research paper, an oral presentation, a thesis, or something else assigned by a supervisor (Lynch, 2013). This process involves identifying, locating, assessing, analysing, and then developing and expressing ideas, which is exactly what was done in this case.

To begin this process, the primary research question was identified, followed by background research into the subject matter, as well as other matters that relate to it. The latter informed the formulation of the instrumentation plan, which comprises of the research tool identification, data collection and data processing. Ultimately, this resulted in the analysis of results from the data processing phase, and ended off with conclusions and recommendations. The following is a brief overview of the research process steps. A graphic illustration of the research process is presented in Figure 2-2.

2.3.1 Research Question

The main research question which set off this study is as follows:
"*How can road safety be improved through user information provision regarding sun glare risk?*"

2.3.2 Background Research

Literature sources on sun glare have shown that sun glare effects on road safety are a critical matter worth further investigation. A study by Hagita and Mori (2013) highlighted that quantitative analysis on the contribution of sun glare to traffic accident occurrence is very important toward developing measures against the serious traffic safety problem of sun glare. In light of this, Hagita and Mori's (2013) analysis of sun glare as a contributing factor to traffic accidents found traffic accidents to be higher when the sun was in front of the vehicle. This is an expected conclusion, because, at the right angle, the sun is highly likely to impair visual acuity when it is in front of the driver.

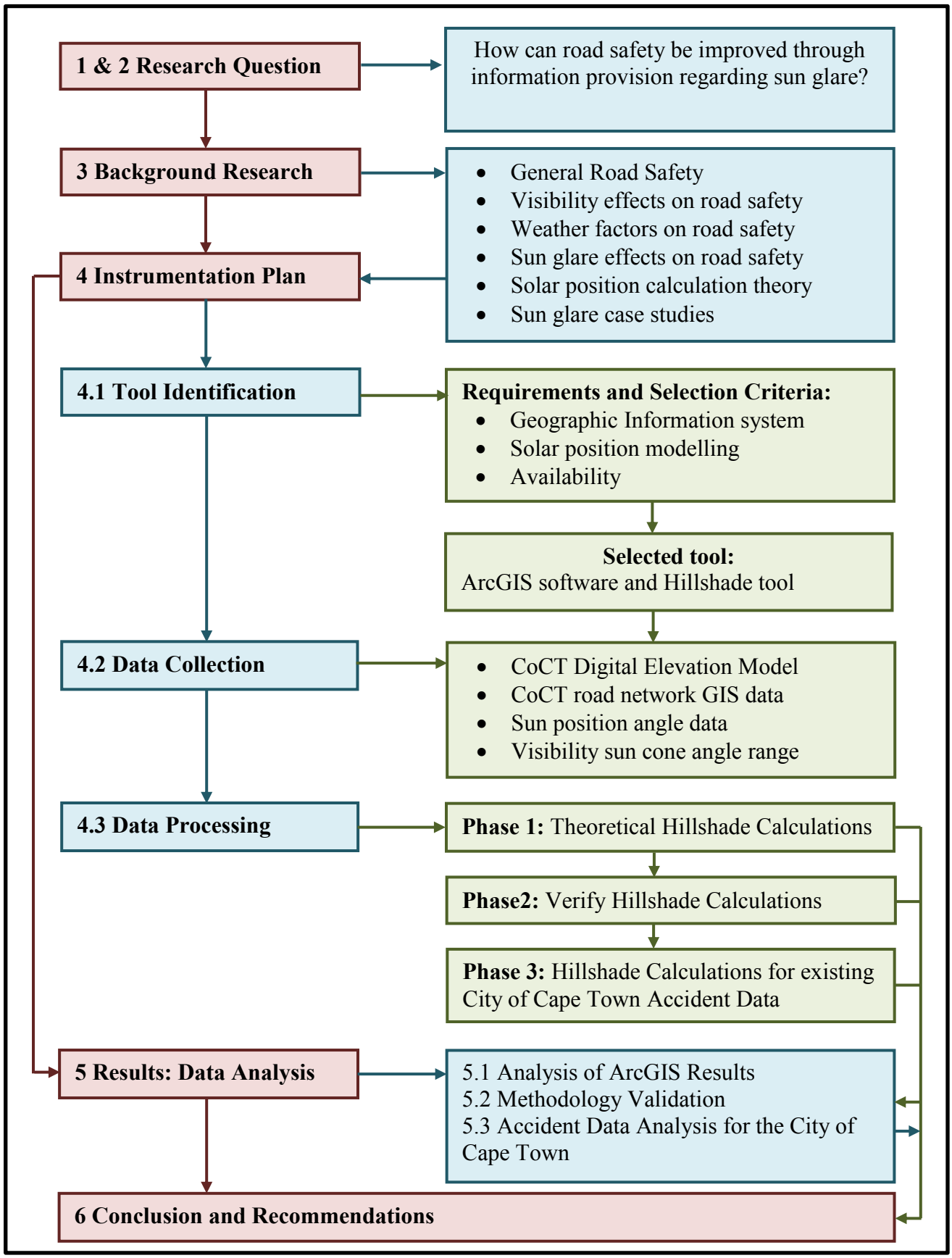

Figure 2-2: Research Process

Furthermore, Hagita and Mori (2013) also indicate that the angle of the sun is most potent to drivers during the times when the sun is closest to the horizon, which is dawn and dusk; typically between 07h30-09h30 and 17h00-18h30, respectively. In agreement, Mitra (2008) also disclosed that the traffic accident rates at dusk and dawn are higher than the rates at other times. This was concluded in a study analysing of traffic accident data, sunset and sunrise time, and road travel directions in Arizona, America. However, Hagita and Mori (2011) argued that this study lacked precision. They pointed out flaws in three key points: firstly, the road travel directions of the subjects were classified into only four categories, the four compass points (north, south, west and east). Secondly, the time periods in which sun glare was considered to contribute to traffic accidents were defined roughly as one hour after sunrise and before sunset. Lastly, they also indicated that the influence of weather was not addressed. On a different note, Jurado-Pina and Pardillo-Mayora (2010) used software tools TRIVIUM and MATLAB to identify and quantify vision impairment problems originated by sun glare, and to facilitate the design of countermeasures to prevent potential safety hazards caused by these situations.

Even though the literature in this field is limited, it is clear that a number of studies have addressed the issue of sun glare on road safety. As pointed out already, this study applies a different tool to achieve similar results, which are all based on the stated research question. Furthermore, a comprehensive review of the literature studied for this thesis is provided in Chapter 3. This includes the following topics: a discussion of road safety in general; analysis of visibility effects on road safety; analysis of weather factors on road safety; sun glare effects on road safety; theory behind coordinate calculations of the solar position; and lastly, sun glare case studies.

2.3.3 Instrumentation plan

2.3.3.1 Research Tool Identification

The identification of tools is an integral part of any research. In this case, it was the identification of tools that will facilitate the investigation of sun glare risk spots in the City of Cape Town (CoCT) road network. As such, several factors were considered before the selection of the appropriate tools to identify sun glare exposure. Given that the study aimed to identify direct sunlight exposure for specific points of location, one of the key tool requirements considered in

this selection process was a tool with the ability to combine spatial data and solar position data. Among others, an additional key factor was availability; meaning the tools had to be accessible for use in this research.

Simple modules for computing sunlight exposure, which require only the surface data and the sun position angles, are available in some Geographical Information System (GIS) programs. For that reason, the ArcGIS software was identified to be the most suitable software program for this study. This software includes a hillshade tool, which was used to model sun illumination.

In view of the selected tool, the next step was the selection of a study area, given that ArcGIS requires geographic data input. Considering accessibility and proximity to the University of Cape Town (UCT), the City of Cape Town was regarded the most convenient study area. A detailed description of the study area is presented in Chapter 4.

2.3.3.2 Data Collection

The essential data needed for this research was grouped into GIS data and analysis data. GIS data entails all the data required which was to execute the proposed methodology. Analysis data on the other hand, consisted of Cape Town accident data, which was used to determine whether individuals involved in sun glare accidents could have been warned had this model been in use. This data was used in the analysis chapter [5]. The following is a list of the GIS data. Note that an in-depth discussion of the listed data is also included in Chapter 4.

- City of Cape Town Digital Elevation Model (DEM),
- City of Cape Town road network data,
- Sun position data (azimuth and altitude angles),
- Sun cone data (horizontal and vertical cones), and
- City of Cape Town accident data.

2.3.3.3 Data Processing

The methodology used in this work comprised of three general phases, two of which have multiple steps. The following is a list of these three phases, as well as the steps within each phase, where applicable. An in-depth discussion of these phases and steps is carried out in Chapter 4, which also includes a graphic illustration (data flow) of the methodology.

Phase 1: Production of Hillshade Maps

This involved the creation of maps for the four chosen representative days and each of the 16 scenarios, which included the morning and afternoon scenarios.

Phase 2: Classification of Road Segments According to Azimuth Sun Cone

- Step 1: Creating Multiple Road Line Features with Constant Direction,
- Step 2: Calculating Road Bearing and Reverse Bearing, and
- Step 3: Attribute Query for Roads within 30° sun cone (azimuth).

Phase 3: Hillshade Map and Road Classification Overlay

- Step 1: Reclassify and Erase Roads in Shadow, and
- Step 2: Producing Final Analysis Data.

2.3.4 Data Analysis

The data analysis chapter was split into three sections. The first section is a comprehensive discussion of the methodology output (ArcGIS results). The second section focuses on validating the proposed methodology by comparing field investigation observations with output from the model. Lastly, in the third section CoCT accident data was analysed to isolate sun glare related accidents, which were be modelled in ArcGIS to determine whether such accidents could have been prevented if drivers were warned based on the information provided by this model.

3 Literature Review

Driving is the primary mode of travel in numerous countries. It facilitates the performance of routine daily activities, employment, and opportunities for social interaction; and is thus, integral with the concept of quality of life (Owsley, 1999). Regardless of the many benefits of vehicular mobility, traffic safety is a worldwide problem of enormous magnitude. The World Health Organisation (WHO) estimates that 1.2 million people are killed on the roads every year, worldwide; and between 20 and 50 million suffer non-fatal injuries because of traffic crashes (WHO, 2009). In 1996, the United States of America (USA) endured 41,907 fatalities and 3,511,000 injuries caused by automobile crashes (Owsley, 1999). Several authors acknowledge that road accidents are a consequence of the combined effects of several different factors, broadly grouped as behavioural, technological and environmental (Andrey and Olley, 1990; Edwards, 1996). According to Edwards (1996) the absence of any of these factors could prevent an accident from occurring.

Other sources of literature apply a different classification system to the factors that contribute to the occurrence of road traffic accidents. While the impact of factors influencing road safety is a complex theme, Statistics SA (2009) and Jun (2010) classify the road accident contributory factors into three factors, which are considered the primary factors. These are human contributory factors, road contributory factors and vehicle contributory factors. In South Africa (SA), human factors (e.g. pedestrian jay-walking) contribute 85% to the occurrence of fatal crashes, while road factors (e.g. poor visibility) and vehicle factors (e.g. tyre burst and faulty brakes) contribute 9% and 6%, respectively (Statistics SA, 2009).

A number of developing countries are rapidly motorising, traffic casualties are increasing rapidly, and the victims are typically the working-age productive members of society (Zein and Navin, 2007). Over 90% of the deaths accounted for occur in low and middle income countries, which have only 48% of the world's registered vehicles. A global status report on road safety by WHO report maintains that low and middle income countries have higher road fatality rates (21.5 and 19.5 per 100,000 population; respectively) than high income countries (10.3 per 100,000 population) (WHO, 2009). Road crashes are the tenth leading cause of human health problems (Zein and Navin, 2007). Several high income countries have been experiencing

declining death rates over the last four to five decades (Eurostat, 2007; NHTSA, 2006; WHO, 2009). Despite this reduction, road traffic injuries remain a significant cause of death, injury and disability (Plainis et al., 2006; WHO, 2009).

In South Africa, road crashes result in 13,000 to 14,000 deaths annually (Jungu-Omara and Vanderschuren, 2006). Data from Statistics SA reveals that road injuries were ranked 18 in a list of top 25 leading causes of death in 2007 (6,038 deaths; 1% of all deaths), which accounts for just over 80% of all deaths (MRC, 2010). The 9th annual report of the National Information Management and Support Systems (NIMSS) has identified fatal injuries, especially as a consequence of motor vehicle collisions and violence, as high priority in South African public health. When compared to water and air transport, land transport contributes the highest proportion (99.8%) to the total transport accident rates in SA (Statistics SA, 2009). Even though a large amount of public resources have been funnelled into the reduction of road accidents, they are still one of the leading causes of death (WHO, 2009; Statistics SA, 2009). However, with the right resources, knowledge, experience and tools, a safer and healthier transport system can be achieved.

Research has shown that the road accident occurrence events are not random. There are numerous explanations of traffic crashes; and given that driving is such a complex task, it is not surprising that so many dimensions appear important (Plainis et al., 2006). A number of these play a major role in the occurrence of accidents, and most of them fall in the road accident factor classifications previously mentioned. For instance, numerous researchers have shown that the time of day influences both the severity and the rate of crashes (Clarke et al., 2006; Konstantopoulos et al., 2009). The risk of a fatal crash has been shown to increase up to four times when driving at night compared to daytime (Williams, 2003). Diminished visibility, alcohol use and driver fatigue are some of the many factors that contribute to the higher death toll at night (Wood and Owens, 2005). A number of research studies have shown that diminished visibility is one of the major causes of night-time accidents (Jun, 2010; Wood and Owens, 2005). Chu et al. (2010) also underlines that degraded visibility during night-time driving increases the risk of crash by reducing the driver's ability to avoid a collision, because of late recognition of other road users. On the contrary, analysis in a study on young driver accidents in the UK

suggests that the problems of accidents in darkness are not a matter of visibility, but a consequence of the way young drivers use the roads at night (Clarke et al., 2006).

It is clear that there are a number of factors affecting road safety. Although there are a number of road safety factors worth investigating, this research focused on the effects of sun glare, which falls under weather conditions. However, the literature in this chapter elaborates on the effects of weather conditions on road safety, as well as provide a brief and concise discussion on three weather conditions considered to have the most impact on road safety (precipitation, fog and snow, respectively). Weather may not be a principal cause of road traffic accidents, but it is an important component; even more so sun glare conditions, whose impacts on road safety are not sufficiently explored and captured in literature. Before the introduction of a comprehensive section on the effects of sun glare on road safety, analysis of road safety statistics on vision related accidents are reviewed. This is followed by a brief discussion of the theory behind the algorithms used to estimate the position of the sun; and concluding with an assessment of sun glare accidents for two case studies.

3.1 Analysis of Visibility Effects on Road Safety

Driving is a highly visual task. Vision is, therefore, inarguably a fundamental component of safe driving. Shepard (1996) highlights that the driving task involves performing a number of functions, some of the more important being guiding the vehicle within the highway geometrics and traffic control devices, while detecting other vehicles, and judging their speed and position, and possible behaviour of their drivers. Furthermore, this task is complicated by conditions of reduced visibility, which may be accompanied by wet surfaces and darkness. The effects of these conditions on driver behaviour have been a matter of concern for many years and subject to several studies over the last two decades, primarily focused on the role of vision in driving (Shepard, 1996; Owsley and McGwin Jr, 2010). Much of this research has been centred on what type and degrees of vision impairment hamper driver safety and performance.

Many studies on vision, driver safety and performance have concluded that vision impairment is more prevalent in later adulthood. Consequently, the focus of these studies is on adults around 40years and older (Owsley and McGwin Jr, 2010; Owsley and McGwin Jr, 1999). Given that

crash rates increase with age, it is possible that observed associations between visual function and driving performance are confounded by age (Owsley and McGwin Jr, 1999). In another study concerning visual impairment with older people, Owsley and McGwin (2010) also highlight that, because of this focus on the older adult population, other medical and functional co-morbidities common in late adulthood are potential confounders in understanding the relationship between vision and driving. For instance, cognitive impairment elevates crash risk and impairs driving performance (Ball et al., 2006; Wood et al., 2008).

The changes in visual function that occur under reduced illumination are well recognised and include reductions in visual acuity in central and peripheral locations, as well as reduced contrast sensitivity for all spatial frequencies (Johnson and Casson, 1995; Wood and Owens, 2005). Although it is well documented that many older drivers minimise or avoid driving at night, crash data show that drivers aged 65 and older have a greater rate of involvement in fatal crashes at night, except for those younger than 25 years (Wood and Owens, 2005).

According to Hyslop (2009) impaired visibility is also a symptom of environmental problems, because it is evidence of air pollution. Additionally, Thach et al. (2010) have shown that improved visibility and mortality are related. On a different note, visibility is also compromised by weather conditions, such as fog and haze, which reduce visibility just like pollution. Road crashes, which occur in fog are, generally, twice as severe as the average crash (Babari et al., 2010). The effects of three prominent weather conditions on road safety, including fog, are discussed in the following section. In addition to the safety problem, reduced visibility is cause of delays and disruption in air, sea and ground transportation for passenger and freight.

In his study, Charman (1997) concluded that there is little doubt that the visual sense provided most of the information used by the vehicle driver, with only relatively minor contributions from hearing, among other things. He further points out that, if this observation is combined with the statistic that some 3620 people are killed in on the United Kingdoms (UK) roads each year, nearly the equivalent of the monthly crash of a fully-loaded jumbo jet, it is natural to ask if road accidents might be linked with defects in vision.

3.2 Analysis of Weather Factors on Road Safety

The state of knowledge on the engineering aspects of weather-related driving risks is quite advanced. In particular, the physical effects of weather on road surface friction and driver visibility are reasonably well understood and researched. Weather plays a significant role in the performance of the surface transportation system. Therefore, weather impact on road accident rates and road visibility is a crucial factor that cannot be overemphasized when it comes to road safety. Extreme weather events, such as snow or thick fog can bring traffic to a standstill (Smith et al., 2003). Such weather conditions, including precipitation, reduce road friction (skid resistance), impair visibility and make vehicle control more difficult (Andrey et al., 2001). These conditions, therefore, create a safety threat for road users and pedestrians. Beyond these extreme conditions, more common weather events have also been shown to impact traffic conditions. Such conditions include temperature, sunlight, wind etc. As a result of the underestimated impact of sunlight on road safety; there is a shortage of literature on sun glare conditions.

Literature contends that weather may explain about 5% of monthly accident/fatality variability (Hermans et al., 2006; Bergel-Hayat et al., 2013). A 1998 Canadian study on weather hazards indicated that 16% of fatal collisions and 18.5% of personal injury collisions occurred during adverse weather conditions i.e. rain, snow, hail and fog (Andrey et al., 2001). The study also indicates that over 25% of property-damage-only collisions occurred during visibility-impairing weather. Reduced visibility resulting from adverse weather conditions, smoke, or dust impairs motorists' ability to see pavement markings, signs and other vehicles, and their ability to react appropriately to changing roadway and traffic conditions (Shepard, 1996). Fog is considered to be one of the most serious meteorological restrictions on visibility. The extreme visibility in fog, especially its density and location, coupled with problems in driver perception and behaviour present a threat to safe traffic operations (NTSB, 1991). A number of other weather-related factors are also known to affect driver visibility; these include droplet size, ambient illuminance, blowing snow, snow bank obstructions at intersections, wiper speed, and splash from other vehicles (Andrey et al., 2001).

Using time series analysis models, Bergel-Hayat et al. (2013) carried out research, which aimed to highlight the link between weather conditions and road accident risk at an aggregate level on a

monthly basis. The main results revealed that weather conditions significantly affect the number of road accidents and casualties, with different effects according to the type of road (motorways, rural roads and urban roads) (Bergel-Hayat et al., 2013). As stated by Yannis and Karlaftis (2010), the interaction between weather effects and the effects of other road safety factors, including roadway, driver, vehicle, and intervention variables on road accident frequency is certainly a complex phenomenon that attracts increasing attention by researchers.

A number of studies have indicated that of all overall weather indicators, the presence of precipitation has the most significant impact on road traffic accidents (Hermans et al., 2002; Mosedale, et al., 2004). In support of this statement, Yannis and Karlaftis (2010) point out that weather conditions, such as air temperature and precipitation are associated with considerable impacts on road safety, mainly through their influence on both the exposure and the behaviour of road users. Malyshkina et al. (2008) also found a positive correlation between extreme temperatures and road accidents. On the contrary, Scott (1986) and Brijs et al. (2008) suggest that higher temperatures appear to have a decreasing effect on accident frequencies and severity both on daily, weekly and monthly bases. According to these two authors the hours of sunlight appear to increase road accidents (Hermans et al., 2002), while deviations from mean daily or monthly temperatures were found to increase road accidents.

Despite creating hazardous driving conditions, weather does not always contribute unfavourably to road accident totals (Foldvary and Ashton, 1962). In certain circumstances, such as snow, people take more care by reducing their speed accordingly, and are thus able to negate the increased hazard (Edwards, 1996). Some weather cases may lead to journeys being cancelled, postponed or re-routed, thus leading to reduction in the number of vehicles at risk (Palutikof, 1983). Seemingly, positive and negative effects of weather conditions on road safety co-exist. However, there is a lack of research that identifies their combined effects. The following sub-sections contain brief and comprehensive discussions of three weather conditions considered to be the most hazardous in literature: Precipitation, fog and snow, in that respective order.

3.2.1 Precipitation

It has been widely acknowledged that rain, with its resultant wet roads, is the weather variable which causes the greatest problems in terms of accidents numbers (TRRL, 1974). Rain

diminishes the visibility distance as a result of the reflection on wet road surfaces. Jun (2010) stressed that the important effect of rain is not only reducing meteorological visibility, but also decreasing contrast and increasing glare especially at night. Precipitation significantly reduces friction of the wet road surface (Doherty, et al., 1993). Many factors affect friction; these include pavement texture, travel speed, tire tread and pressure, and ambient temperature. However, it is generally accepted that wet road friction is always less than that for the least skid-resistant dry road surface (Andrey and Olley, 1990). With increasing speed, the friction of a dry road surface is constant, while the friction of a wet road surface is rapidly decreasing (Doherty, et al., 1993). Consequently, braking distance of the vehicle is increased and the driver cannot sufficiently adapt their speed to compensate for their difference in friction between dry and wet roads, ergo the higher accident rate on wet roads than on dry roads (Jun, 2010).

Regardless of the variety of methods and data sources employed, results from prior studies examining the relationship between precipitation and traffic crashes have been nearly universal. In each case, precipitation has been estimated to increase overall traffic crashes. For instance, Andrey and Olley (1990) found that relative risk of crash during rain is 1.6; while Brodsky and Hakkert (1988) found a 2.2 relative risk during rain for injury accidents in Israel and 2.18 for fatal crashes in the US. Additionally, the NTSB (1980) discovered the relative risk for fatal crashes on wet pavement to be about 4. Furthermore, several studies have concluded that crashes increase during rainfall by 100% or more, while others find more moderate (but still statistically significant) increases (NTSB, 1980; Andreescu, 1998; Andrey and Olley, 1990).

On the contrary, a study by Yannis and Karlaftis (2010) on the impact of weather conditions on traffic safety found that increases in rainfall reduce the total number of accidents and fatalities, as well as the pedestrian accidents and fatalities. Although this appears counter to what would seem logical, it may be attributed to the safety offset hypothesis resulting from more cautious and less speedy driver behaviour. Yannis and Karlaftis (2010) argue that this may also be a characteristic of Southern European drivers who are not accustomed to driving in wet conditions. Several studies have managed to interpret positive effects of rainfall on road accidents. Keay and Simmonds (2006) showed that increased rainfall in centimetres results in decreased daily traffic volume, both day-time and night-time, winter and spring. Bergel-Hayat and Depire's (2004) findings are more or less along the same lines, only difference being that they decomposed the

global effect of monthly rainfall in two components. These are (1) a direct effect on the number of injury accidents and fatalities, and (2) an indirect effect on traffic volume.

On a different note, Smith et al. (2003) concluded that rainfall has a significant impact on freeway capacity and operating speed. He also argued that in the case of capacity, the impact of rainfall is a function of its intensity. In his investigation into the impact of rainfall on freeway traffic flow Smith et al. (2003) makes reference to work by Lamm et al. (1990) who concluded that operating speeds are not affected by wet pavement until visibility is also impacted, and therefore light rain does not impact operating speeds, while heavy rain does. Findings from this study indicate that light rain (intensity of 0.01–0.25 inches/hour) decreases freeway capacity by 4%-10%; while heavy rain (intensity of 0.25 inches/hour or greater) decreases freeway capacity by 25%-30%. In addition, regardless of intensity, the presence of rain results in approximately a 5%-6.5% average decrease in operating speeds. On the subject of visibility, preliminary results from research on driver visibility during rainfall indicate that driver visibility decreases within increased rainfall intensity, due mainly to the film of water on the windshield rather than to the reduction in meteorological visibility, and is accentuated by low ambient illuminance, slow wiper speed, and splash and spray from other vehicles (Morris et al., 1977).

To sum up, hundreds of studies have examined the tire-pavement interaction in wet conditions, such that the knowledge, and literature, of the effects of rainfall surface friction is very good (Andrey and Olley, 1990). Rain is considered the most common hazard, and being a year-round phenomenon in some parts of the world, Smith (1982) as cited by Edwards (1996) concluded that it influences driving conditions much more than either fog or snow.

3.2.2 Fog

Fog is simply a cloud on the ground composed of tiny droplets of water, or ice crystals in rare cases (Shepard, 1996). According to Shepard, the transparency of fog primarily depends on the concentration of droplets; the more droplets, the denser the fog. Thick fog (40 – 200 microns), therefore, represents the most important visibility range for road users. A study by Codling (1971), analysing the frequency and duration of thick fog in Great Britain for the period 1958-1967, revealed that the highest mean annual number of days with thick fog at recording sites was

17 at 0900 Greenwich Mean Time at Watnall (Nottinghamshire). The study found thick fog in general to be relatively infrequent, patchy, rarely widespread, and of short duration.

In practice, fog is recorded as the prevailing weather in very few road accidents. Fog is a relatively infrequent phenomenon, which is less prevalent than rain, even in those regions most prone to fog (Edwards, 1996). Consequently, road accidents in fog make up a diminutive proportion of total accidents. In accord, data collected in a study on weather-related road accidents in England and Wales (Edward, 1996) indicates that only a small portion of accidents occur in fog. According to Moore and Cooper (1972) overall 2% of all road casualties occur in foggy weather. Essentially, this implies that even if such accidents in fog were eradicated, overall accident totals would only be slight reduced. Nevertheless, fog is still considered the one weather condition that seems to seize media attention and weather hazard that drivers fear most (Edwards, 1996; Musk, 1991).

In 1990 and 1991, the National Transportation Safety Board (NTSB) noted that 4 accidents caused by fog on limited-highways in the United States (US), involving more than 240 vehicles, has resulted in 21 fatalities and more than 90 injuries (NTSB, 1991). In addition to this, the NTSB also noted that between 1981 and 1989, accidents where fog was present on all classes of highways in the US had resulted in more than 6 000 deaths. Although this is a small percentage of the total accidents, they are catastrophic and generally attract national media attention. Moreover, even though the total number of motorway for accidents is small, Moore and Cooper (1972) highlight that accidents per kilometre are more numerous than on other roads and more serious. Furthermore, they also note that despite a drop of 20% in the amount of traffic in thick fog there was an increase of 16%. Additionally, fog-accidents tend to be multi-vehicular accidents and often occur in a few ‘black-spots’, frequently on motorways (Codling, 1971).

A study by Hogema and Van Der Horst (1998) revealed that drivers reduce their free driving speed in fog, but not sufficiently to avoid a collision when they would be confronted with a stationery or much slower lead vehicle. In a different study, Hogema and Van Der Horst (1994) highlight that accidents in foggy weather are usually thought to be attributable to unreasonable risk taking on the part of drivers. Their interpretation is based on the observation that driving speeds are often too high for the visibility distance. A decrease in temporal headway between cars has been observed under certain traffic conditions in foggy weather (White and Jeffery,

1980). However, a number of authors contend that the problem lies in perceptual difficulties brought about by an alteration in fundamental processes of space and motion perception of fog (Cavallo et al., 2001). A driving simulation study by Snowden et al. (1998) supports this hypothesis. Snowden's study shows that participants who were instructed to drive at a certain speed drove faster as the visual scene became foggier. Brown (as cited in Snowden et al., 1998) pointed out that in conditions of reduced visibility produced by fog, drivers are reluctant to divert their gaze from the road to the speedometer for fear of missing an object emerging from the fog. Hence drivers rely on their own perceptual judgement of speed in conditions of reduced visibilitu caused by fog. This finding by Snowden et al. could also explain why drivers leave less headway in fog: in underestimating their speed, drivers tend to adopt a shorter safety distance.s

Nevertheless, (Cavallo et al., 2001) hypothesises that distance perception itself is affected by the presence of fog and that this alteration contributes to the observed behavioural modifications. Therefore, two experiments in a fog chamber reveal an average increase of 60% in the perceived distance of vehicles in fog as compared with normal visibility conditions. Distance overestimation was particularly pronounced when the vehicle had only one fog light instead of two and when the lights were close together. These results suggest that the perception of vehicle distance in nighttime fog could be significantly improved by the presence of 2 lights with maximal spacing.

In a nutshell, fog is a twofold effect: it both improverishes and distorets distance cues. Only the rear lights of the vehicle in front are visible in conditions of fog. The distance to that vehicle is perceived on the basis of the visible characteristics of the car's lights: their angular size, their luminance, and the angular distance between them (if there are two) (Cavallo et al., 2001).

3.2.3 Snow

Snow cover is cited as a hindrance to transportation more often than any other meteorological phenomenon, and that surface icing and glaze are considered to be only slightly less severe (Rooney, 1967). Much work on the problem of vehicle performance on roads covered by snow or ice has been done by tire manufacturers, and is proprietary (Jean et al., 2001). Jean et al. (2001) argues that the snow/ice issue is somewhat more complex than rainfall, because the greater importance of temperature, traffic, and maintenance activities. Edwards (1996) points out

that in the United Kingdome (UK) snow can cause extensive disruption to road transport, partly because of its unpredictability and infrequency. Marked fluctuations can be observed in its occurrence, amount, persistence and seasonality, with wide variations being observed from year to year (Hargreaves, 1976). Consequently, snow and fog are considered insignificant weather hazards when viewed in terms of annual road accident total; also given that they account for less than 2% of annual accidents (Edwards, 1996).

When blowing and whirling, snow reduces direct road visibility; an even more severe direct visibility reduction occurs with increasing wind speed (Jun, 2010). In addition, visibility impairment may be also associated with snow banks, obstructing visibility intersections, snow cover obscuring roadway markers, and the reduced contrast within the field of view due to snow on the ground/road (OECD, 1976), although these are not as well documented (Andrey et al., 2001). According to Bullough and Rea (2001), light reflected from particles in perturbed atmospheres (such as falling snow, rain and fog) impairs visibility because it acts as a luminous veil in the case of fog, or as visual "noise" in the case of falling rain and snow. As cited by Bullough and Rea (2001); Bisonnette (1992) and Hutt et al. (1992) also add that some of the light from headlamps will be reflected from falling rain and snow back toward the driver.

A number of studies provide empirically derived estimates of weather-related driving risks. Snow reduces the friction of the road, even much more than the reduction made by rain; therefore considerable evidence has shown that snowfall has greater effect than rainfall on collision occurrence and risk of injury, although snow-related collisions tend to be less serious than other collisions (Andrey et al., 2001; Jun, 2010). In spite of this, snowfall-related collisions tend to be associated with fewer fatalities than other collisions (Andrey et al., 2001). A study by Suggett (1999), on the effect of precipitation on road safety in Regina (Canada), uncovers that the calculated risk of a collision was 2.11 in snow and 1.47 in rain; while the calculated relative risk of an injury was 1.68 in snow and 1.42 in rain. Similarly, Lane et al. (1995) found that, in Highways and feeder highways in Ontario London, 8% of fatal accidents and 9% of injury accidents occurred during rain; while 12% of fatal accidents and 16% of injury accidents occurred during snow. Also, 13% of fatal accidents and 18% of total injury accidents occurred on snow covered roads.

Several literature sources debate whether snowfall is associated with a net increase or net decrease in injuries; but Canadian studies are consistent in finding that injury rates increase during snowfall, although to a lesser extent than property damage collisions (O'Leary, 1978). Suggett (1999) discovered that driving during a snow event was twice as likely to result in a crash, and 70% more likely to result in injury. Moreover, periods of elevated risk caused by residual snow were found to last up to a week after measurable snow had fallen. However, it is less clear for fatal collisions, mostly because of the small numbers involved. However, some studies note fewer fatalities during snowfall, probably because of the reduced speed (Datla and Sharma, 2008). Overall, the hazards associated with snowy conditions are a well-recognised and well researched subject; nevertheless, there are still a number of subject-matters that need further research and improvement.

3.3 Sun Glare Effects on Road Safety

3.3.1 Definition of Glare and Forms of Glare

The *Dictionary of Visual Science* (as cited by Auffray et al., 2007) defined glare as a relatively bright light, or the dazzling sensation of relatively bright light, which produces unpleasantness or discomfort, or which interferes with optimal vision. Nakagawara et al. (2004) defines glare as a temporary sensation produced by luminance (brightness) within the visual field that is significantly greater than that to which the eyes are adapted and is not associated with biological damage. In his research on the effect of glare on the brightness difference threshold, Stiles (1929) indicates that there are three different components of the glare effect: the disability caused by it; the sensation of discomfort; and the recovery time. Traditionally, glare has been classified into two well-recognised forms: *discomfort glare* or *disability glare* (Jurado-Pina and Pardillo-Mayora, 2010).

Discomfort glare (also known as psychological glare) produces discomfort or annoyance without necessarily interfering with the visual performance of the driver (Vos, 2003). Discomfort glare is a result of illumination that is too intense or variable for a particular person, place, and time. Is it essentially a normal response to abnormal illumination; whereas *photophobia* is an abnormal response to normal illumination exaggerated by abnormal light exposure (Mainster and Turner,

2012). Mainster and Turner (2012) also highlight that discomfort glare threshold (*photosensitivity*) varies considerably between individuals. According to Theeuwes et al. (2002) discomfort glare is determined primarily by rating scales, whereby participants indicate how annoying a light source is while looking at its direction. He goes on to highlight that although there is no consensus about which rating scale should be used, the 9-point DeBoer scale is most widely used in the field of automotive and public lighting. However, only five different glare index values have the descriptive meaning; these ratings are listed in Table 3-1 (Fekete et al., 2005). In addition, unlike disability and scotomatic glare, discomfort glare varies little with age (Mainster and Turner, 2012).

Table 3-1: The Different Index Levels of the De Boer Glare Rating Scale

Index	Glare	General Impression
1	Unbearable	Bad
2	-	-
3	Disturbing	Inadequate
4	-	-
5	Just admissible	Fair
6	-	-
7	Satisfactory	Good
8	-	-
9	Unnoticeable	Excellent

(Source: Fekete et al., 2005)

On the other hand, disability glare (also known as physiological glare) causes reduced visual performance resulting from apparent scattering of light within the eye (Knott, 1983). Basically, disability glare causes reduced contrast sensitivity (Theeuwes et al., 2002). However, Vos (2003) points out that there are large individual differences in people's sensitivity to disability glare; the average reduction in contrast sensitivity can be calculated objectively. The cause of disability glare is intraocular light scattering (straylight) that reduces the contrast of retinal images by spreading a veiling of luminance across them (Mainster and Turner 2012). Mainster and Turner (2012) also underline that disability glare and discomfort glare can range from insignificant to incapacitating; they are usually concurrent but can occur independently. For example, brilliant

street lighting can produce discomfort without disability glare, whereas poor street lighting can cause disability without discomfort glare (Vos, 2003).

In his paper, Nakagawara et al. (2004) identifies two other types of glare: *flashblindness* and *afterimage*. Flashblindness is a visual interference effect that persists even after the source of illumination has been removed. While afterimage is a transient image left in the visual field after exposure to bright light. Mainster and Turner (2012) classifies these two types of glare as scotomatic glare (also termed photostress), which is glare that causes afterimages and visual disability when a brilliant but localised light exposure excessively bleaches macular photopigment. An additional type of glare is also acknowledged in this paper, dazzling glare (dazzle). Mainster and Turner (2012) define dazzle as glare that produces squinting, annoyance, aversion, and visual disability when bright environments spread high illuminance across large retinal areas. Dazzling glare is considered a type of discomfort glare, and of course it is uncomfortable as well, but phenomenologically it is an entirely different phenomenon (Vos, 2002). According to Vos (2003) the observer in dazzle looks at an extended field of view, and shows avoidance rather than attraction reactions. Dazzling glare is also termed adaptation glare if brief, saturation or blinding glare if prolonged (Boyce, 2009).

3.3.2 Glare Contributing Factors

Be it from a natural or artificial light source, glare can result in temporary visual impairment, increasing the risk of an accident (Nakagawara et al., 2004). Due to high-glare conditions, low contrast objects may be rendered invisible as a result of the reduction in object visibility associated with such conditions. A statistical comparison carried out by Choi and Singh (2005) found that glare, whether from headlights or sunlight, has a statistically significant impact on the likelihood of vehicle crashes. In agreement with this conclusion, Monsere et al. (2008) also points out that glare generated by vehicle headlights or other artificial light sources also causes significant reductions in vision performance. The most common sources of glare include street lighting, electric head lamps, direct sunlight, and headlights of other vehicles, or other light sources, which can cause substantial reductions in vision performance (Auffray et al., 2008). In essence, the effect of glare remains the same whether it comes from headlamps or sunlight: it obstructs drivers' vision and affects driving performance (Choi and Singh, 2005).

Moreover, a study by Theeuwes et al. (2002) drew attention to the fact that discomfort glare and disability glare may not always be affected by all and the same aspects of lighting. Discomfort glare is assumed to cause discomfort without necessarily impairing the vision of objects, meaning that there may be aspects of lighting that do not affect disability glare but increase discomfort glare. A good example is a headlamp size, which influences discomfort glare but not disability glare (Van Derlofske and Bullough, 2003). An earlier study by Bullough et al. (2002) reveals that the relative influences of lamp spectrum, light level and viewing angle appear to be much different for discomfort glare than they are for disability glare. According to Bullough et al. (2002), for the same illuminance at the eye, High-Intensity Discharge (HID) headlamps seem to produce greater discomfort than halogen headlamps, despite their similar scotopic content.

Moreover, in an investigation to analyse the impact of sun glare (Jurado-Pina and Pardillo-Mayora 2010) indicate several factors determine the occurrence of sun glare along a roadway at a given time. These include the position of the sun relative to the driver's eye, the direction of the driver's line of sight, and the configuration of the terrain. The sun position is discussed in Section 2.4. The direction of line of sight is the spot where the driver aims his/her line of sight while driving. This spot obviously varies with vehicle speed and layout of the roadway. In their analysis (Jurado-Pina and Pardillo-Mayora 2010) assumed the driver's line of sight to be directed to a point on the road axis 90m ahead of his position.

Furthermore, the terrain profile refers to the physical features of the environment under investigation, e.g. the topography. These features play a significant role in the occurrence of invasive sun glare conditions. For instance, at certain angles of the sun, terrain features, such as mountains may shield the driver's eyes from the sun, thus preventing the occurrence of glare. For this reason, it is essential that the analysis of sun glare situation incorporate the profile defined by the terrain within the driver's visual field (Jurado-Pina and Pardillo-Mayora 2010).

Given that the occurrence of glare varies according to location and time, certain combinations of the horizontal and vertical geometry of the roadway contribute directly to sun glare conditions by placing the driver's line of sight in a situation to be susceptible to glare effects (Auffray et al., 2007). Due to the axial tilt of the Earth, the trajectory of the sun through the sky changes over the course of the year (Churchill et al. 2012). Therefore, glare conditions are highly dependent on

geographical locations. Furthermore, mountainous areas (terrain profile) are less susceptible to sun glare conditions, since the sun may be occluded when it might be most problematic. Similarly, cloud cover potentially blocks direct sunlight exposure on drivers as well.

3.3.3 Relation between Glare and Driving Performance

Despite the existing knowledge and research output, there are not a lot of solutions that exist to mitigate sun glare effects. When the sun is moderately high in the sky, its effects can be mitigated by proper use of sun visors, sunglasses, and/or other means reducing glare. However, when the sun is low in the sky, no more than a few degrees above the roadway ahead, there is no way to block the sun and prevent glare, without also losing forward preview information. Normally, a driver will squint, look down at the roadway in the near foreground, or use other strategies to continue to navigate and drive, thus making him/her unable to keep watch for potential obstacles or problems further ahead (Ayres et al., 2004). Nonetheless, there is consensus that glare within the range that causes discomfort does not significantly reduce the ability to perceive information (Theeuwes et al., 2002). Granted if a glare source causes only feelings of discomfort then one expects that driving behaviour is not affected by the presence of the glare source. However, Theeuwes et al. (2002) also indicates that if the discomforting glare source results not only in feelings of discomfort but also in strategic adaptations to reduce discomfort, then one may expect to see changes in driving behaviour.

As a first step towards understanding driver decision-making and response to sun glare conditions, Ayres et al. (2004) carried out a study of speed adjustment to solar glare. In this study driver behaviour, including travel speed is unobtrusively (video) observed on two public roadways during conditions in which the sun ahead was expected to create difficulty, as well as in more benign conditions. Video observations of drivers approaching a setting afternoon sun found only a small decrease compared with a non-glare condition; in addition, speed variability appeared to increase somewhat in the sun condition. These effects, which are similar to reported driver behaviour in for and other impaired-visibility conditions, increase the risk of accidents (Shepard, 1996). Ayres et al. (2004) also investigated the visual performance by using contrast detection. The data from his findings indicates that when the sun is low in the sky it can impair visual performance in the form of contrast sensitivity for objects ahead. The use of a visor or other means of blocking intrusive direct sun light greatly improves target detection, but does not

completely eliminate performance decrement. Thus, in certain times of the day, driving towards the sun in the morning or afternoon can interfere with a driver's ability to see features on the road and environment ahead, even if efforts are made to block the glare. Essentially, behaviour varies when drivers are faced with degraded-visibility conditions. Some drivers slow down, and some do not, and generally nobody slows down very much, probably not enough to compensate for the degraded visibility (Ayres et al., 2004).

In accord, Theeuwes (2002) draws attention to the fact that with increasing glare there is a reduction in the ability to perceive small contrasts; this reduction may affect a number of visual tasks required in traffic such as detecting critical objects, controlling headway, reading signs and evaluating critical encounters. Certain changes in factors aggravate the effects of sun glare. Generally, the effect of glare will increase when the source of luminance increases, the background luminance decreases, and the angle between the line of sight and the direction of the light source decreases (Alferdinck, 1996; Alferdinck and Varkervisser, 1991).

3.3.4 Glare in Traffic

Intuitively, when thinking about the impact of glare, one would expect the measured flow and speed to drop slightly while glare is occurring, and impacting drivers (Auffray et al., 2007). It's safe to assume that during conditions of direct (bright) sunlight exposure drivers will reduce their speed and increase their headways, due to a tentative feeling and lack of visibility of other vehicles and lane markings. Depending on the age and visual health, people do not react homogenously to the discomfort of glare. Naturally, an individual driver could slow down in response to a sun glare situation. As a result of such a situation, an individual driver or group of drivers slowing down together could generate significant traffic congestion (Churchill et al., 2012). On the contrary, Theeuwes et al.'s (2002) study on the relation between glare and driving performance indicates that only when roads are winding and dark and lane keeping becomes a problem do drivers slow down to compensate for the negative effects of a glare source. However, there is no behavioural adaptation if the road is wide and fairly predictable because lane keeping is easy even when glare is present.

Moreover, Auffray et al. (2007) hypothesises that speed would decrease during periods of sun glare, because of a new dynamic bottleneck created by the glare. His paper examines the

potential impact between measured traffic flow characteristics and the potential for vehicles to be impacted by sun glare. Although the empirical data did not always show this glare effect, his investigations reveal that the presence of potential for sun glare can apparently affect the speed and flow distributions during congested and uncongested periods. While far from conclusive, the study has revealed a potential for future research.

On a different note, to shed some lights on the effects of glare in airway transportation, Nakagawara et al. (2004) investigated the relationship between visual impairment from natural sunlight and aviation accidents. The National Transportation Safety Board Aviation Accident/Incident Database was queried for the period January 1, 1988 to December 31, 1998 for terms which relate to sun glare conditions, such as "sun", "glare", "vision" etc. there were 130 accidents in which glare was found to be a contributing factor. This investigation concluded that exposure to glare from natural sunlight has contributed to aviation accidents, primarily under otherwise optimal visual conditions at low altitude in congested airspace.

In a preliminary investigation, Choi and Singh (2005) employ descriptive statistical and contingency analyses on crash data compiled in National Automotive Sampling System-General Estimates System (NASS-GES) to study the glare issue and some of its aspects, which in this study include: age, sex, travel speed, manoeuvre, crash hour, traffic-way flow, number of lanes, manner of collision, roadway profile and vehicle role. The results of this investigation show that a driver's age plays a significant role in conjunction with glare, while sex does not. The driver's manoeuvring on the other hand is not associated with his/her crash involvement due to being exposed to glare. Furthermore, factors such as traffic flow, roadway profile, and number of lanes are likely to contribute to crash involvement when a driver is exposed to glare. Additionally, the findings also suggest that vehicle-related factors, vehicle speed, crash hour, manner of collision, and vehicle role are also significantly associated with glare.

3.4 Sun Position: The Theory behind Coordinate Calculations

A number of astronomical algorithms can be used to determine the position of the sun relative to a specific location and time. An algorithm is a step-by-step procedure for calculations that is followed by a computer. At a given time and location, the sun position is defined in global

coordinates, local coordinates, and the relative elevation angle. The global coordinates consist of the right ascension and declination, while the local coordinates consist of the hour angle, zenith and azimuth angle (Grena, 2008). As stated by Jurado-Pina (2010), the successive solar positions throughout a day define the solar path.

However, the sun positions used in this thesis were obtained from a credible website, which applies algorithm calculations to produce sun position (and hour angle) results for a specific location. Nevertheless, the literature in this section will briefly explore the science behind the sun algorithms, among other things.

3.4.1 Computing the Position of the Sun

As previously stated, when the sun is low in the sky either setting or rising, the problem of sun glare is most prevalent. As the roadway tends to be quite small form a geometric perspective and the sun is no more than a few degrees above the roadway ahead, there is no way to block the sun and prevent glare without losing forward preview information (Ayres et al., 2004). Furthermore, atmosphere plays a significant role in refracting sunlight, ultimately causing the sun's apparent position to be different than its true position (Churchill et al., 2012). This phenomenon makes the analysis of the solar position slightly more complicated. Nevertheless, several authors have proposed various solutions to this conundrum. These solutions, inter alia, include the use of a refraction correction formula in the algorithm calculations procedure.

According to Churchill et al. (2012) and Jurado-Pina and Pardillo-Mayora (2010), Spencer (1971) was one of the early approaches to propose a method for the efficient establishment of the position of the sun. This was later followed by Walraven (1978). Many subsequent authors (Walraven, 1979; Archer, 1980; Ilyas, 1983; Spencer, 1989) provided corrections and improvements on the Walraven algorithm. In the same year, the Pitman and Vant-Hull (1978) algorithm was introduced. Blanco-Muriel et al. (2001) and Grena (2008), two of the more recent approaches, took a systematic approach to comparing errors of these various models, as well as ease of use.

In computing the position of the sun, relative to an observer, several factors have to be considered. Among others, these include terrain profile (i.e. topography); the geometric design of

the roadway; cloud cover for that instance under investigation; the sun cone relative to the terrain profile and the driver's line of sight; and seasonal variation (time of year).

3.4.2 Sun Position Algorithms

Two of the most prominent algorithms for the determination of the sun coordinates are the *Solar Position Algorithm* (SPA) by Grena (2008) and the Plataforma Solar de Almerýa (PSA) by Blanco-Muriel et al. (2001). The following sections are brief discussion of these two algorithms, respectively.

Solar Position Algorithm

The SPA algorithm requires several inputs in order to determine the position of the sun. These are: fractional Universal Time (UT) of the day, the date and the difference (Δ) between UT and Terrestrial Time (TT). UT, or Greenwich civil time, is measured in hours form the Greenwich midnight; the minutes and seconds must be converted into fractions of an hour. The date is presented as the day (D), months (M) and years (Y). Lastly, the difference between UT and TT is the time scale for ephemeres. For this algorithm, this difference is required to be given in seconds; longitude and altitude remains in radians, pressure (in atmospheres) and temperature (in ^{o}C). The following is an outline of the steps which Grena (2008) adopted for the computation of the position of the sun:

a) Time Scales

The time scales in this computation, Julian Day (t_G) and Ephemeris Julian Day (t), are shifted to make them start at noon, 1st January 2003. The following formulae give values for t_G and t times scales. For Eq.2, if M is 1 or 2, it must be increased by 12 and Y must be decreased by 1:

$$t_G = INT\big(365.25(Y - 2000)\big) + INT\big(30.6001(M + 1)\big) + D + \frac{UT}{24} - 1158.5 \qquad (2)$$

$$t = t_G + \frac{\Delta}{86400} \qquad (3)$$

The standard Julian Day (JD) and Ephemeris Julian Day (JDE) equations, starting at noon 1 January 4712 BC, are as follows:

$$JD = JD_t + 2452640 \quad (4)$$

$$JDE = t + 2452640 \quad (5)$$

(Grena, 2008)

Where,

t_G = Julian Day

t = Ephemeris Julian Day

Y = Years

M = Months

D = Day

UT = Universal Time

INT = a function that indicates rounding towards zero: i.e., INT(3.7) = 3

Δ = Difference between Terrestrial Time and Universal Time (TT - UT)

JD = Standard Julian Day (starting at noon, 1st January 4712 B.C.)

JDE = Ephemeris Julian Day (starting at noon, 1st January 4712 B.C.)

b) Calculation of the heliocentric longitude of the earth

Heliocentric means considered in relation to the centre of the sun; meaning, the position of the earth is calculated with respect to the centre of the sun. In order to avoid errors, and for convenience, this calculation step is broken down into the following four steps.

i. Linear increasing with annual oscillation

$$\Sigma = 1.72019e - 2t - 0.0563 \quad (6)$$

$$L_y = 1.74094 + 1.7202768683e - 2t + 3.34118e - 2\sin\Sigma + 3.488e - 4\sin 2\Sigma \quad (7)$$

ii. Moon perturbation

$$L_m = 3.13e-5\sin(0.2127730t - 0.585) \quad (8)$$

iii. Harmonic correction

$$L_h = 1.26e-5\sin(4.243e-3t + 1.46) + 2.35e-5x\sin(1.0727e-2t + 0.72) + 2.76e-5x\sin(1.5799e-2t + 2.35) + 2.75e-5x\sin(2.1551e-2t - 1.98) + 1.26e-5x\sin(3.1490e-2t - 0.80) \quad (9)$$

iv. Polynomial correction

$$t_2 = 0.001t \quad (10)$$

$$L_p = \left((-2.30796e-7t_2 + 3.7976e-6)t_2 - 2.0458e-5\right)t_2 + 3.976e-5\Big)t_2^2 \quad (11)$$

Finally, Eq. (12) gives the value of the longitude (L), which is the sum of the four terms calculated in the preceding four steps.

$$L = L_y + L_m + L_h + L_p \quad (12)$$

Where,

L = Longitude (in degrees)

L_y = Linear increasing with annual oscillation term

L_m = Moon perturbation term

L_h = Harmonic correction term

L_p = Polynomial correction term

t_2 = time scale introduced in order to have more homogeneous quantities in the products within the polynomial, avoiding too rough rounding approximation.

c) Correction to geocentric longitude due to nutation

$$\Delta\gamma = 8.33e-5\sin(9.252e-4t-1.173) \quad (13)$$

d) Earth axis inclination

$$\varepsilon = -6.21e-9t+0.409086+4.46e-5\sin(9.252e-4t+0.397) \quad (14)$$

e) Geocentric global solar coordinates

i. Geocentric solar longitude

$$\gamma = L+\pi+\Delta\gamma-9.932e-5 \quad (15)$$

ii. Geocentric right ascension

$$\alpha = a\tan2(\sin\gamma\cos\varepsilon,\cos\gamma)$$

The output of this calculation is a value in radians, between –π and π (Grena 2008).

The right ascension is usually measured in hours, from 0 to 24 (Grena 2008). In hours, this can be easily obtained using Eq. (16):

$$\alpha^{hr} = 12mod(\alpha,2\pi)/\pi \quad (16)$$

iii. Declinations

$$\delta = a\sin(\sin\varepsilon\sin\gamma) \quad (17)$$

Where,

α = Ascension

α^{hr} = Right ascension in hours (h); 1h =15º

f) Local hour angle of the sun

$$h = 6.30038809903t_G + 4.8824623 + 0.9174\Delta\gamma + \theta - \alpha \quad (18)$$

Where,

θ = Longitude

g) Parallax correction to right ascension

$$\Delta\alpha = -4.26e - 5\cos\varphi \sin h \quad (19)$$

Where,

φ = Latitude (radians)

h) Topocentric Sun Coordinates

Topocentric means relative to an observer. The sun position is calculated with respect to the observer's local position at the Earth surface (Reda and Andreas, 2004). This is established by using the following equations.

i. Topocentric right ascension:

$$\alpha_t = \alpha + \Delta\alpha \quad (20)$$

ii. Topocentric declination:

$$\delta = \delta - 4.26e - 5(\sin\varphi - \delta\cos\varphi) \quad (21)$$

iii. Topocentric hour angle:

$$h_t = h - \Delta\alpha \quad (22)$$

$$ch_t = \cos h + \Delta\alpha\sin h\,(approximate\ cosine\ of\ h_t) \quad (23)$$

$$sh_t = \sin h - \Delta\alpha\cos h\,(approximate\ sine\ of\ h_t) \quad (24)$$

Where,

α_t = Topocentric right ascension

δ = Topocentric declination

h_t = Topocentric hour angle

i) Solar elevation angle, without refraction correction

$$e_0 = a\sin(\sin\varphi \sin\delta_t + \cos\varphi \cos\delta_t ch_t) \quad (25)$$

j) Atmospheric refraction correction to the solar elevation

Eq. (26) is the same as the one used by Reda and Andreas (2004), except that they use degrees, while this one by Grena (2008) uses radians. Grena (2008) points out that since this formula is independent from the other steps of the algorithm, it can be replaced by any formula for refraction correction that includes all the parameters one chooses to consider, or ignore in the case that refraction is considered negligible.

$$\Delta e = \frac{0.084217P}{\left[(273+T)\tan\left(e_0+\frac{0.0031376}{(e_0+0.089186)}\right)\right]} \quad (26)$$

k) Local Topocentric sun coordinates

i. Zenith:

$$z = \frac{\pi}{2} - e_0 - \Delta e \quad (27)$$

ii. Azimuth:

$$\Gamma = a\tan2(sh_t, ch_t \sin\varphi - \tan\delta_t \cos\varphi) \quad (28)$$

Where,

z = Zenith angle (degrees)

Γ = Azimuth (degrees)

The azimuth (Γ) obtained in Equation 28 varies from $-\pi$ to π; while the one calculated by Reda and Andreas (2004) ranges from 0° to 360°. Evidently, the two authors are carrying out the same calculations but are using different units: Reda and Andreas are using degrees, while Grena is using radians. $\Gamma = 0$ towards the south direction, and positive in the western hemisphere (Grena, 2008).

Plataforma Solar de Almerýa

Blanco-Muriel's Plataforma Solar de Almerýa (PSA) algorithm, which calculates atmospheric refraction correction based on a few modifications, is crucial when getting the true position of the sun. The impact of refraction is illustrated in Figure 3-1. According to Churchill et al. (2012), compared to others, the PSA procedure has a good combination of computational performance and predictive accuracy. Without the refraction correction, the PSA algorithm has a maximal error of 0.008°, and is applicable for the period between 1995 and 2015 (Grena, 2008). To facilitate the processing of the traditional specification of the highway geometry data, the data must first be converted into a format that can be easily processed by a computer (Churchill et al., 2012). Figure 2-2 is an illustration of the algorithm methodology established by Churchill et al. (2012). The converted data is projected onto a map to locate various stations in traditional geographic coordinates. Subsequently, the relative position of the sun is calculated at some interval along the centreline using the processed highway alignment data. Upon establishing the solar position and viewing the direction, the last phase of the methodology (glare analysis) is carried out.

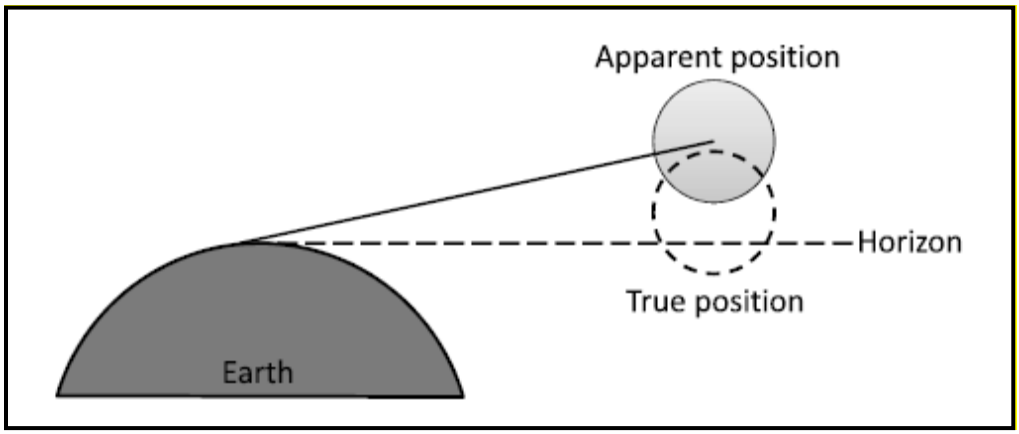

Figure 3-1: Impact of Refraction on Apparent Solar Position

Source: *(Churchill et al., 2012)*

In order to determine the sun position using this algorithm, three types of input data are required: time, location and atmospheric conditions. The latter is input data for the modified part of the PSA algorithm, atmospheric refraction correction. It is desirable that the position of the sun be described relative to a specific position at a specific time; hence, the need for the time and location input data. In this situation, the reference point would be the observer's location. The time at which the solar position is calculated is given as the date (year, month and day) and the Universal Time (hours after midnight, minutes and seconds as fractions of an hour) (Churchill et al., 2012). The location is given as the longitude (positive east) and latitude (positive north) of the observer. Lastly, the atmospheric conditions of temperature and pressure are specified to accurately model refraction (Churchill et al., 2012). Ultimately, the algorithm output is the solar position relative to the specified viewer's position.

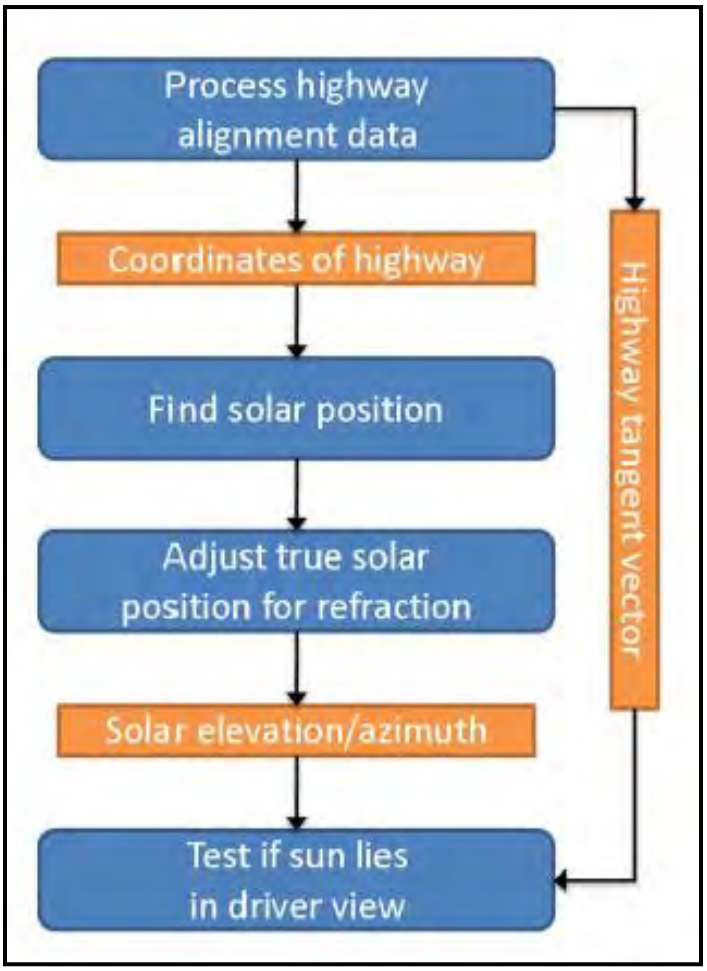

Figure 3-2: Sun Glare Algorithm Flow Chart

Source: *(Churchill et al., 2012)*

Churchill et al. (2012) breaks the modified PSA algorithm into 6 distinct calculations. These are as follows:

a) Compute Julian Day

The initial step consists of the computation of the Julian Day (JD) of the time being considered. The Julian Day refers to a continuous count of days, and fractions of a day, elapsed since March 2, 4800 BCE (Churchill, 2012). The following is a formula to calculate JD (Eq. 29):

$$\boldsymbol{jd} = \frac{1461}{4}\left[y + 4800 + \frac{m-14}{21}\right] - \frac{3}{400}\left[y + 4900 + \frac{m-14}{21}\right] + d + \frac{h}{24} - 31708.5 \quad (29)$$

$$\boldsymbol{n} = \text{jd} - 2451545$$

Where,

jd = julian day

n = value used to normalise the julian day value obtained above, so that zero now corresponds with the J2000.0 epech (noon on January 1, 2000)

b) Compute Location of Sun in Ecliptic Coordinates

Ecliptic coordinates are coordinates based on the celestial coordinate system (coordinate system for mapping positions on the celestial sphere) that uses the ecliptic for its fundamental plane. The sun ecliptic coordinates are calculated as a function of the Julian Day. The ecliptic is the sun's apparent path across the sky over the course of a year (Churchill, Tripodis et al. 2012). To begin this computation, the auxiliary variable (Ω) is calculated first, followed by the mean longitude (L) and mean anomaly (g), and finally the ecliptic longitude (l) and obliquity of the ecliptic (ep) are calculated. The following are the respective equations for these calculations.

i. *Auxiliary variable:*

$$\Omega = 2.1429 - 0.0010394594n \quad (30)$$

ii. *Mean Longitude:*

$$\boldsymbol{L} = 4.8950630 + 0.017202791698n \quad (31)$$

iii. *Mean anomaly:*

$$\boldsymbol{g} = 6.2400600 + 0.0172019699n \quad (32)$$

iv. *Ecliptic Longitude*:

$$\boldsymbol{l} = L + 0.03341607\sin(g) + 0.00034894\sin(2g) - 0.0000203\sin(\Omega) - 0.0001134 \quad (33)$$

v. *Obliquity of the ecliptic ep:*

$$\boldsymbol{ep} = 0.4090928 - 6.2140310x10^{-9}n + 0.0000396\cos\Omega \quad (34)$$

Where,

Ω = Auxiliary variable

L = Mean Longitude

g = Mean anomaly

l = Ecliptic Longitude

ep = Obliquity of the ecliptic *ep*

c) Convert Ecliptic to Celestial Coordinates

To define the established location in equatorial coordinates it is transformed from ecliptic coordinates to celestial coordinates. The equatorial coordinate system uses as its fundamental the projection of the Earth's equator onto the celestial sphere (Churchill, Tripodis et al. 2012). This transformation simply requires the calculation of the right ascension (ra) and the declination (δ). The following respective equations are used to calculate these values.

$$ra = \tan^{-1}\left[\frac{\cos(ep)\sin(l)}{\cos(l)}\right] \quad (35)$$

$$\delta = \sin^{-1}[\sin(ep)\sin(l)] \quad (36)$$

Where,

ra = Right Ascension

δ = Declination

d) Convert Celestial to Horizontal Coordinates

Finally, the solar position which is in equatorial coordinates is converted to horizontal coordinates. The calculation of the horizontal coordinates, which express the position of the sun relative to the location of the observer, completes this process (Churchill, Tripodis et al. 2012). Several sub-steps make up this final step. These are as follows:

i. Firstly, calculate the Greenwich Mean Sidereal Time (GMST) as shown in Equation 37. Sidereal Time means "star time"; basically how long it takes the earth to spin 360° with respect to the "fixed" stars instead of the sun (http://docs.kde.org/).

$$\boldsymbol{gmst} = 6.6974243242 + 0.0657098283n + h \quad (37)$$

ii. Secondly, the GMST is further adjusted to Local Mean Sidereal Time (LMST).

$$\boldsymbol{lmst} = 15gmst + \lambda \quad (38)$$

iii. Thirdly, calculate the hour angle as a function of the LMST and the right ascension.

$$\boldsymbol{\omega} = lmst - ra \quad (39)$$

iv. All the transformations are now complete, so the direct calculation of the relative position of the sun can now be carried out. Eq. (40) calculates the azimuth angle, which is a function of the hour angle, declination and latitude.

$$\boldsymbol{\gamma} = \tan^{-1}\left[\frac{-\sin(\omega)}{\tan(\delta)\cos(ø) - \sin(ø)\cos(\omega)}\right] \quad (40)$$

v. The Zenith angle is computed using Eq. (41).

$$\boldsymbol{\theta_{z,n}} = \cos^{-1}[\cos(ø)\cos(\omega)\cos(\delta) + \sin(\delta)\sin(ø)] \quad (41)$$

Given that the zenith angle is measured relative down from the zenith (the point on the celestial sphere furthest from the fundamental plane, rather than up from the fundamental plane itself), Eq. (42) is applied for a transformation (Churchill, Tripodis et al. 2012). To arrive at the solar elevation angle, a slight correction for parallax is applied as well.

$$\boldsymbol{\theta_s} = \frac{\pi}{2} - \left[\theta_{z,n} + \frac{6371.01}{149597890}\sin(\theta_{z,n})\right] \quad (42)$$

The diagram in Figure 3-3 gives a set of example outputs for the algorithm.

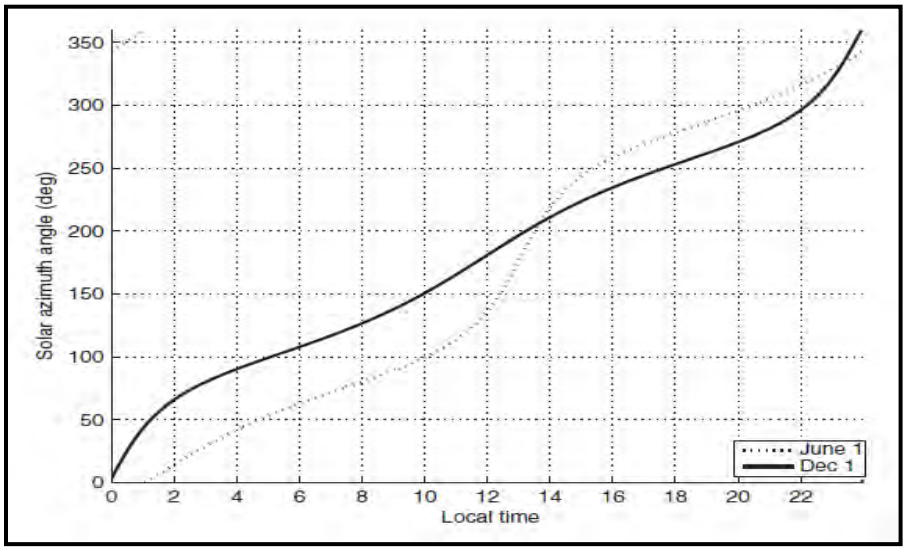

Figure 3-3: Sun Glare Algorithm Flow Chart

Source: *(Churchill et al., 2012)*

Where,

gmst = Greenwich Mean Sidereal Time

lmst = Local Mean Sidereal Time

ω = hour angle

γ = Azimuth angle (degrees)

$\theta_{z,n}$ = Zenith angle (degrees)

θ_s = Zenith angle fundamental plane measurement transformation and parallax correction

e) Adjust Apparent Solar Position for Atmospheric Refraction

When passing from one medium to another light waves change direction. This also occurs when they pass through the atmosphere on earth. This occurrence is known as refraction; it causes the apparent position of the sun to an observer to differ from the actual position of the sun. In this application, it is the apparent position which is more important (Churchill, Tripodis et al. 2012). In view of that, the true position of the sun obtained in step d) is adjusted to that which is seen by the observer. Figure 3-1 is an illustration of this concept.

The following equation (Eq. 43) can be used for a refraction correction when the true elevation angle of a star is known. The formula assumes 1.010mbar atmospheric pressure and 10°C air temperature.

$$\boldsymbol{\theta_{s,r}} = \theta_s + \frac{1.02}{\tan\left(\theta_s + \frac{10.3}{\theta_s + 5.11}\right)} \tag{43}$$

According to Meeus (1988), quoted by (Churchill et al., 2012), refraction increases with increased pressure or decreased temperature. Accordingly, Meeus (1988) provided an update to the above refraction formula. In the following equation (Eq.44) P represents the atmospheric pressure and T the temperature:

$$\boldsymbol{\theta_{s,r}} = \theta_s + \left[\frac{P}{1010}\right]\left[\frac{283}{273+T}\right]\left[\frac{1.02}{\tan\left(\theta_s + \frac{10.3}{\theta_s + 5.11}\right)}\right] \tag{44}$$

Where,

$\theta_{s,r}$ = refraction correction

P = Atmospheric Pressure (mbar)

T= Temperature (ºC)

f) Change Coordinate Systems

Lastly, for numerical convenience, the spherical coordinates are converted to rectangular coordinates using Eq. (45), and the vector is normalised to unit length using Eq. (46).

$$\hat{s} = [\sin\gamma\,, \cos\gamma\,, \tan\theta_s\,, r] \tag{45}$$

$$s = \frac{\hat{s}}{\|\hat{s}\|} \tag{46}$$

3.4.3 Glare Analysis after Computation

As the final step in identifying glare conditions, a test to determine if the view of the driver will approach the sun is applied (Churchill et al., 2012). As seen in Figure 3-4, Churchill et al. (2012) presents a diagram, which illustrates the horizontal geometry of this test. According to this diagram, the driver is likely experiencing glare if the centre of the sun lies in the areas swept out in both the horizontal and vertical planes, (a) and (b), respectively. It is important to note that the models described by Churchill et al. (2012) do not take into account the surrounding topography. Furthermore, the viewing region of the driver, which might be affected by sun glare, is represented by a sun cone with a circular base whose apex lies at the driver's position.

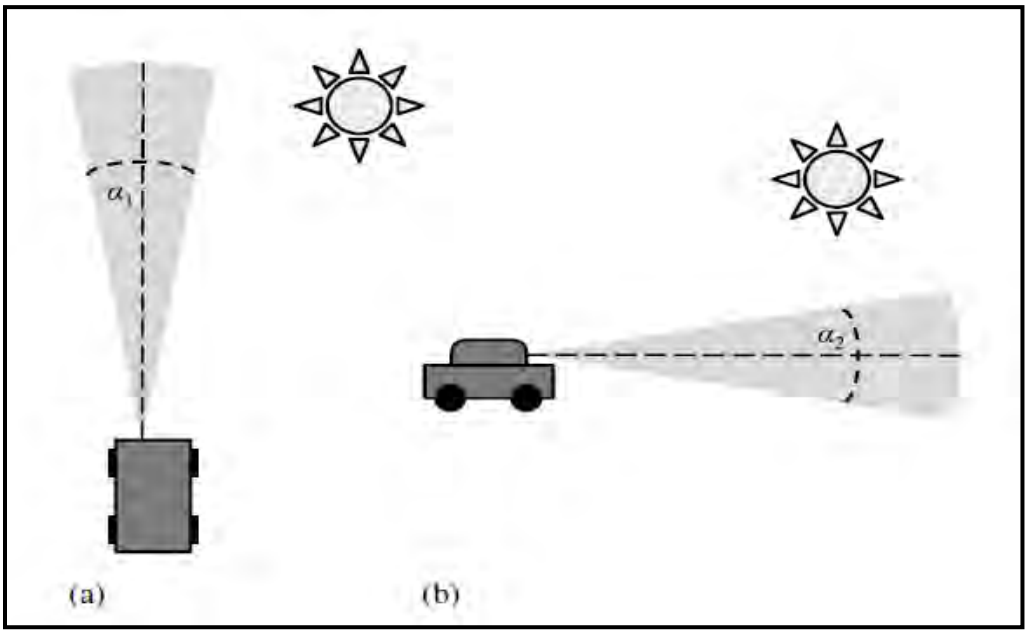

Figure 3-4: Geometry of Sun Glare Test

Source: *(Churchill et al., 2012)*

Alternatively, a methodology by Jurado-Pina and Pardillo-Mayora et al. (2010) indicates that the solar paths throughout a year at any specific position can be plotted on a cylindrical solar chart (see Figure 3-5). The establishment of this graph is based on the projection of the solar trajectory in a cylinder surrounding the observer. With its azimuth as the abscissa value and its elevation as the ordinate value, the sun position at a specific time is represented by a point on the chart. The driver's field of view is represented on this chart, thus allowing the analysis of the impact the sun has on the visual conditions on the road. As seen in Figure 3-5, for a specific driver position, the direction of the line of sight is determined by its azimuth and elevation angle (both in degrees). Contrary to Churchill's model, the cylindrical chart takes into account all the factors that intervene in the issue of visual obstructions that may exist between the driver and the sun position, which are represented in the graph i.e. terrain. For this model, the days and times of the year when sun glare may result in driver vision impairment are those in which the sun position is within the glare cones (the two circles) and above the line defining the terrain profile (dotted line).

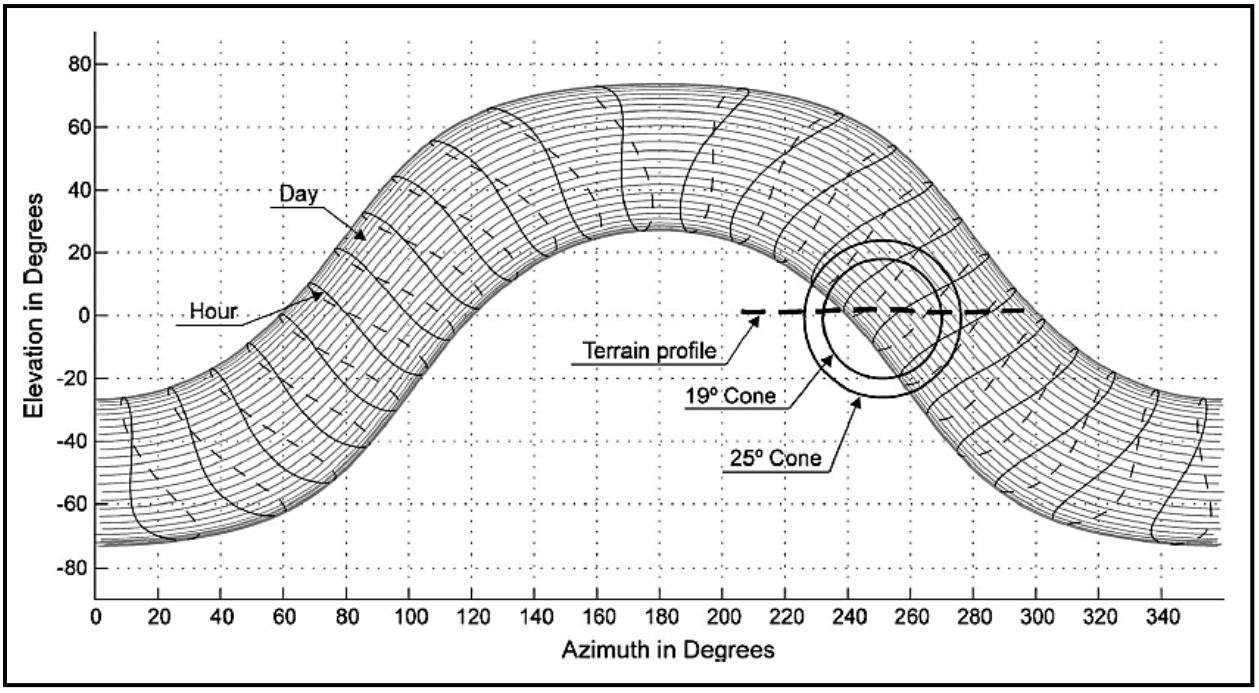

Figure 3-5: Factors Representation in a Cylindrical Chart

Source: (*Jurado-Piña and Pardillo-Mayora, 2010)*

To sum up, there are a number of models proposed by several authors to analyse the impact of glare on driver vision based on the sun position, among other factors. Irrespective of the common goal, most of these models do not have a homogenous approach to the analysis of the sun glare issue.

3.5 Case Studies: Sun Glare Accidents

Sun glare has contributed to a number of road traffic accidents. When commuters are driving into the sun, it can cause hazardous glare that leads to them not seeing their lane markings, brake lights on the cars in front of them, the cars next to them, signal lights or stops, and bicyclists or pedestrians crossing the street. This section presents six case studies where sun glare was the cause of the accident. The section aims to show evidence of the danger associated with sun glare conditions. It should be noted that five of the case studies presented here occurred in the United States of America (USA). As stated in Chapter 1, very few sun glare accidents are captured in literature, and majority of those occurred in the USA.

3.5.1 Case Studies

Schuylkill County, Pennsylvania, USA (Times News Online, 11 August 2014)

On the 11th of August 2014 morning, an elderly woman was injured after sun glare caused her to crash while driving along Route 309 in West Penn Township, Schuylkill County. The crash occurred just after 07h00 as the victim was travelling south while climbing Blue Mountain. According to the article, the woman, as well as many of the first responders, was blinded by the rising sun and windshields that instantly fogged up with sudden temperature changes. As she was climbing the mountain and lost her vision, she drove into the rear of a car that had slowed down due to sun glare. She was treated at the scene by paramedics and transported to a nearby hospital.

Paddington, London, United Kingdom (Brent & Kilburn Times, 15 August 2014)

A 42 year old male motorcycle courier (Frank Chaves) from Wembley crashed into the back of a delivery truck and died after being momentarily blinded by the sun. This accident occurred on the morning of the 16th of February, 2014. Chaves suffered massive chest injuries and was pronounced dead at the scene half an hour later. The collision was captured on CCTV and showed Chaves, as well as the glare from the sun along the road where the accident occurred.

Clark County, Washington, USA (Hastings, 2012)

A number of accidents resulting from sun glare conditions were reported by the Clark County Columbian newspaper. An article by Hastings (2012) reports a couple of these accidents. On the 23rd of August 2012, an 86 year old male crossing West Eight Street just after 19h00 on a motorised scooter was hit by a pickup vehicle. He died at the scene. On the 10th of September 2012, a woman was seriously injured at 17h52 when her Grand Cherokee collided with an Acura SUV and rolled on its top against a building at Broadway and East 20th Street. She survived, but lost a few fingers. A 23 year old female was driving west on East 45th Street, about a block of Main Street, around 18h30 on the 29th of August, when she turned into the Pacific Point Apartments and hit a 58 year old male who was on a bicycle passing the entrance to the complex.

The common trend in all these accidents is that all the vehicles were travelling west, facing the sun as it was setting. A police officer from the Vancouver Police Departments pointed out that drivers don't always adjust the way they drive when the sun is blinding them. He stated that he often hears "I didn't see them" after accidents.

Nebraska, United States of America (Department of Health & Human Services, 2011)

A police crash data report in the Department of Health and Human Services (DHHS) in Nebraska revealed that during the years 2002-2009 there was an average of one sun glare-related motor vehicle crash per day. In the 8-year period, September was indicated as the month with the most glare-related crashes, which is 21% of the total crashes. During this month, most sun glare-related crashes occurred between 07h00-09h00 (399 crashes, 61% of total) and 17h00-20h00 (191 crashes, 29% if total). This report on sun glare-related accidents also revealed the following findings:

- An average of 2 deaths occurred per year, which sums up to 16 deaths between 2002 and 2009;
- An average of 20 severe injuries occurred per year, which totals to 160 severe injuries between 2002 and 2009;
- An average of 70 moderate injuries occurred per year, which totals to 563 moderate injuries between 2002 and 2009; and

- An average of 158 possible injuries were recorded per year, which sums up to 1 267 possible injuries in the 8 year period (2002-2009).

Syracuse, New York, USA (Ha, 2011)

An article by Ha (2011) reports a fatal sun glare accident which took place on the 29th of February 2000, near a large office complex in Syracuse, New York. On that day, Derek Klink, the driver, struck a female pedestrian (Irene Lifson) while she was crossing the street near the complex, causing her death. Klink claimed to have been temporarily blinded by sun glare when the accident occurred. According to Klink, he stopped at the stop sign to make a left turn on a street, but his view of oncoming traffic was partially obstructed by parked cars in the left-hand lane of the street. He had to "creep up" in order to see the approaching vehicles. He noticed that there were pedestrians crossing the street to his left, but he also asserted that he had looked in that direction and "cleared the road" before making a turn. He testified that he had been looking to his right, toward oncoming traffic when he started turning. Klink maintained that, when he looked back to his left, mid-turn, he was blinded by the sun, "all of sudden". He reacted by looking down and to his right, and when he looked up Lifson was in front of the vehicle. Although he applied breaks, he was unable to avoid her, having seen her only a fraction of a second prior to impact.

Colorado Springs, United States of America (Stone, 2007)

The Police Department in Colorado Springs has blamed the sun's glare on at least two accidents in the month of September 2007. One accident was reported whereby a woman had to have her leg amputated after she was hit by a car on North Carefree road. Police report that the driver who hit her may have been blinded by the sun. Additionally, four Coronado High School students landed in hospital in the month of September after they were hit by a van while crossing the street in the cross walk. Similarly, the driver in this case was blinded by the sun. He was going into an easterly direction into the sun.

3.5.2 Résumé

While there are limited solutions for a sun that sets every evening, some countries are changing traffic laws to prevent accidents caused by sun glare. For instance, since 2009, Canadian drivers

have been required to use daytime running lights, which the Nova Scotia Department of Transportation and Infrastructure Renewal says reduces daytime injury crashes by 3% to 10% (Hastings, 2012). In the case studies presented in the preceding sections, police officers and experts typically offer the same recommendations for dealing with sun glare. These include the following:

- Changing the driving time. Drivers should delay unnecessary drives at sunrise or before sunset when the sun's glare may obstruct the vision of drivers and compromise road safety;
- Taking a different route on shaded roads, in a direction different from the one with direct sunlight exposure;
- Keeping windshields clean, inside and outside, to prevent a film of dirt and grime. The film will reflect the sun, worsening visibility;
- Avoid using high-gloss products on the dashboard, which can contribute to extra glare;
- Laying down a dark-coloured towel on a light-coloured dashboard, to reduce glare;
- Slowing down if blinded, and being mindful of obstructions;
- Make use of sun visors;
- Wearing polarised sunglasses to minimise the effect of sun glare, since little protection is offer by a car's sun visor when the sun is on the horizon; and
- If glare is problem, leaving extra space between your car and others in the event of sudden stopping or other road hazards.

4 Tool and Study Area Selection

The purpose of this chapter is to give a comprehensive discussion of five aspects of the research framework provided in Chapter 2. In their respective order, the following topics will be discussed: identified research tool, selected study area, data collection, data processing and data analysis.

4.1 Identified Research Tools

As stated in Chapter 2, ArcGIS and hillshade (tool in ArcGIS) were identified as the best tools to employ in this study. ArcGIS is Geographic Information System software, produced by ESRI, which allows people to collect, organise, manage, analyse, communicate, and distribute geographic information (http://resources.arcgis.com/). GIS can be used to store geographic data, make maps and analyse spatial data (Atkinson, 2012). ArcGIS has several products, which are: ArcGIS Online, ArcGIS Explorer Desktop, ArcGIS Desktop and ArcGIS for mobile.

Based on the functionality requirements of this study and software availability, ArcGIS Desktop was selected for use in this study. ArcGIS Desktop is the industry standard in GIS software, designed for advanced mapping and spatial analysis. Beyond showing data as points on a map, ArcGIS Desktop gives you the power to manage and integrate data, perform advanced analysis, model and automate operational processes, and display results on professional-quality maps (http://resources.arcgis.com/). Additionally, the role of ArcGIS in applications such as urban planning and transportation provides users, managers and decision makers, powerful tools for solving complex spatial problems. In this study, ArcGIS was used to model the exposure of the Cape Town road network to direct sunlight. Moreover, ArcGIS possesses a number of attributes, inter alia; these include the following (http://resources.arcgis.com/):

- *Create, Edit, Ensure the Quality of Your Geographic Data*
  Manipulate data with a minimum number of clicks and automate your editing workflow with the powerful suite of editing tools provided by ArcGIS for Desktop. Advanced editing and coordinate geometry (COGO) tools simplify your data design, input, and clean up.

- *Perform the Complete Cartographic Production within Your GIS*

  Easily create professional-quality, publication-ready maps with ArcGIS for Desktop software's simple wizards, predefined map templates, an extensive suite of map elements, and advanced drawing and symbolisation tools.

- *Manage Your Data More Efficiently*

  ArcGIS for Desktop is also a universal data integration system. ArcGIS for Desktop supports more than 70 data formats, so you can easily integrate all types of data for visualization and analysis.

- *Get Started Immediately with Ready-to-Use Data*

  You can begin your visualization and analysis right away with a range of ready-to-use geospatial data acquired from ArcGIS Online or via DVD, including the following: basemaps, demographic data, imagery etc.

- *Customise ArcGIS for Desktop to Meet Your Unique Needs*

  ArcGIS for Desktop includes developer tools that make it easy to build and deploy GIS applications on multiple platforms.

- *Add Even More Capabilities with Optional Extensions*

  A wide-ranging suite of optional extensions dramatically expands the functional capabilities of ArcGIS for Desktop with specialized GIS tools. These extensions can add powerful, 3-D visualization and analysis; comprehensive raster-based spatial modelling and analysis; advanced routing, closest facility, and service area analysis; and much more.

Hillshade is an ArcGIS tool that was employed to model the effects of solar exposure. Hillshade is a shaded relief technique where a lighting effect is added to a map based on elevation variations within the landscape (http://landtrustgis.org/). Hillshade is a grayscale 3D model of the surface, with the sun's relative position taken into account for shading the image (http://resources.arcgis.com/). The hillshade function intends to mimic the sun's effects –

illumination, shading and shadows – on hills and canyons, thus, obtaining hypothetical illumination of a surface by determining illumination values for each cell in a raster (Hegazy and Effat, 2011). This function uses the latitude and azimuth properties to specify the sun's position, which are the function's inputs, including a Digital Elevation Model (DEM) and z factor. A DEM is the presentation of continuous elevation values over topographic surface by a regular array of z-values, referenced to a common datum. DEMs are typically used to represent terrain relief (http://support.esri.com/).

Additionally, a hillshade model is a derivative of a DEM that stimulates relative solar insolation for each grid cell based on its slope, aspect and the position of the sun (as defined by altitude and azimuth angle) (Bricher et al., 2008). The azimuth is the sun's relative positions along the horizon, and is expressed in positive degrees ranging from 0 to 360, measured clockwise from north. The altitude is the sun's angle of elevation above the horizon, and is expressed in positive degrees ranging from 0 to 90˚, with 0° at the horizon and 90° directly overhead (http://www.esri.com/). An illustration of the orientation of the azimuth and altitude, relative to the ground plane, can be seen in Figure 4-1.

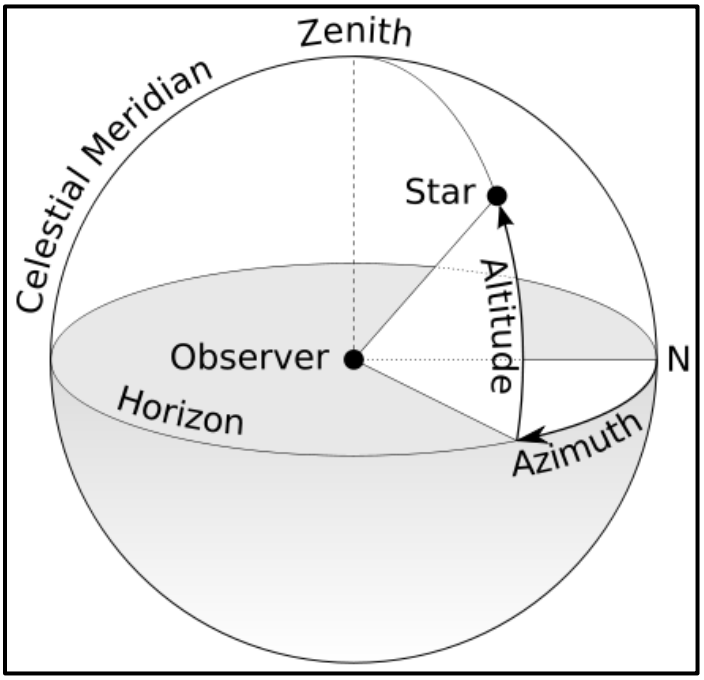

Figure 4-1: Azimuth and Altitude Schematic

Source: *http://m.teachastronomy.com/*

While a DEM's dataset contains actual elevation values, the hillshade dataset – although also a raster – contains brightness values. According to Land Trust GIS (http://landtrustgis.org/), these two data layers can be used individually or in combination. The latter was employed in this research as it will be explained in the sections to follow. Furthermore, hillshade gives you a three dimensional (3D) feel for the landscape. In fact, this effect can be enhanced by using the transparency tool with the DEM and hillshade grids. In summation, hillshade is a Spatial Analyst toolset found in the Surface Analysis tools in ArcGIS. Section 4.4 relays the steps taken to produce results for this study in ArcGIS.

4.2 Selected Study Area

As already mentioned in Chapter 2, the chosen study area for this research was the City of Cape Town (CoCT) in South Africa, which occupies the south-western most point of Africa (see Figure 4-2). Cape Town is a legislative capital of South Africa and capital of the Western Cape Province, and is located at 33°55'31"S latitude and 18°25'26"E longitude in the Southern Hemisphere. The city is the second largest city in South Africa, based on population, and is the largest in land area at 2 455km2 (http://geography.about.com/). Furthermore, Cape Town lies at the northern end of the Cape Peninsula some 50km, at its southernmost boundary, north of the Cape of Good Hope (http://www.britannica.com/). The City centre lies embedded between Table Mountain, Devils Peak, Lions Head and Signal Hill on the one side and borders on the Table Bay and the Atlantic Ocean on the other side.

Cape Town climate is Mediterranean, with mild, moderately wet winters and dry, hot summers (Global Atmosphere Watch Station Information System). The climate is locally modified by the mass of Table Mountain and by the cold Benguela Current of the South Atlantic Ocean. Winter in Cape Town starts as soon as the cold front from the Atlantic Ocean rolls in, with significant precipitation and strong north-westerly winds which start turning from the Cape Doctor (South Easter).

The winter season runs from the end of May to the end of August (http://www.capetownmagazine.com/). Data from the World Weather Information Service website suggests that Cape Town temperatures in winter range between 8.5°C and 18°C, and the

total rainfall averages 515ml. Summer lasts from December to March and November to March. Summer temperatures range between 19°C and 35°C. The summer season is usually hot and sunny with very little rain.

Figure 4-2: The City of Cape Town, South Africa

Source: *http://www.capeintern.com/cape-town-map/*

Three national roads start in Cape Town: the N1, N2 and the N7. The N1 links Cape Town with Bloemfontein, Johannesburg, Pretoria and Zimbabwe; while the N2 links Cape Town to Port Elizabeth, East London and Durban. The N7 links Cape Town with the Northern Cape Province and Namibia. The N1 and N2 both start in the Central Business District (CBD), and split to the east of the CBD, with the N1 continuing to the north east and the N2 heading south east past Cape Town International Airport. The N7 starts in Mitchells Plain and runs north, intersecting with N1 and the N2 before leaving the city. Additionally, CoCT has a system of freeway and dual carriageway (M-roads), which connect different parts of the city.

4.3 Data Collection

Data collection in this study was informed by the research framework and research process as seen in Figure 2-1 and Figure 2-2. This means that from each step in the methodology, subsequent data is required. At the onset of this study, the factors that impact road safety as a

result of sun glare were informed by the literature review. As a key part of the development of the data collection phase, a set of procedures setting out the research approach and process were developed. The following sections give brief and concise descriptions of the data required to execute the next phases of this study, which are data processing (GIS data) and data analysis (analysis data), respectively.

4.3.1 GIS Data

4.3.1.1 City of Cape Town Digital Elevation Model

In simpler terms, a DEM is a digital model or 3D representation of a terrain's surface created from terrain elevation data. Consequently, a DEM of Cape Town was one of the most important data sets required for modelling the effects of direct sunlight exposure in Cape Town. This data was obtained from the University of Cape Town (UCT) GIS laboratory. A 10m spatial resolution DEM was used. The reference system was the World Geodetic System 1984 (WGS84). The DEM was derived from 10m (interval) contour lines. The slope and aspect of the DEM played a key role in the creation of hillshade layers.

According to research by the National Oceanic and Atmospheric Administration (NOAA; 2007) in the US, the accuracy of DEMs (and hillshades) depends on the source and resolution of the data samples. The accuracy of DEM data is derived by comparing linear interpolation elevations in the DEM with corresponding map location elevations and computing the statistical standard deviation or Root-Mean-Square Error (RMSE); which is used to describe the DEM accuracy. However, Van Niekerk (2012) stated that contours are not ideal for interpolating DEMs as their densities vary with slope and gradient. He further pointed out that contour density is further reduced as the vertical interval of the contours increases (i.e. contours with a 5m vertical interval generally produce better DEMs than contours with a 20m vertical interval) and as scale increases. Based on this analysis, the accuracy of the DEM used in this study is acceptable given that the selected contour interval (10m) is relatively low.

4.3.1.2 City of Cape Town Road Network GIS Data

Given that this thesis largely focused on road network analysis, it was crucial to acquire the appropriate CoCT road network data to facilitate this analysis. Similar to the DEM, this GIS data

was also obtained from the UCT GIS laboratory. The road network layer was derived from a 10m topographical map.

4.3.1.3 Horizontal Sun Cone: Azimuth Angle Range

Churchill et al. (2012) pointed out that there is a long history of research to quantify the angular distance at which glare causes distraction. Upon pointing out that the problem is related to identifying the appropriate angular displacement of a driver's view, Churchill et al. (2012) cited Zwahlen (1989) who suggested the use of a 20° maximum aperture for visibility.

All things considered, it was decided that for this study the visibility aperture would be a 30° azimuth cone (±15° of the line of sight, see α in Figure 4-3), which represents the viewing region of the driver that is affected by sun glare. The 30° cone facilitated the selection of road segments whose azimuth (bearing) is ±15° of the sun azimuth for that particular time snapshot. The theory behind the sun cone is discussed in Chapter 3, Section 3.4.3. See Figure 4-3 for an illustration of the sun cone concept, where α_1 represents one half of the azimuth sun cone (15°).

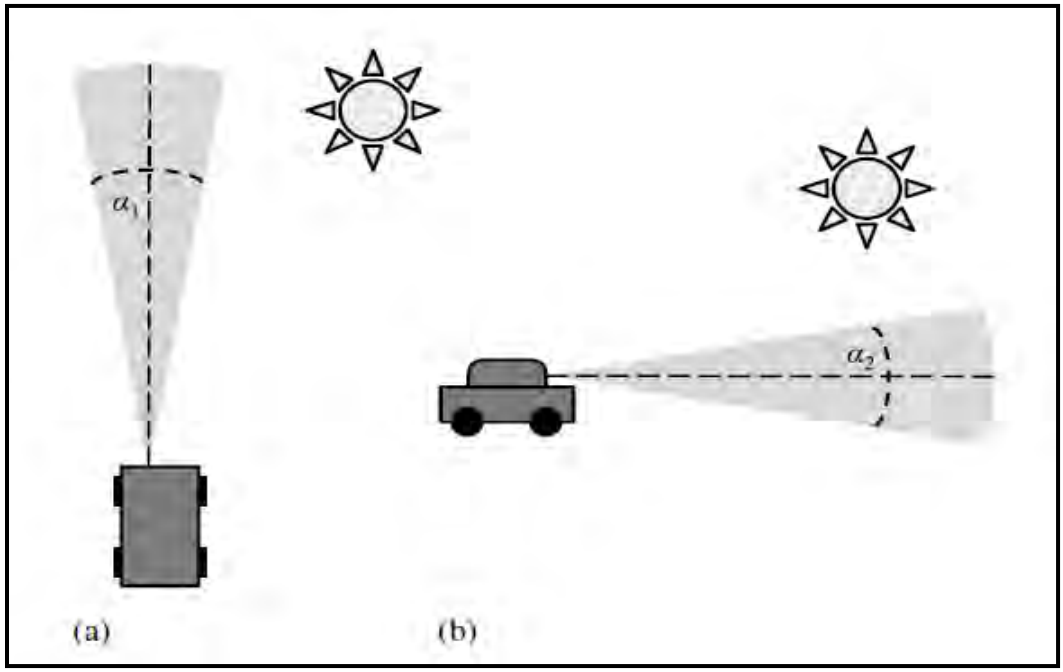

Figure 4-3: Azimuth and Altitude Sun Cones

Source: *(Churchill et al., 2012)*

4.3.1.4 Vertical Sun Cone: Critical Altitude Angle Range

In a study of driver impairment situations as a result of sun glare, Jurado-Pina and Pardillo-Mayora (2009) adopted two values of the angle of glare to characterise problem situations corresponding to drivers aged 40 and 60 years. The corresponding values are 19° and 25° (altitude), respectively. Consequently, this study adopted the same values to define the altitude sun cone, whereby the range of angles between – and including – 19° and 25° define a time period when sun glare is at its worst. See Figure 4-3 for an illustration of the vertical sun cone, where α_2 represents one half of the angle range. It is worth pointing out that, given the geographical differences between Jurado-Pina and Pardillo-Mayora (2009)'s study location (Madrid) and the location of this study, it is not certain that these angles are also valid in Cape Town. The study was merely used as a point of reference.

4.3.1.5 Sun Position Data (Azimuth and Altitude Angles)

The analysis instruments provided by the ArcGIS Spatial Analyst hillshade tool allow map drawing and an analysis of the sun's effects on a geographical area during a certain specific time frame. This means that the hillshade azimuth and altitude angle input defines the sun position for a specific date and time. For that reason, two astronomical events (solstice and equinox) each of which occur twice a year – and have the added benefit of seasonal variation – were selected for use in this research. The following section delivers a detailed discussion on these two astronomical phenomenons. It is worth pointing out that the use of specific time snapshots limits the quality of conclusions that can be drawn since the output is not generic, rather specific to a day and time of the year.

A decision was made to select time snapshots – for the four days – whose altitude values are defined by the vertical sun cone (19° and 25°). This means each of the scenarios/time snapshots modelled in this study only had a 19° or 25° altitude value. Sun position data (azimuth and altitude) for these four days, for both the morning (AM) and afternoon (PM) snapshots was obtained from the Astronomical Applications Department of the U.S. Naval Observatory server (aa.usno.navy.mil/) which is considered a credible source. Both altitude and azimuth are measured in decimal degrees.

For example, in the Autumnal Equinox (AE) – which occurred on the 20th of March – the time snapshots for the morning period are at 08h30 and 08h55, whereby the altitude angles are 19.9° and 24.8°, respectively. The same applies to the afternoon period. Table 4-1 shows a larger selection of the solar position data obtained for this day. The altitude angles chosen to define the sun cone range are as close as possible to 19° and 25°, but still within the range. As seen in the table, the azimuth angles for the two altitude values are 76.2° for the 08h30 snapshot and 72.1° for the 08h55 one.

Table 4-1: Southern Hemisphere Autumnal Equinox Angles

20 March (Autumnal Equinox)					
Morning			**Afternoon**		
Time	**Altitude**	**Azimuth (E of N)**	**Time**	**Altitude**	**Azimuth (E of N)**
h/min	°	°	**h/min**	°	°
08:30	19.9	76.2	16:30	29.2	292
08:35	20.9	75.4	16:35	28.3	291.1
08:40	21.9	74.6	16:40	27.3	290.2
08:45	22.9	73.8	16:45	26.3	289.4
08:50	23.8	73	16:50	25.3	288.5
08:55	24.8	72.1	16:55	24.4	287.7
09:00	25.8	71.3	17:00	23.4	286.8
09:05	26.8	70.4	17:05	22.4	286
09:10	27.8	69.5	17:10	21.4	285.2
09:15	28.7	68.6	17:15	20.4	284.4
09:20	29.7	67.7	17:20	19.4	283.6

Source: *Astronomical Applications Department of the U.S. Naval Observatory*

4.3.1.6 Solstice and Equinox Time Snapshots/Scenarios

A total of 16 scenarios were formulated for this model. First and foremost, there are the four days, which are split into 2 equinox days and 2 solstice days. For each of these four days, there was the morning (AM) and afternoon (PM) scenario. Each of the AM and PM scenarios were further split into two time snapshots each of which is for the 19° and 25° altitudes as seen in

Table 4-1. This section will, therefore, focus on defining the equinox and solstice concepts, as well as presenting the sun position data obtained for all 16 scenarios.

The first two days were the 20th of March and the 22nd of September. These are the days when the sun is in its zenith over the equator and the Earth experiences day and night of generally equal length (http://www.nationalgeographic.com/). These days are called equinoxes; autumnal equinox and spring equinox in the Southern Hemisphere, respectively. According to the Nuttall Encyclopaedia by James Wood (1907), equinoxes are two annually recurring times at which the sun arrives at the equinoctial, whereby at these times the sun is directly over the equator, and day and night is then of equal length over the whole globe. Equinoctial points are the two points at which the celestial equator intersects the ecliptic, so called because the days and nights are of equal duration when the sun is at these points. Figure 4-4 gives a visual illustration of the equinox concept.

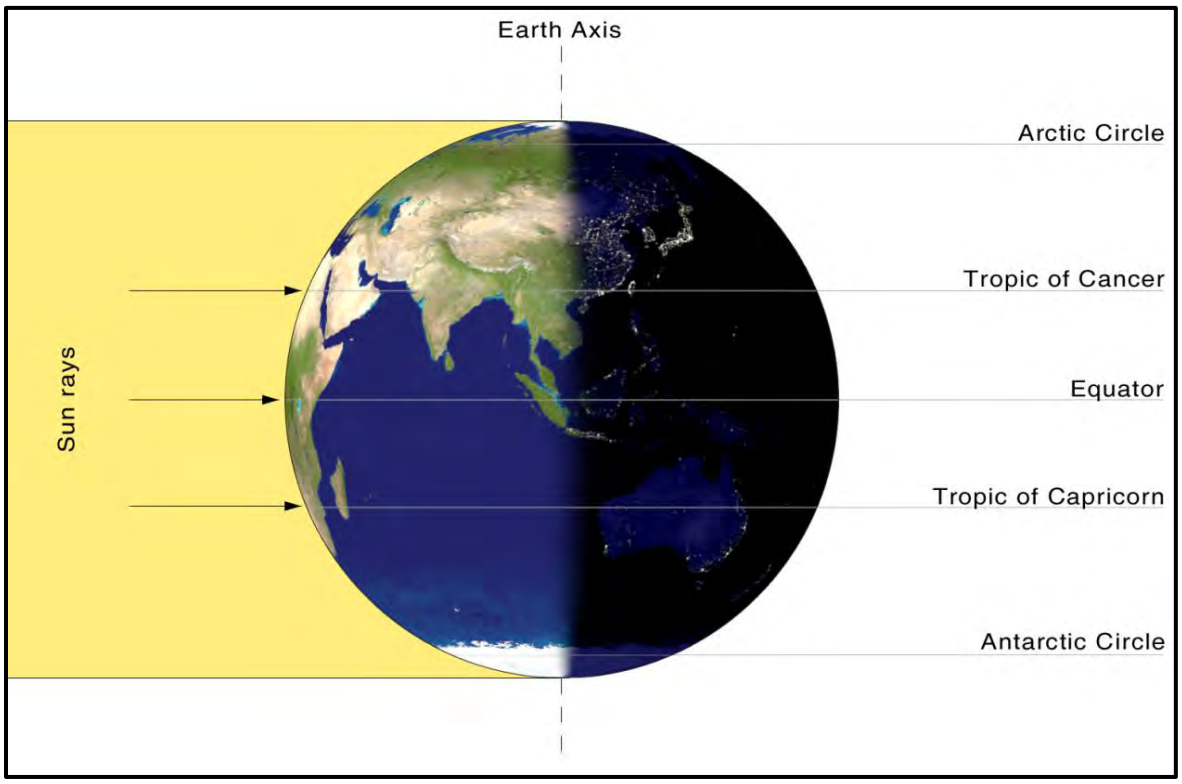

Figure 4-4: Illumination of Earth by Sun on the Day of Equinox in the Eastern Hemisphere

Source: *http://www.timeanddate.com/*

As discussed earlier, in the preceding sections, the sun cone angle values (19° and 25°) obtained from Jurado-Pina and Pardillo-Mayora (2010)'s study were used to determine which angles to use for each of the four days. Therefore, each equinox produced a total of four hillshade maps, two for the morning and another two for the afternoon. Table 4-2 shows the selected angles as well as the time of day that each angle occurs at. The data obtained from the Astronomical Applications Department of the U.S. Naval Observatory server was in increments of 5 minutes, so it did not produce exact 19° and 25° angles. Therefore, the angles closest to these two angles, but still within the range, were used.

Table 4-2: Southern Hemisphere Equinox Azimuth and Altitude

Day and Month	Equinox	Time Period	Time (h/min)	Altitude (°)	Azimuth [E of N] (°)
20 March 2014	Autumnal	Morning	08h30	19.9	76.2
			08h55	24.8	72.1
		Afternoon	16h55	24.4	287.7
			17h20	19.4	283.6
23 September 2014	Spring	Morning	08h15	19.8	76.1
			08h40	24.8	72
		Afternoon	16h40	24.4	287.5
			17h05	19.5	283.4

The other two days selected for this study were the 22nd of June and the 22nd of December. These days are the winter solstice and summer solstice (in the Southern Hemisphere), respectively (http://www.nationalgeographic.com/). The winter solstice is the shortest day of the year in the Southern Hemisphere, which is when the Earth's Northern Hemisphere is tilted toward the sun. Whereas in the summer solstice the Earth's Southern Hemisphere is the tilted toward the sun, which is why the 22nd of December is the longest day of the year in the Southern Hemisphere. In the Nuttall Encyclopaedia, James wood (1907) defines the solstice as the two recurring periods of the year at which the sun is farthest distant north or south from the equator, which mark midsummer and midwinter; also applied to the two points in the ecliptic which the sun appears to reach on these two dates. Figure 4-5 gives a visual illustration of the solstice concept.

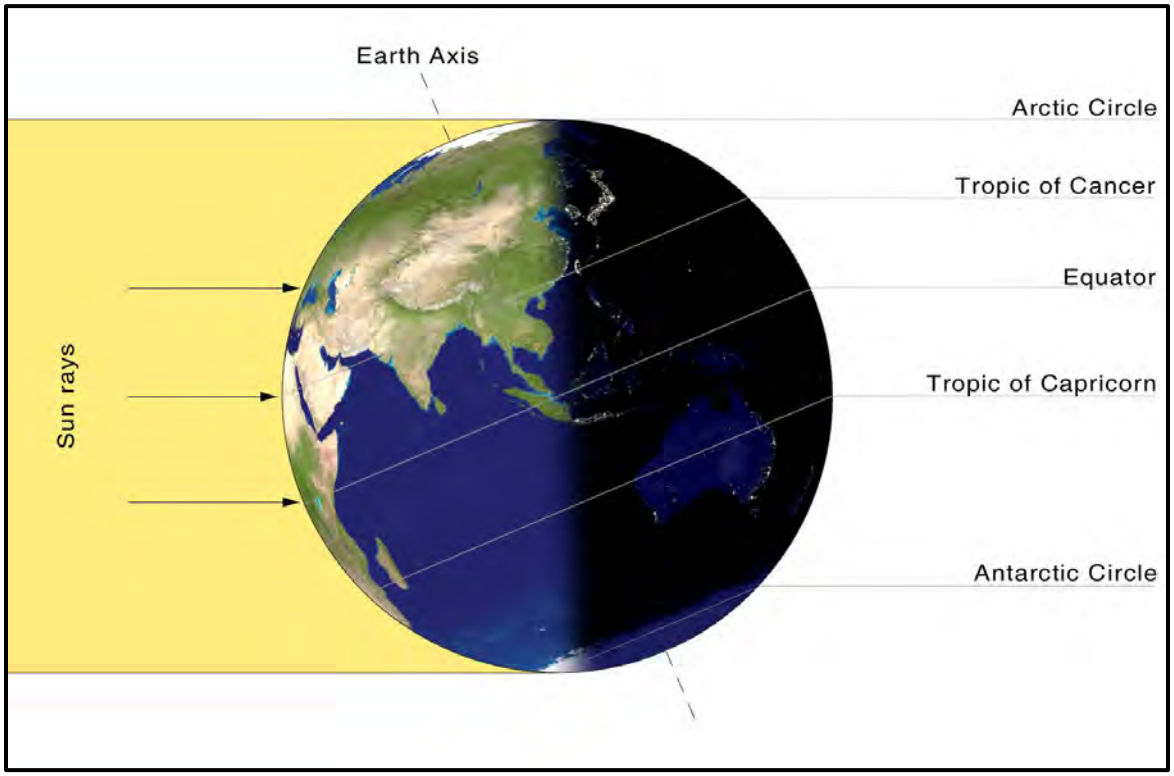

Figure 4-5: Illumination of Earth on the Day of the Winter Solstice on Northern Hemisphere

Source: *http://www.timeanddate.com/*

The sun position data for each of the solstice days is shown in Table 4-3. Figure 4-6 shows the timings of the equinox and solstice days in the Earth's orbit.

Table 4-3: Southern Hemisphere Solstice Altitude and Azimuth

Day and Month	Solstice	Time Period	Time (h/min)	Altitude (°)	Azimuth [E of N] (°)
21 June 2014	Winter	Morning	09h55 10h35	19.4 24.5	41.9 33.7
		Afternoon	15h00 15h40	24.7 19.7	326.8 318.5
22 December 2014	Summer	Morning	07h20 07h45	19.8 24.8	105.5 102.6
		Afternoon	17h45 18h10	24.8 19.8	257.5 254.5

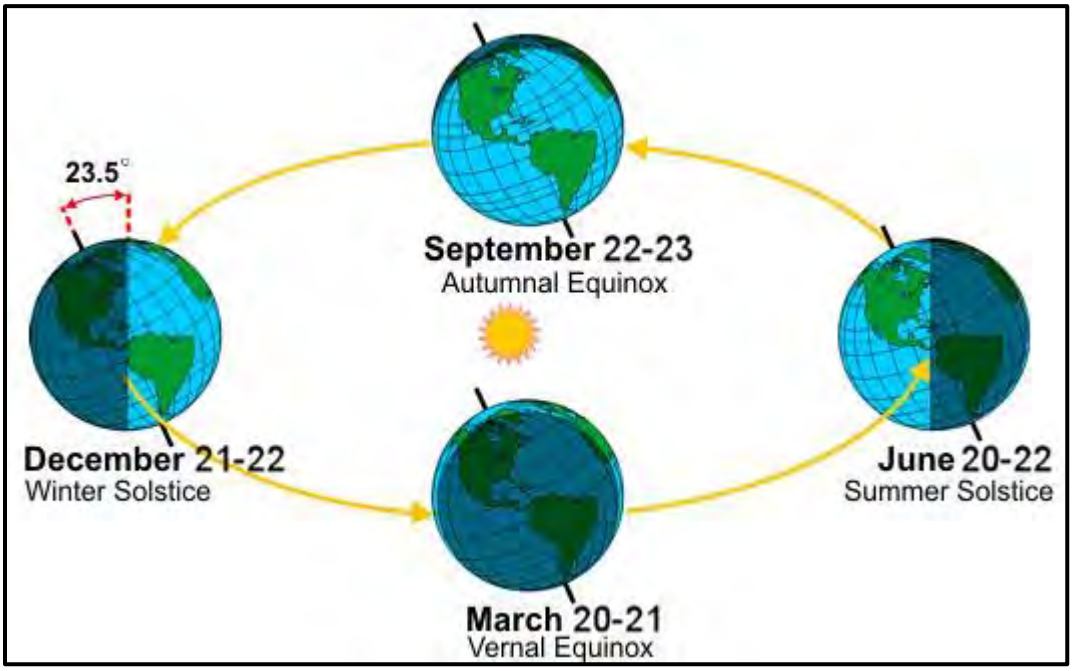

Figure 4-6: Solstice and Equinox Timings

Source: *http://www.perceptions.couk.com/precess.html*

4.3.2 Analysis Data

As per the discussion in Chapter 2, the last phase of the analysis made use of CoCT accident data for analysis. This information was obtained from the City of Cape Town municipal offices.

4.4 Data Processing

As already mentioned in Chapter 2, the methodology used in this work comprised of three general phases, and these are illustrated in the methodology data flow in Figure 4-7.

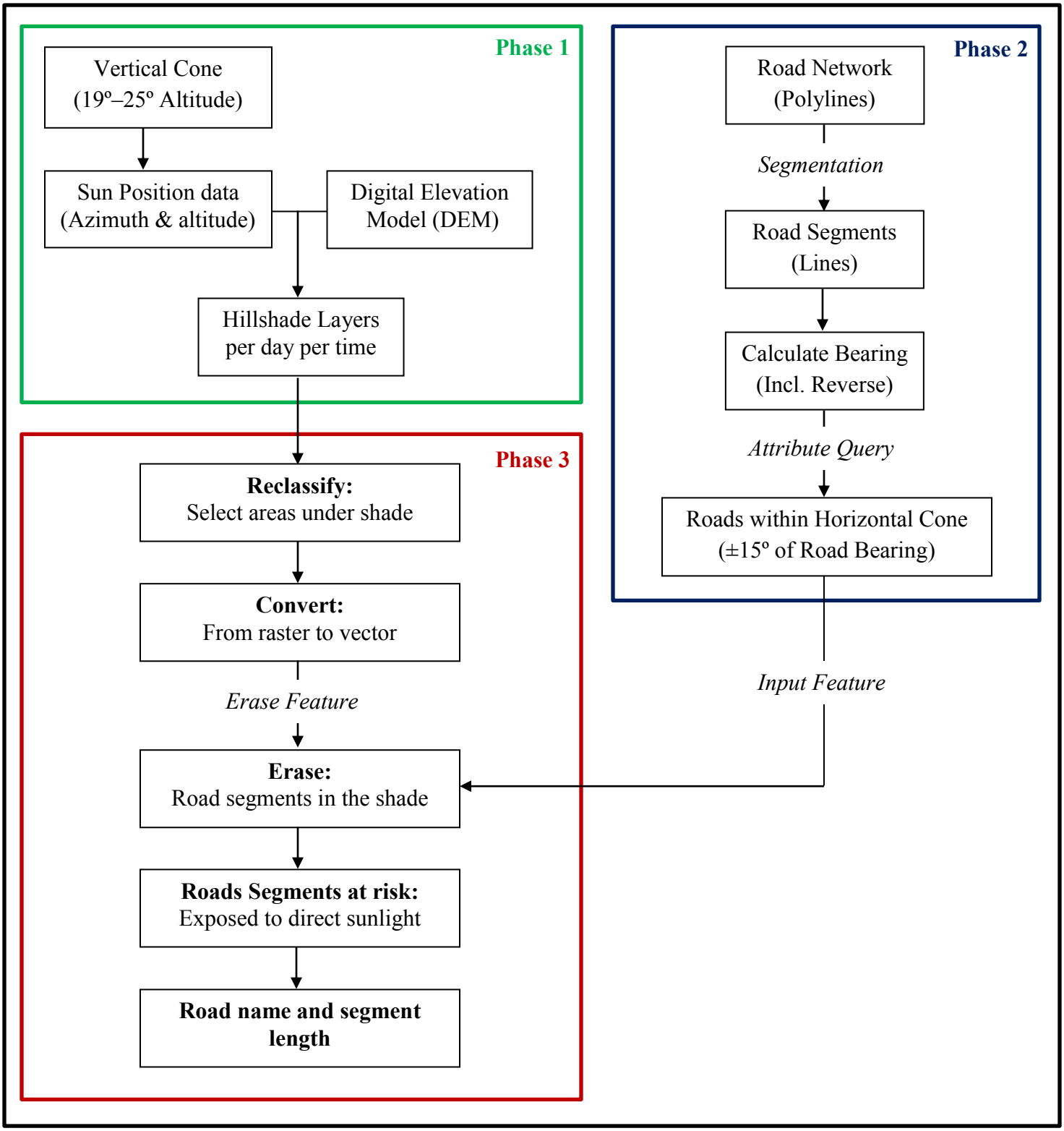

Figure 4-7: Methodology Data Flow

4.4.1 Phase 1: Production of Hillshade Maps

The sun position data (azimuth and altitude) defined in Section 4.3 was used as Hillshade input to produce 16 maps for each of the four days. Note that the hillshade layers produced here are defined by the vertical sun cone (19º – 25º); meaning, 8 of the 16 maps have an altitude approximately 19º, while the other half have an approximately 25º altitude (see Table 4-2 and Table 4-3). In this phase, hillshade essentially uses an algorithm to calculate the shade value for each day. Once the angles have been input into the hillshade tool, these sun coordinates are processed by the tool to determine the final hillshade value for each cell in the output raster. Basically, to obtain a hypothetical illumination of a surface, hillshade sets a position for a hypothetical light source (the sun) and calculates the illumination values of each cell in relation to neighbouring cells. The output shaded relief raster considers both local illumination angles and shadows. The output raster contains values ranging from 0 to 255, with 0 representing the shadow areas, and 255 the brightest. Essentially, shadow and light are shades of grey associated with integers from 0 to 255 (increasing from black to white).

The alternative option would have been an output shaded relief raster that only considers local illumination angles, meaning the effects of shadows would not be considered. Given that this option doesn't consider the shading effect of hills and canyons relief with respect to solar exposure, it is safe to assume that the illumination values produced would not be the best representation of sun exposure in the study area. This is why the exclusion of shadows was not a preferred option. At the end of this phase, a total of 16 hillshade maps were generated for the four days and different time snapshots listed in Table 4-2 and Table 4-3.

4.4.2 Phase 2: Classification of Road Segments According to Azimuth Sun Cone

As derived from the literature analysis, this study acknowledged 3 main factors that contribute, or determine, the occurrence of sun glare conditions: the position of the sun, the driver's line of sight and the configuration of the terrain and road network. Phase 1 of this study addressed two of these factors (the sun position and the configuration of the terrain), and this phase addresses the road network alignment. In order to produce a comprehensive discussion of the potential sun glare areas in Cape Town, the CoCT road networks were used along with the maps produced in Phase 1 to highlight sun glare problem areas on the road networks rather than on the DEM. This

overlay was, however, carried out in phase 3. In order to be able to use the road network data in phase 3, several processes had to be carried out. These included changing the data from polylines to single lines (step 1); calculating the road bearing and reverse bearing (step 2); and carrying out an attribute Query for roads within the 30° sun cone. These steps are discussed in the following sub-sections, in the respective order.

4.4.2.1 Step 1: Creating Multiple Road Line Features with constant direction

The road network was initially divided into straight line segments with constant geometry (polylines). In order to get line elements that are manageable, the road network had to be divided into straight line segments with constant direction, thus, allowing for the establishment of the bearing for each segment. These segments were the basis for the proposed methodology. Therefore, using the *Split Line at vertices* tool in ArcGIS, the road network polylines were split up into multiple line features (road segments) such that each segment was its own entity with a unique identity and bearing. Figure 4-8 shows an illustration of the *Split Line* tool input and output. This figure shows that a line is made up of segments joint together, which the tool splits at vertices to form straight line segments. Furthermore, the unique identity assigned to each line segment was in the form of a number starting from 1 to the last number, which was also equivalent to the total sum of the existing line segments.

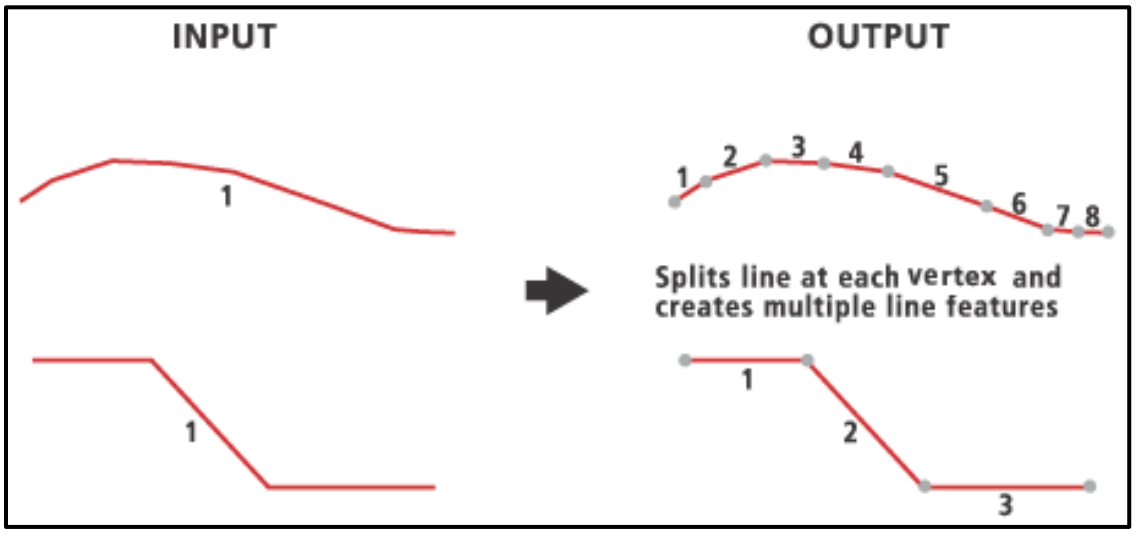

Figure 4-8: Split Line at Vertices

Source: *http://resources.arcgis.com/*

4.4.2.2 Step 2: Calculating Road Bearing and Reverse Bearing

The literature in this study points out that the elevation and direction of the road network plays a key role in the occurrence of sun glare conditions. Therefore, it was crucial to factor in these features (bearing and reverse bearing) of the road network in the execution of the methodology, which ultimately produced results indicating which roads are likely to experience sun glare conditions in Cape Town. Accordingly, the *Linear Directional Mean* tool in ArcGIS was used to calculate these bearing values, which is the mean direction for each line segment from the North. The reverse bearing was calculated by adding 180° to these output bearings. The road segment bearings calculated here were used in the next step to select road segments, which have an identical direction (±15º) with the sun azimuth of each time snapshot.

4.4.2.3 Step 3: Attribute Query for Roads within 30° sun cone (azimuth)

Using the selection tool in ArcGIS (selection by attributes), an attribute query was performed for all 16 scenarios to select the road segments whose direction was within ±15° of the sun azimuth for each time snapshot. The 15° is one half of the 30° sun cone described in Section 3.2.2.4 and illustrated in Figure 4-3. For instance, Figure 4-9 shows an example of this attribute query for the winter solstice (21 June 2014) at 09:55 in the morning. The outcome of this query was all the road segments, in the defined road network, that are exposed to direct sunlight with respect to the defined 30º horizontal sun cone; whereby the road segment direction lies between 26.9° and 56.9° (which is ±15° of the 41.9° sun azimuth). Road segments produced in this step were used in step 1 of the next phase (Phase 3).

```
(CompassB >= (41.9-15) AND CompassB <= (41.9+15)) OR (CompassA >= (41.9-15)
AND CompassA <= (41.9+15))
```

Figure 4-9: Attribute Query for Winter Solstice at 09h55

4.4.3 Phase 3: Hillshade Map and Road Classification Overlay

The final maps produced in this phase were a combination of the hillshade layers and the Phase 2 outcome. The final product of this phase was 16 layers with a distribution of road segments exposed to direct sunlight in each scenario. This phase consisted of only two steps.

4.4.3.1 Step 1: Reclassify and Erase Roads in Shadow

Ultimately, hillshade shows the amount of sunlight a pixel will get at a certain date and time. The production of hillshade maps, therefore, enables the selection of road segments in shadowed areas. Since the main focus of this research was those pixels that receive sunlight, the hillshade layers produced in phase 1 were reclassified to eliminate pixels that were exposed to sunlight so that only the shadows were left. This process resulted in the exclusion of shadowed road segments. A value of 1 was given to all pixels in complete shade. All other pixels were classified as NO DATA. This is how layers representing shadowed areas, in the DEM, were created. Using these reclassified hillshade layers as shadow maps, the roads that were in shadow were converted from raster to polygon, after which they were erased, thus, leaving behind road segments that were of interest to the subject matter of this research – exposed to direct sunlight. Roads located in shadowed areas were considered safe and thus, excluded from further analysis. The reclassification and erasing produced the final outcome of the defined methodology, this being the layers of road segments exposed to direct sunlight for each time snapshot, defined by both the horizontal (azimuth) and vertical (altitude) sun cone. An overview of the actual input into the reclassification, conversion and erase processes can be seen in Appendix A.

4.4.3.2 Step 2: Producing Final Analysis Data

The last phase of this investigation consisted of the production of publication-ready maps for the final segment output produced in Step 1 of this phase. A total of 16 maps were produced for the 16 scenarios, each of which indicated the road segments exposed to direct sunlight in the Cape Town road network. The output data for these layers was the lengths of road segments exposed to direct sunlight. Since the road network was segmented (multiple line segments for individual roads), the output data was summarised by street names in order to determine the total lengths of road segments exposed to direct sunlight in each road/street, thus, enabling easier analysis of the individual roads, and areas, in the Cape Town road network. A comprehensive analysis of the results and findings from the methodology is carried out in the next chapter, Chapter 5.

5 Results: Analysis and Findings

According to research by Hagita and Mori (2013), the sun is most potent to drivers when it is on the immediate horizon, typically between 07h30-09h30 and 17h00-1830 – which is an hour or so after sunrise and sunset. The angles and time snapshots used as input data in this thesis correlate with these times. This means that each of the sun position time snapshots for the 19° and 25° sun cone altitude angles (for both morning and afternoon) fall in the time periods assumed to be the most potent period in terms of sunlight exposure.

In the methodology the vertical sun cone (altitude) was defined to be between 19° and 25°, based on Jurado-Pina and Pardillo-Mayora (2009)'s extensive study on predicting driver vision impairment situations caused by sun glare. In order to model the effect of direct sunlight on road networks, sun angle data was required for input into the hillshade tool, in ArcGIS. Regarding the solar radiation distribution on the Earth's surface, the analysis instruments provided by ArcGIS Spatial Analyst allow a map drawing and an analysis of sun's effects on a geographical area during a certain specific time frame. Similarly, angle data from the United States Naval Observatory server required specific data to produce sun position data reflecting sun position during a specified time period. On account of their seasonal variation, the equinox and solstice days were, therefore, chosen for the purposes of this investigation. The days are the Autumnal Equinox (AE) (20 March 2014), Spring Equinox (SE) (23 September 2014), Winter Solstice (WS) (21 June 2014) and Summer Solstice (SS) (22 December).

Aside from the benefits of seasonal variation, another benefit of these time periods, with the exception of the winter solstice on most days, is that they allow for an interpretation of the results for cloud free days. The assumption is that the AE, SE and SS are mostly experienced on cloud free days, however, this has not been validated. It is worth noting that one of the basic assumptions of the ArcGIS method is the absence of atmospheric effects, such as cloud cover, precipitation, etc. Moreover, during the time periods of the obtained angles, more drivers are exposed to risk due to increased road traffic – peak traffic.

Table 5-1 shows the complete angle data and time snapshots used in this study, along with the code names for each scenario. Instead of using full names, the code names will sometimes be

used to label scenarios in tables, graphs, images or maps to follow. This table can, therefore, be used as a point of reference.

Table 5-1: The 16 Scenarios Chosen for the Study

Day	Period	Altitude	Azimuth	Time	Code Name
Autumnal Equinox	Morning	19.9	76.2	08h30	AE08h30
		24.8	72.1	08h55	AE08h55
	Afternoon	19.4	283.6	17h20	AE17h20
		24.4	287.7	16h55	AE16h55
Spring Equinox	Morning	19.8	76.1	08h15	AE08h15
		24.8	72.0	08h40	SE08h40
	Afternoon	19.5	283.4	17h05	SE17h05
		24.4	287.5	16h40	SE16h40
Winter Solstice	Morning	19.4	41.9	09h55	SE09h55
		24.5	24.5	10h35	WS10h35
	Afternoon	19.7	318.5	15h40	WS15h40
		24.7	326.8	15h00	WS15h00
Summer Solstice	Morning	19.8	105.5	07h20	SS07h20
		24.8	102.6	07h45	SS07h45
	Afternoon	19.8	254.5	18h10	SS18h10
		24.8	257.5	17h44	SS17h44

The methodology used in this study produced road networks whose direction is ±15° of the solar azimuth for each time snapshot, and with a gradient that falls within the 19°-25° vertical sun cone. This essentially produced road segments defined by the horizontal and vertical sun cones. Given the defined sun cones, it was assumed that angles outside these cones have no detrimental effect on the road networks with respect to direct sunlight exposure. Before the application of these road network selections, a '*split lin*e' was applied to transform the road networks into straight line segments with constant geometry, thus, producing segmented roads with 112 661km of total length. Overall, this process produced 16 hillshade images, as listed in Table 5-1, and 16 layers of road segments exposed to direct sunlight; in which case direct sunlight exposure implies vulnerability to accident occurrence as a result of impaired vision.

The hillshade maps produced during the data processing phase characterise and compare textures of the shaded-relief for the different days and times modelled. To begin to understand the direct

sunlight exposure variance between the four days – as well as the morning (AM) and afternoon (PM) period within each day – the analysis was structured in the most effective manner, which is illustrated in Figure 5-1.

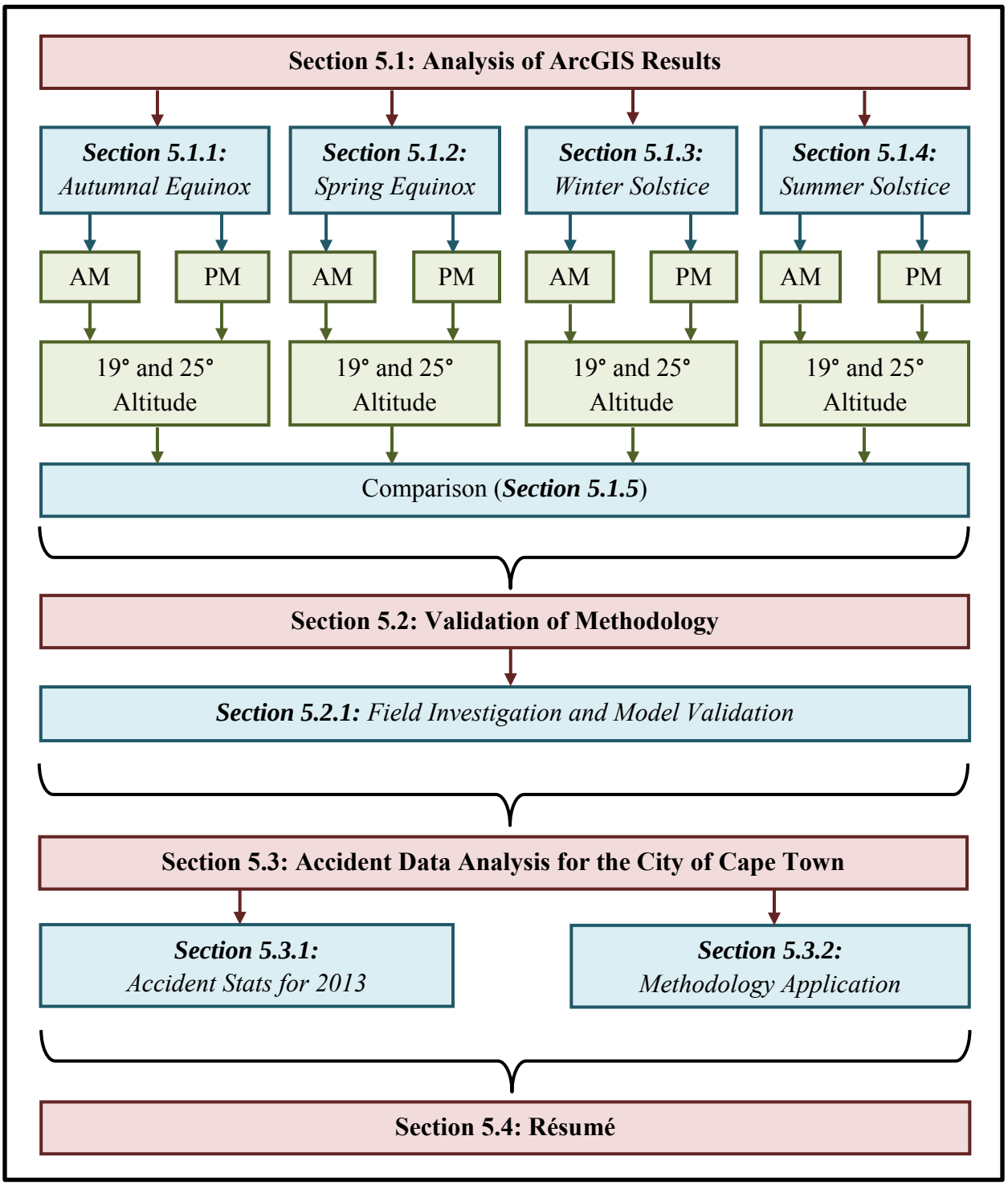

Figure 5-1: Map of Data Analysis and Findings Chapter

5.1 Analysis of ArcGIS Results

The analysis in this section is split into two different parts. The first part (Section 5.1.1 to 5.1.4) analyses the morning and afternoon results in each day, and also includes a concise discussion of the results from a statistical comparison of the morning and afternoon data using the Wilcoxon Signed-Rank Test (WSRT). The Wilcoxon signed rank test is a non-parametric test procedure for the analysis of paired data (e.g. consisting of pre- and post-treatment measurements) based on independent unit of analysis (Rosner et al., 2005; Rey and Neuhauser, 2011; Woolson, 2008). This test compares two sets of scores that come from the same participants. In this case it is comparing road segment length results for individual roads, in the different scenarios. The aim was to investigate any change in scores from one time point to another. As the Wilcoxon signed-rank test does not assume normality in the data, it can be used when this assumption has been violated and the use of independent t-test is inappropriate. The null hypothesis in this test was that the differences, or individual observations in the single-sample case, have a distribution centered about zero (Woolson, 2008).

Given that there were too many entries in the output data, running a statistical analysis on the full dataset was over-powering. As a result, a 1% random cluster sample was taken where street name was considered to be a cluster. By taking a cluster sample, all the observations (i.e. day and time) were included in the sampling procedure by default. This is important as comparison must be for the morning and afternoon measurements form the same street. The summary information for the sample data are shown in Table 5-2 and 5-3.

Table 5-2: Sample Data for the Different Days

Day	Frequency	Percentage	Cumulative Percentage
AE	330	26.48	26.48
SE	331	26.57	53.05
WS	260	20.87	73.92
SS	325	26.08	100.00
Total	**1,246**	**100.00**	

Table 5-3: Sample Data for the Different Times

Day	Time	Frequency	Percentage	Cumulative Percentage
AE	08h30	88	7.06	7.06
	08h55	87	6.98	14.04
	16h55	74	5.94	19.98
	17h20	81	6.50	26.48
SE	08h15	88	7.06	33.54
	08h40	88	7.06	40.6
	16h40	74	5.94	46.54
	17h05	81	6.50	53.04
WS	09h55	62	4.98	58.02
	10h35	65	5.22	63.24
	15h00	70	5.62	68.86
	15h40	63	5.06	73.92
SS	07h20	73	5.86	79.78
	07h45	79	6.34	86.12
	17h44	89	7.14	93.26
	18h10	84	6.74	100.00
Total		**1 246**	**100.00**	

As can be seen in the tables, all the days and times are represented in the sample. Furthermore, the two morning and afternoon values of percentage road segment coverage are averaged, to give one morning (AM) and one afternoon (PM) value, per street, per day. The averaged AM and PM values, per day, are compared using a paired test, since there are morning and afternoon measurements on the same streets, so the data are paired. This ultimately led to the use of the WSRT as it is the non-parametric equivalent of the parametric t-test, which cannot be used if the data are not normally distributed, as is the case here.

Overall, the analysis in this section, for each day, was broken up into the morning period analysis, afternoon period analysis and statistical analysis. Each of the AM and PM sections consists of a quantitative data analysis and map analysis for the two sun cone altitudes (19º and 25º).

The second part of this analysis (Section 5.1.5) is comparison of the ArcGIS output of the four days, which also includes a statistical analysis over all days and times – comparing AM and PM

and all four days, across all streets. It is worth noting that roads exposed to direct sunlight in each scenario are only affected in one direction, which is dependent on the position of the sun. However, the ArcGIS results do not indicate this direction, though it can be deduced based on the coordinates of the sun position used to produce each hillshade image. All in all, the overall expectation is that the result presented in this chapter will evaluate the risk on road networks in Cape Town, with regards to vulnerability to sun glare conditions. Several things should be noted before proceeding to read this chapter, these are as follows:

- The term 'road segments' will often be used to refer to parts of a road/road network exposed to direct sunlight.
- Several terms will be used to refer to sunlight exposure. These are: solar insulation, solar radiation and solar illumination.
- 'Scenarios' refers to the different data sets produced for each day, which totals up to 16 as seen in Table 5-1. For example, the autumnal equinox is one day which has the morning and afternoon periods modelled, which in turn each have two data sets: one for the 19° angle one for the 25° angle, thus, making it a total of four scenarios in one day.
- The 16 scenarios obtained from the four days will either be referred to as 'scenarios', 'time snapshots' or just 'snapshots'.
- Each of the four days will either be referred to in their full name or by their abbreviations. For example AE for autumnal equinox.
- Lastly, the chapter mainly consists of discussions of road segments and actual roads/streets exposed to direct sunlight. The difference between the two is that road segments (sometimes referred to as segments) are the multiple straight lines that make up the road; whereas 'road'/street' refers to the actual road, e.g. Voortrekker road, Main road etc. To avoid any confusion, the word 'streets' will mostly be used to refer to whole roads.

The image in Figure 5-2 displays the different locations in the City of Cape Town (also termed Cape Metropolitan. As seen in Figure 5-2, these are the Western Seaboard, Northern Suburbs, City Bowl, Atlantic Seaboard, Southern Suburbs, Cape Flats and the Southern Peninsula.

Figure 5-2: Locations in the Cape Metropolitan

Source: http://www.pamgolding.co.za/

Figure 5-3 shows a map of the City of Cape Town and the road network distribution.

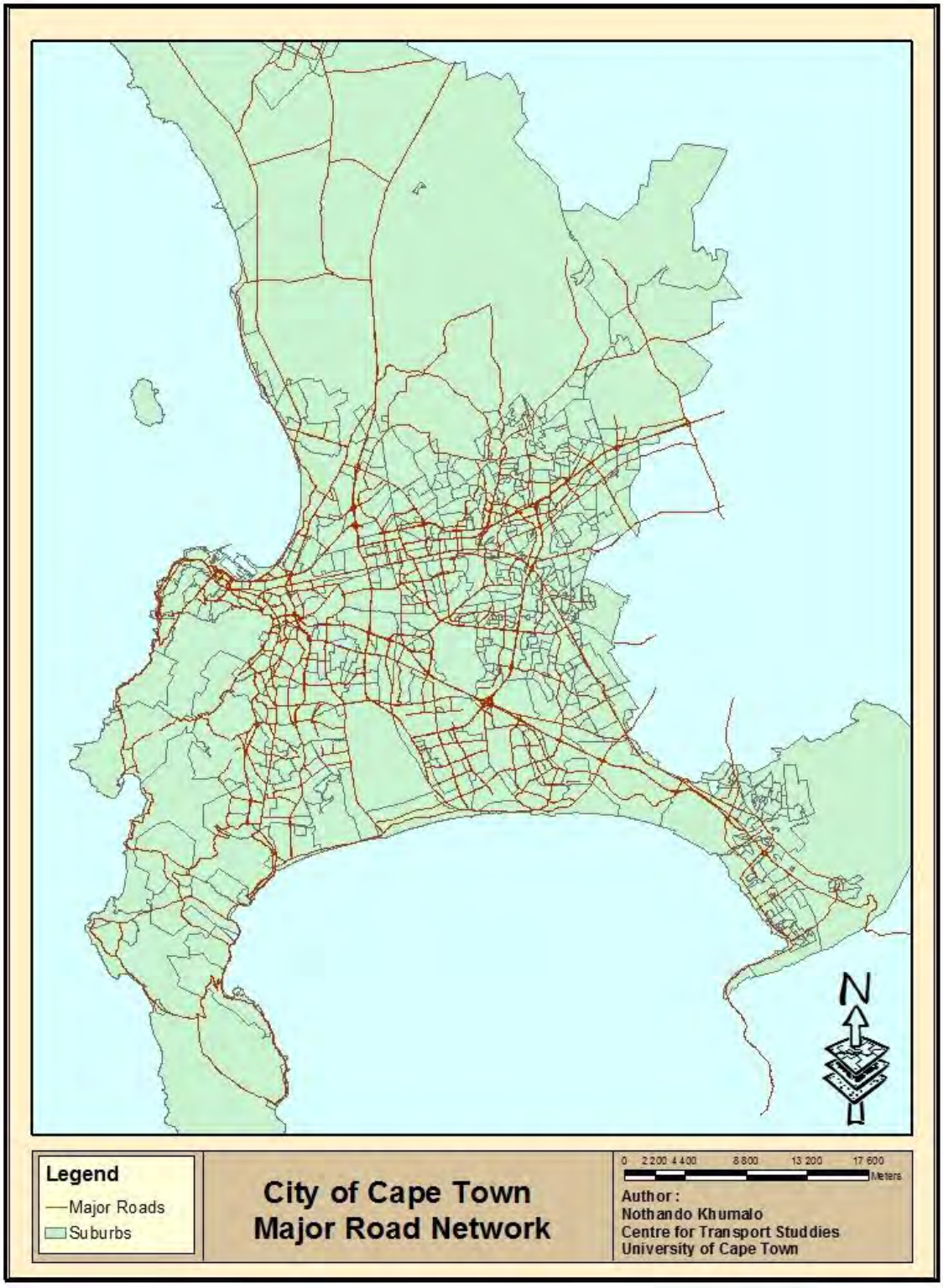

Figure 5-3: Map of the City of Cape Town and Road Network Distribution

5.1.1 Autumnal Equinox

5.1.1.1 Morning Period

a) Analysis of Quantitative Data

According to the model, the most insulated surface in Cape Town for this day is the southern cental part of the city, which includes a portion of the Southern Suburbs, Northern Suburbs and Cape Flats (see Figure 5-2). While the upper northern regions experience less or no direct sunlight exposure on their road networks (see AE map of exposed road segments in Figure 5-4 and Figure 5-5). Visual interpretation of the shaded relief image in Figure 5-4 and Figure 5-5 also reveals that the hills in the south-western part of the map, facing west, are not experiencing any insulation as a result of the elevation which provides shadowing. As already stated in Chapter 3, the physical environment is one of the influencing factors in the occurrence of sun glare. The hill and mountain exposure are two parameters that influence the solar radiation while the altitude and latitude set the temperature's distribution.

Moreover, the total length of road segments identified to be exposed to direct sunlight exposure in the AE was an average total of 2 247km. A longer length of direct sunlight exposure simply implies that there is a greater risk, compared to a road which has a much shorter length of road segments exposed. For instance, in the morning 1 347m of Voortrekker Road is exposed to direct sunlight, while 708m of the N1 is exposed. Assuming equal speed in both roads, it takes twice as long to drive through the high risk part of the network in Voortrekker road.

The road segment lengths were catergorised into eight classes as seen in Table 5-4. According to the results in the table a total sum of 2 169km length of segments were exposed to direct sunlight at 08h55, compare to the 2 325km at 08h30. Furthermore, compared to the other classes, the 0-1<km class has the most road segments exposed to direct sunlight. A total number of 8 896 streets are exposed to direct sunlight at 08h30, and 8 566 of those streets have exposed segments less than 1km (0-1<km class). At 08h55, a total of 7 674 streets fall within this 0-1<km class out of a total of 8 554 streets exposed. Table 5-5 gives a summary of the number of streetss exposed in each class, out the total 16 056 streets in Cape Town.

Table 5-4: Road Segments Length Exposed to Direct Sunlight in the Autumnal Equinox AM

Autumnal Equinox - Morning					
AE08h30 (19°)			AE08h55 (25°)		
Length (km)	Total Length (km)	Mean Length (km)	length (km)	Total Length (km)	Mean Length (km)
0-1<	1505.6	0.2	0-1<	1410.2	0.2
1-2<	295	1.4	1-2<	257.5	0.4
2-3<	125.1	2.4	2-3<	118.7	0.9
3-4<	83.9	3.5	3-4<	85.7	1.6
4-5<	61.2	4.4	4-5<	57.9	1.7
5-6<	32.2	5.4	5-6<	21.2	1.3
6-7<	32.1	6.4	6-7<	44.7	3.2
7+	189.8	15.8	7+	173.4	12.4
Sum	**2324.9km**			**2169.2km**	
Min	**0.00001km (=0.01m)**		**Min**	**0.00015km (=0.15m)**	
Max	**43.8km**		**Max**	**44.4km**	

Table 5-5: Numbers of streets exposed to direct sunlight in the autumnal equinox AM

Autumnal Equinox - Morning			
AE08h30 (19°)		AE08h55 (25°)	
Length Class (km)	No. of Streets Exposed to Direct Sunlight	Length Class (km)	No. of Streets Exposed to Direct Sunlight
0-1<	8566	0-1<	7674
1-2<	217	1-2<	581
2-3<	52	2-3<	136
3-4<	24	3-4<	54
4-5<	14	4-5<	34
5-6<	6	5-6<	16
6-7<	5	6-7<	14
7+	12	7+	14
Sum	**8896**	**Sum**	**8554**

b) Map Analysis: Visual Interpretation

It is worth noting that the affected road segments (exposed to direct sunlight) in each scenario have a defined orientation (cardinal direction). In view of the fact that the road segments in each map are actually parts of a road/street that is exposed to direct sunlight, the angle attributes of these segments were used to determine a directional range of the streets vulnerable to sun glare in each scenario. For example, the red segments in Figure 5-4 indicate that the roads exposed to direct sunlight in the morning period of the autumnal equinox are facing the northeast direction,

from the southwest, with a slope ranging between 60° and 90° clockwise from the north. The values for the 25° altitude snapshot (08h55) are not too far off from this range. With the same orientation, the angle range is between 59° and 83°. It should be noted that, in determining these values, including those for the other scenarios, one area of the road segment layers was magnified, whereby only segments that fall in that area were used to determine the directional values. The main purpose of using the same area for all values was to increase the accuracy of the results. In addition, both morning segment layers (each one for the 19° and 25° altitude) were overlaid to determine the angles of segments that don't fall in both scenarios, thus, allowing for the determination of even more precise results.

Moreover, there is a noticeable uneven distribution of the road segments at 08h30 (as seen in Figure 5-4). The northern part, which is the Western Seaboard, and the top part of the Northern Suburbs (see Figure 5-2), have significantly less roads exposed to direct sunlight, as indicated by the sparse distribution of road segments. The same observation was made in the 08h55 map in Figure 5-5. Majority of the roads segments are concentrated in the southern part of the city, which includes the Southern Suburbs, Cape Flats, and parts of the Northern Suburbs and Southern Peninsula. Given that these parts of the city exhibit a plain topographic profile, they experience more exposure to direct sunlight, as a result of the lack of mounds or raised areas of land to provide shadowing. Meanwhile, the areas shadowed by the raised land (combination of hills and mountains) in the Atlantic Seaboard and Southern Peninsula have significanly less roads vulnurable to sun glare, ergo the meagre distribution of road segments.

Additionally, there is an observed clustering of road segments in both maps in Figure 5-4 and 5-5. This simply signifies that where there are clusters there is a concentration of streets that fall in the directional range of streets exposed to direct sunlight in these scenarios. Taking everything into account, there is an apparent similarity in the road segment distribution of the two morning time snapshots. Nonetheless, there still are small differences between the two, as can be seen in the map overlaying the outcomes of the two scenarios in Appendix B.

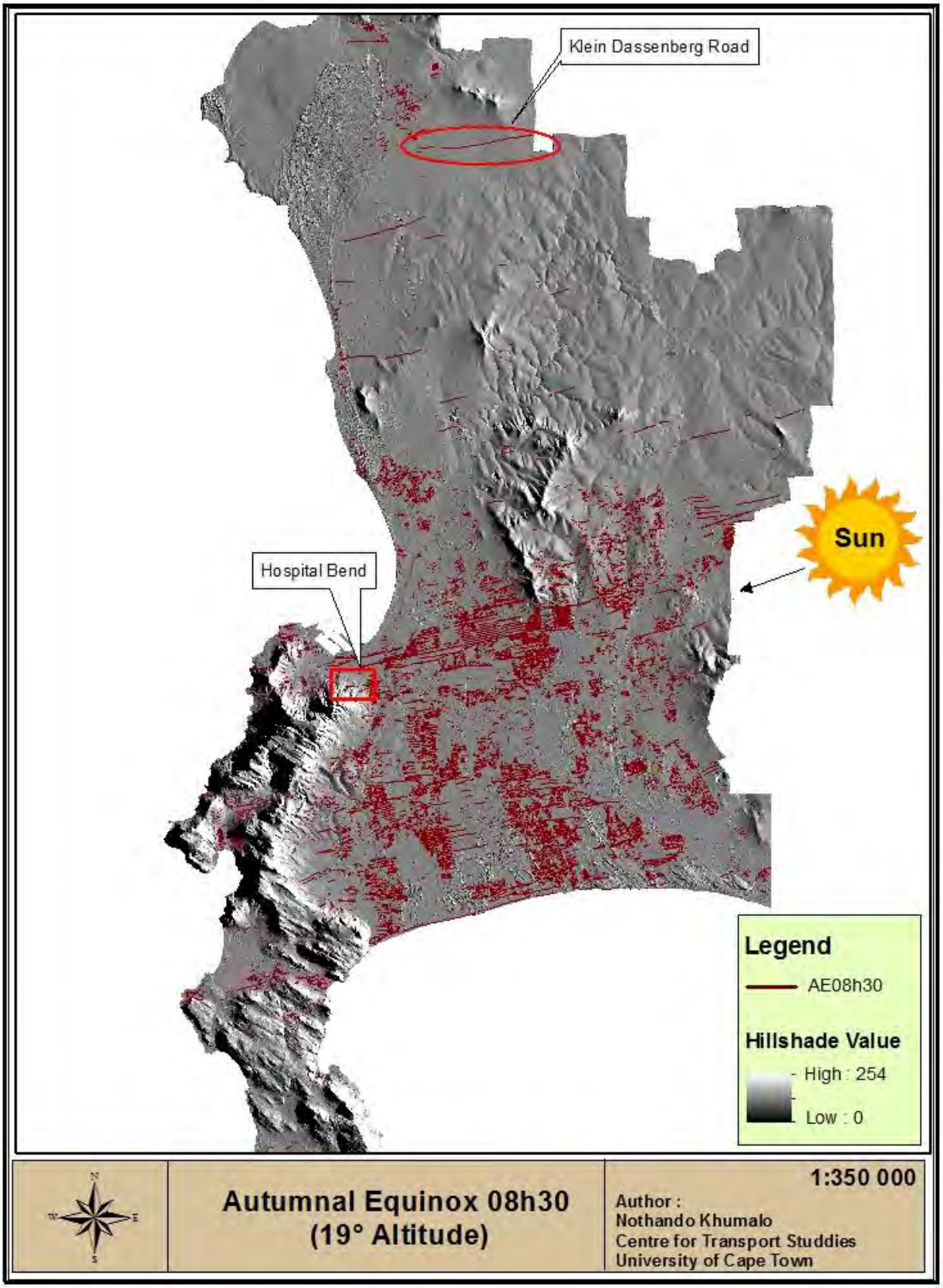

Figure 5-4: Road Segments Exposed to Direct Sunlight in the Autumnal Equinox at 08h30

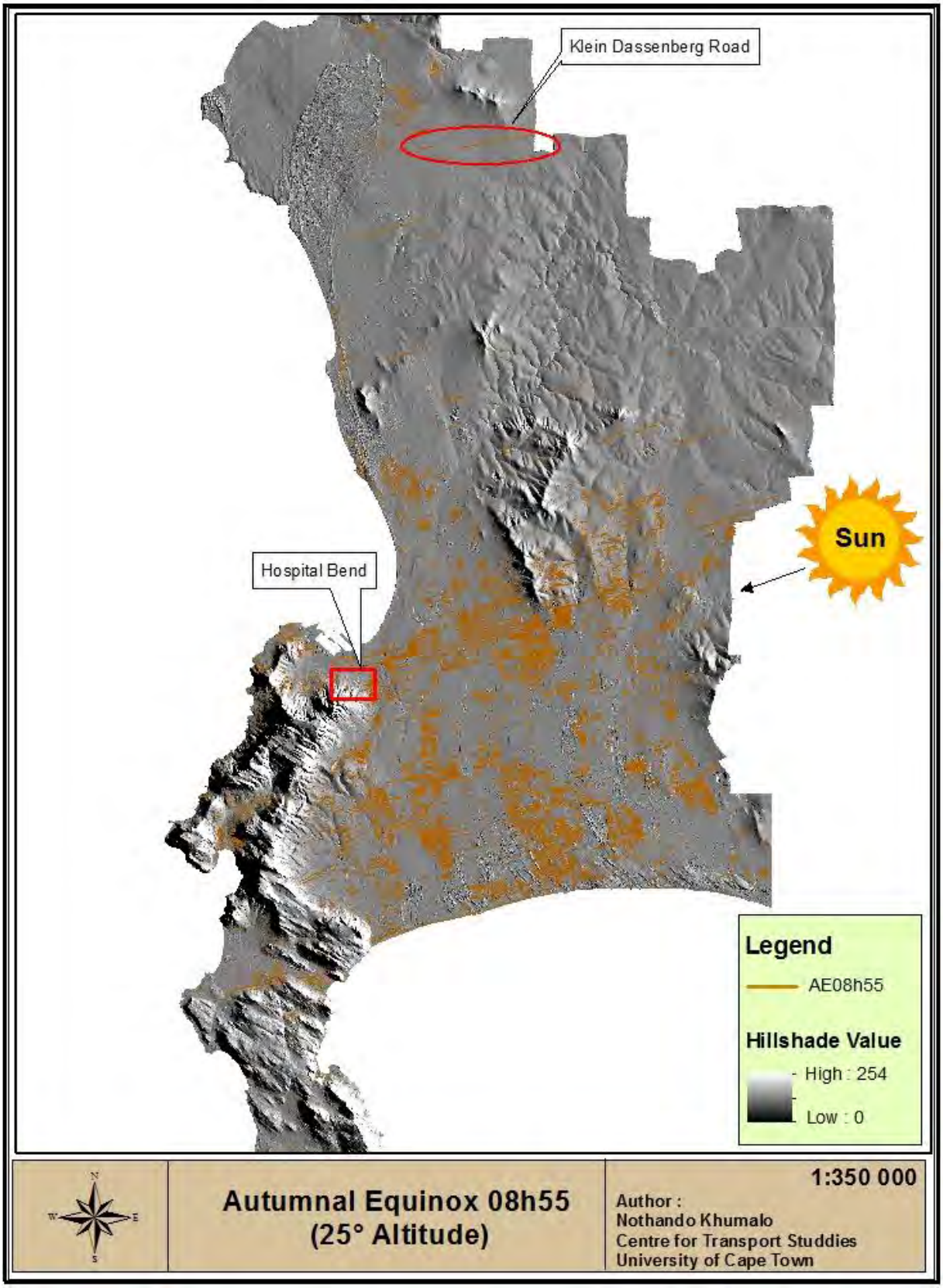

Figure 5-5: Road Segments Exposed to Direct Sunlight in the Autumnal Equinox at 08h55

5.1.1.2 Afternoon Period

a) Analysis of Quantitative Data

An average total of 1 674km (in length) of road segments are exposed to direct solar radiation in the afternoon of the autumnal equinox. Table 5-6 shows a total length of 1 749km road segments exposed to direct sunlight at 17h20, and a total of 1 599km exposed at 16h55. From these results it can be observed that the afternoon period starts out with less road segments, in length, and ends up with more at the other end of the sun cone (at 19°). With respect to the length classes, the same observations made in the morning period can be made here, that is, the 0-1<km class has significantly more road segments in length than the other classes.

Table 5-6: Road Segments Length Exposed to Direct Sunlight in the Autumnal Equinox PM

Autumnal Equinox - Afternoon					
AE17h20 (19°)			**AE16h55 (25°)**		
Length (km)	**Total Length (km)**	**Mean Length (km)**	**length (km)**	**Total Length (km)**	**Mean Length (km)**
0-1<	1199.7	0.2	0-1<	1072.5	0.1
1-2<	187.2	1.4	1-2<	199.5	1.4
2-3<	93.8	2.4	2-3<	80.0	2.4
3-4<	60.1	3.5	3-4<	43.1	3.6
4-5<	31.5	4.5	4-5<	17.4	4.3
5-6<	17.1	5.7	5-6<	27.5	5.5
6-7<	6.6	6.6	6-7<	6.8	6.8
7+	153.2	15.3	7+	152.1	16.9
Sum	**1749.3**		**Sum**	**1599.0**	
Min	**0.000004km (=0.004m)**		**Min**	**0.00014km (=0.14m)**	
Max	**42.0km**		**Max**	**50.1km**	

In terms of the number of exposed streets in each class, these values are shown in Table 5-7. According to the data in this table, the later period in the afternoon, which is at 17h20, has a lot more streets esposed to direct sunlight (8 129 streets) than the ealier period at 16h55 (7 646 streets). These observations are in line with the ones made in the afternoon period. What is apparent here is that when the sun is lower in the sky (at 19°), more streets are exposed to direct sunlight compared to the relatively higher altitude of 25°.

Table 5-7: Numbers of Streets Exposed to Direct Sunlight in the Autumnal Equinox PM

Autumnal Equinox - Afternoon			
AE17h20 (19°)		**AE16h55 (25°)**	
Length Class (km)	**No. of Streets Exposed to Direct Sunlight**	**Length Class (km)**	**No. of Streets Exposed to Direct Sunlight**
0-1<	7915	0-1<	7434
1-2<	137	1-2<	147
2-3<	39	2-3<	34
3-4<	17	3-4<	12
4-5<	7	4-5<	45
5-6<	3	5-6<	5
6-7<	1	6-7<	1
7+	10	7+	9
Sum	**8129**	**Sum**	**7646**

b) Map Analysis: Visual Interpretation

The road segments in this scenario take a northwest direction, from the southeast, which is actually a perpendicular direction to that of the morning period. Compared to the morning period, the segments here are oriented a couple more degrees further away from the north point (clockwise). Case in point, at 19° altitude the slope of the road segments in the afternoon period ranges from 88° to 113°; while those of the same altitude in the morning period range from 60° to 90°. Comparison of the two lower end and upper end values in both periods (88° with 60°, and 113° with 90°) reveals that there is an average 25° clockwise orientation shift (from the north) in the road segments exposed to direct sunlight from the morning to the afternoon period. The same observations apply for the 25° altitude values, whereby they range from 95° to 120° in this scenario. In addition, through visual interpretation of the map, it is possible to determine a rough estimation of the position of the sun in each map for any of the four days. A good indicator of the solar position and direction of illumination is the shading of the Atlantic Seaboard in Figure 5-2. For example, in Figure 5-6 and 5-7 the hills and mountains in this area are shaded (lower hillshade values; dim illumination) on the east side and brightly illuminated on the west side (higher hillshade value), which means that the sun is on the west part of the map shining towards the east. This means that the northwest bound traffic is experiencing direct sunlight exposure. Conversely, the sun is shining towards the west in the morning period, in which case the northeast bound traffic is experiencing direct exposure. Going forward, the defined orientation of

the road segments in the following sections for SE, WS and SS will also be referring to the direction of traffic exposed to direct sunlight.

On the subject of road segment map distribution, the two time snapshots (16h55 and 17h20) display very similar results. Given the level of similarity it would be difficult to spot any differences. A map overlaying the two segments can be observed in Appendix C. Compared to the morning period, there is an observed decrease in road segments in some parts of the Southern Suburbs, Northern Suburbs and Cape Flats. Some streets are experiencing comparatively less insulation in the afternoon period, or just none at all. These include streets like Vanguard Drive and Baden Powell Drive. In the morning Vanguard Drive has zero exposure to direct sunlight, while in the afternoon about 14m (0.03%) of the streets is vulnerable to sun glare; although it is still not a significant figure considering that 14m is not a very long distance. On the other hand, Baden Powell Drive is exposed in both the morning and afternoon periods. About 591m (1.8% of the total road length) of the streets is exposed in the morning, while only 34m (0.1%) is exposed in the afternoon.

5.1.1.3 Statistical Comparison: Morning and Afternoon Period

The null hypothesis (H_0) in this study is "there is no difference in average sunlight exposure between the two periods (AM and PM)". The null hypothesis is a type of hypothesis used in statistics that proposes that there is no significant difference in the data to be compared (Anderson et al., 2000). To quantify the significance of a test statistic, the so-called p-value is used. The p-value essentially answers this question: "if the data were sampled from a population with a median equal to the hypothetical value entered, what is the chance of randomly selecting N data points and finding a median as far (or further) from the hypothetical value as observed here".

Since the p-value (probability value) for this test was 0.0117 (1.17%). This implies that there is actually a significant difference in the median amount of average sunlight between AM and PM. This means the null hypothesis is rejected in favour of an alternative hypothesis (H_1 – there is an actual difference in average sunlight exposure between time periods). Table 5-8 and 5-9 show the AE sample data as well as results from the WSRT calculations, respectively.

Table 5-8: Autumnal Equinox Sample Data

Time	Frequency	Percentage	Cumulative Percentage
08h30	88	26.67	26.67
08h55	87	26.36	53.03
16h55	74	22.42	75.45
17h20	81	24.55	100.00
Total	**330**	**100.00**	

Table 5-9: Wilcoxon Signed-Rank Test

Sign	Observation	Sum Ranks	Expected
positive	34	1250	907.5
Negative	21	565	907.5
zero	5	15	15
all	**60**	**1830**	**1830**

Often in social science research, a 5% level of significance is used as a boundary at which to assume that there is significant evidence to reject or accept the null hypothesis (Gardner and Altman, 1986; Hall and Wilson, 1991). If $p \leq 5\%$, the null hypothesis is rejected, in favour of the alternative hypothesis. On the other hand, $p > 5\%$ gives little evidence against the null hypothesis, so it is accepted. Additionally, a larger sample increases the ability of a test to reject a false null hypothesis.

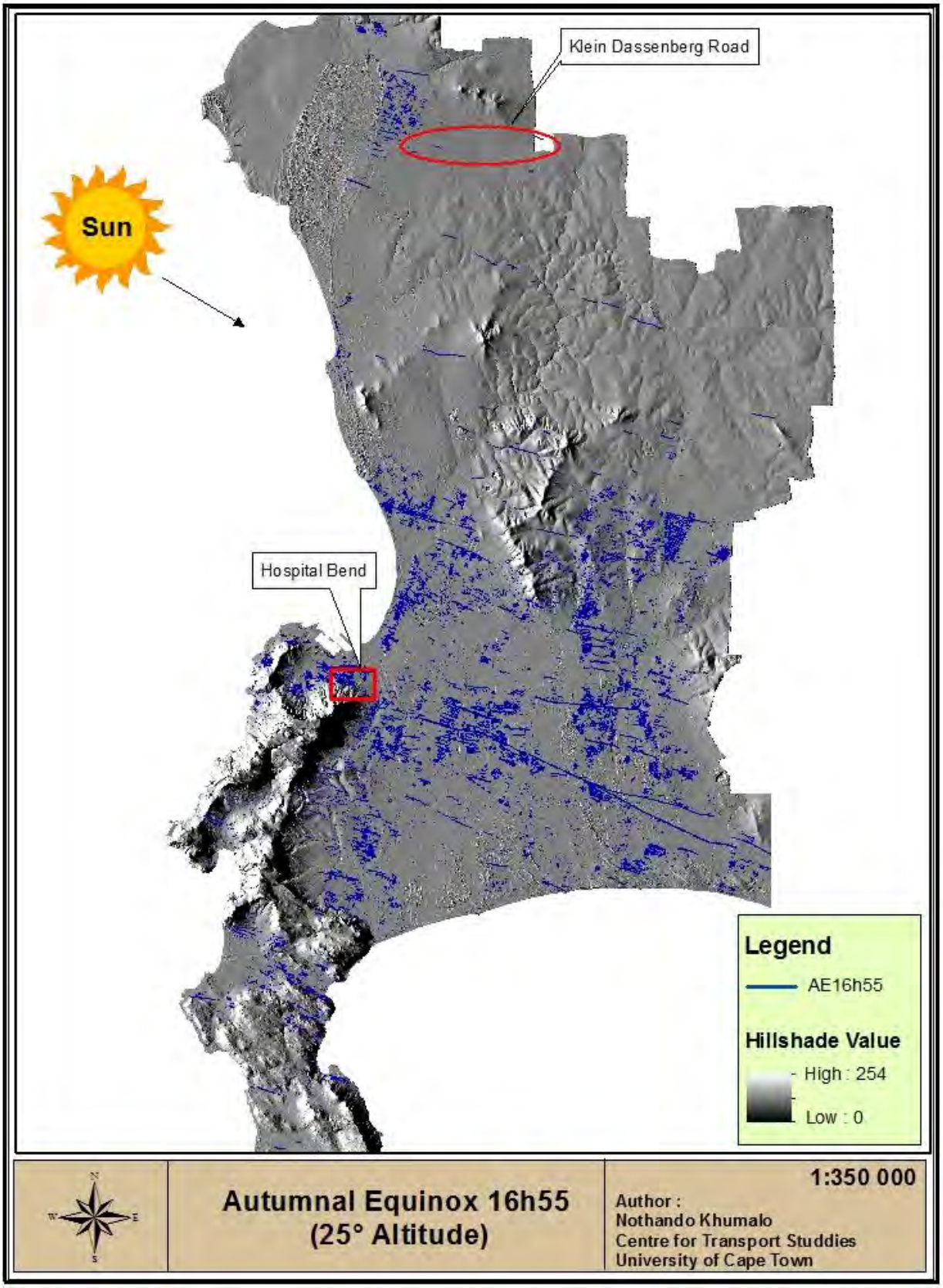

Figure 5-6: Road Segments Exposed to Direct Sunlight in the Autumnal Equinox at 16h55

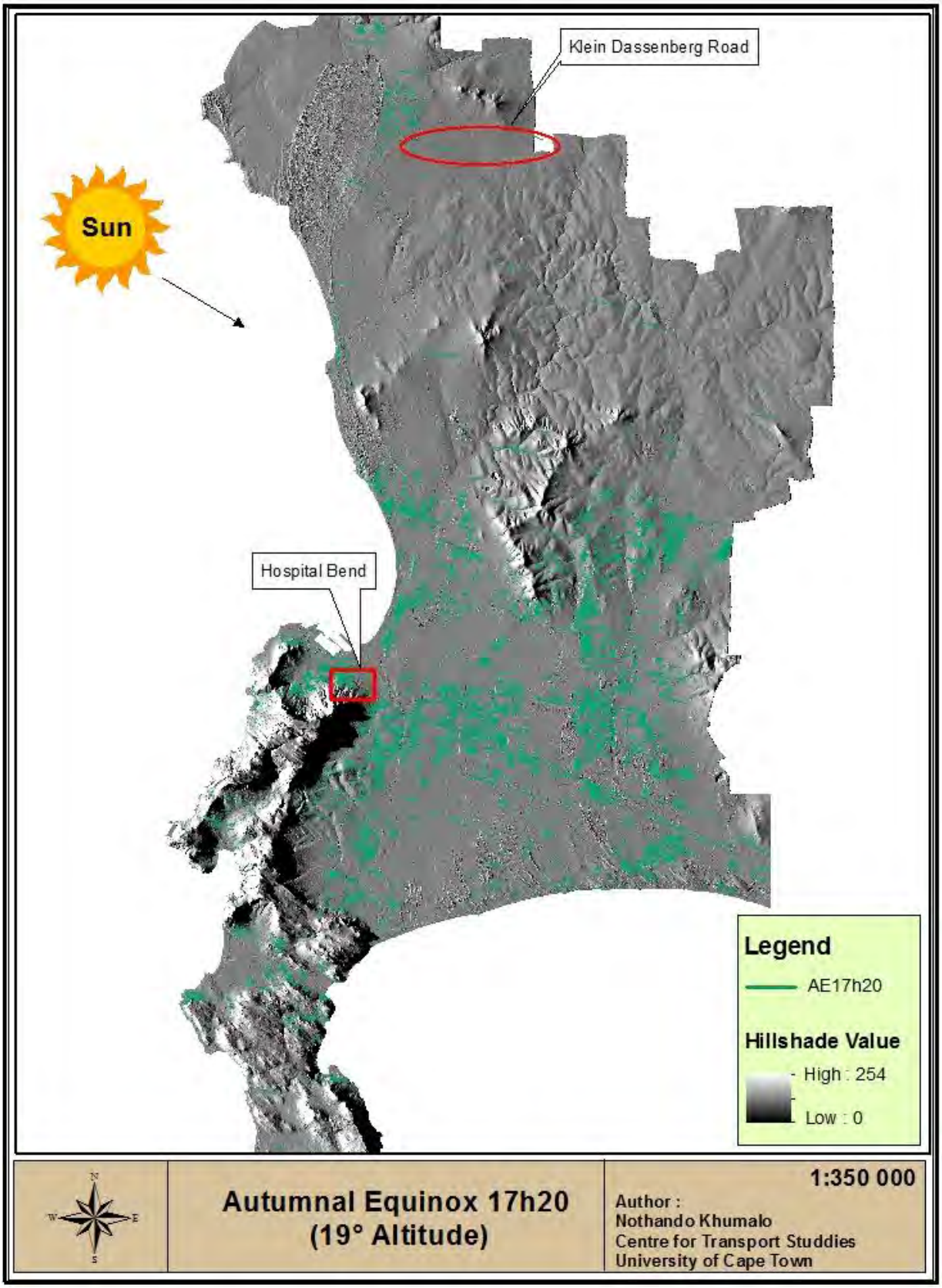

Figure 5-7: Road Segments Exposed to Direct Sunlight in the Autumnal Equinox at 17h20

5.1.2 Spring Equinox

5.1.2.1 Morning Period

a) Analysis of Quantitative Data

The outputs in the spring equinox (SE) morning period are more or less similar to the ones in the autumnal equinox morning period. For instance, in this scenario a total of 2 323km road segment are exposed to direct sunlight at 19° altitude, while 2 325km are exposed in the AE. Additionally, the same streets in both periods have the maximum length of road segments exposed. At 19° altitude, the N1 has the longest length of road segments exposed to direct sunlight in both the autumnal and spring equinox. The same applies with the 25° altitude, whereby 44km of the N2 is exposed on both days. The SE values of road segment lengths affected in each class and altitude can be seen in Table 5-10.

Table 5-10: Road Segments Length Exposed to Direct Sunlight in the Spring Equinox AM

Spring Equinox - Morning					
SE08h15 (19°)			**SE08h40 (25°)**		
Length (km)	**Total Length (km)**	**Mean Length (km)**	**length (km)**	**Total Length (km)**	**Mean Length (km)**
0-1<	1501.9	0.2	0-1<	1416.8	0.2
1-2<	293.3	1.4	1-2<	259.6	1.4
2-3<	129.4	2.4	2-3<	126.5	2.4
3-4<	83.7	3.5	3-4<	75.5	3.4
4-5<	61.2	4.4	4-5<	57.0	4.4
5-6<	32.3	5.4	5-6<	32.2	5.4
6-7<	31.9	6.4	6-7<	44.7	6.4
7+	189.8	15.8	7+	171.5	17.1
Sum	**2323.5km**		**Sum**	**2183.8km**	
Min	**0.00001km (=0.01m)**		**Min**	**0.00015km (=0.15m)**	
Max	**43.7km**		**Max**	**44.4km**	

With respect to the number of streets affected, the same observations made for the road segment lengths between SE and AE can also be applied here. At 08h15, a total of 8 135 streets are exposed to direct solar insulation in the SE, which varies only by five additional streets from the AE value (8 896 streets) at the same altitude (19°). See Table 5-11 for an outline of the numbers of streets exposed in the spring equinox morning period.

Table 5-11: Numbers of Roads Exposed to Direct Sunlight in the Spring Equinox AM

Spring Equinox - Morning			
SE08h15 (19°)		**SE08h40 (25°)**	
Length Class (km)	**No. of Streets Exposed to Direct Sunlight**	**Length Class (km)**	**No. of Streets Exposed to Direct Sunlight**
0-1<	8569	0-1<	8304
1-2<	217	1-2<	192
2-3<	54	2-3<	53
3-4<	24	3-4<	22
4-5<	14	4-5<	13
5-6<	6	5-6<	6
6-7<	5	6-7<	7
7+	12	7+	10
Sum	**8901**	**Sum**	**8607**

b) Map Analysis: Visual Interpretation

The SE morning period exhibits more or less the same characteristics as that of the autumnal equinox, with respect to road segment distribution. The Western Seabord and the top part of the Northern suburbs have a considerably sparse distribution of road segmens. Whereas, the Southern Surburbs, Cape Flats, south part of the Northerern Surburbs and a small portion of the north part of the Southern Peninsula have a significant concentration of road segment clusters. As previously stated, these areas are located in areas of land with a relatively plain topographic profile. It is, therefore, expected that all the 16 scenarios will have a significantly sparse distribution of segments in the northern part of the Cape Metropolitan, which includes Western Seaboard and north part of Northern Suburbs; and a comparatively dense distribution in the Southern Surburbs, Cape Flats, south part of the Northerern Surburbs and a small portion of the north part of the Southern Peninsula.

The road segments in this scenario are orientated towards the northeast, from the southwest, which is similar to the autumnal equinox direction. The similarities also apply to the slope of the segments. The 08h15 time snapshot has a slope ranging between 63° and 90°, while the 08h40 slope ranges between 57° and 83°. The slight differences between the AE and SE may be attributed to, either, accuracy errors or seasonal differences. An overlay of the two SE morning scenarios is presented in Appendix B.

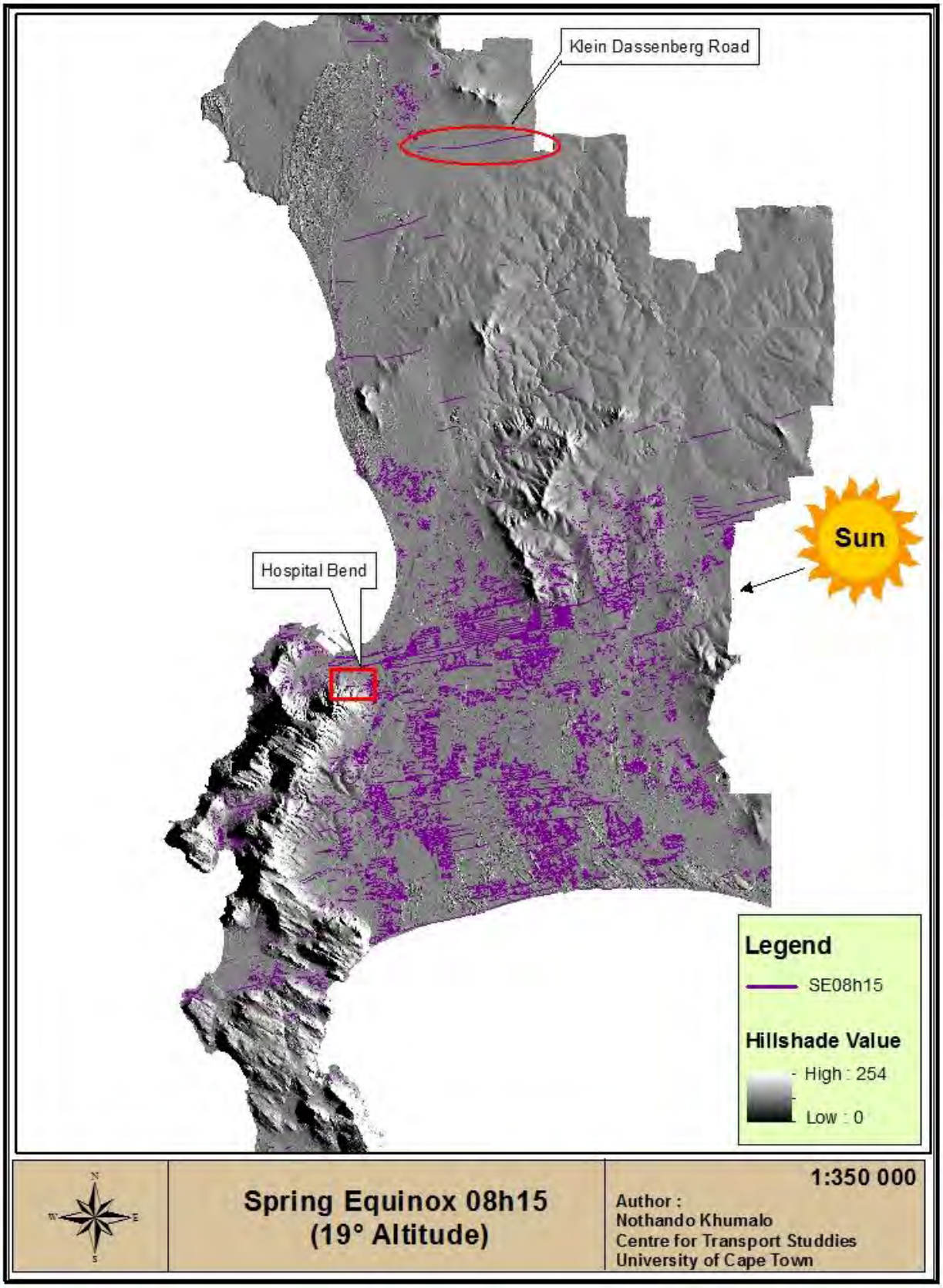

Figure 5-8: Road Segments Exposed to Direct Sunlight in the Spring Equinox at 08h15

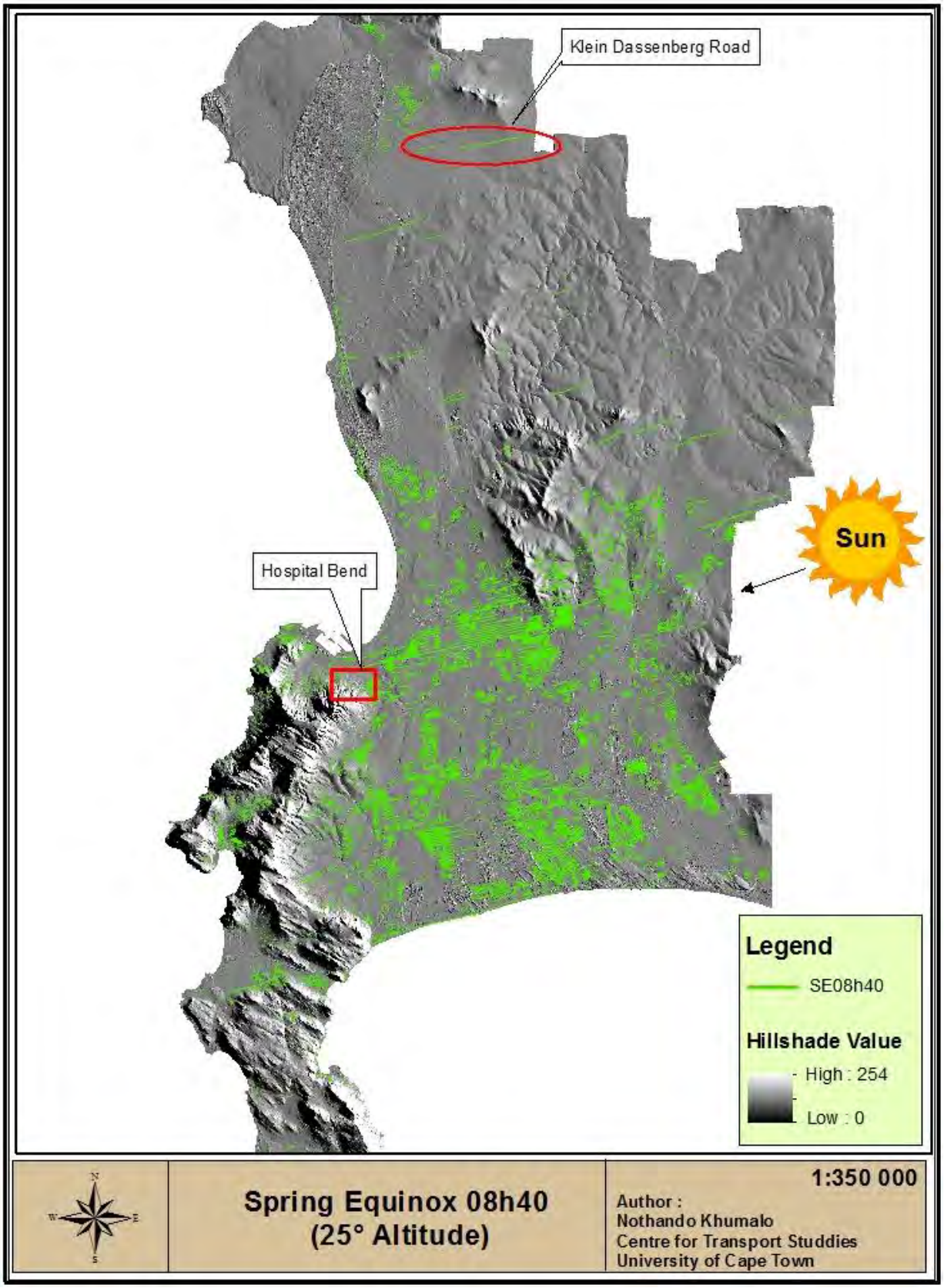

Figure 5-9: Road Segments Exposed to Direct Sunlight in the Spring Equinox at 08h40

5.1.2.2 Afternoon Period

a) Analysis of Quantitative Data

Similar to the autumnal equinox, the road segment length values in the afternoon period are less than those of the morning period. A total length of 1 599km road segments are exposed to direct sunlight in the 25° altitude for the spring equinox afternoon period, while a greater value of 2 184km is observed for the afternoon period. Table 5-12 highlights the road segment values in each of the eight classes as well as the lengths of the minimum and maximum road segment lengths exposed in each of the two altitudes.

Table 5-12: Road Segments Length Exposed to Direct Sunlight in the Spring Equinox PM

Spring Equinox - Afternoon					
SE17h05 (19°)			**SE16h40 (25°)**		
Length (km)	**Total Length (km)**	**Mean Length (km)**	**length (km)**	**Total Length (km)**	**Mean Length (km)**
0-1<	1198.2	0.2	0-1<	1072.8	0.1
1-2<	189.5	1.4	1-2<	199.7	1.4
2-3<	93.8	2.4	2-3<	80	2.4
3-4<	60.1	3.5	3-4<	43.1	3.6
4-5<	31.5	4.5	4-5<	17.4	4.3
5-6<	17.2	5.7	5-6<	27.5	5.5
6-7<	6.7	6.7	6-7<	6.8	6.8
7+	153.3	15.3	7+	152.1	16.9
Sum	**1750.3**		**Sum**	**1599.4km**	
Min	**0.000004km (=0.004m)**		**Min**	**0.00014km (=0.14m)**	
Max	**42.1km**		**Max**	**50.1km**	

There is a direct correlation between the road segment length and number of streets values. A decrease of the road segment length in the afternoon, also results in a decrease in the number of streets at sun glare risk. For instance, the road segment length in the 19° altitude decreases from 2 324km in the morning to 1 750km in the afternoon. On the other hand, the number of streets affected also decrease from 8 901 streets in the morning to 8 135 streets in the afternoon (see Table 5-13 for SE afternoon values). Overall, this implies that there is less insulation in the afternoon period compared to the morning period.

Table 5-13: Numbers of Roads Exposed to Direct Sunlight in the Spring Equinox PM

Spring Equinox - Afternoon			
SE17h05 (19°)		**SE16h40 (25°)**	
Length Class (km)	**No. of Streets Exposed to Direct Sunlight**	**Length Class (km)**	**No. of Streets Exposed to Direct Sunlight**
0-1<	7919	0-1<	7438
1-2<	139	1-2<	147
2-3<	39	2-3<	34
3-4<	17	3-4<	12
4-5<	7	4-5<	4
5-6<	3	5-6<	5
6-7<	1	6-7<	1
7+	10	7+	9
Sum	**8135**	**Sum**	**7651**

b) Map Analysis: Visual Interpretation

The road segments in this scenario are orientated towards the northwest from the southeast, which is similar to the AE in the same period. The slope is also more or less the same to that of the autumnal equinox. At the 19° altitude (17h05) the angle values of the slope, clockwise for the north, range from 88° to 113°, while those at 25° altitude (16h40) range from 92° to 120°.

The spring equinox road segment distribution is very similar to that of the autumnal equinox distribution. Aside from visual observation and interpretation of the maps, this is also evidenced by the similarity in the total road segment length and total number of streets values found in the tables of the respective sections. For example, at 19° altitude the spring equinox has a total length of 1 750km road segments and total number of 8 135 streets exposed to direct sunlight; while the autumnal equinox has a total 1 750km road segments and a total number of 8 129 streets exposed. Between the two time snapshots in this scenario, the 16h40 map in Figure 5-10 appears to have more segments than the 17h05 map in Figure 5-11, thus, implying a decrease in road segment quantity with decrease in altitude. The circles in both maps indicate the more noticeable differences between the two, otherwise anymore differences can be seen in the overlay map in Appendix C.

5.1.2.3 Statistical Comparison: Morning and Afternoon Period

Similar to the SE, the probability value (p-value) for this test was also 0.0117, implying there is a significant difference in the median amount of average sunlight between AM and PM. In other words, this means there was strong evidence against the null hypothesis in favour of the alternative (AM ≠ PM). This result gives additional evidence for the observed similarities between AE and SE in the quantitative data and map analysis discussions. The SE sample data and WSRT results can be observed in Table 5-14 and 5-15.

Table 5-14: Spring Equinox Sample Data

Time	Frequency	Percentage	Cumulative Percentage
08h15	88	26.59	26.59
08h40	88	26.59	53.17
16h40	74	22.36	75.53
17h05	81	24.47	100.00
Total	**331**	**100.00**	

Table 5-15: Wilcoxon Signed-Rank Test

Sign	Observation	Sum Ranks	Expected
positive	34	1268	938
Negative	22	608	938
zero	5	15	15
all	**61**	**1891**	**1891**

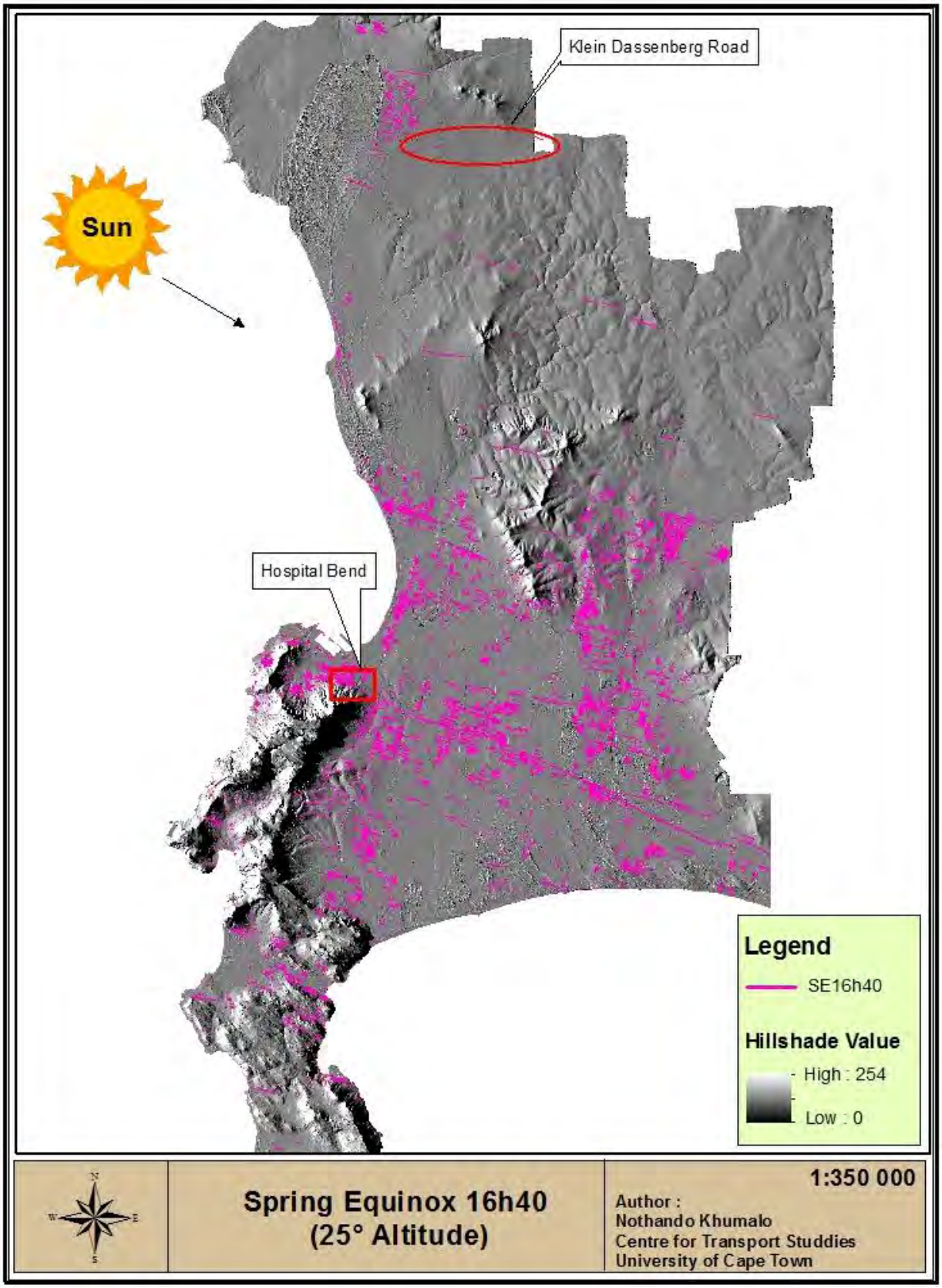

Figure 5-10: Road Segments Exposed to Direct Sunlight in the Spring Equinox at 16h40

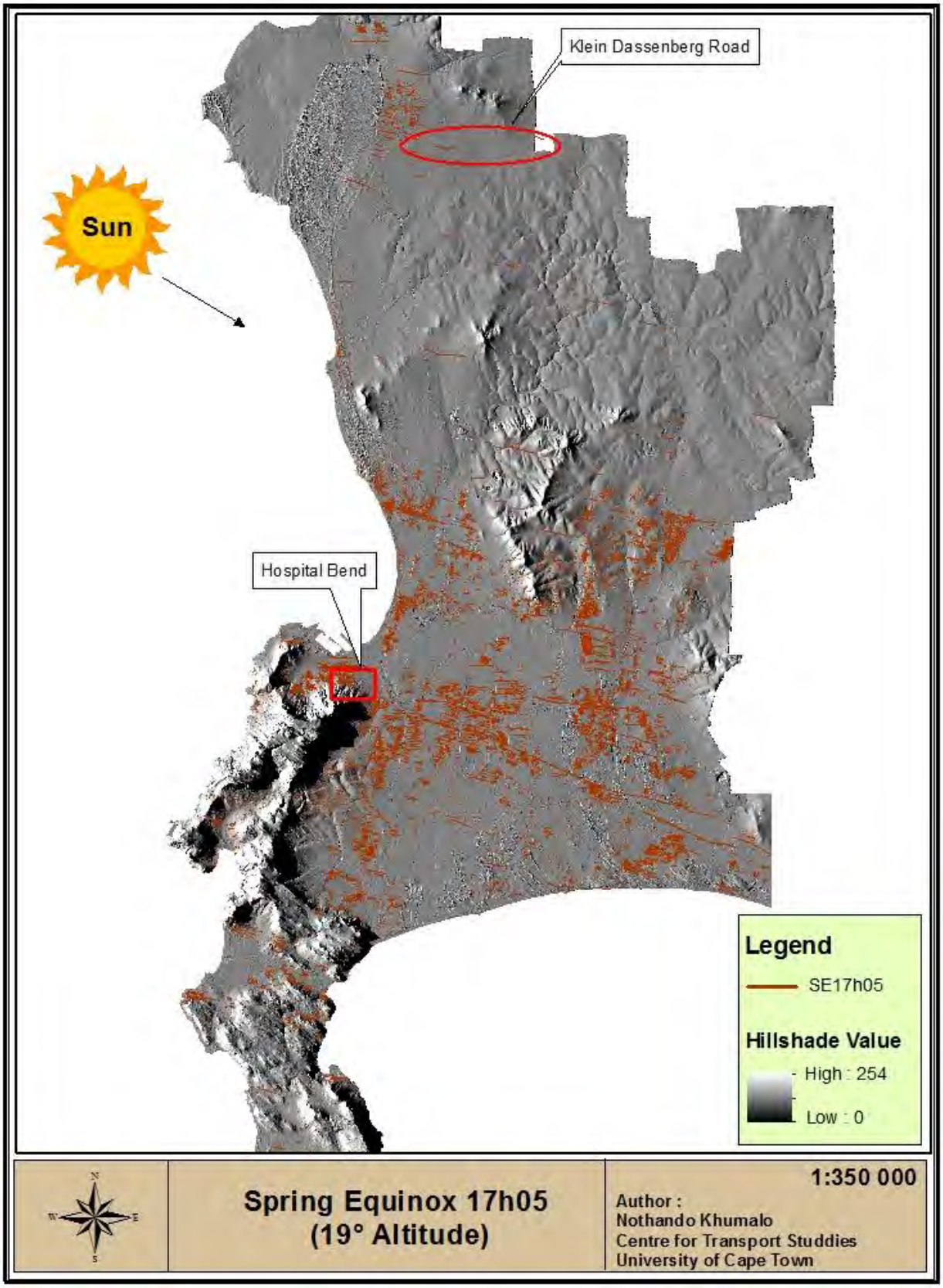

Figure 5-11: Road Segments Exposed to Direct Sunlight in the Spring Equinox at 17h05

5.1.3 Winter Solstice

5.1.3.1 Morning Period

a) Analysis of Quantitative Data

Compared to the results presented for AE and SE, the winter solstice results indicate conditions of decreased solar illumination, which is comprehensible given that the winter season experiences the least sun exposure and intensity. At 09h55 in the morning, a total length 1 463km road segments are exposed to direct solar insulation. Similar to the autumnal and spring equinox mornings, this value decreases with increasing altitude (from 19° to 25°) to 1 332km at 10h35. See Table 5-16 for an outline of the road segment values in each altitude and length classes.

Table 5-16: Road Segments Length Exposed to Direct Sunlight in the Winter Solstice AM

Winter Solstice - Morning					
WS09h55 (19°)			**WS10h35 (25°)**		
Length (km)	**Total Length (km)**	**Mean Length (km)**	**length (km)**	**Total Length (km)**	**Mean Length (km)**
0-1<	940.5	0.1	0-1<	910.9	0.1
1-2<	203.9	1.3	1-2<	165.6	1.4
2-3<	112.3	2.4	2-3<	54.0	2.5
3-4<	23.5	3.4	3-4<	38.8	3.5
4-5<	44.9	4.5	4-5<	39.8	4.4
5-6<	32.9	5.5	5-6<	26.4	5.3
6-7<	12.8	6.4	6-7<	25.0	6.2
7+	92.1	11.5	7+	71.8	12.0
Sum	**1462.9km**		**Sum**	**1332.3km**	
Min	**0.00014km (=0.14m)**		**Min**	**0.00014km (=0.14m)**	
Max	**23.4km**		**Max**	**18.0km**	

With respect to the number of streets affected, the expectation is that more streets are affected in the earlier time snapshot at 09h55 compared to the later period at 10h35. As you can see in Table 5-17 this is the case; 7 225 streets are affected by direct sun exposure at 09h55 and 7 152 streets are affected at 10h35.

Table 5-17: Numbers of Roads Exposed to Direct Sunlight in the Winter Solstice AM

Winter Solstice - Morning			
WS09h55 (19°)		**WS10h35 (25°)**	
Length Class (km)	**No. of Streets Exposed to Direct Sunlight**	**Length Class (km)**	**No. of Streets Exposed to Direct Sunlight**
0-1<	6993	0-1<	6975
1-2<	152	1-2<	120
2-3<	47	2-3<	22
3-4<	7	3-4<	11
4-5<	10	4-5<	9
5-6<	6	5-6<	5
6-7<	2	6-7<	4
7+	8	7+	6
Sum	**7225**	**Sum**	**7152**

b) Map Analysis: Visual Interpretation

The orientation of the road segments in the winter solstice morning scenario is the northeast direction, from the southwest, which is similar to the moring direction of the segments in the autumnal and spring equinox. The orientation angles, however, are considerably much less (closer to the north point) than those of the two days. The 19° snapshot at 09h55 has range of 44° - 56°, while that of the 25° snapshot is between 20° and 48°. Considering the 40min glare window period in the WS (time duration of the solar position shift from 19° to 25° altitude - see glare window discussion in Section 5.1.5), the substantial difference between the angle ranges of the snapshots is an expected outcome. This difference can also be accredited to the extreme weather characteristics of the winter season.

Unlike the autumnal and spring equinox, there is a noticeable change in the magnitude of road segments between the two morning scenarios here. From visual interpretation of the images in Figure 5-12 and 5-13, it is apparent that there are more road segments at 09h55 than at 10h35. Furthermore, another form of evidence of this difference is the relatively long segment northwest of Klein Dassenberg Street (indicated in both maps) in the 09h55 time snapshot map, which is no longer visible in the 10h35 map. These differences are more evident in the overlay map of the two morning scenarios in Appendix B.

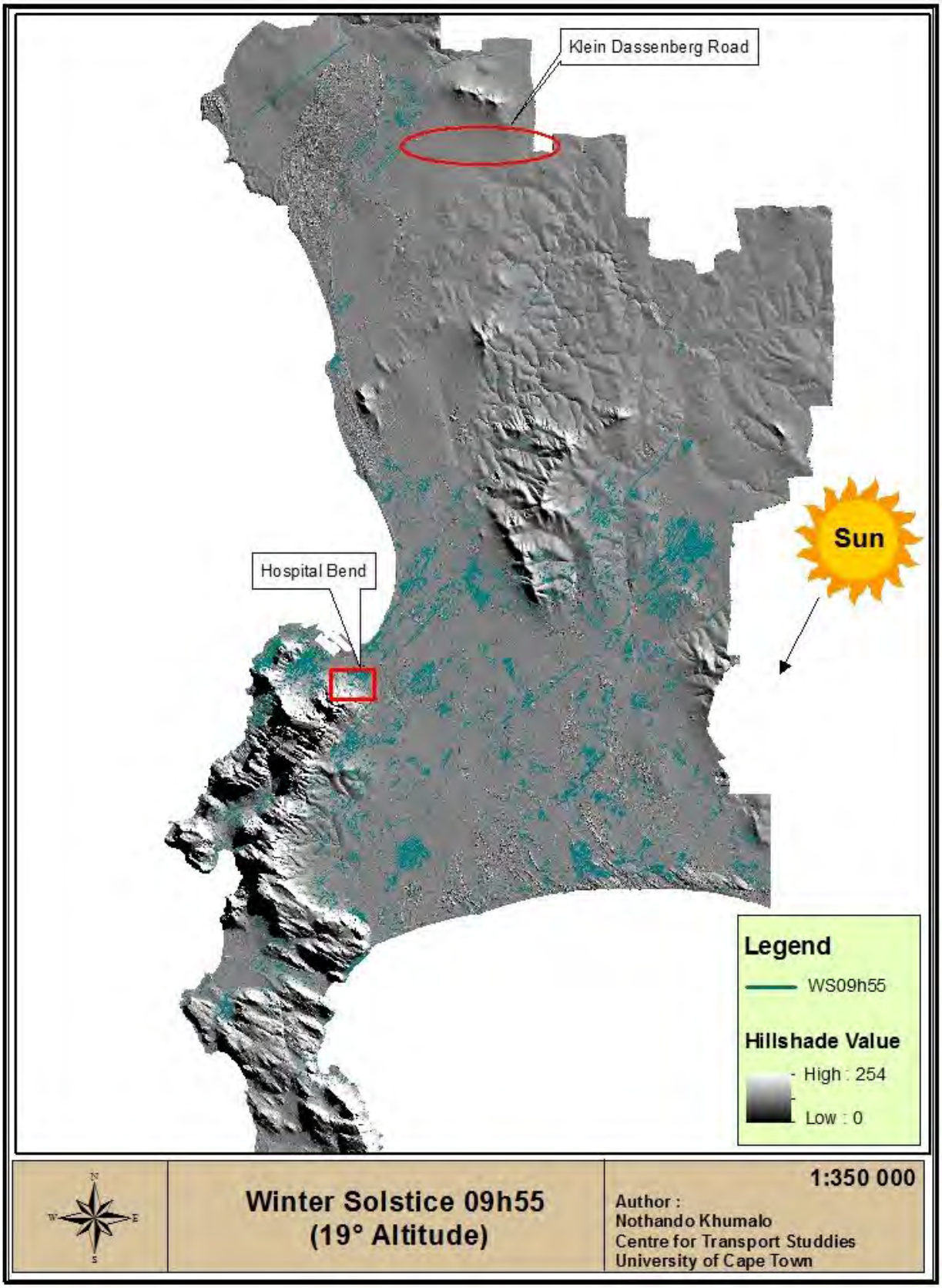

Figure 5-12: Road Segments Exposed to Direct Sunlight in the Winter Solstice at 09h55

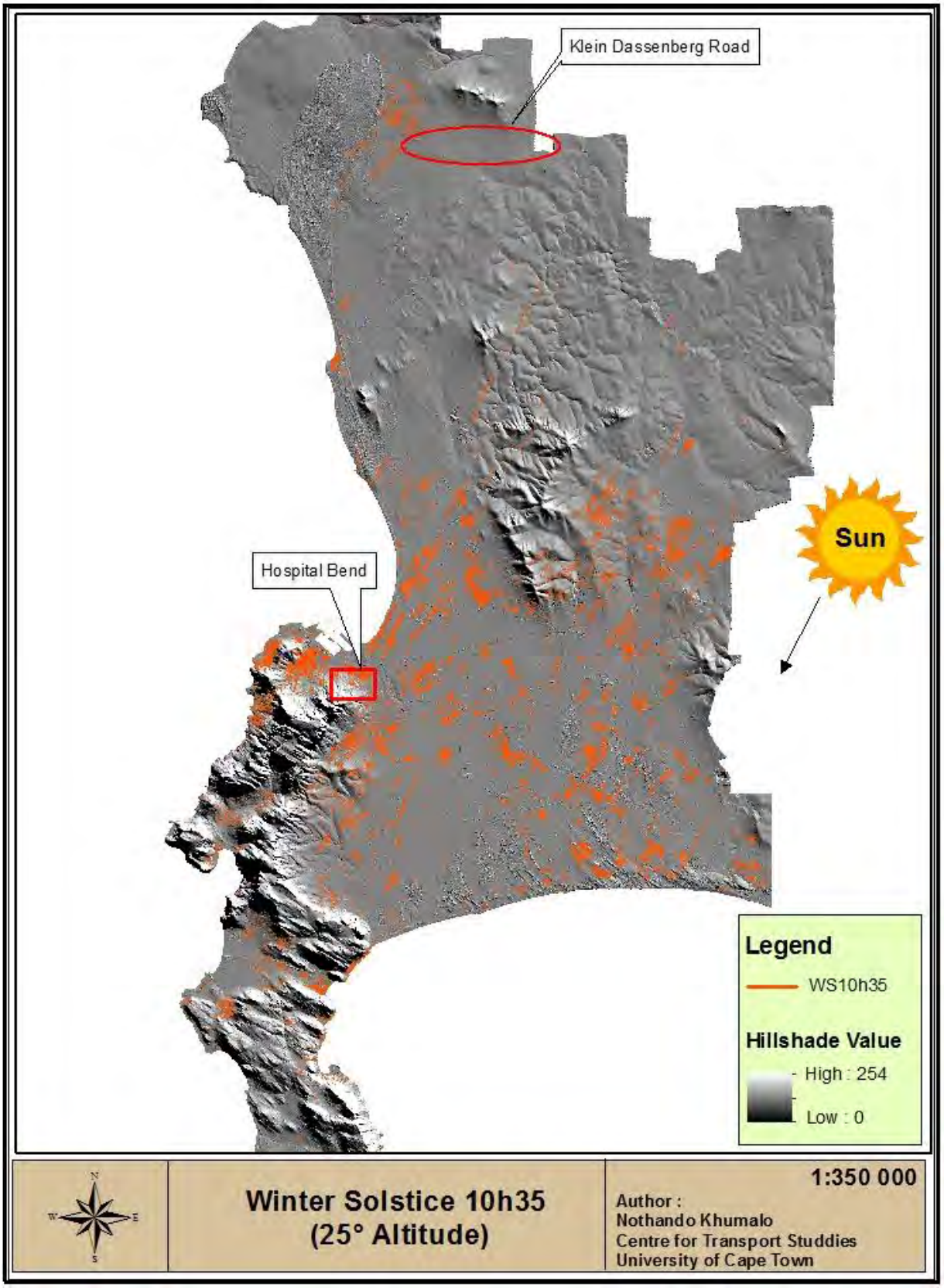

Figure 5-13: Road Segments Exposed to Direct Sunlight in the Winter Solstice at 10h35

5.1.3.2 Afternoon Period

a) Analysis of Quantitative Data

Normally, when a scenario has relatively more road segments exposed to direct sunlight it also has more streets exposed – there is an observed direct proportionality. On the contrary, this WS scenario (PM) has a smaller total length of road segments compared to those of the morning period, and significantly more streets exposed to direct sunlight. For example, for the 19° altitude, the morning period has total length of 2 639km road segments and 7 225 streets exposed, while the afternoon period has a total length of 1 542km road segments and 7 345 streets. See Table 5-18 for values of the road segment lengths and Table 5-19 for the number of streets affected in each class of the winter solstice afternoon.

Table 5-18: Road Segments Length Exposed to Direct Sunlight in the Winter Solstice PM

Winter Solstice - Afternoon					
WS15h40 (19°)			**WS15h00 (25°)**		
Length (km)	**Total Length (km)**	**Mean Length (km)**	**length (km)**	**Total Length (km)**	**Mean Length (km)**
0-1<	993.9	0.1	0-1<	1095.1	0.1
1-2<	206.5	1.4	1-2<	225.3	1.4
2-3<	76.5	2.4	2-3<	84.7	2.4
3-4<	59.8	3.5	3-4<	55.8	3.5
4-5<	26	4.3	4-5<	35.2	4.4
5-6<	16.3	5.4	5-6<	11.1	5.6
6-7<	12.3	6.2	6-7<	6.6	6.6
7+	150.9	15.1	7+	170.8	12.2
Sum	**1542.2km**		**Sum**	**1684.6km**	
Min	**0.00014km (=0.14m)**		**Min**	**0.00014km (=0.14m)**	
Max	**28.8km**		**Max**	**25.9km**	

Table 5-19: Numbers of Streets Exposed to Direct Sunlight in the Winter Solstice PM

Winter Solstice - Afternoon			
WS15h40 (19°)		**WS15h00 (25°)**	
Length Class (km)	**No. of Streets Exposed to Direct Sunlight**	**Length Class (km)**	**No. of Streets Exposed to Direct Sunlight**
0-1<	7123	0-1<	7555
1-2<	152	1-2<	163
2-3<	32	2-3<	36
3-4<	17	3-4<	16
4-5<	6	4-5<	8
5-6<	3	5-6<	2
6-7<	2	6-7<	1
7+	10	7+	14
Sum	**7345**	**Sum**	**7795**

b) Map Analysis: Visual Interpretation

Comparatively, the winter solstice road segments in the afternoon period are angled the furthest away from the north point, in the clockwise direction. With a southeast to northwest orientation, the slope of the road segments at 15h40 (19° altitude) ranges from 125° to 153°, and from 143° to 160° at 15h00 (25° altitude). The orientation of the segments in this scenario is similar to that of the autumnal and spring equinox. However, as indicated by the angle values, the segment slope is relatively steeper.

Visual interpretation of the maps in Figure 5-14 and 5-15 reveals a couple of differences between the two, as indicated by the two black circles in the maps. From these differences it is evident that the change in the number of road segments exposed to direct sunlight is inversely proportional to the change in altitude in the afternoon. This means when the altitude decreases in the afternoon from 25° to 19° (towards sunset), some parts of the city, such as the Atlantic Seaboard and Southern Suburbs, experience an increase in the number and total length of road segments exposed. Another difference between the two snapshots, which is actually a good indicator of the differences between the slopes of the segments in the two periods, is the road segment in the black square in Figure 5-15. Overall, the difference between the 15h00 and 15h40 snapshots are insignificant, as can be seen in the overlay map of the two scenarios in Appendix C.

5.1.3.3 Statistical Comparison: Morning and Afternoon Period

Contrary to that of the AE and SE, the p-value for this test (0.5779) was greater than the 5% significance level; implying there is no evidence for a statistically significant difference in the median amount of average sunlight between AM and PM. Unlike the AE and SE, the p-value here shows that there is not enough evidence against the null hypothesis, in favour of the alternative, ergo the insignificant statistical difference. Table 5-20 gives the sample data used for the WS, while the WSRT results are shown in Table 5-21.

Table 5-20: Winter Solstice Sample Data

Time	Frequency	Percentage	Cumulative Percentage
09h55	62	23.85	23.85
10h35	65	25.00	48.85
15h00	70	26.92	75.77
15h40	63	24.23	100.00
Total	**260**	**100.00**	

Table 5-21: Wilcoxon Signed-Rank Test

Sign	Observation	Sum Ranks	Expected
positive	22	496	451.5
Negative	20	407	451.5
zero	0	0	0
all	**42**	**903**	**903**

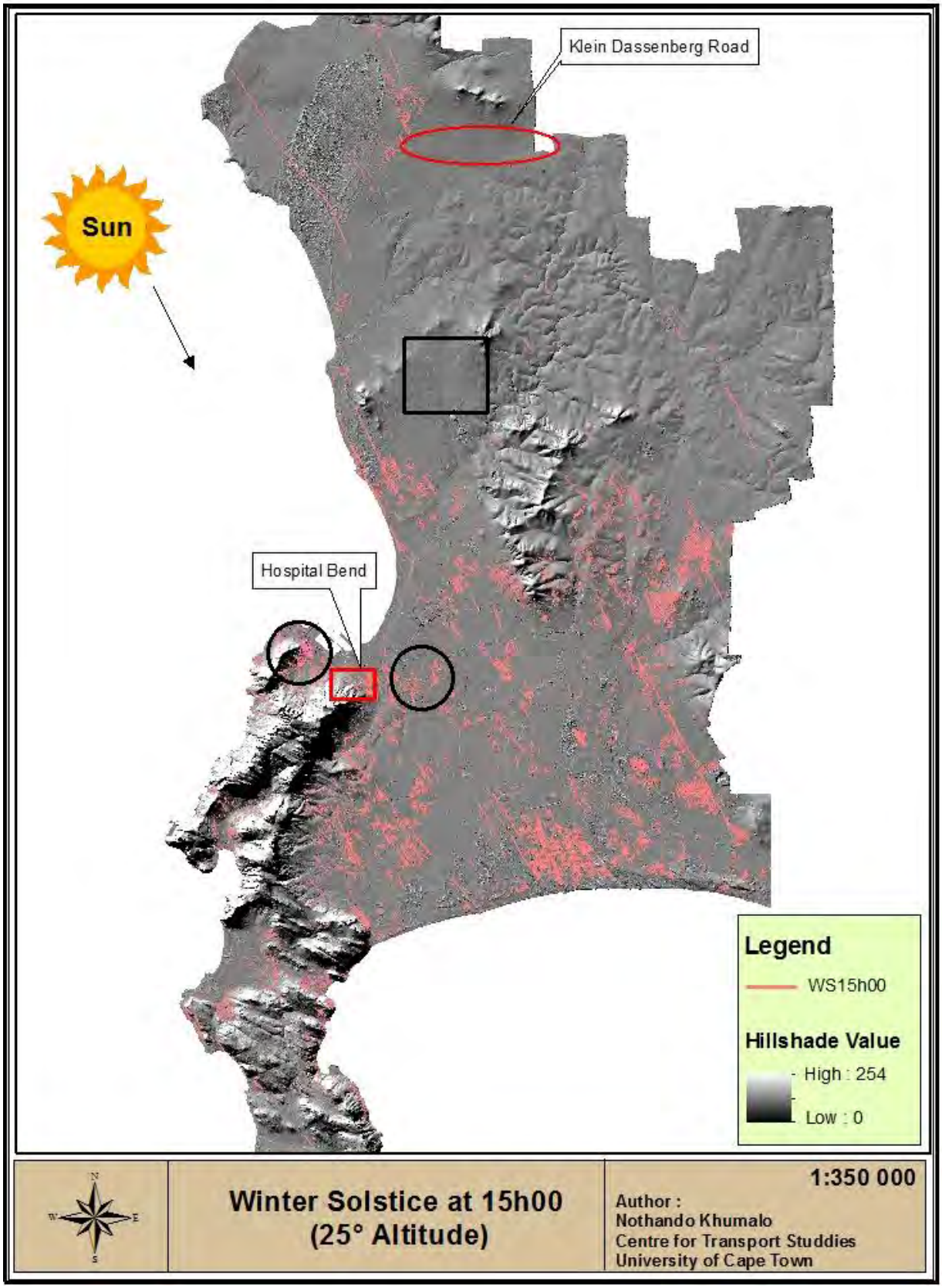

Figure 5-14: Road Segments Exposed to Direct Sunlight in the Winter Solstice at 15h00

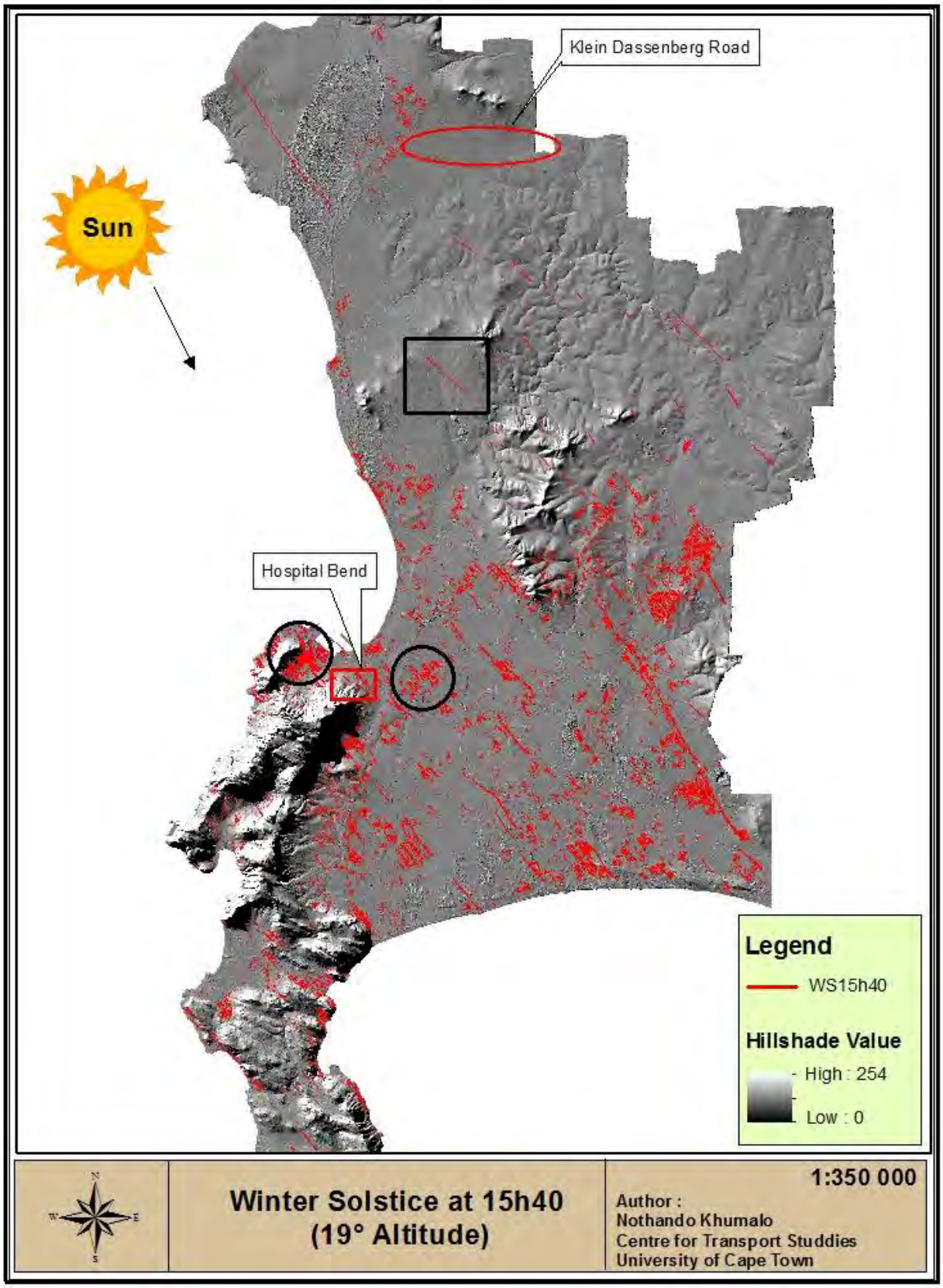

Figure 5-15: Road Segments Exposed to Direct Sunlight in the Winter Solstice at 15h40

5.1.4 Summer Solstice

5.1.4.1 Morning Period

a) Analysis of Quantitative Data

In summer, the sun rises relatively much earlier than in other seasons. This is evident in the potent glare window on this day, that being between 07h20 and 07h45. A total road segment lengths of 1 654km are exposed to direct sunlight at 07h20, which increases with increasing altitude (from 19° to 25°) to 1 749km at 07h45. These values are shown in Table 5-22, along with the total lengths of road segments in each of the eight classes. The same observations made in the other three days also apply here, that being the 0-1<km class which has the longest total length of segments exposed to direct sunlight. This value drastically decreases with ascending classes, with the exception of the 7+km class.

Table 5-22: Road Segments Length Exposed to Direct Sunlight in the Summer Solstice AM

Summer Solstice - Morning					
SS07h20 (19°)			**SS07h45 (25°)**		
Length (km)	**Total Length (km)**	**Mean Length (km)**	**length (km)**	**Total Length (km)**	**Mean Length (km)**
0-1<	1120.2	0.1	0-1<	1203.1	0.2
1-2<	193.9	1.4	1-2<	180.7	1.3
2-3<	80.6	2.4	2-3<	91.4	2.4
3-4<	49.5	3.5	3-4<	59.6	3.5
4-5<	31.6	4.5	4-5<	36.5	4.6
5-6<	17.0	5.7	5-6<	11.0	5.5
6-7<	0.0	0.0	6-7<	20.2	6.7
7+	161.5	16.2	7+	146.4	16.3
Sum	**1654.3 km**		**Sum**	**1748.9km**	
Min	**0.00014km (=0.14m)**		**Min**	**0.000004km (=0.004m)**	
Max	**49.5km**		**Max**	**41.6km**	

Out of the 16 056 streets in the Cape Town road network, a total of 7 767 streets are affected in the morning of the SS, at 07h20. This value increases with change in altitude, from 19° to 25°, to 8 176 streets at 07h45. These values can be seen in Table 5-23, along with the class values.

Table 5-23: Numbers of Roads Exposed to Direct Sunlight in the Summer Solstice AM

Summer Solstice - Morning			
SS07h20 (19°)		**SS07h45 (25°)**	
Length Class (km)	**No. of Streets Exposed to Direct Sunlight**	**Length Class (km)**	**No. of Streets Exposed to Direct Sunlight**
0-1<	7557	0-1<	7964
1-2<	141	1-2<	135
2-3<	34	2-3<	38
3-4<	14	3-4<	17
4-5<	7	4-5<	8
5-6<	3	5-6<	2
6-7<	0	6-7<	3
7+	10	7+	9
Sum	**7767**	**Sum**	**8176**

b) Map Analysis: Visual Interpretation

Compared to the other three days, the orientation of the road segments in the morning period of the summer solstice are towards the southeast direction from the northwest, which is about a 90° change from the direction of the other three days (southwest to northeast). The slope orientation, clockwise from the north point, ranges from 92° to 120° at 07h20 and from 88° to 110° at 07h45. The differences in these range values resemble those of the winter solstice. Similarly, they can also be attributed to extreme weather characteristics. The road segments here get closer to the north with the change in time and altitude in the morning.

The road segment concentration, on the other hand, has no resemblance to the observed change in concentration in the WS morning period (see Figure 5-16 and 5-17). There are, however, a few noticeable changes between the two morning periods. The segment clusters in the two black circles in Figure 5-16 and 5-17 reveal that the roads exposed to direct sunlight decrease with change in time and altitude. Overall, the distribution in the two morning snapshots is more or less similar. However, the similarity is comparatively less than that of the autumnal and spring equinox. See Appendix B for an overlay map of the two distributions.

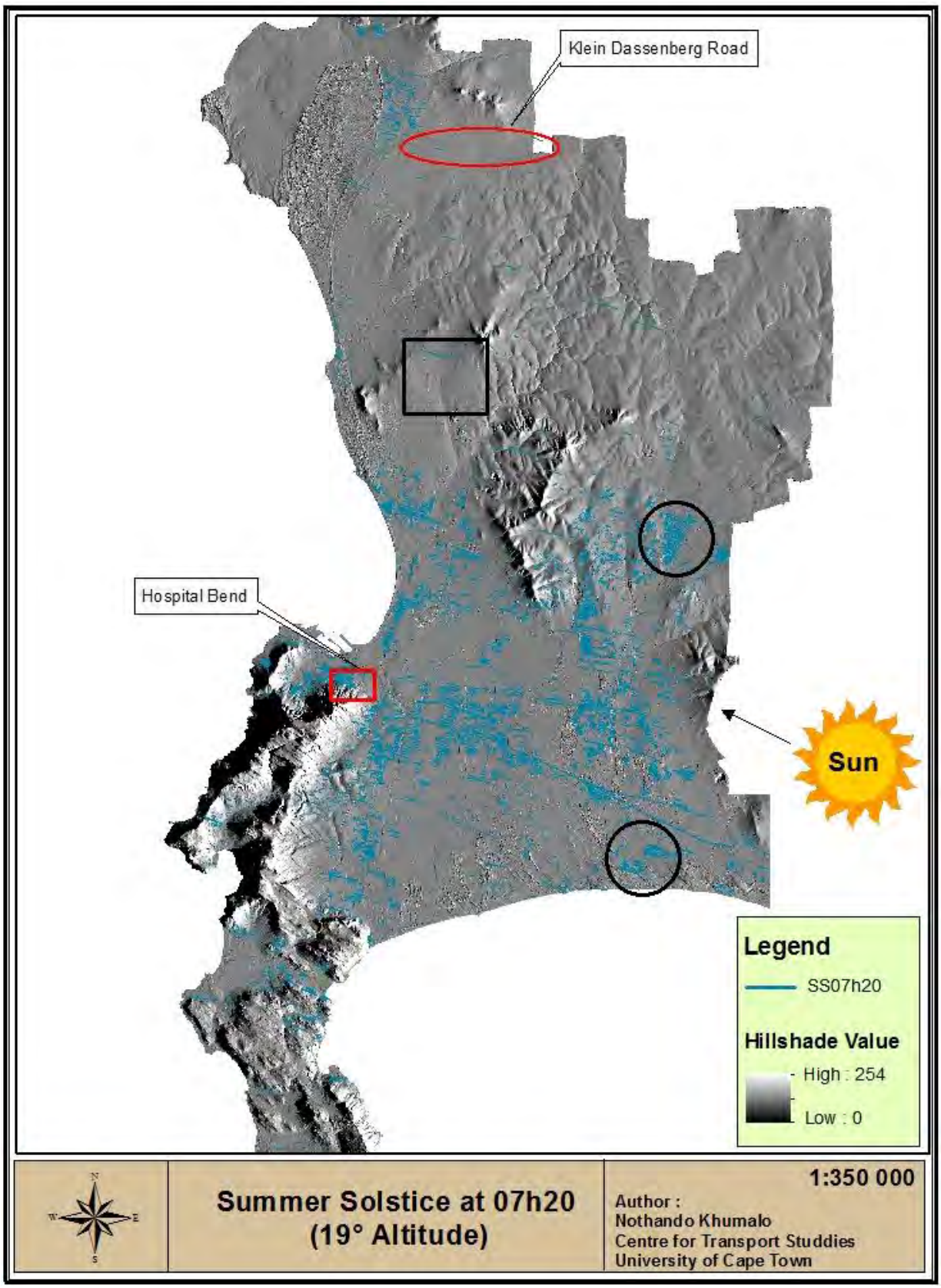

Figure 5-16: Road Segments Exposed to Direct Sunlight in the Summer Solstice at 07h20

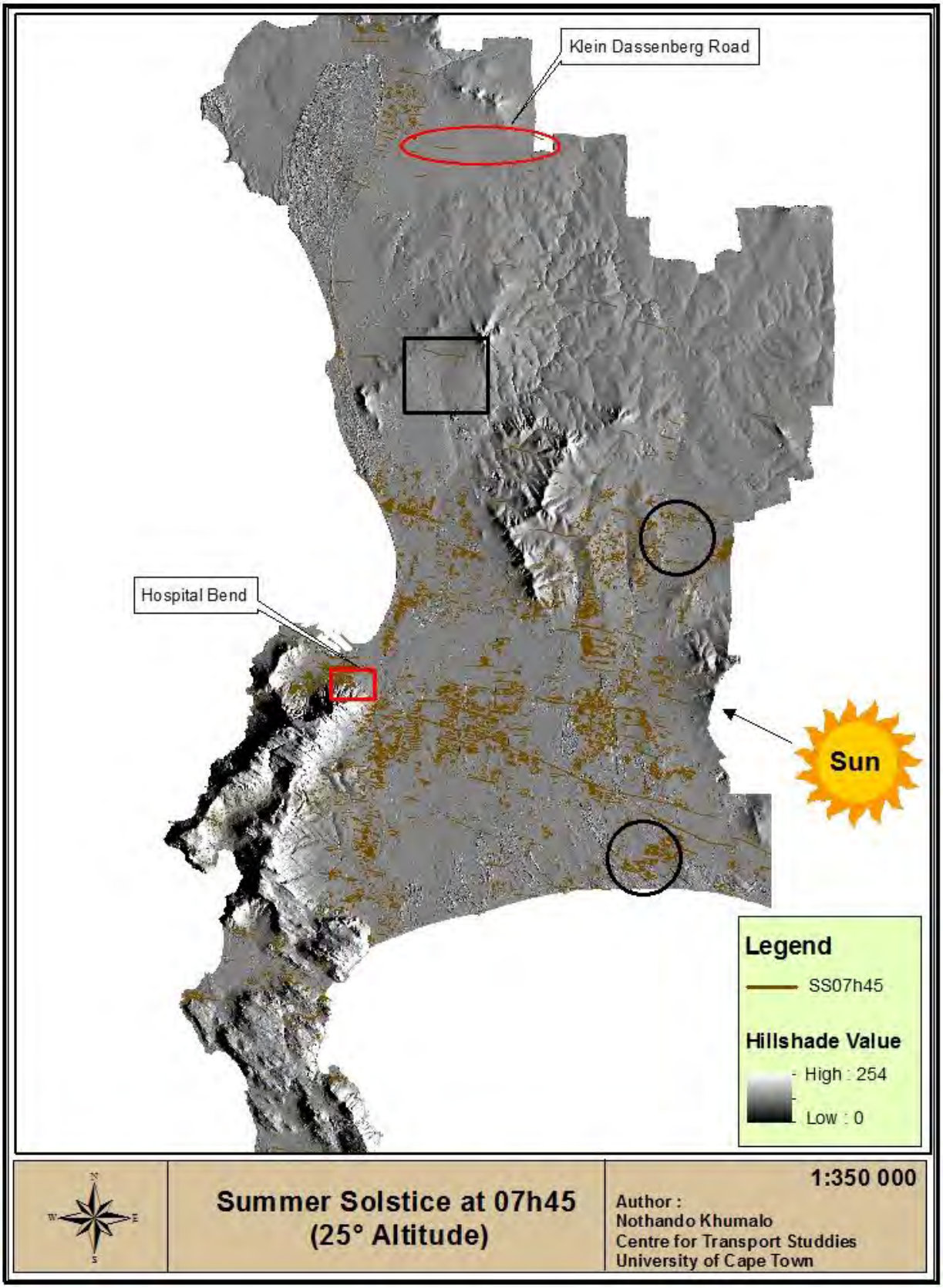

Figure 5-17: Road Segments Exposed to Direct Sunlight in the Summer Solstice at 07h45

5.1.4.2 Afternoon Period

a) Analysis of Quantitative Data

Compared to the 1 702km in the morning period, an average total of 2 293km road segments are exposed to direct sunlight in the afternoon period. These results imply that the exposure is greater in the afternoon compared to the morning period. In agreement, the results also indicate that more streets are exposed in the afternoon (8 826 streets on average), while less are exposed in the morning (7 972 streets on average). There is a significant difference of approximately 854 streets not exposed to the sun glare risk in the morning period. Table 5-24 gives values of the total road segment lengths exposed to direct sunlight, while Table 5-25 gives the total number of streets exposed in each length class.

Table 5-24: Road Segments Length Exposed to Direct Sunlight in the Summer Solstice PM

Summer Solstice - Afternoon					
SS18h10 (19°)			**SS17h45 (25°)**		
Length (km)	**Total Length (km)**	**Mean Length (km)**	**length (km)**	**Total Length (km)**	**Mean Length (km)**
0-1<	1466.5	0.2	0-1<	1511.7	0.2
1-2<	269.4	1.4	1-2<	286.3	1.4
2-3<	127.3	2.4	2-3<	122.3	2.4
3-4<	85.1	3.4	3-4<	86.7	3.5
4-5<	48.3	4.4	4-5<	71.1	4.4
5-6<	31.7	5.3	5-6<	32.3	5.4
6-7<	44.4	6.3	6-7<	19	6.3
7+	182.7	16.6	7+	200.3	15.4
Sum	**2255.4km**		**Sum**	**2329.7km**	
Min	**0.00015km (=0.15m)**		**Min**	**0.00001km (=0.01m)**	
Max	**44.5km**		**Max**	**42.1km**	

Table 5-25: Numbers of Roads Exposed to Direct Sunlight in the Summer Solstice PM

Summer Solstice - Afternoon			
SS18h10 (19°)		**SS17h45 (25°)**	
Length Class (km)	**No. of Streets Exposed to Direct Sunlight**	**Length Class (km)**	**No. of Streets Exposed to Direct Sunlight**
0-1<	8418	0-1<	8596
1-2<	199	1-2<	211
2-3<	53	2-3<	51
3-4<	25	3-4<	25
4-5<	11	4-5<	16
5-6<	6	5-6<	6
6-7<	7	6-7<	3
7+	11	7+	13
Sum	**8730**	**Sum**	**8921**

b) Map Analysis: Visual Interpretation

The summer solstice in this period also exhibits road segment orientation qualities dissimilar to those of the other three days, from the preceding sections. The road segments in this case are orientated towards the southwest direction, from the northeast, which is also directionally perpendicular to the morning period direction and that of the other days. Clockwise from the north, the segment slope is angled between 60° and 83° at 18h10 (19° altitude), and between 63° and 93° at 17h45 (25° altitude). With respect to the clockwise orientation from the north, the segments in the afternoon lean relatively more towards the north compared to the morning.

Regarding the magnitude of road segments in this period, it is apparent that there are more segments in the afternoon period than the morning period; meaning more roads are at risk in the afternoon period. Considering that the quantitative data in both periods revealed an increase in the total number of roads insulated in the afternoon, this is an expected deduction. Moreover, understandably so, there is also an increase in the number of streets affected in the Southern Peninsula and the east part of the Atlantic Seaboard. This can be accredited to the change in the direction of solar illumination, which in this case is insulating the west side of the Atlantic Seaboard, hence the increase in road segments. Last of all, with the aim to highlight any differences, Appendix C shows an overlay map of the two afternoon scenarios.

5.1.4.3 Statistical Comparison: Morning and Afternoon Period

The p-value for this test was 0.0221. Similar to the AE and SE, the p-value here also implies a significant difference in the median amount of average sunlight between AM and PM. However, the AE and SE have relatively stronger evidence considering that the evidence against the null hypothesis in favour of the alternative increases with a decreasing p-value. The sample data for this test and the results from the WSRT can be seen in Table 5-26 and 5-27.

Table 5-26: Summer Solstice Sample Data

Time	Frequency	Percentage	Cumulative Percentage
07h20	73	22.46	22.46
07h45	79	24.31	46.77
17h45	89	27.38	74.15
18h10	84	25.85	100.00
Total	**325**	**100.00**	

Table 5-27: Wilcoxon Signed-Rank Test

Sign	Observation	Sum Ranks	Expected
positive	20	555	850.5
Negative	34	1146	850.5
zero	4	10	10
all	**58**	**1711**	**1711**

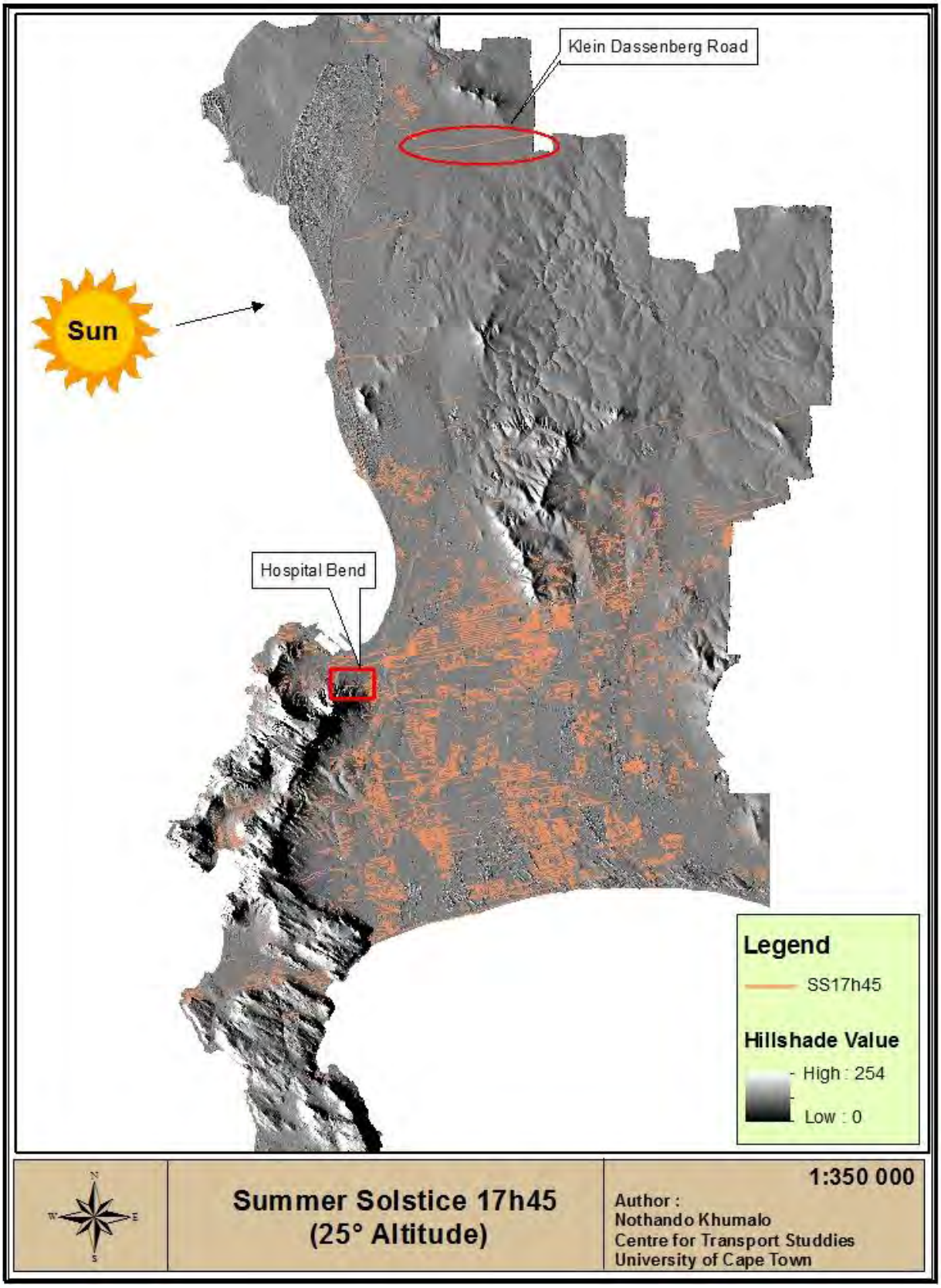

Figure 5-18: Road Segments Exposed to Direct Sunlight in the Summer Solstice at 17h45

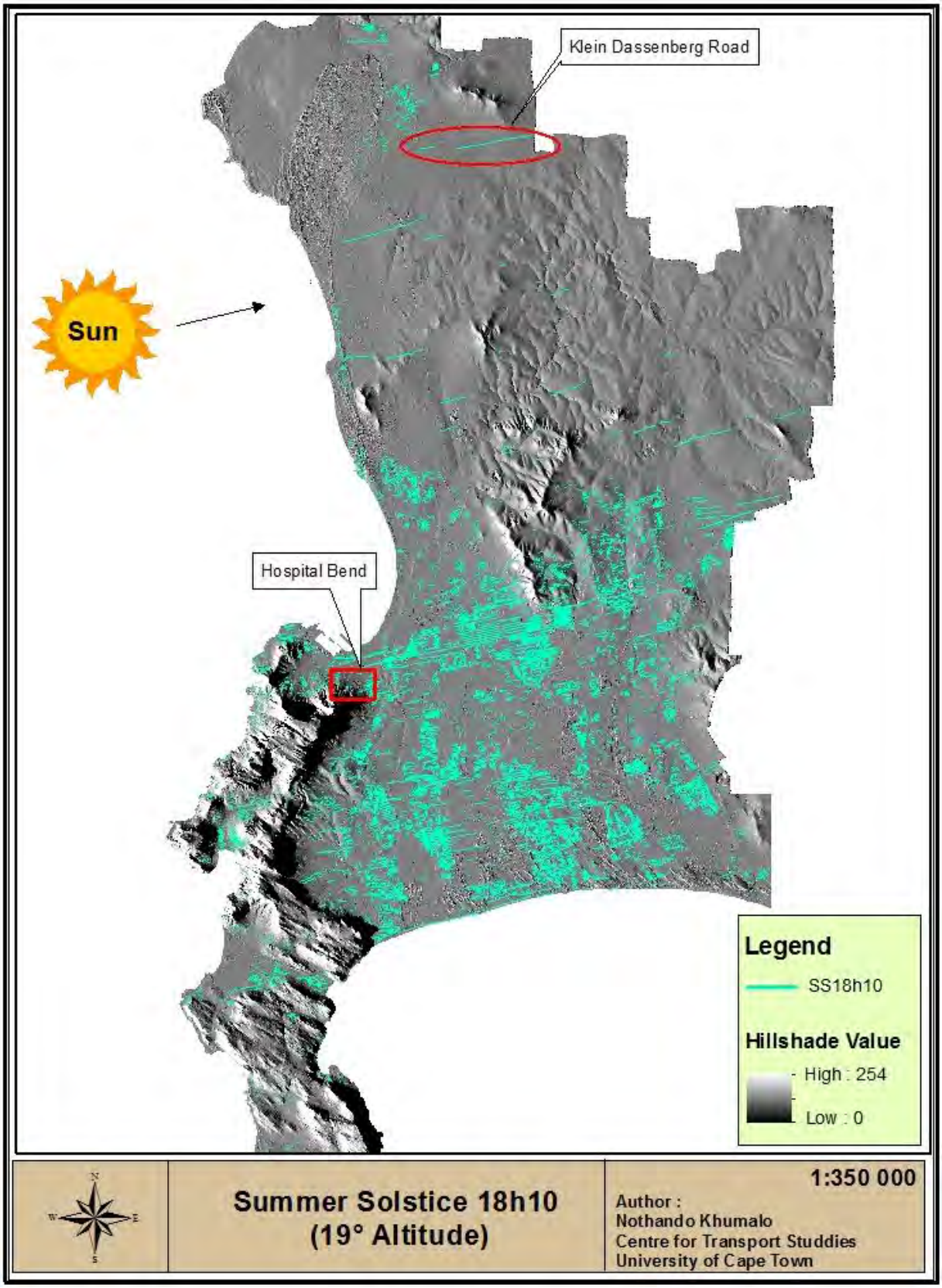

Figure 5-19: Road Segments Exposed to Direct Sunlight in the Summer Solstice at 18h10

5.1.5 Comparison of All Four Scenarios

Summer is the warmest season of the year, with long days and short nights. Winter on the other hand consists of the coldest months of the year, with short days and long nights. Autumn is a transition phase between summer and winter, while spring is a transitory season between winter and summer. In contrast to summer and winter, autumn and spring are not severe seasons, but simple transitory seasons as already stated. It, therefore, makes sense that visual interpretation of the autumn and spring results would appear very similar, as was observed in Sections 5.1.1 and 5.1.2. It is also expected that the winter season will have relatively fewer road segments exposed to direct sunlight, whilst the summer season gets more road segments as a result of the brighter sun and clear sky. Nevertheless, be it minor or major, there still were some differences between the four days. To characterise these differences in a more objective manner, this section first compares the glare window period of the four days, followed by a comparison of the quantitative data (exposed road segments lengths) and a visual interpretation of the maps, respectively. The section ends off with an overview of the statistical analysis results.

5.1.5.1 Comparison of Sun Glare Risk Window Period

In winter, the potent glare window occurs at a relatively much later time in the morning (between 09h55 and 10h35), while in the afternoon it occurs the earliest (between 15h00 and 15h40). This can be attributed to the winter having shorter days. On the contrary, because of the longer days, the identified risk period occurs much earlier in the summer morning, which in this case was between 07h20 and 07h45; and the latest in the afternoon (between 17h44 and 18h10). Autumn and spring on the other hand have more or less the same sun glare risk window period. In autumn this was between 08h30 and 08h55 in the morning, and between 16h55 and 17h20 in the afternoon. While in spring this occurred between 08h15 and 08h40 in the morning and between 16h40 and 17h05 in the afternoon.

Furthermore, with the exception of the winter solstice, it appears that there was a consistent 25min time gap in the glare window period for both the morning and afternoon pairs for each of the other three scenarios (see Table 5-1 for values and times). For example, when the solar altitude in the AE morning period changes from 19.9° at 08h30 to 24.8° at 08h55 it takes 25min, the same thing occurs in the afternoon. However, in the winter solstice the same angle change in

the morning and afternoon takes 40min, which is almost two times longer than the other three days. Based on the sun cone assumptions made in this study, this implies that the sun is at its most potent for only a period of 25min in the AE, SE and SS; and 40min in the WS. It should, however, be noted that this does not mean that glare is only likely to occur between these times; it can occur outside the defined sun cones. Nonetheless, the assumption here was that it is not as intense outside the defined times, but can still be the source of sun related problems.

5.1.5.2 Comparison of Quantitative Data

The total lengths of road segments at risk (exposed to direct sunlight) were all summed up for each of the 16 scenarios. This computation was split into two: there was one for all the streets in the City of Cape Town (ranging from residential streets to major roads) and one that only looked at the major roads (national roads, the freeway and dual carriageways (M-Roads)). Since the former consists of all the streets, this data was used for the quantitative analysis. The major roads data was mainly used to relay the different effects on individual streets, with respect to the direct sunlight exposure in each scenario.

The data for all the total road segment lengths exposed to direct sunlight for each of the scenarios was summarised in Table 5-28. This broke it up into the morning (am) and afternoon (pm) period for each day. The road network data consisted of a total of a total of 16 056 streets, whose road segments totalled up to 112 661km in length.

Table 5-28: Total Lengths and Percentages of Road Segments Exposed to Direct Sunlight

Astronomical Day	Time Period	Total Road Length Exposed to Sunlight					
		Distance in km			Percentage		
		19°	25°	Average	19°	25°	Average
Autumnal Equinox	am	24064	22452	**23258**	21.4	19.9	**20.6**
	pm	18104	16538	**17321**	16.1	14.7	**15.4**
Spring Equinox	am	24039	22605	**23322**	21.3	20.1	**20.7**
	pm	18113	16545	**17329**	16.1	14.7	**15.4**
Winter Solstice	am	15063	13748	**14406**	13.4	12.2	**12.8**
	pm	16134	17565	**16850**	14.3	15.6	**15.0**
Summer Solstice	am	17149	18110	**17629**	15.2	16.1	**15.6**
	pm	23321	24140	**23730**	20.7	21.4	**21.1**

A graphical comparison of the values in Table 5-28 is presented in Figure 5-20 and Figure 5-21, where it can be seen that the autumnal and spring equinox have the greatest road segment exposure in the morning, while the summer solstice has the greatest exposure in the afternoon. In spite of having a longer glare window (40min), it is not surprising to observe that the winter solstice has the least road segments (in length) exposed to direct sunlight in both the morning and afternoon period. Presumably, this is attributable to the winter season receiving relatively less sun and more cloud coverage; and also that the sun is much higher in the sky in winter compared to other days, as indicated by the altitude values in Table 5-1.

Another similarity which singles out the winter solstice was that the maximum road segment length exposed to direct sunlight ranged between 42km and 50km in the other 3 days (AE, SE and SS); while the range in the winter solstice was between 18km and 29km. These results imply that the three days have a relatively longer distance of vulnerability compared to the winter solstice, thus, making them a greater risk.

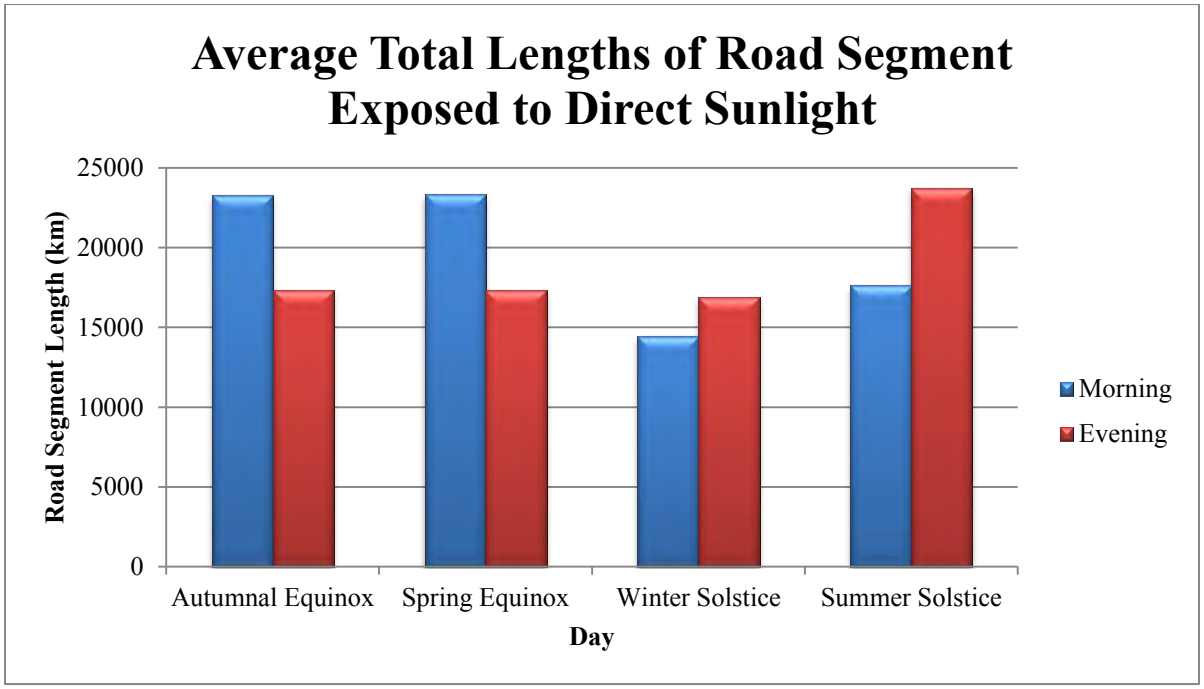

Figure 5-20: Graph of Average Total Lengths of Road Segments Exposed to Direct Sunlight

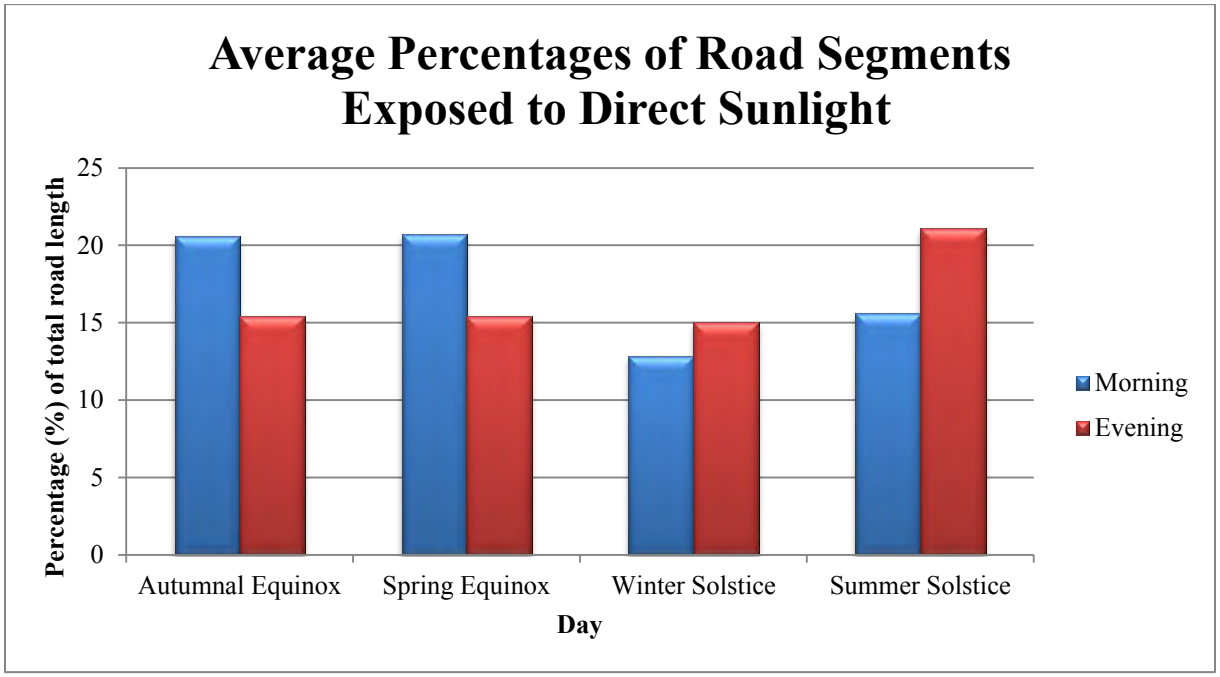

Figure 5-21: Average Percentages of Road Segments Exposed to Direct Sunlight

As mentioned in Section 5.1.1, in order to simplify the amount of data to be analysed the road segment lengths were grouped into eight classes as seen in Figure 5-21 and Figure 5-22. The assignment of data from the 16 time snapshots into each of these classes facilitated the comparison of outputs. It is apparent that for both outputs (19° snapshots in Figure 5-21 and 25° snapshots in Figure 5-22) more than half of the road segments were less than 1km. Considering that this data was obtained by summing up the lengths of all the road segments in each class, the disparity between the 0-1<km and 7+km classes implies that there were very few streets whose segment exposure totalled up to 7km and above. An average of 7 825 streets and 7 800 streets fall in the 0-1<km class in the morning and afternoon, respectively. This means that drivers have a larger risk to be surprised by sun glare regularly. Conversely, an average of 11 streets falls in the 7+km class in both the morning and afternoon period.

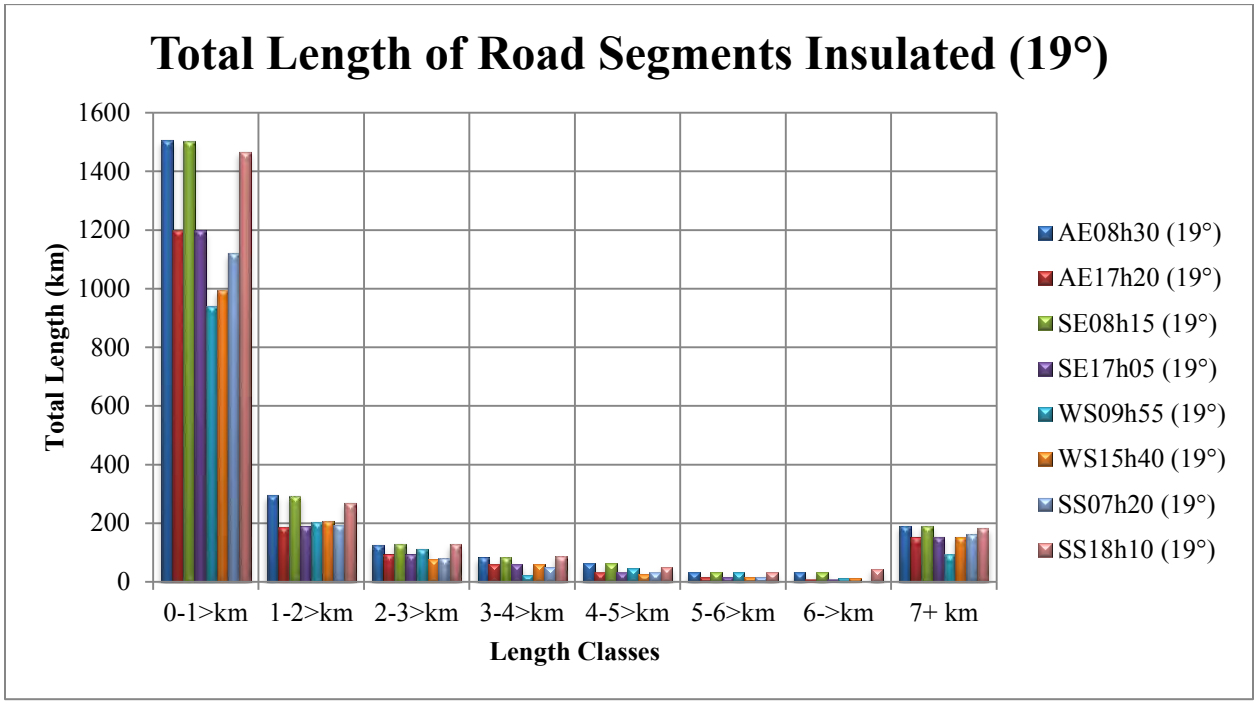

Figure 5-22: Total Lengths of Road Segments Insulated in 8 Length Groups for the 19° Altitude

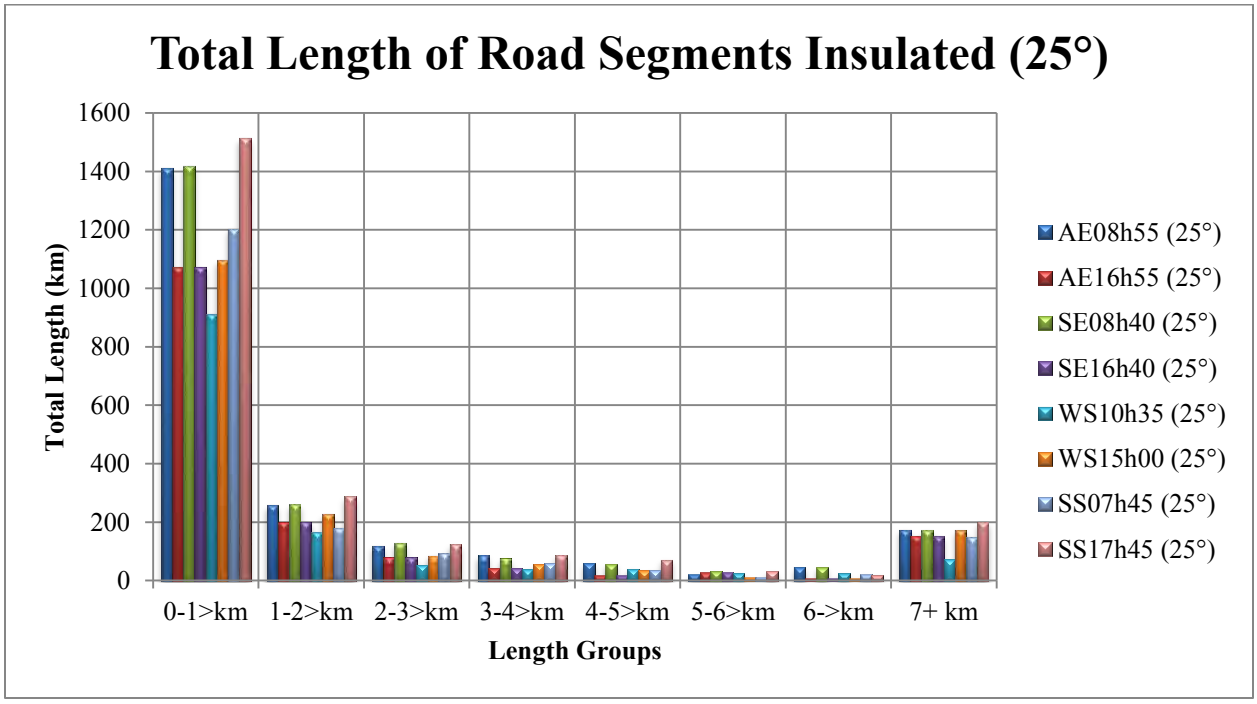

Figure 5-23: Total Lengths of Road Segments Insulated In 8 Length Groups for the 25° Altitude

Furthermore, there is a fair amount of road overlap in all 16 snapshots; meaning a number of roads are exposed to direct sunlight in more than one scenario, although there are very few roads affected in all 16 snapshots. Table 5-29 gives a summary of the top four roads which have the highest sum of road segment lengths exposed to direct sunlight in each snapshot. The N1 and N2 (national roads) are top of the list in a number of the scenarios in both the morning and afternoon periods, respectively. Conversely, the N2 has the maximum sum of road segment lengths in the morning of the summer solstice, and the N1 holds the same spot in the afternoon period. Among other things, this exchange is presumably an indicator of the change in the direction of the sun illumination. Furthermore, a number of other streets make an appearance in more than one scenario, as seen in Table 5-29. These include Voortrekker, Frans Conradie, Klipfontein, Settlers Way and Main Road.

It is, however, worth noting that it is illogical to use the total road segment lengths exposed to sunlight (in each road/street) as a basis for the ranking of sun glare hotspots in the city. Given the wide range of street/road lengths, this method produces an outcome that is biased against the lengthier roads, such as highways and arterials. For that reason, considering major roads only (i.e. Primary and Secondary Arterials, Expressways and Freeways), Table 5-30 gives a summary of the top four major roads which have the highest percentage of road segments exposed to direct sunlight in each snapshot. Similar to Table 5-29, most of the streets in Table 5-30 make an appearance in more than one scenario. For example, all the roads that appear in the two equinox days also appear in the summer solstice snapshots. Although it should be noted that, the roads that appear in the morning of the equinox days, appear in the evening snapshots of the summer solstice, the same switch applies to the equinox evening snapshots.

Table 5-29: Top Four Roads with the Highest Sum of Road Segment Lengths in Each Scenario

Day	Morning		Afternoon	
	Time	**Road Name**	**Time**	**Road Name**
Autumnal Equinox	08h30	1. N1 (43.8km) 2. Voortrekker (27.6km) 3. Frans Conradie (20.3km) 4. Baden Powell (18.3km)	16h55	1. N2 (50.1km) 2. Klipfontein (18.5km) 3. Settlers (16.9km) 4. Main (15.5km)
	08h55	1. N1 (44.4km) 2. Voortrekker (27.6km) 3. Frans Conradie (20.3km) 4. Spine (15.9km)	17h20	1. N2 (42.0km) 2. Settlers (20.7km) 3. Klipfontein (18.2km) 4. Stellenbosch (15.4km)
Spring Equinox	08h15	1. N1 (43.7km) 2. Voortrekker (27.6km) 3. Frans Conradie (20.3km) 4. Baden Powell (18.3km)	16h40	1. N2 (50.1km) 2. Klipfontein (18.5km) 3. Settlers (16.9km) 4. Main (15.5km)
	08h40	1. N1 (44.4km) 2. Voortrekker 27.4km) 3. Frans Conradie (20.3km) 4. Spine (16.1km)	17h05	1. N2 (42.0km) 2. Settlers (20.8km) 3. Klipfontein (18.2km) 4. Stellenbosch (15.4km)
Winter Solstice	09h55	1. N1 (23.3km) 2. Main (12.3km) 3. Marine (11.5km) 4. Robert Sobukwe (10.5km)	15h00	1. Van Riebeeck (25.8km) 2. West Coast (24.3km) 3. Main (19.0km) 4. N2 (14.3km)
	10h35	1. Koeberg (17.9km) 2. Main (13.2km) 3. Kuils River (12.0km) 4. N1 (10.4km)	15h40	1. N2 (28.8km) 2. Van Riebeeck (25.2km) 3. Old Main (17.7km) 4. Main (16.9km)
Summer Solstice	07h20	1. N2 (49.5km) 2. Settlers (21.3km) 3. Klipfontein (18.1km) 4. Stellenbosch (15.3km)	17h45	1. N1 (42.1km) 2. Voortrekker (27.7km) 3. Frans Conradie (20.3km) 4. Baden Powell (18.4km)
	07h45	1. N2 (41.6km) 2. Settlers(21.1km) 3. Klipfontein (18.2km) 4. Stellenbosch (15.5km)	18h10	1. N1 (44.5km) 2. Voortrekker (27.6km) 3. Frans Conradie (20.0km) 4. Baden Powell (17.6km)

Table 5-30: Top Four Roads with the Highest Percentage of Road Segments Directly Sunlit

Day	Morning		Afternoon	
	Time	**Major Road Name**	**Time**	**Major Road Name**
Autumnal Equinox	08h30	1. Avonwood Road (43.3%) 2. Avonwood Ave. (10.9%) 3. Station (10.3%) 4. Steenberg (8.2%)	16h55	1. Sable (20.2%) 2. Tokai (16.8%) 3. Constantia (11.6%) 4. Trovato Link (11.0%)
	08h55	1. Avonwood Road (43.3%) 2. Avonwood Ave. (10.9%) 3. Station (10.3%) 4. Hendrik Verwoed (5.3%)	17h20	1. Sable (20.2%) 2. Tokai (16.8%) 3. Constantia (14.5%) 4. Kendal (10.0%)
Spring Equinox	08h15	1. Avonwood Road (43.3%) 2. Avonwood Ave. (10.9%) 3. Station (10.3%) 4. Steenberg (8.2%)	16h40	1. Sable (20.2%) 2. Tokai (16.8%) 3. Constantia (11.6%) 4. Trovato Link (11.0%)
	08h40	1. Avonwood Road (43.3%) 2. Avonwood Ave. (10.9%) 3. Station (10.3%) 4. Hendrik Verwoed (5.3%)	17h05	1. Sable (20.2%) 2. Tokai (16.8%) 3. Constantia (14.5%) 4. Kendal (10.0%)
Winter Solstice	09h55	1. Paarden Eiland (16.5%) 2. Newlands Avenue (10.8%) 3. De Villiers (10.6%) 4. Boyes Drive (10.2%)	15h00	1. Lower Main (61.6%) 2. De Waal Drive (37.2%) 3. Brackenfell Blvd. (12.5%) 4. Newlands (9.9%)
	10h35	1. Newway (38.8%) 2. Paarden Eiland (16.5%) 3. Protea (11.0%) 4. Sir Lowr's (9.5%)	15h40	1. De Waal Drive (37.2%) 2. Section Street (23.8%) 3. Brackenfell Blvd. (11.5%) 4. Newlands (10.3%)
Summer Solstice	07h20	1. Sable (20.2%) 2. Tokai (16.8%) 3. Constantia (14.5%) 4. Kendal (10.0%)	17h45	1. Avonwood Road (43.3%) 2. Avonwood Ave. (10.9%) 3. Station (9.8%) 4. Steenberg (8.2%)
	07h45	1. Sable (20.2%) 2. Tokai (16.8%) 3. Constantia (14.5%) 4. Kendal (10.0%)	18h10	1. Avonwood Road (43.3%) 2. Avonwood Ave. (10.9%) 3. Station (10.3%) 4. Hendrik Verwoed (5.3%)

According to the values presented Table 5-31 over half of the streets in Cape Town have a certain portion of their segments exposed to direct sunlight in the autumnal and spring equinox morning period. Although, it should be noted these values don't indicate the degree of exposure in the individual roads. The same observation was made in the afternoon period for the 19° altitude. The values in the 25° altitude on the other hand, indicate a decrease slightly below 50%. Nonetheless, there still is a significant percentage of streets at risk in both scenarios. The winter and summer solstice exhibit insignificantly different changes and values to those of the autumnal and spring equinox. The percentages of streets affected in the winter solstice in both periods are slightly below 50%, with an average of 45% and 47% in the morning and afternoon period, respectively. With the exception of the 19° altitude value, the summer solstice values are also slightly above 50%, as can be seen in Table 5-31 and 5-31.

In comparing the morning and afternoon period percentage values, the apparent trend is a decrease from the morning to the afternoon period in the autumnal and spring equinox, and an increase for the same change in the winter and summer solstice. For example, at 25° altitude, the percentage of roads in the autumnal equinox changes from 53.3% in the morning to 47.6% in the afternoon. At the same altitude the percentage of roads at risk in the summer solstice increases from 50.9% in the morning period to 55.6% in the afternoon period. Presumably this implies that the solar illumination in the afternoon period of the winter and summer solstice has a relatively greater effect than the morning period, which means the opposite applies to the autumnal and spring equinox. Figure 5-24 presents a graphical comparison of the average changes in the percentages between the morning and afternoon period in the four days.

Table 5-31: Total Number and Percentage of Roads Affected in Each Day for the AM Period

Morning Period				
Day	**19° Altitude**		**25° Altitude**	
	Total No. of roads affected	**% of total roads in CoCT**	**Total No. of roads affected**	**% of total roads in CoCT**
Atumnal Equinox	8896	55.4%	8554	53.3%
Spring Equinox	8901	55.4%	8607	53.6%
Winter Solstice	7225	45.0%	7152	44.5%
Summer Solstice	7767	48.4%	8176	50.9%

Table 5-32: Total Number and Percentage of Roads Affected in Each Day for the PM Period

Afternoon Period				
Day	19° Altitude		25° Altitude	
	Total No. of roads affected	% of total roads in CoCT	Total No. of roads affected	% of total roads in CoCT
Atumnal Equinox	8129	50.6%	7646	47.6%
Spring Equinox	8135	50.7%	7651	47.7%
Winter Solstice	7345	45.7%	7795	48.5%
Summer Solstice	8730	54.4%	8921	55.6%

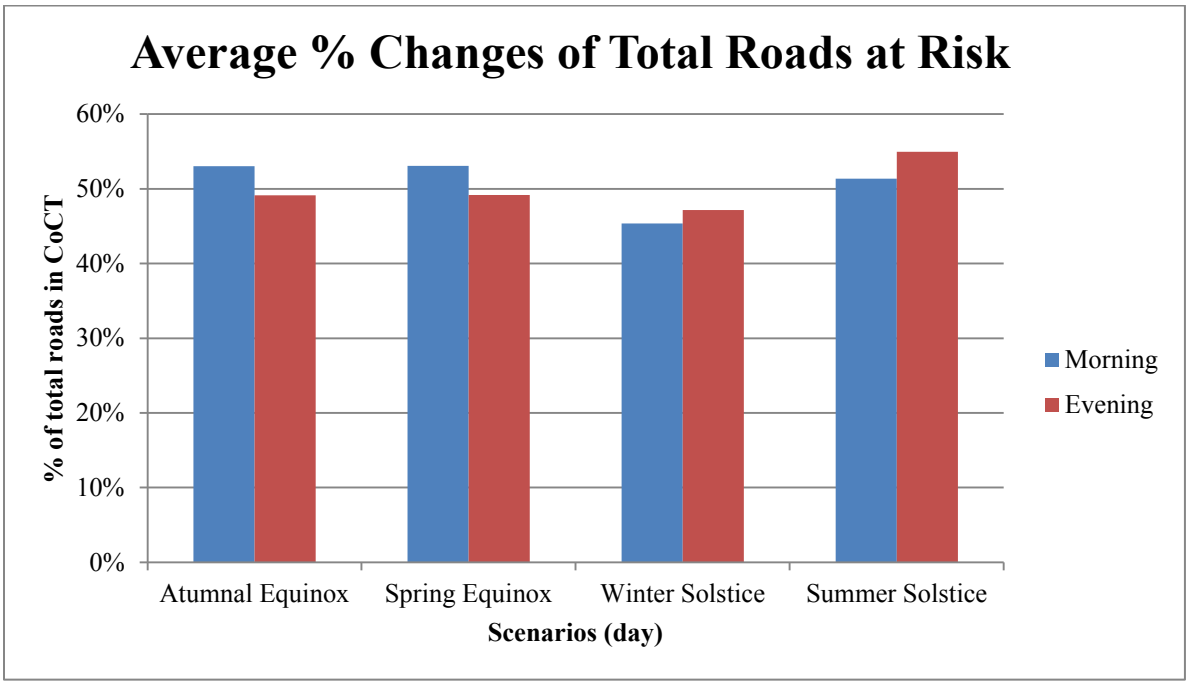

Figure 5-24: Graphical Comparison of Average % Changes of Total Roads at Risk

5.1.5.3 Comparison of Map Analysis (Visual Interpretation)

In order to closely examine the features of the 16 ArcGIS maps already presented in Sections 5.1.1 to 5.1.3, shaded relief images for two smaller areas were prepared. The areas are marked in the respective maps in Sections 5.1.1 to 5.1.4. The first mark, in the red ellipse, is Klein Dassenberg Road, and the second mark, in the red square, is a magnification of the roads surrounding hospital bend. The main purpose of this section was to give a general idea of the minor and major differences between the 16 scenarios.

The following tables give an overview of the road segment orientation and slope in each scenario, which have already been discussed in the preceding sections (5.1.1 to 5.1.4). The information in Table 5-33 and 5-33 will facilitate the discussions to follow.

Table 5-33: Cardinal Directions of Road Segments in Each Day for the Morning Period

Season (day)	Morning	Approx. Road Segment Direction (Angle from clockwise North)	
		19°	25°
Autumnal Equinox	Southwest to Northeast	60° – 90° (08h30)	59° – 83° (08h55)
Spring Equinox	Southwest to Northeast	63° – 90° (08h15)	57° – 83° (08h40)
Winter Solstice	Southwest to Northeast	44° – 56° (09h55)	20° – 48° (10h35)
Summer Solstice	Northwest to Southeast	92° – 120° (07h20)	88° – 110° (07h45)

Table 5-34: Cardinal Directions of Road Segments in Each Day for the Afternoon Period

Season (day)	Afternoon	Approx. Road Segment Direction (Angle from clockwise North)	
		19°	25°
Autumnal Equinox	Southeast to Northwest	88° – 113° (17h20)	95° – 120° (16h55)
Spring Equinox	Southeast to Northwest	88° – 113° (17h05)	92° – 120° (16h40)
Winter Solstice	Southeast to Northwest	125° – 153° (15h40)	143° – 160° (15h00)
Summer Solstice	Northeast to Southwest	60° – 83° (18h10)	63° – 93° (17h45)

a) Zooming into Klein Dassenberg Road

In the autumn and spring maps in Section 5.1.1 and Section 5.1.2, it is apparent that there is little variation in the road segment distribution for both morning and afternoon period. This is most likely attributable to the similar sun conditions in both seasons. Nevertheless, there are still small differences between the two, which are indicative of the variation in degree/angle of exposure, meaning the bearing variation of roads affected in each scenario.

To illustrate some of these differences, a red ellipse was used in all the maps, in Sections 5.1.1 to 5.1.4, to single out two segments that have much more noticeable differences in all the scenarios (see maps in these sections). Comparing these two segments in the autumnal and spring equinox, it is clear that the segments in both scenarios have more or less the same slope (81.1° from the north point; southwest to northeast direction). However, there is an apparent difference in the gap

between the two segments. The autumnal equinox segments have a much smaller gap compared to those of the spring equinox. The two segments in both maps form part of a road called Klein Dassenberg road (as labelled in all the maps). A total length of 7.7km of Klein Dassenberg road is exposed to direct sunlight in the AE, while 6.6km is exposed in the SE. As indicated in the methodology, road networks are formed of multiple segments joined together at vertices, which were split in the data processing phase to form straight line segments with constant geometry. Klein Dassenberg road was, therefore, split into a number of segments defined by a variety of bearings, which explains the gap variation between the two maps - some of the segments affected in the AE were not in the SE. These observations also apply for the afternoon period.

On the contrary, Klein Dassenberg road was not exposed to any direct sunlight in the winter solstice, which is presumably a result of the differences in the direction of road segments in each scenario (see Table 5-33 for segment directions). The summer solstice, on the other hand, does affect a portion of Klein Dassenberg road, however, not as long (length) as the ones in the autumnal and spring equinox. Only 8.9m of the road is affected in the summer solstice, which means one of the many split segments in this road has a bearing similar to the segments affected on this day. In general, there have been other minor differences observed and these can be clearly seen in the overlay maps in Appendices B to D.

b) Zooming into the Hospital Bend Area

For further comparison of the differences and similarities in the map outputs, the area surrounding hospital bend (intersection of De Waal drive and Settlers Way in the west of side of CoCT) was magnified and compared. A pictorial comparison of this enlarged area, in all the scenarios, can be observed in Figure 5-25 to 5-32 in the morning period discussion and Figure 5-33 to 5-40 in the afternoon period discussion. The following paragraphs give a comparison of the snapshots in the morning and afternoon, respectively.

i. Morning Period

From Figure 5-25 to 5-26 and Figure 5-27 to 5-28 it is apparent that the autumnal and spring equinox have a very similar distribution of road segments around hospital bend, any differences don't appear to be significant ones. Conversely, the winter and summer solstice have

significantly few segments around this area. The hillshade values around the two illuminated segments in De Waal Drive (marked X in red) are approximately 172 (at 08h30) and 182 (at 08h55) for the autumnal equniox. The values are more or less the same for the spring equinox, with 174 at 08h15 and 183 at 08h40.

The summer soltice consists of hillshade values about 145 at 07h20 and 149 at 07h45, which appear to be much lower values than the other days. This implies that there was relatively less illumination in this area of Cape Town on this day/season, although it does not necessarily mean that glare doesn't occur as you can see the segments in Figure 5-31 to 5-32. The winter solstice exhibits the following hillshade values: about 195 at 09h55 and 197 at 10h35, which appears to be brighter than all the other days. This would be expected because the glare window in the winter solstice occurs much later in the morning, when it is much brighter. Given that the hillshade scale is in the form of a gradient, even small areas such as the one around hospital bend have a wide range of values. The values above simply give an idea of a range of values in that one particular area.

Autumnal Equinox

Figure 5-25: Autumnal Equinox at 08h30

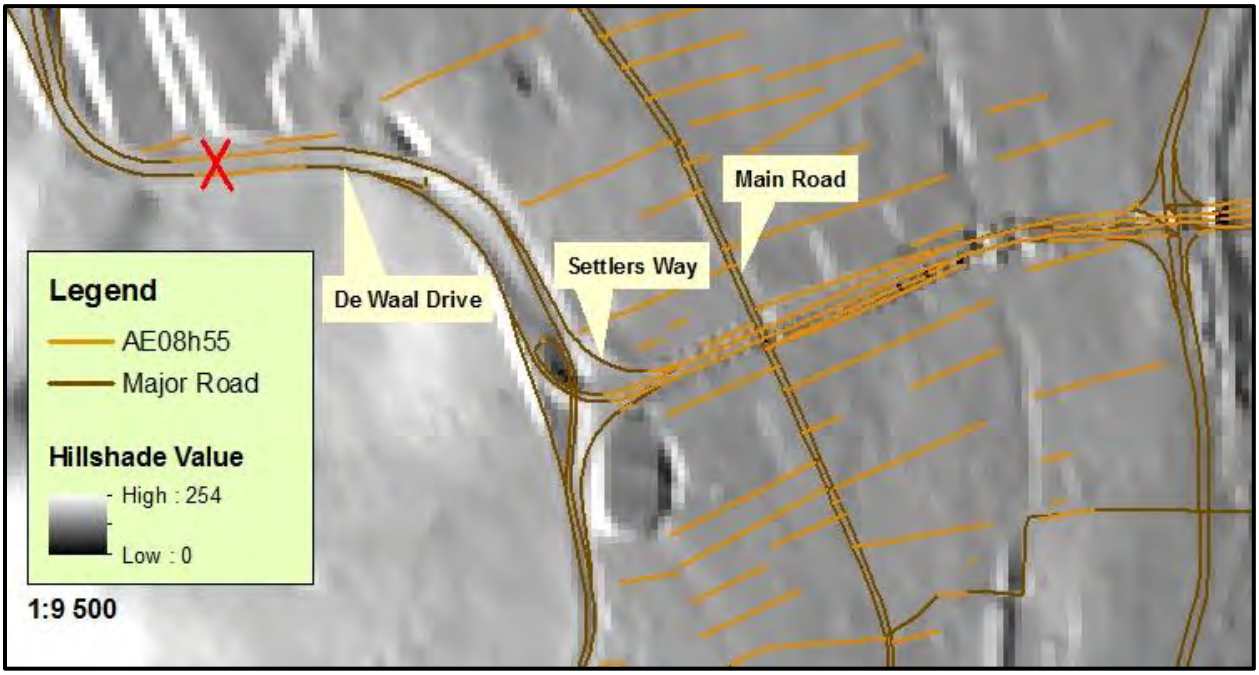

Figure 5-26: Autumnal Equinox at 08h55

Spring Equinox

Figure 5-27: Spring Equinox at 08h15

Figure 5-28: Spring Equinox at 08h40

Winter Solstice

Figure 5-29: Winter Solstice at 09h55

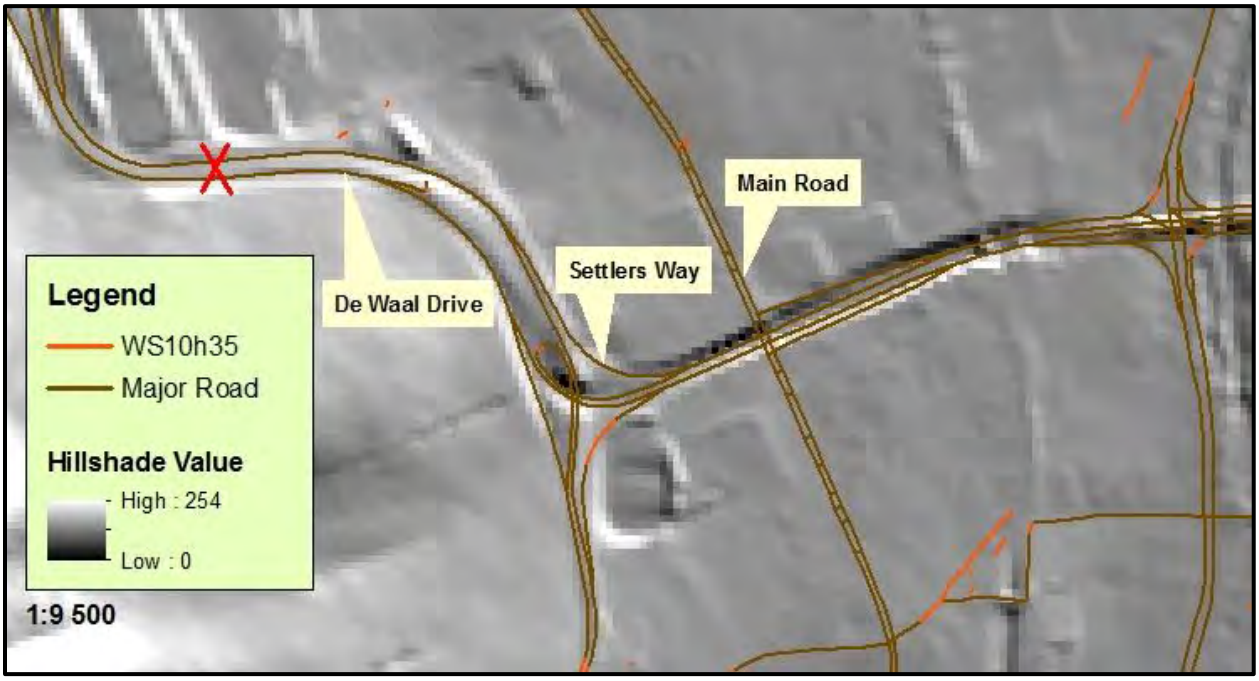

Figure 5-30: Winter Solstice at 10h35

Summer Solstice

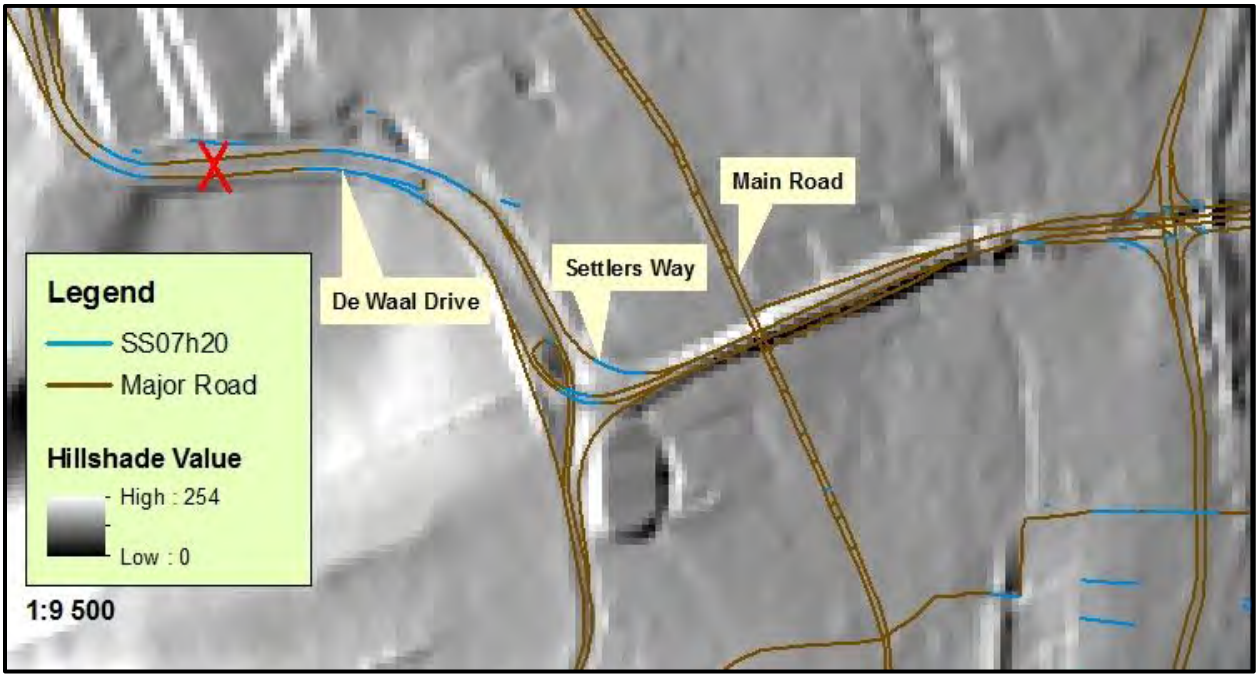

Figure 5-31: Summer Solstice at 07h20

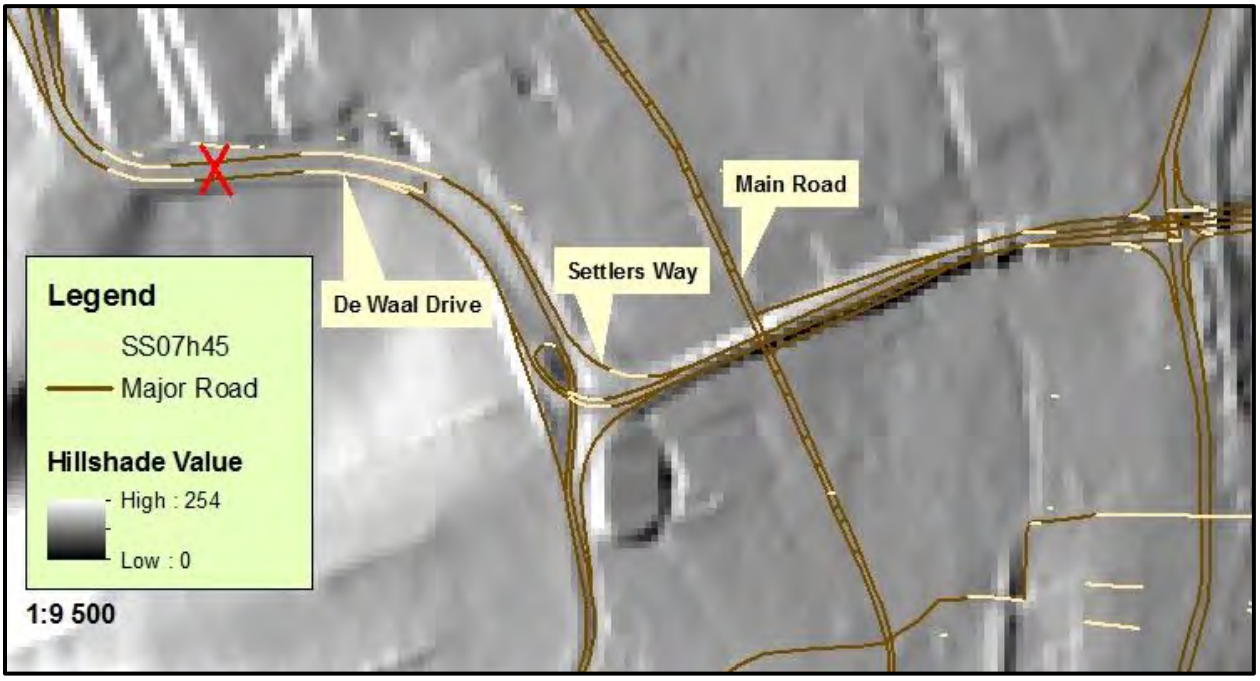

Figure 5-32: Summer Solstice at 07h45

ii. Afternoon Period

Similar to the morning period, the AE and SE still have comparable road segment distribution in the afternoon period as well, with no apparent significant differences. The winter and summer solstice, on the other hand, both comprise of segments with a completely different direction from any of the other snapshots. The segments in the WS intersect all three roads, although only a very small portion of Settlers Way is intersected since it changes direction after hospital bend, towards the east. Earlier in the sun glare window (at 15h00) most of main road is exposed to direct sunlight, compared to the later snapshot at 15h40. There are also more affected segments at 15h00 than at 15h40, which is expected because the sun is actually approaching the immediate horizon at this time, getting lower in the sky (decreasing in altitude).

Considering the direction of the road segments in the summer solstice, no part of Main road is exposed to direct sunlight. However, the road segments intersecting Main road are vulnerable to sun glare. There is an insignificant difference between the segments at 17h45 and 18h45. However, it is surprising to observe that the segment in the red ellipse in Figure 5-39 and 5-40 is much shorter at 17h45 and much longer at 18h10. Given that the expectation would be shorter

and less segments with change in time in the afternoon, a possible explaination for this would simply be that as the sun gets lower in the sky it becomes a greater risk.

Together with sections of De Waal and Settlers Way, a number of streets near Settlers Way (with the same direction) are at sun glare risk in the morning, while there are significantly less road segments at risk in the afternoon. Alternatively, the winter and summer solstice have more road segments exposed to direct sunlight in the afternoon than in the morning. All in all, this is a further indicator of the differences in sun position and illumination in all four days.

One does not need to obtain hillshade illumination values to conclude, based on the observation in the figures, that the afternoon period experiences significantly less illumination than the morning period – as evidenced by the images from Figure 5-33 to 5-40. Nonetheless, the hillshade values in the AE are around 121 at 16h55 and 123 at 17h20. While those of the SE are around 125 at 16h40 and 119 at 17h05. The winter solstice values range around 170 at 15h00 and 166 at 15h40. The summer solstice appears to have the least illumination of all in the afternoon, with values ranging around 88 at 17h45 and 83 at 18h10.

Autumnal Equinox

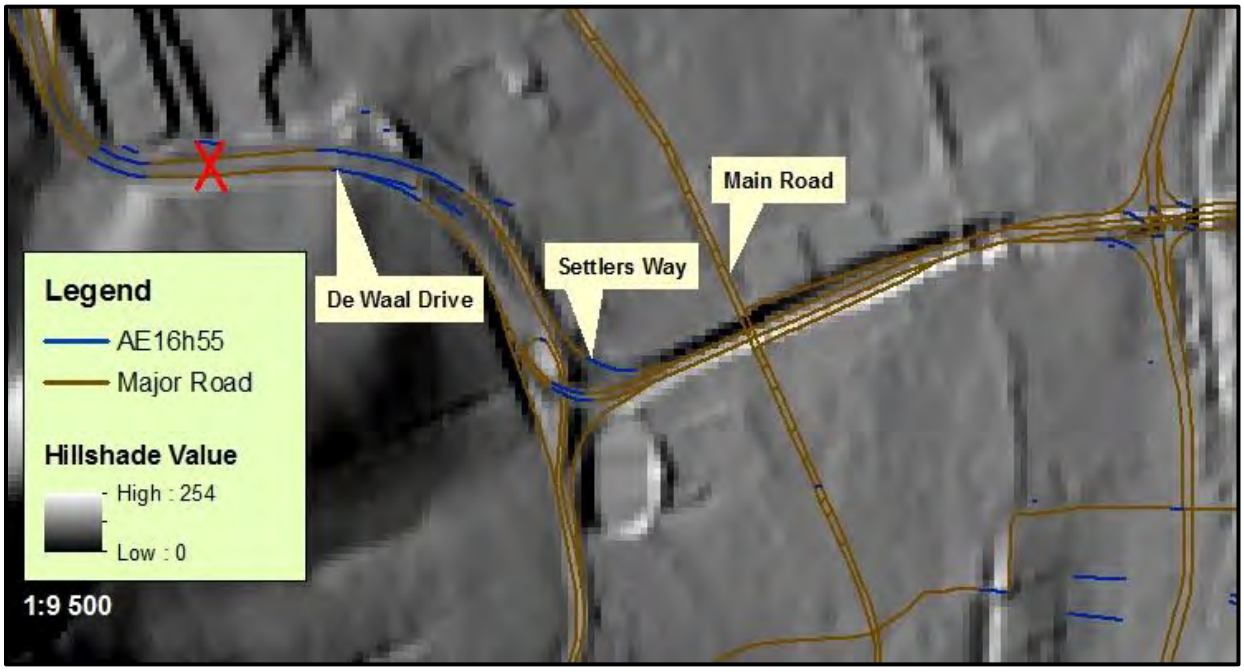

Figure 5-33: Autumnal Equinox at 16h55

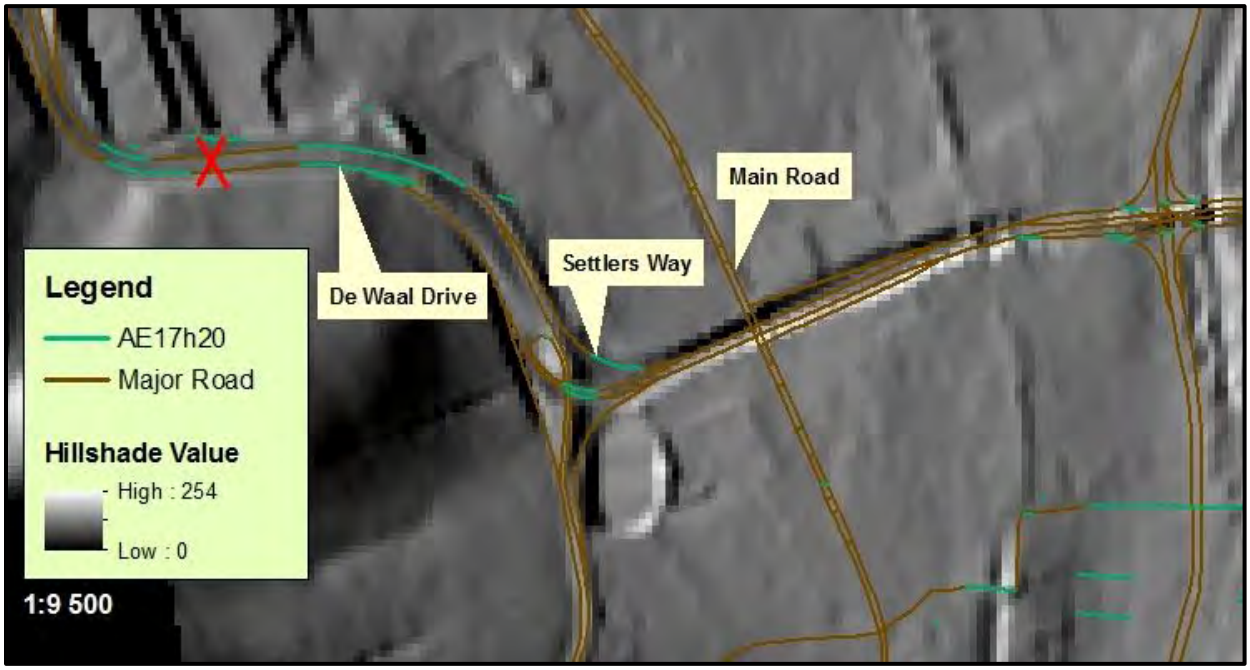

Figure 5-34: Autumnal Equinox at 17h20

Spring Equinox

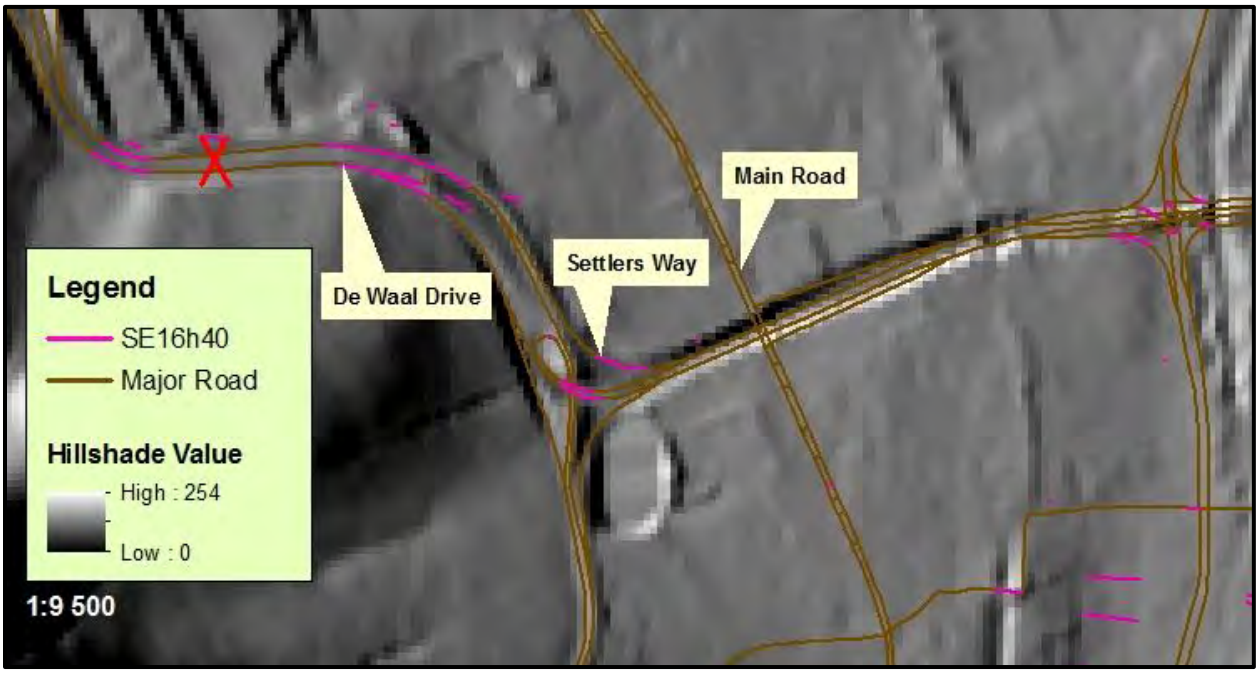

Figure 5-35: Spring Equinox at 16h40

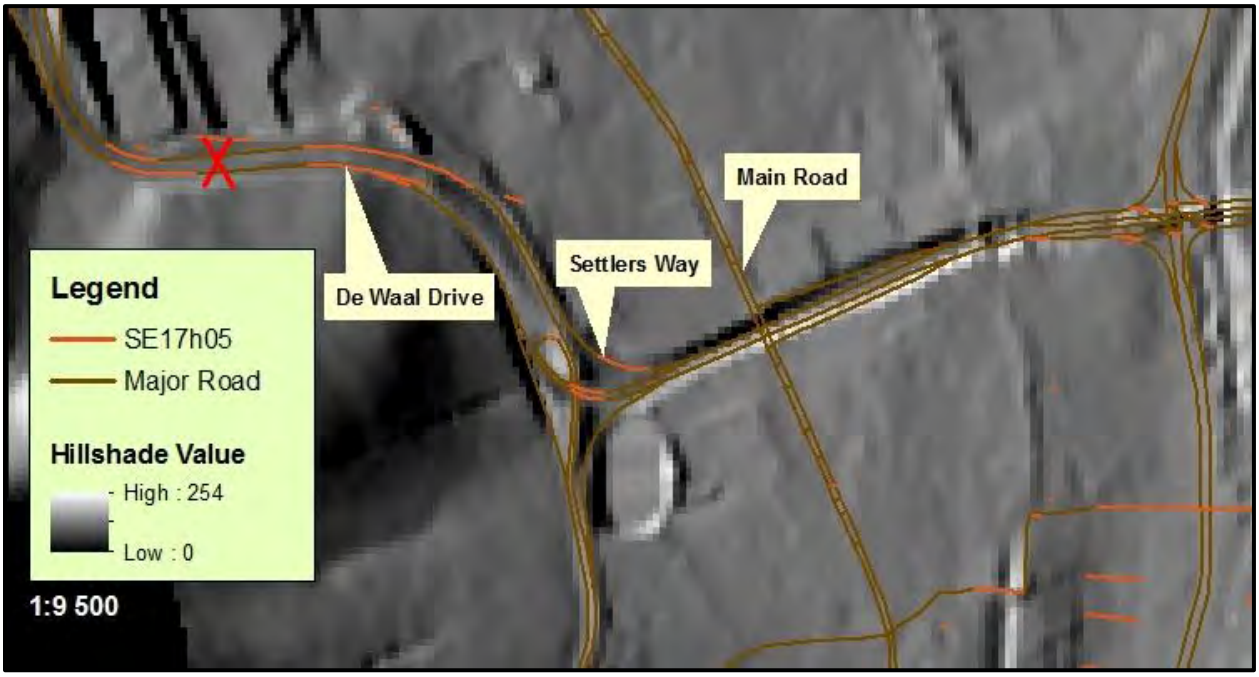

Figure 5-36: Spring Equinox at 17h05

Winter Solstice

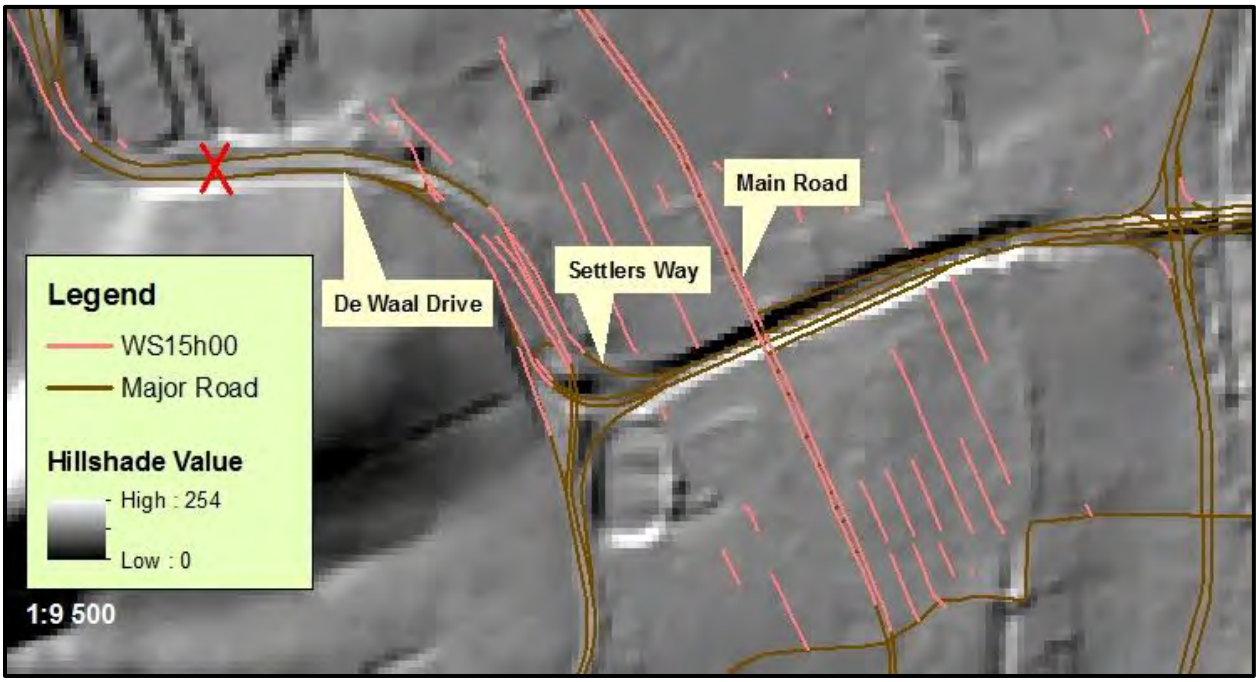

Figure 5-37: Winter Solstice at 15h00

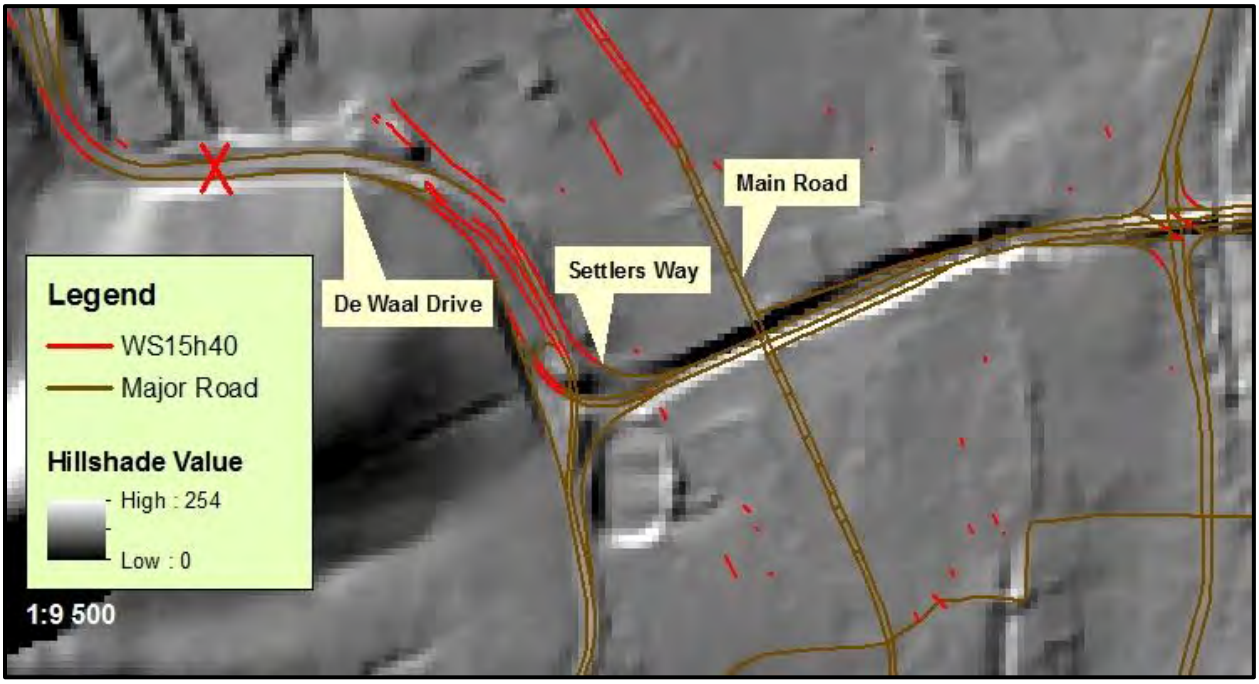

Figure 5-38: Winter Solstice at 15h40

Summer Solstice

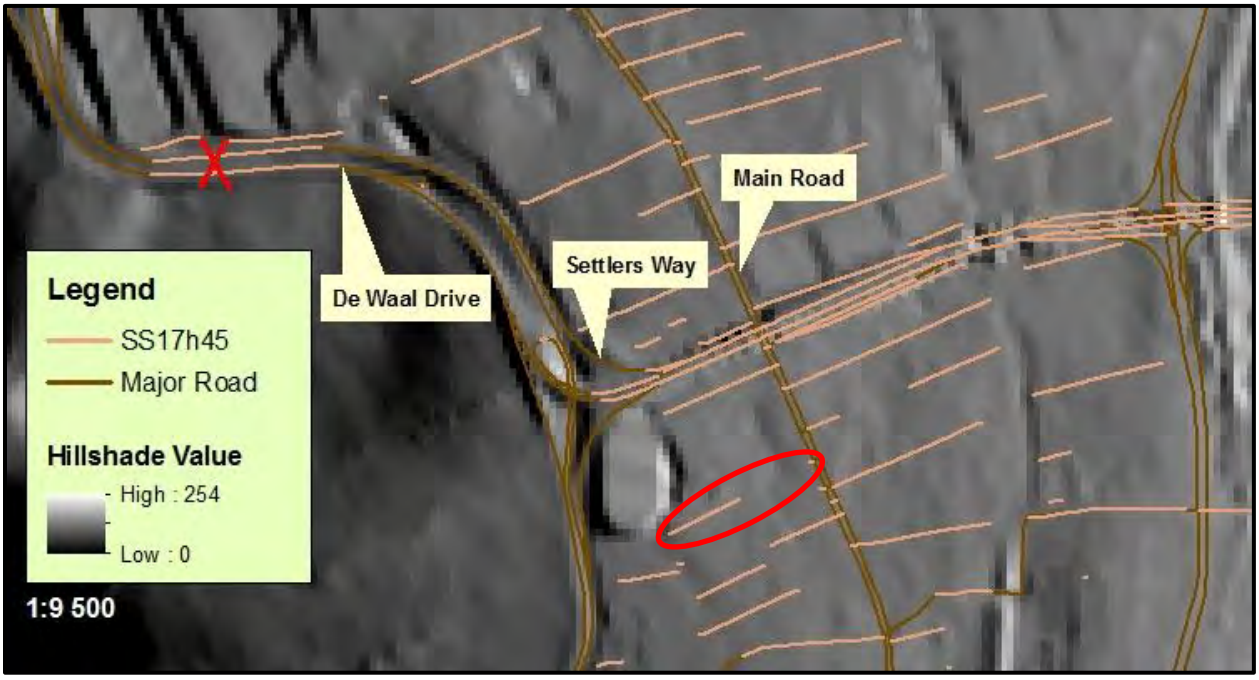

Figure 5-39: Summer Solstice at 17h45

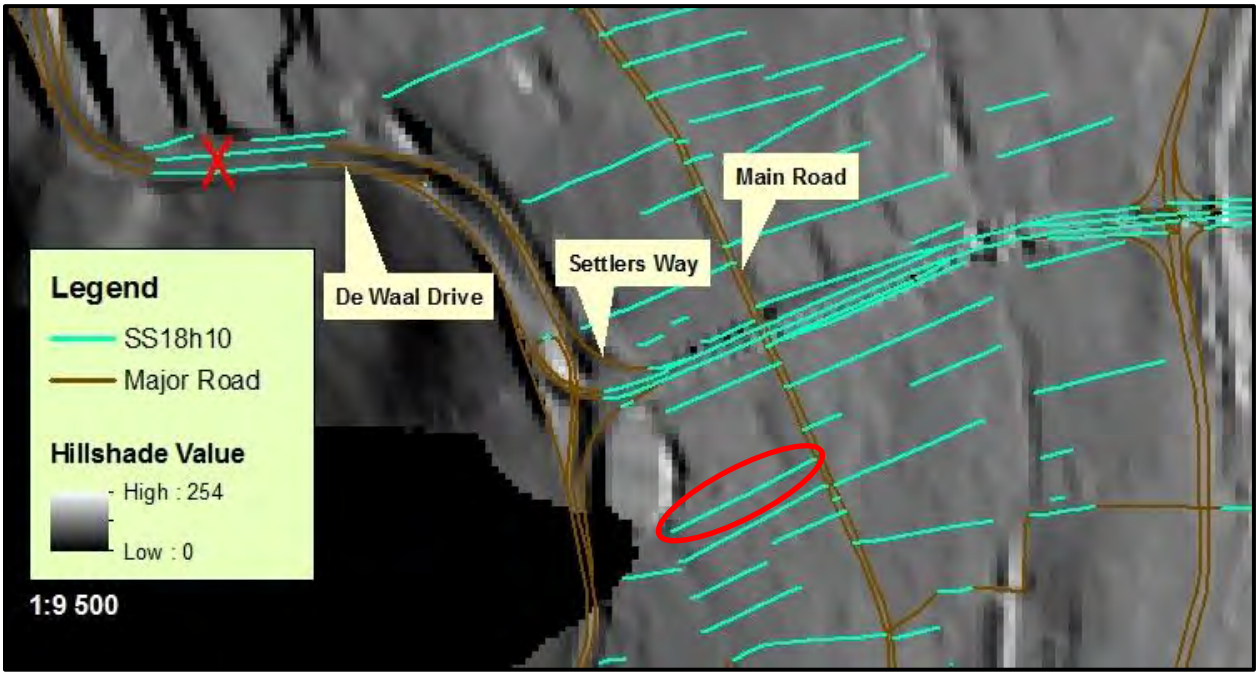

Figure 5-40: Summer Solstice at 18h10

5.1.5.4 Statistical Comparison: All Days and Times

a) Per day analysis: comparing all four times

The Friedman test was used to carry out an analysis of each day, comparing the four different times (two AM times and two PM times). The Friedman test is a non-parametric equivalent of the so-called ANOVA test. It tests if there is a significant difference in the median sunlight levels between the four time periods on any given day. The results can be seen in Table 5-35.

Table 5-35: Friedman Test Results

Percentage	Friedman test stat	p-value
AE	75.25	0.002
SE	75.25	0.002
SS	89.50	<0.001
WS	47.17	0.018

All the p-values for each day are significant, indicating a significant difference in percentage sunlight exposure between the different times of day, when each day is considered separately.

b) Over all days and times analysis: comparing morning and afternoon and all four days, across all streets

A linear mixed-effects model was executed to compare across all four days and the two time periods simultaneously. The streets were modelled as random effects as there are multiple measurements per street. AM and PM were also interacted with day to see if there is an effect. The output for this model can be seen in Table 5-36. The reference category is AE in the AM.

Table 5-36: Linear Mixed Effects Model

Linear Mixed effects model			
Percentage	**Effect size**	**Standard Error**	**p-value**
SE	-0.16	1.86	0.933
SS	-11.15	2.05	<0.001
WS	-10.10	2.22	<0.001
PM	-11.32	2.05	<0.001
SE:PM	0.16	2.72	0.954
SS:PM	22.32	3.06	<0.001
WS:PM	11.75	3.16	<0.001
Constant	53.90	3.04	<0.001
Standard deviations			
Between-street		0.32	
within-street/error		0.17	

The output reveals that, on average, there is less sunlight in the afternoon compared to the morning, as the effect of PM is negative and statistically significan (see box and whisker plot in Figure 5-41).

The main effects of SE, SS and WS were not interpreted seeing as the interactions are all statistically significant. However, it is evident in Figure 5-42 that they all have less sunshine than AE.

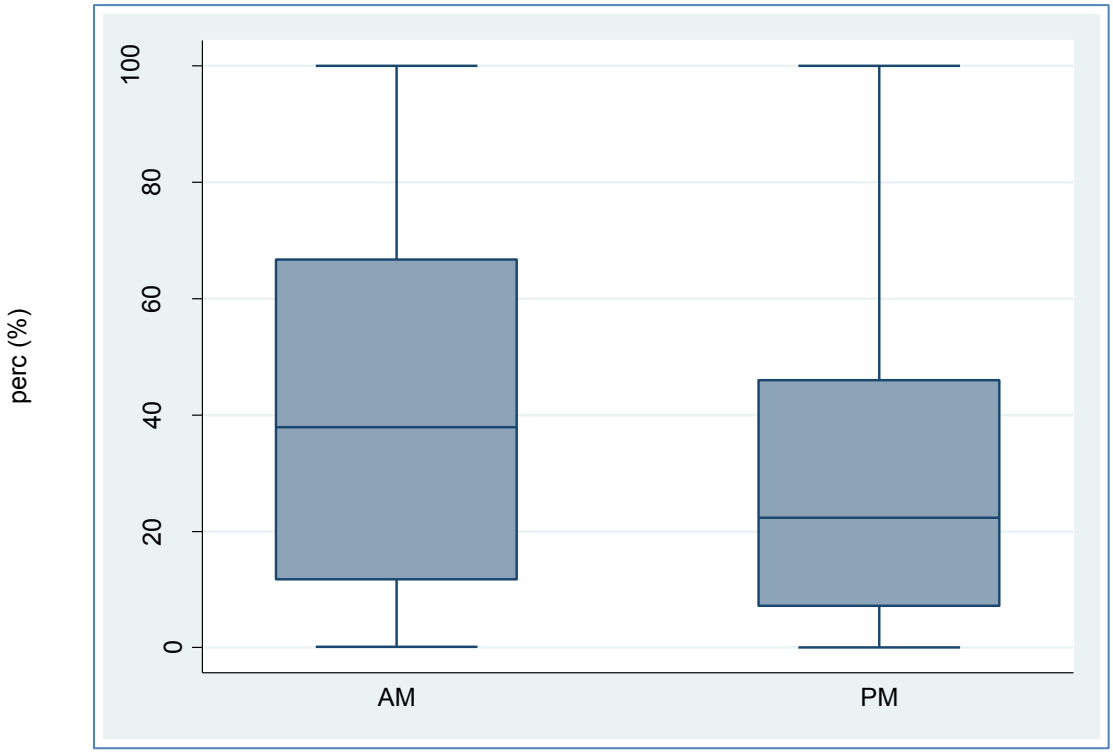

Figure 5-41: Box and Whisker Plot for Interactions Between AM and PM

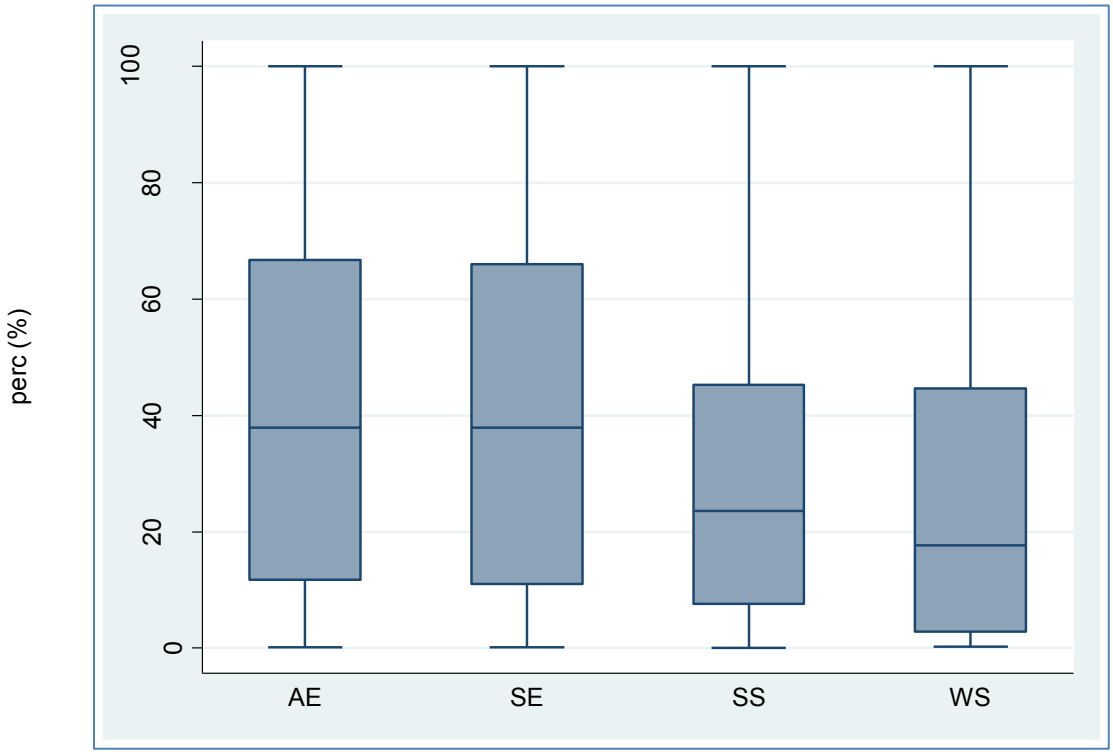

Figure 5-42: Box and Whisker Plot for Interactions Between the Four Days

With regards to the other interactions, for SE:PM the p-value (0.954) is not statistically significant so the effect size was not interpreted. Conversely, for SS:PM and WS:PM, the effect size was positive indicating more sunshine in the afternoons compared to the morning on these days, as well as more sunshine compared to the afternoon of AE. The graph in Figure 5-43 illustrates all the interactions between the four days for the AM and PM periods. In addition, a standard deviation of the two random effects produces a $(0.32)^2$ between-street variance and $(0.17)^2$ within-street variance; meaning that, together, they explain 13% of the variation in the data.

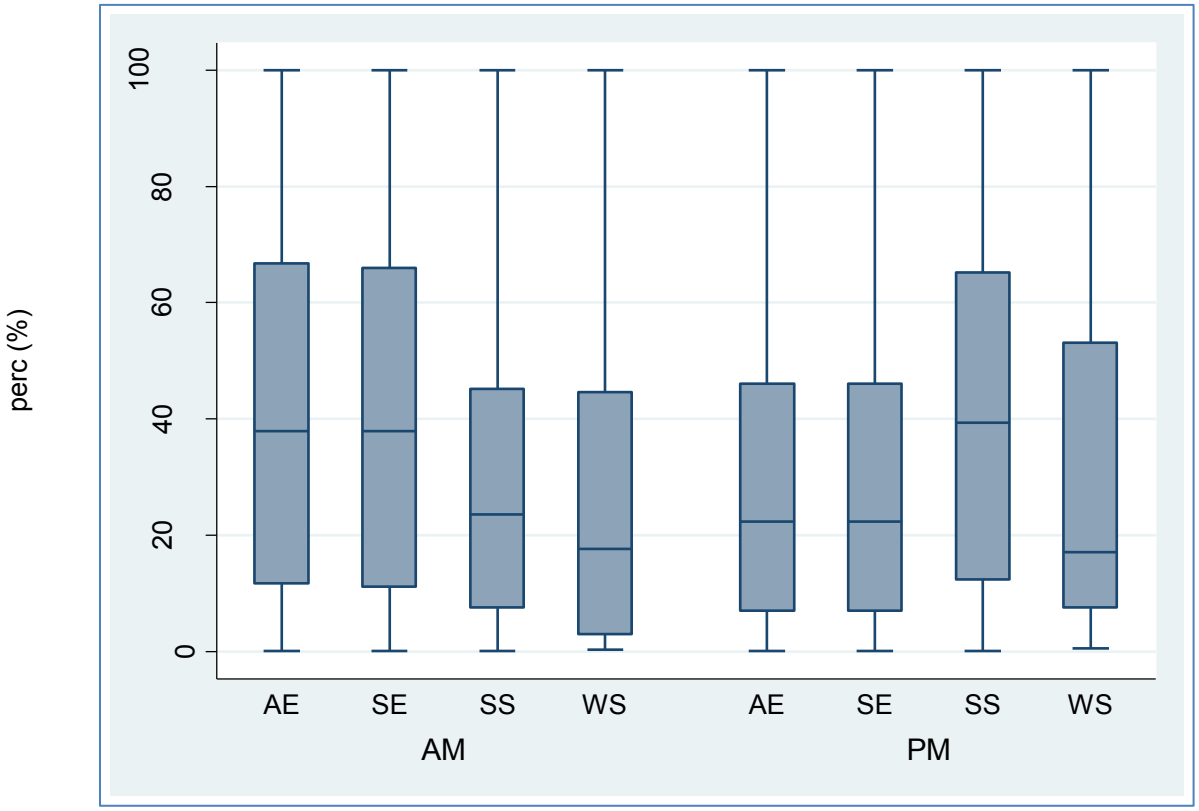

Figure 5-43: Box and Whisker Plot for All Interactions

Note that one possible problem with the model was that it assumed that percentage (perc) is normally distributed. However, this is not the case and the model was carried out anyway, because there is no non-parametric equivalence to the linear mixed effects model so the data could not be modelled non-parametrically. The most appropriate transformation of perc is the square root transformation. The model was run with this as the outcome and it did not change the direction of the effects (negative effects stayed negative and positive effects stayed positive) or

p-values. Only the size of the effects became smaller since the outcome was square root transformed. Thus, in terms of interpreting the direction of the effects, the model run on the raw data can be used.

5.2 Validation of Methodology

The principal aim of this part of the thesis was to validate the methodology established in this thesis and, subsequently concludes whether ArcGIS and Hillshade are the right tools for establishing a real time database for road networks exposed to direct sunlight. The validation consisted of two parts, the first being the recording of a sun glare events for a selected roads in the study area, in both the morning and afternoon period. The recording was carried out in Freeway segments where sun glare problems occur in the course of the year. Using the proposed methodology, the selected streets were modelled in ArcGIS. The comparison of the results from these two processes facilitated the drawing of conclusion on the validity of the proposed model.

This investigation was carried out using a Road Eye JS-300 camera (see picture in Appendix F), which is an intelligent electronic device designed to record the driving parameters of the vehicle using an advanced camera with Wide Dynamic Range function – a black box for the car (http://www.carblackbox.ro/). The camera used is a 120 degree 0.3 MP Complementary Metal-Oxide Semiconductor (CMOS; a digital sensor whose sensitivity normally ranges between 6 and 15 lux), and has a H.264 Video Graphics Array (VGA) resolution of 640 pixels wide by 480 pixels tall up to 30fbs. Apart from its use in this investigation, the JS-300 has diverse utilisation potential, which includes uses by traffic regulation authorities, taxicab companies, police, insurance agencies, ambulances, etc.

Considering that this was the only equipment available for (recording) use in the field investigation, any reliability issues with it is not something that could be addressed considering the lack options. Nevertheless, the camera has been used in several research investigations in the Department of Civil Engineering, and has proven to provide reliable and valid results.

5.2.1 Field Investigation and Model Validation

On the 15th of August, 2014, video footage of four Freeway and Primary arterial roads in the Cape Metropolitan CBD was taped for the morning and afternoon periods during the time periods when sun was considered to be at its worst – which in this case was defined by the 19º-25º sun cone. These roads are Buitenkant Street, Roeland Street, Adderley Street and Strand Street. The descriptions of these segments for the morning and afternoon period can be seen in Table 5-37 and 5-37, respectively. It is worth mentioning that only two roads were recorded in both time periods: are Buitenkant Street and Adderley Street. Roeland and Strand Street were only captured in the afternoon period. Nonetheless, this had an inconsequential effect on the outcome and conclusions of this validation. Table 5-37 and 5-37, also show the coordinates of the segments taped, as well as the direction of traffic on that road, which is also the road orientation. Footage was recorded while travelling at a speeds ranging between 40 and 60km/h. The terrain around these four roads is relatively flat.

In the morning the 19º-25º sun cone occurred between 09h15 and 09h45; while in the afternoon it occurred between 15h55 and 16h30. Considering that these times were well within an hour or so after sunrise (07h24) and before sunset (18h16), a decision was made to record sun glare footage between these periods. The clear weather condition on this day also made for a suitable recording environment.

Different routes were used to get to the four roads in the morning and afternoon period. Even though they were not part of the analysis, observations of the roads enroute to the selected roads also facilitated the analysis process. In the morning period, one of these roads is Penzance Street, the N2-of ramp from Main Road and Liesbeek Parkweg Road. Plein Street, Spin Street and Bureau Street were the roads recorded in the afternoon. Overall, the results from these roads correlate to those of the four roads used in this analysis.

Table 5-37: Road Segments Recorded in the Morning Period

Morning Period		
Road Name	**Description of Recorded Segment**	**Traffic Direction**
Buitenkant St	Between Buitenkant/Darling intersection (18º25'31"E; 33º55'34"S) and Buitenkant/Glynn intersection (18º25'14"E; 33º55'51"S)	NE & SW
Darling St	Between Buitenkant/Darling intersection (18º25'31"E; 33º55'34"S) and Darling/Adderley intersection (18º25'18"E; 33º55'24"S)	NW & SE
Adderley St	Between Darling/Adderley intersection (18º25'18"E; 33º55'24"S) and Adderley/Hans Strijdom roundabout (18º25'34"E; 33º55'11"S)	NE & SW

Table 5-38: Road Segments Recorded in the Afternoon Period

Afternoon Period		
Road Name	**Description of Recorded Segment**	**Traffic Direction**
Buitenkant St	Between Buitenkant/Darling intersection (18º25'31"E; 33º55'34"S) and Buitenkant/Glynn intersection (18º25'14"E; 33º55'51"S)	NE & SW
Roeland St	Between Roeland/Buitenkant intersection (18º25'18"E; 33º55'45"S) and Roeland/Plein intersection (18º25'10"E; 33º55'40"S)	NW & SE
Strand St	Between Strand/Adderley intersection (18º25'23E; 33º55'19"S) and Strand/Hudson intersection (18º25'2E; 33º55'3"S)	NW & SE
Adderley St	Between Adderley/Bureau (18º25'16E; 33º55'31"S) and Adderley/Hans Strijdom roundabout (18º25'34"E; 33º55'11"S)	NE & SW

Figure 5-44 and 5-45 present a graphical display of the directions of the roads/streets recorded, as well as the periods that they were taped.

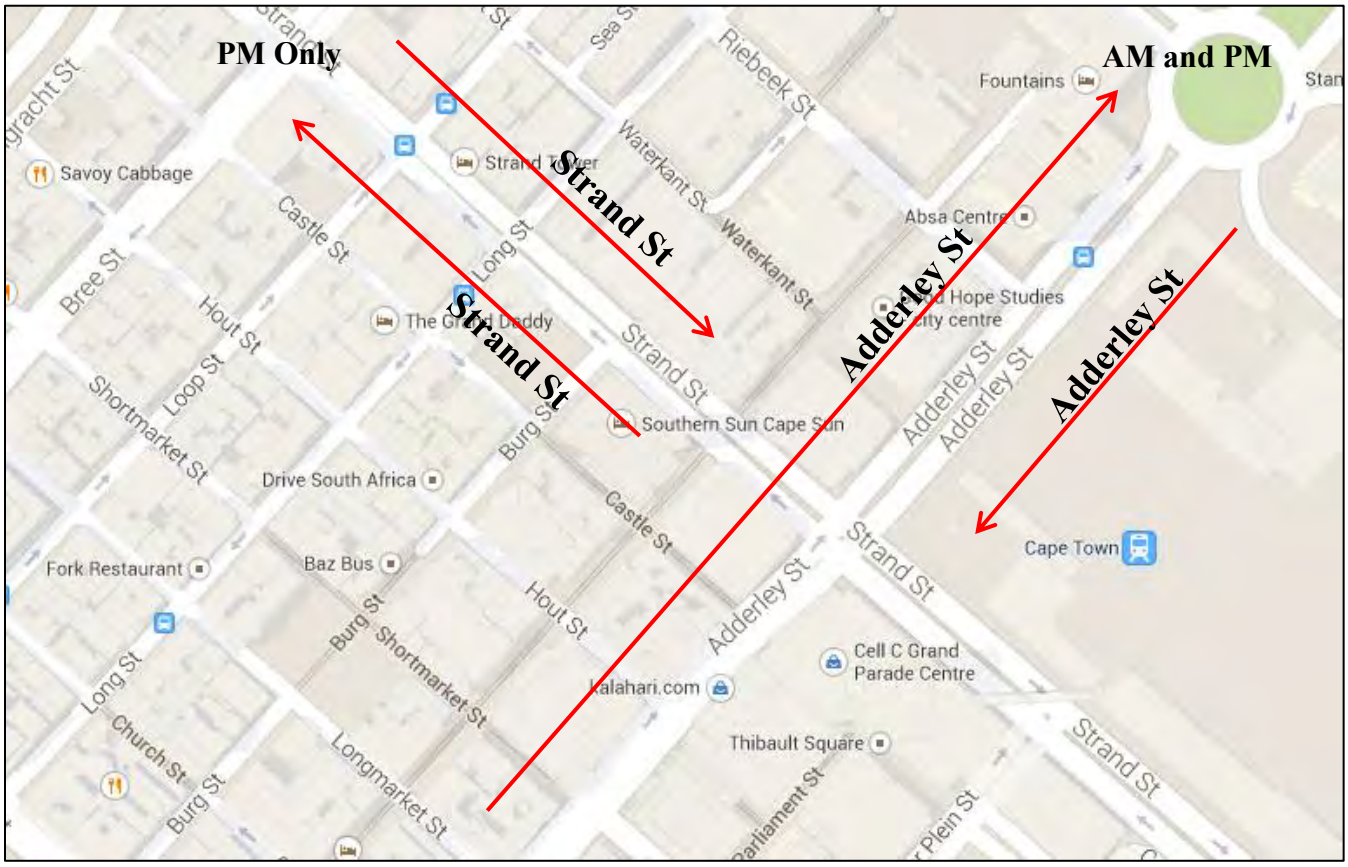

Figure 5-44: Adderley Street and Strand Street

Figure 5-45: Darling Street, Buitenkant Street and Roeland Street

5.2.1.1 Morning Period

The first street to be recorded was Buitenkant Street between the Darling Street and Glynn Street intersections, recorded in both directions (see Figure 5-45). As a dual carriageway road, Buitenkant Street can experience sun glare in either one of the directions; and like most primary arterial roads the different segments within the road itself take different orientations. The

changing sun position in the Liesbeek Parkway Road (northbound from Settlers Way exit in Observatory) video footage snapshots proves this to be true (see Figure 5-46).

Figure 5-46: Snapshots of Liesbeek Parkweg Street in Observatory (North Bound)

For that reason, some parts of Buitenkant Street are free of direct sunlight exposure, as was observed in the field investigation. Buitenkant Street has a southwest orientation, with a wide range of road segment slopes. Measured clockwise from the north, the slope range of the segments between Darling Street and Roeland Street intersections is 41°-45°, while for the segments between the Roeland Street and Glynn Street intersections the range is 23°-32°. It is, therefore, not surprising to learn that only the northeast bound traffic in the 41º-45º segments (segments between Darling Street and Roeland Street intersections) were vulnerable to direct sunlight exposure, as seen in the ArcGIS map in Figure 5-51 and video snapshots in Figure 5-47. However, because of shading by the high-storey buildings, some segments on this road were not exposed to any direct sunlight. Similarly, the images of the segments between Glynn Street and Roeland Street intersections indicate that some parts of this road – for the northeast bound traffic – were actually shaded from the sun by the buildings on the right-side, as seen in the snapshots in Figure 5-48. As the map in Figure 5-51 is time-specific it may not show that at some point in the morning period this segment may have actually been exposed to direct sunlight. Moreover,

according to quantitative data from ArcGIS – out of a total length of 3.2km – 0.54 km of the road was illuminated, which is 16.7% of the total road length.

Figure 5-47: Snapshots of Buitenkant St from Roeland St Int. to Darling St Int. (NE Bound)

Figure 5-48: Snapshots of Buitenkant St from Roeland St Int. to Darling St Int. (NE Bound)

Taking a left turn onto Darling Street from Buitenkant Street provided considerable relief from the dazzling sun experienced in Buitenkant Street. Traffic in the northwest bound direction was free from any sun glare effects on Darling Street (see Figure 5-49 for video footage snapshots). However, the same cannot be said for Adderley Street. Turning right onto Adderley Street, from Darling Street, drivers in the northeast bound direction experienced a 'dazzling' change in visual conditions, due to the overwhelming amount of sun glare on this road. In concurrence, the map in Figure 5-52 shows significant solar exposure in Adderley Street, while none is shown in

Darling Street. Furthermore, quantitative data reveals that about 14% (1.4km out of 9.9km) of the road segment lengths are exposed to direct sunlight. Contrary to the observations made in the video footage, this data also indicates that about 7% of Darling Street is illuminated. What this means is, even though Darling Street is not exposed to direct sunlight, it was still experiencing solar insolation. The images in Figure 5-50 show snapshots of the video footage from Adderley Street.

Figure 5-49: Snapshots of Darling St from Buitenkant St Int. to Adderley St Int. (NW Bound)

Figure 5-50: Snapshots of Adderley St from Darling St Int. to Heerengracht St (NE Bound)

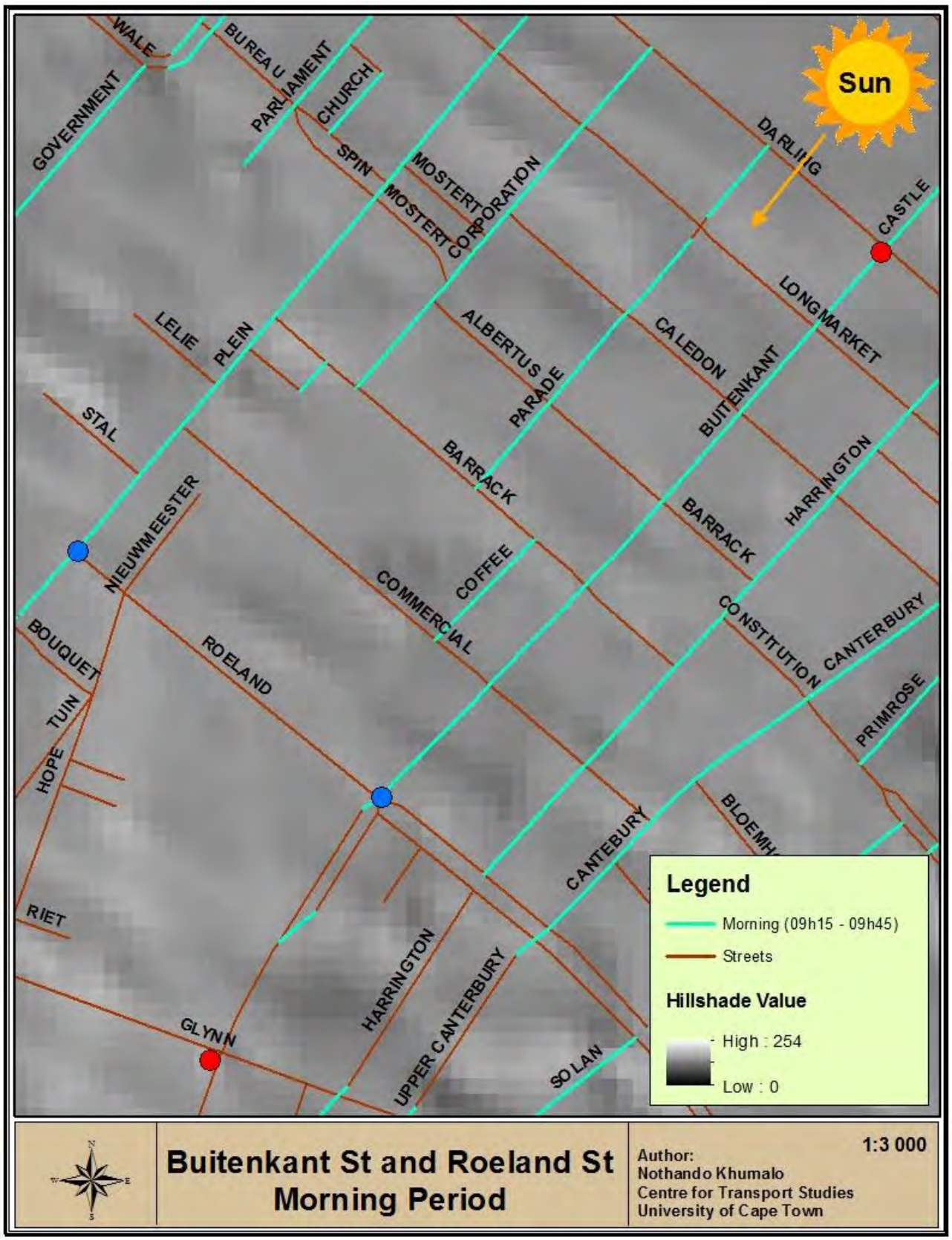

Figure 5-51: Segment Distribution Map for Buitenkant St and Roeland St in the Morning Period

Figure 5-52: Segment Distribution Map for Adderley St and Strand St in the Morning Period

5.2.1.2 Afternoon Period

Contrary to the morning period, roads exposed to direct sunlight in the afternoon period intersect Buitenkant Street (northwest and southeast orientation), which means that traffic in Buitenkant Street was not at sun glare risk in either direction (northeast and southwest bound). In accord, the map in Figure 5-60 shows no segment illumination in Buitenkant, all the way from the Darling St intersection to the Glynn St intersection. Additionally, the qualitative data also shows that not a single length of the total road segments is insolated. Nevertheless, because of veiling glare, traffic on this road could still be at risk given the amount of reflective surfaces along it. The image in the centre of the bottom strip of snapshots in Figure 5-53 is indicative of the presence of veiling glare in Buitenkant, in the southwest bound direction.

Figure 5-53: Snapshots of Buitenkant St from Darling St Int. to Glynn St Int. (SW Bound)

Figure 5-54: Snapshots of Buitenkant St from Glynn St to Roeland St Int. (NE Bound)

An overwhelming burst of sun glare was encountered turning left onto Roeland Street from Buitenkant Street, in the northwest bound direction. As already pointed out, the roads affected by sun glare risk in the afternoon period intersect Buitenkant Street, as was the case with Roeland Street. Roeland Street can be seen in Figure 5-60 (between the two blue circles), which according to the model was one of the streets exposed to direct sunlight in the afternoon. Although, only the northwest bound traffic was encountering direct exposure. The images in Figure 5-55 show snapshots of Roeland Street in the northwest bound direction.

Figure 5-55: Snapshots of Roeland St from Buitenkant St Int. to Plein St Int. (NW Bound)

In essence, the model in this study simply highlighted the roads that were exposed to direct sunlight at a particular time, relative to the solar position. However, in spite of the identified exposure, the model does not indicate the exact direction to which traffic is facing the sun, as evident in the map outcomes for Strand Street. The map in Figure 5-61 shows that both directions in Strand Street were exposed to direct sunlight. Pursuant to this, the northwest bound traffic in Strand Street was enduring immense sun glare conditions in the afternoon (see video snapshots in Figure 5-56). On the contrary, the field recordings show that traffic in the opposite direction (southwest bound) experienced no direct exposure, seeing as it was facing away from the sun (see Figure 5-57). Although, similar to Buitenkant Street, the southwest bound traffic was also likely to experience veiling glare regardless of the traffic direction relative to sun the

sun radiation. Moreover, the quantitative data reveals that 54% (6.3km of the 11.8km) of Strand Street is exposed to direct sunlight. Furthermore, even though this was not highlighted in the morning period map in Figure 5-52, it is also worth noting that the output data ascertained a 0.15% road segment exposure of Strand Street in the morning period.

Figure 5-56: Snapshots of Strand St from Adderley St Int. to Hudson St Int. (NW Bound)

Figure 5-57: Snapshots of Strand St from Hudson St Int. to Adderley St Int. (SE Bound)

Adderley Street in the afternoon period was free of any direct solar exposure, according to the snapshots in Figure 5-58 and 5-59. This applied for traffic travelling in both directions, northeast and southwest bound. The map outcome in Figure 5-61 also indicated the same results, as can be seen between the two red circles. In spite of these observations, the quantitative data shows that about 45m (0.45%) of Adderley Street was exposed to direct sunlight. This value can be attributed to segments of the roundabout that joins Adderley Street to Hans Strijdom Street, whereby some of its segments have the same orientation as the road networks exposed to direct sunlight in this period – as seen in the Figure 5-61 map.

Figure 5-58: Snapshots of Adderley St from Bureau St Int. to Heerengracht St (NE Bound)

Figure 5-59: Snapshots of Adderley St from Heerengracht St to Strand Int. (NE Bound)

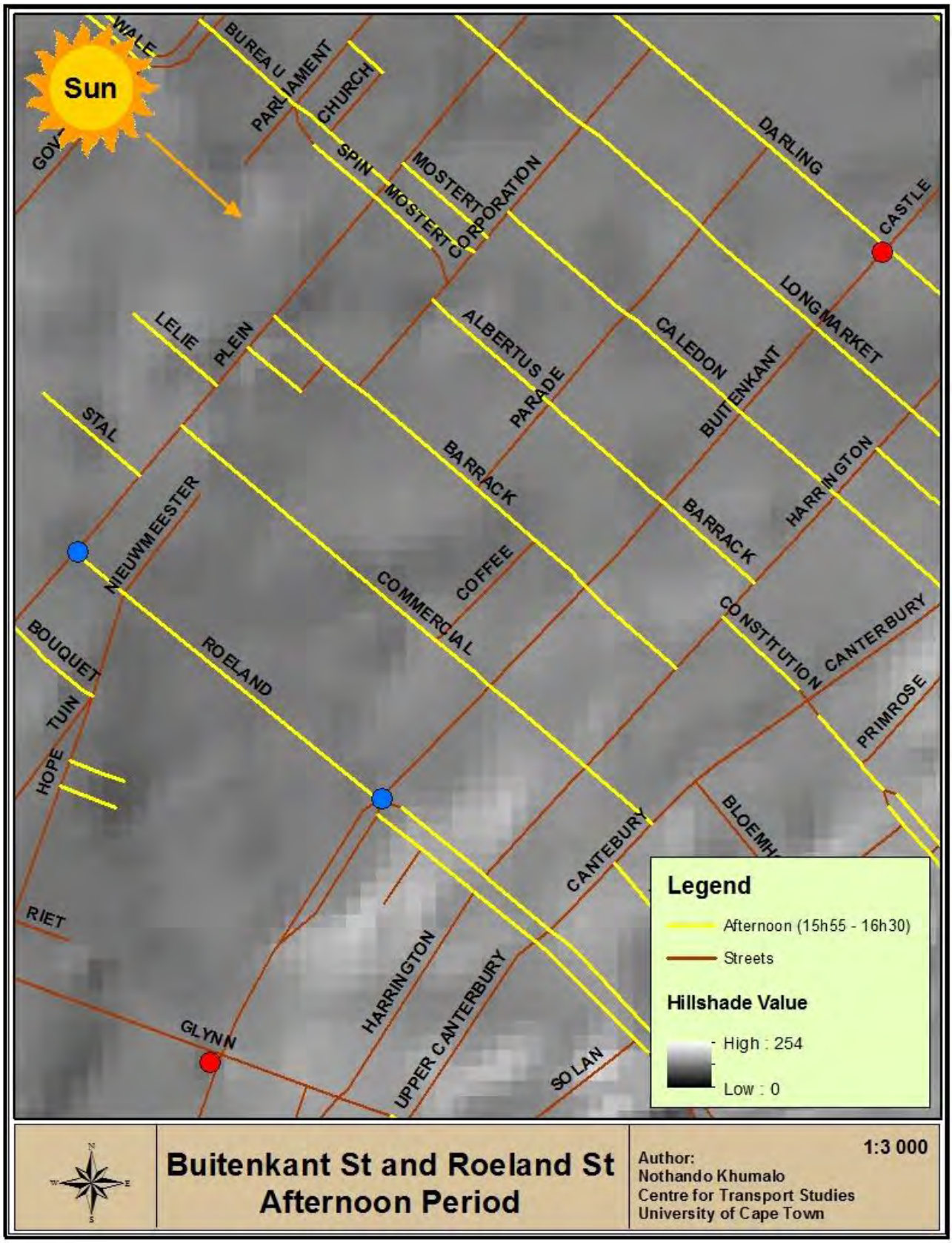

Figure 5-60: Segment Distribution Map for Buitenkant St and Roeland St in the PM Period

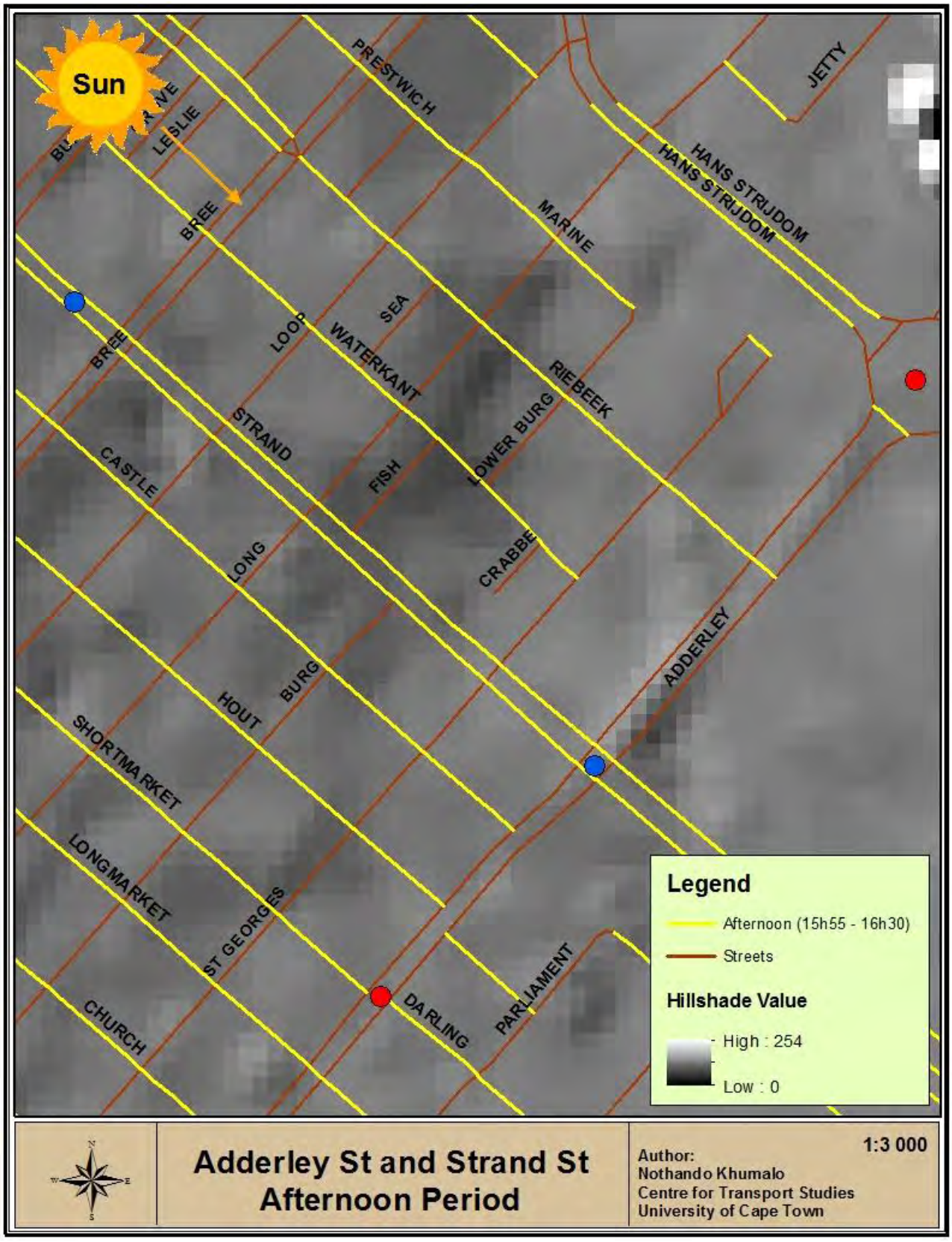

Figure 5-61: Segment Distribution Map for Adderley St and Strand St in the PM period

5.3 Accident Data Analysis for the City of Cape Town

Road accident data used in this analysis, obtained from the Metropolitan Accident Database (MADB), was extracted from copies of the Accident Report (AR) forms, which were forwarded by the South African Police Services (SAPS) stations and Metropolitan/Traffic Police Officers within the City of Cape Town. The first part of this analysis was a review of recorded CoCT accident data with the intention to isolate sun-glare-related accidents. Subsequently, only four of these events were selected for ArcGIS modelling to determine whether such accidents could have been prevented if people were warned, prior to the period of accident occurrence, through the provision of real time information based on information generated by the developed model.

5.3.1 Accident Statistics for 2013

A critical review of accident data recorded for the year 2013 revealed that, out of 141 563 recorded accidents, 209 accidents (0.15%) were result of drivers being 'blinded'. Considering the ambiguity of recorded accident causes, key words such as 'vision', 'sun', 'visibility' and 'blind' were used to isolate the data to be most likely related to sun glare conditions. Consequently, out of the many causes identified for the 141 563 accidents, it was decided that 'blinded' was a cause that closely related to sun glare.

The bar chart in Figure 5-62 illustrates the total number of recorded accidents between the years 2006 and 2013. The statistics belie the danger of sun glare. Prior to 2013, with the exception of four recorded accidents in 2009, the accident data did not list 'blinded' as category for accident cause. The accident data from 2013 had relatively more accidents with 'blinded' as a cause, ergo the decision to use 2013 accident data for this analysis.

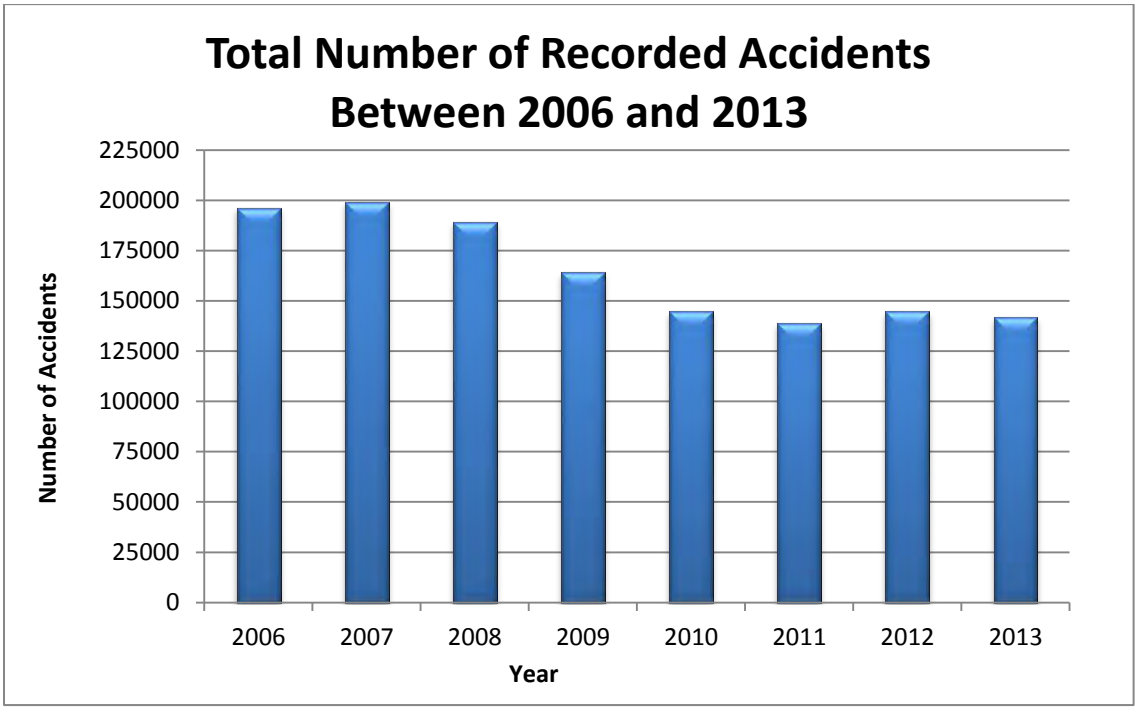

Figure 5-62: Total Number of Recorded Accidents Between 2006 and 2013

Out of the 209 'blinded' accidents, only 4 resulted in serious injuries and 20 with slight injuries. No fatalities were recorded in this period. The following sections only examine the 209 accidents whose specified cause was identified to be 'blinded'. These sections present a variety of classifications for this data, which were also used as criteria for the selection of four accidents events to be modelled in ArcGIS. In the respective order, these are classifications by accidents per month, light conditions, weather and accident type. Overall, the data gives insight into the circumstances of the accidents.

5.3.1.1 Accidents per Month

According to Figure 5-63, the monthly accident peaks occurred in the wet, winter months when it is, generally, believed that more accidents occurred due to poor visibility and wet roads. Out of a total of 5 'blinded' accidents recorded in the whole year, 3 of them occurred in June, while 2 occurred in April. Although glare can be dangerous year-round, it is an especially big problem at this time of the year (June/July) when several factors – such as the early setting sun - conspire against pedestrians and drivers during the worst traffic hours of the day: rush hour.

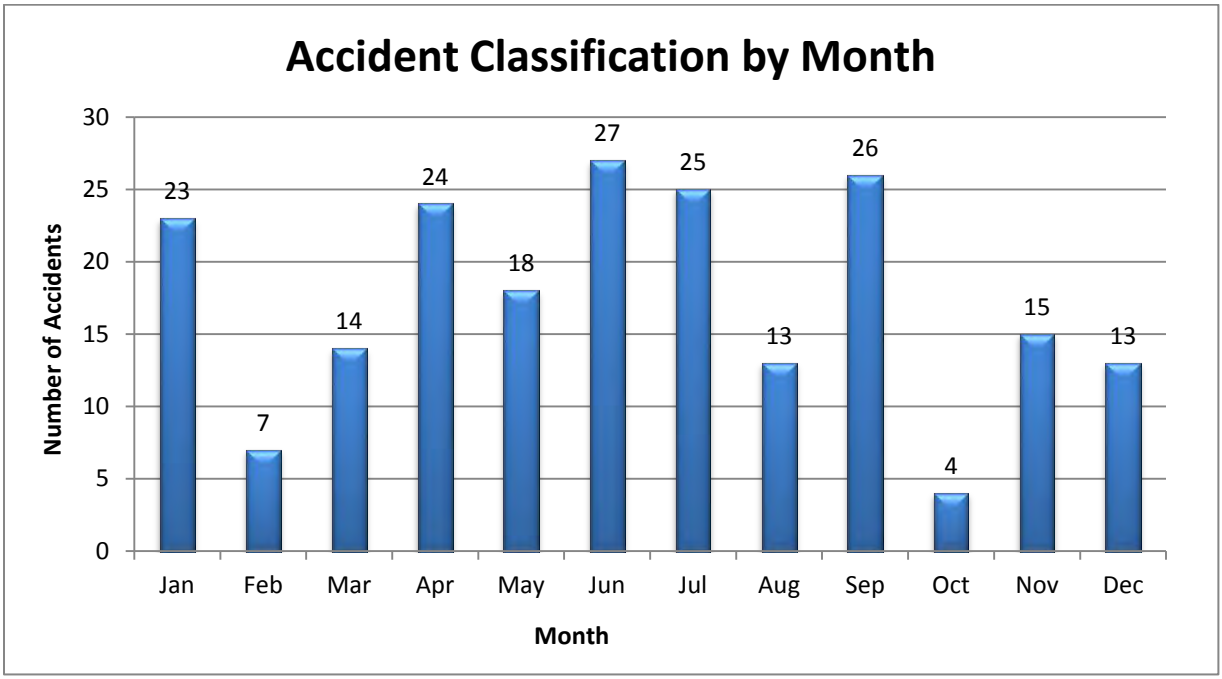

Figure 5-63: Total Number of 'Blinded' Accidents per Month

5.3.1.2 Accidents by Light Conditions

At a glance it appears that fewer accidents occur at night, due to lower traffic volumes being present and less risk of sun glare. According to Figure 5-64, majority of the accidents classified as 'blinded' occur at daylight. These accidents (187 in total) make up 89% of the total 209 'blinded' accidents. Furthermore, the results in Figure 5-64 contradict the literature findings, which state that the vulnerability to sun glare significantly increases when the sun is low in the sky at dawn and dusk.

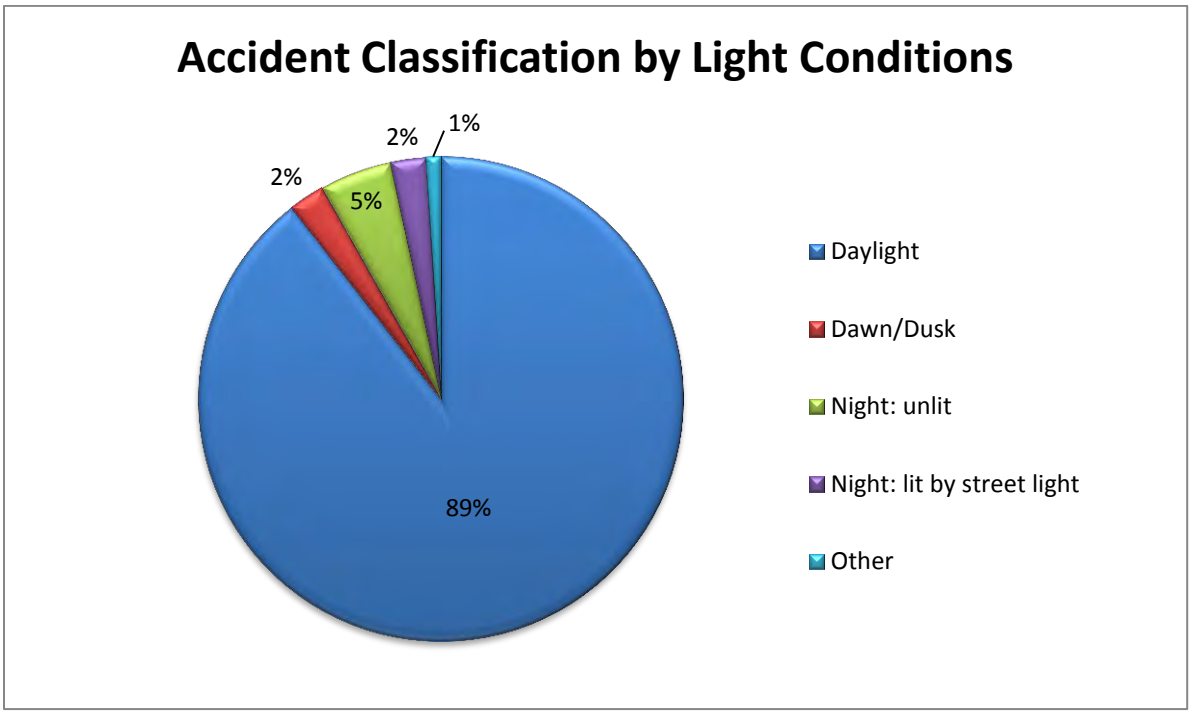

Figure 5-64: Percentage of Road Accidents in Different Light Conditions

5.3.1.3 Accidents by Weather

Almost 90% of the 'blinded' accidents recorded occurred in clear weather, while 4% of these occurred in overcast and rainy weather, as seen in Figure 5-65. Accidents occurring in mist/fog totalled up to 5% of the total accidents. Given that sunny weather is depicted by clear sky, these results are highly indicative of the potential involvement of sun glare in the occurrence of these accidents.

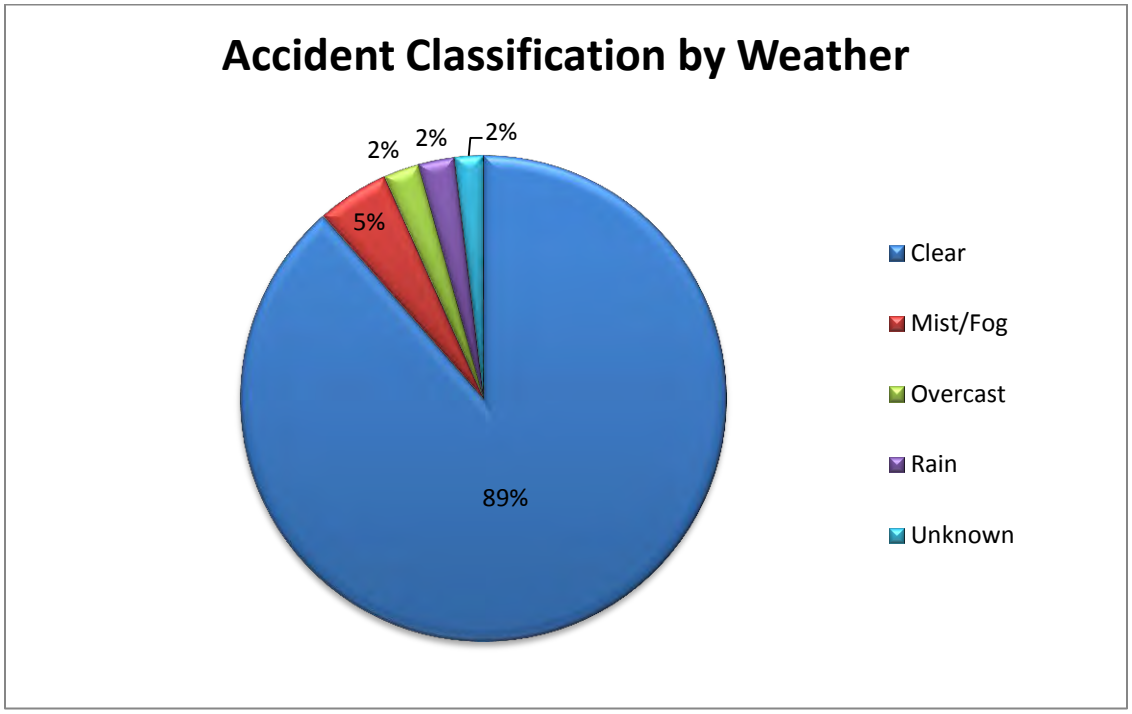

Figure 5-65: Percentage of Road Accidents in Each Weather Condition

5.3.1.4 Accidents by Accident Type

Compared to all the 'blinded' accident types, 'head/Rear end' accidents occurred most frequently, which is 44% of all known and recorded 'blinded' accidents. As made evident by the results presented in Figure 5-66, the 'sideswipe-same direction' had the second highest number of accidents (24), which is 11% of all known 'blinded' accidents.

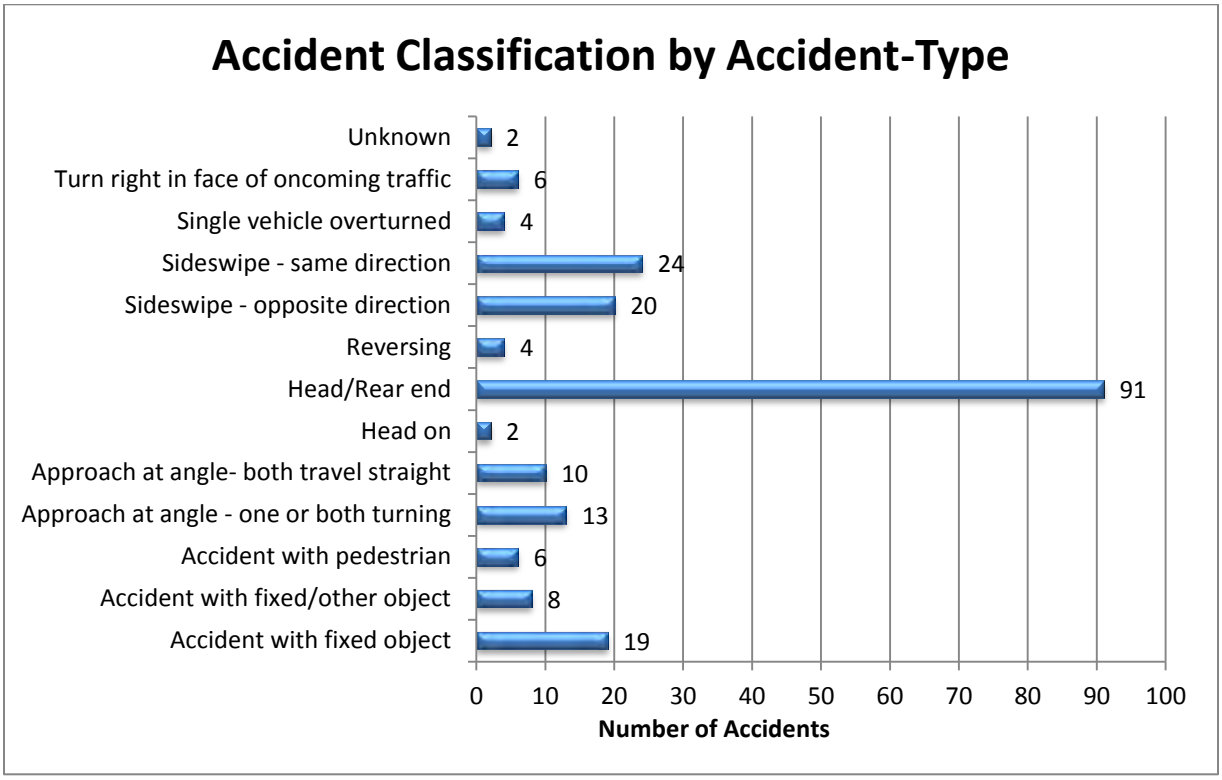

Figure 5-66: Total Number of Accidents per Accident Type

5.3.1.5 Accidents by Vehicle Manoeuvre

The results in Figure 5-67 indicate that in 48% (101 accidents) of the 'blinded' accidents the vehicles were travelling straight, while 13% (27 accidents) and 11% (22 accidents) of these were stationery or turning right, respectively.

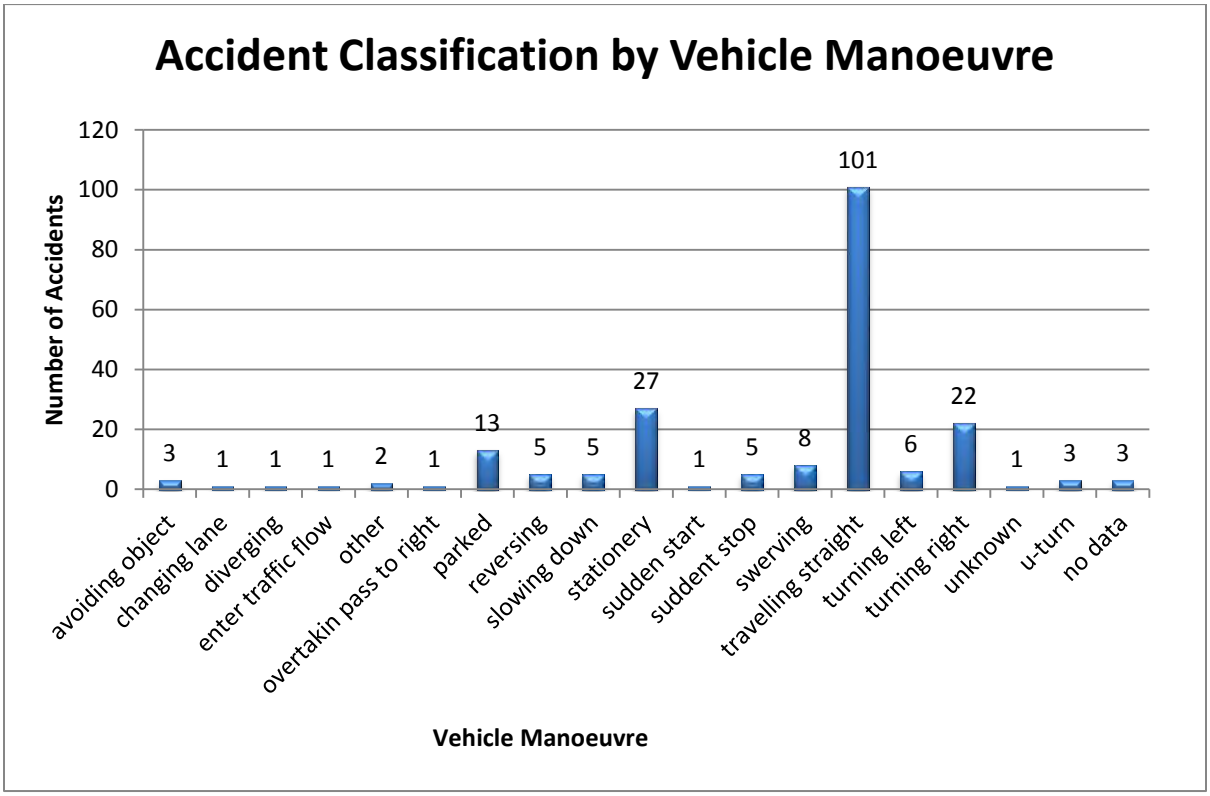

Figure 5-67: Total Number of Accidents per Vehicle Manoeuvre

5.3.2 Methodology Application: Results Analysis

Bearing in mind that the sun is most potent to drivers at dawn or dusk, two of the five 'blinded' accidents identified to have occurred at dusk/dawn were selected for this analysis. The other two cases were randomly selected from the 187 daylight cases based on the classification criteria from Section 5.3.1 – two for the morning period and another for the afternoon period. Overall, the road accident cases presented in Table 5-39 possess the following properties:

- Light Conditions = Daylight
- Weather = Clear
- Accident type = Sideswipe – same direction (SSD) and Head/Rear End (HRE)
- Vehicle Manoeuvre = travelling straight

Table 5-39: Accident Information for 'Blinded' Accidents

Light Conditions	Road Description	Acc. Type*	Date (2013)	Time	Altitude (º)	Azimuth (º)
Daylight	Plattekloof RD, Milnerton	HRE	25 Jan	07h35	17.8º	101.2º
Daylight	Kloof Nek RD, Gardens, Cape Town	HRE	22 Apr	08h20	12.1º	66.1º
Daylight	Highlands DR, Mitchells Plain	SSD	08 Aug	16h58	13.2º	299.8º
Daylight	Hennop RD, Bonnie Brae, Kraaifontein	SSD	20 Aug	16h45	17.6º	298.7º
Daylight	Stellenbosch (arterial)/Polkadraai RD	HRE	07 Nov	17h17	24.1º	265.8º
Dawn/Dusk	Plattekloof RD, Milnerton	HRE	30 Nov	06h00	5.3º	112.7º
Dawn/Dusk	TR009 (N1)	SSD	13 Dec	05h50	3.3º	116º

**HRE – Head/Rear End; SSD – Sideswipe Same Direction*

5.3.2.1 Quantitative Data Analysis

Quantitative output data from modelling the four 'blinded' accidents events (selected from the ones in Table 5-39) in ArcGIS is presented in Table 5-40. The two morning events, as seen in the table, occurred on the 25th of January and the 30th of November; of which, coincidentally, both occurred in the same road. The dates for the afternoon events are the 20th of August and 30th of November.

Considering the sun cone used in this study, it is worth noting that the 7th of November event has an altitude within the identified sun cone range as seen in Table 5-39 (24.1º at 17h17). This, however, does not mean that the rest of the accident events might not have been a result of sun glare. As pointed out in the preceding sections, the 19°-25° sun cone was only assumed to present a period when solar exposure is the most potent to drivers. The 25 of January and 20th of August altitudes (17.8° and 17.6°) are notably close to the altitude in the lower end of the sun cone range (19°).

Table 5-40: ArcGIS Results for the Selected Accident Events

Accident Event		Street Name	Total Road Length (m)	Length of exposed segment (m)	Percentage of total road length (%)
Date	Time				
25 January	07h35	Plattekloof	12307.7	2124.9	17.3
20 August	16h45	Hennop	747.1	232.0	31.1
07 November	17h17	Stellenbosch	16977.3	14131.1	83.2
30 November	06h00	Plattekloof	12307.7	4372.1	35.5

Regarding the percentage of total road segments exposed to direct sunlight in each event, it is apparent that 83% of Stellenbosch road - 14km of the total 17km road length - is exposed to direct sunlight, which is the highest percentage coverage of all the roads. This is a significantly high risk road. Assuming an average speed of 60km/h, it would take 14minutes to drive through the exposed segments in this road.

5.3.2.2 Map Analysis: Visual Interpretation

I. 25 January 2013 at 07H35 (unknown location in Plattekloof Road)

Figure 5-68 provides a magnified view of Plattekloof road, which stretches between the two red circles. A complete map of the road segment distribution in Cape Town at 07h35, on this day, can be viewed in Appendix E. The road segments in this time snapshot are orientated towards the southeast from the northwest, with a road segment slope ranging between 90º and 115º (clockwise from the north).

The accident data does not indicate where in Plattekloof the accident occurred, although, in view of the exposed segment located between Durbanville road and Koeberg road (blue line), it is

likely that it occurred in that road stretch (approx. 2km). Considering the orientation of the sun in this scenario (shining from the southeast towards the northwest), in a case whereby these vehicles were travelling in the southeast direction (facing the sun), then there is a possibility that sun glare could have been a factor in the occurrence of the accident.

As a result of reflection, vision impairment can still play a key role in 'blinded' accident events where the vehicle was not facing the blinding sun. Previous research by Hagita and Mori (2011) indicates that the higher occurrences of accidents at azimuthal angles, near 180º, are attributed to rear-end accidents. In that situation, the sun is behind the first vehicle concerned, and the higher occurrence of accident is attributed to the sun shining from behind the first vehicle concerned. It is assumed that the driver is dazzled by the sun causing a glare in the rear window of the preceding vehicle or in the back or side mirror of the first vehicle concerned. No clear conclusion has been reached on this (Hagita and Mori, 2011).

Hagita and Mori (2011) also found that accidents tend to be more frequent when the sun is in a position that blinds the first party. Overall, with the implementation of mitigation measures it is possible that the accident could have been avoided only if the speculation behind the cause is correct.

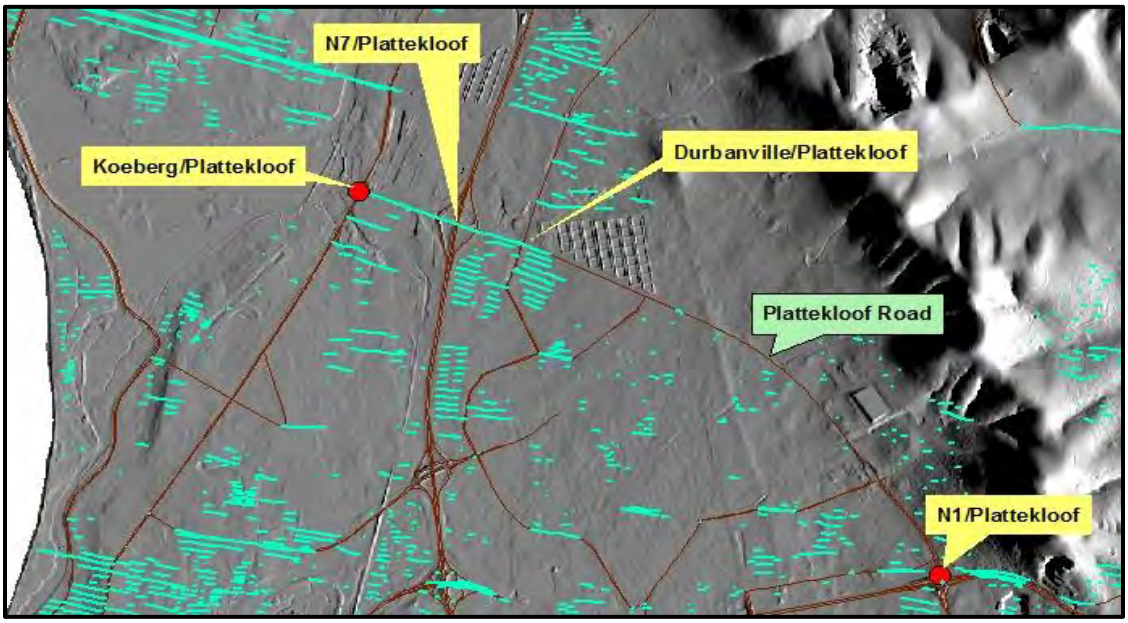

Figure 5-68: Road Segment Distribution in Plattekloof Road for the 25th Of January

II. 20 August 2013 at 16h45 (Hennop Road and Okavango Road node)

The orientation of road segments in this scenario is towards the southeast from the northwest, as can been seen in the road segment distribution map in Appendix E. Clockwise from the north, the slope of the road segments ranges between 107º and 130º. A magnified view of Hennop Road is displayed in Figure 5-69. The exact location of the accident in Hennop road is also not indicated in this case (see Hennop road between the two red circles in Figure 5-69). Although, the only road segment vulnerable to sun glare in this road (yellow lines) is between the Sara/Hennop intersection and the cul-de-sac road after the Limanie/Hennop intersection.

Similar to the head/rear end accident, reflection can also be blamed here in the case that the sun was shining from behind the vehicles. The same assessment can be applied here, although the direction of the sun at this time is in the opposite direction to that in Section I. Since the sun is shining towards the southeast in this case, traffic moving towards the northwest in the yellow segment in Figure 5-69 would be facing the sun. Even though the sun position altitude is not within the sun cone range in this event, the sun is still well within an hour or so before sunset which – according to Hagita and Mori (2011) - is around the time when the sun is the worst for drivers. At this time of the year glare is a problem from about 08h30 to 10h00, and from 16h00 to 17h30 – the height of rush hour traffic.

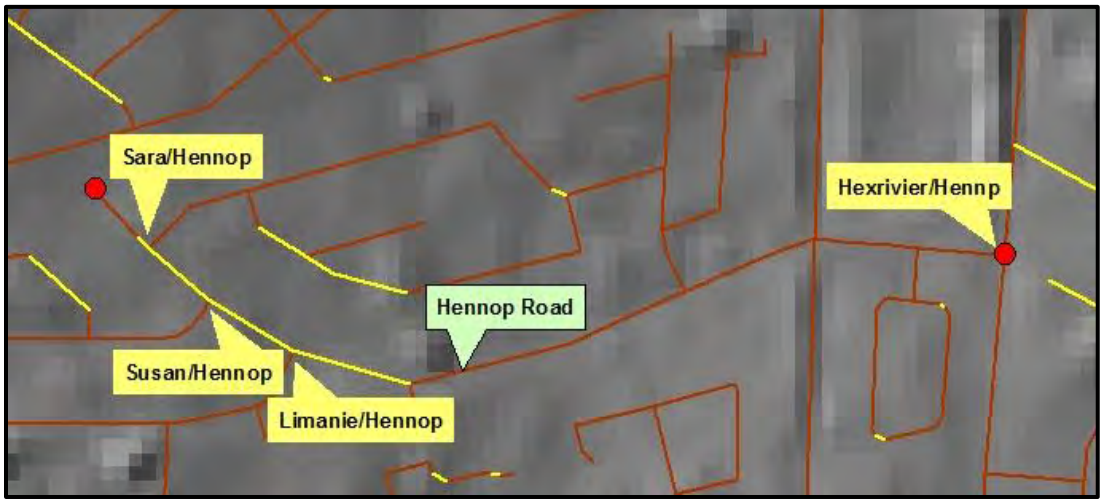

Figure 5-69: Road Segment Distribution in Plattekloof Road for the 20th Of August

III. 07 November 2013 at 17h17 (Stellenbosch Road and unknown location)

Bearing in mind the 83% road segment coverage presented in Table 5-40, the segment distribution in Figure 5-70 also shows evidence of high sun glare risk in Stellenbosch road. Taking into account the road segment (green line) covering Stellenbosch road from the Erica DR/Stellenbosch intersection to the Range RD/Stellenbosch intersection, there is a number of places along the road where an accident might have occurred as a result of direct sunlight exposure in which case individuals involved could have claimed to have been "blinded". The implementation of sustainable mitigation measures, such as trees could reduce vulnerability to sun glare. In implementing such, the orientation and slope of the segments would have to be considered, which in this case is southeast (with a 90º to 115º slope clockwise from north).

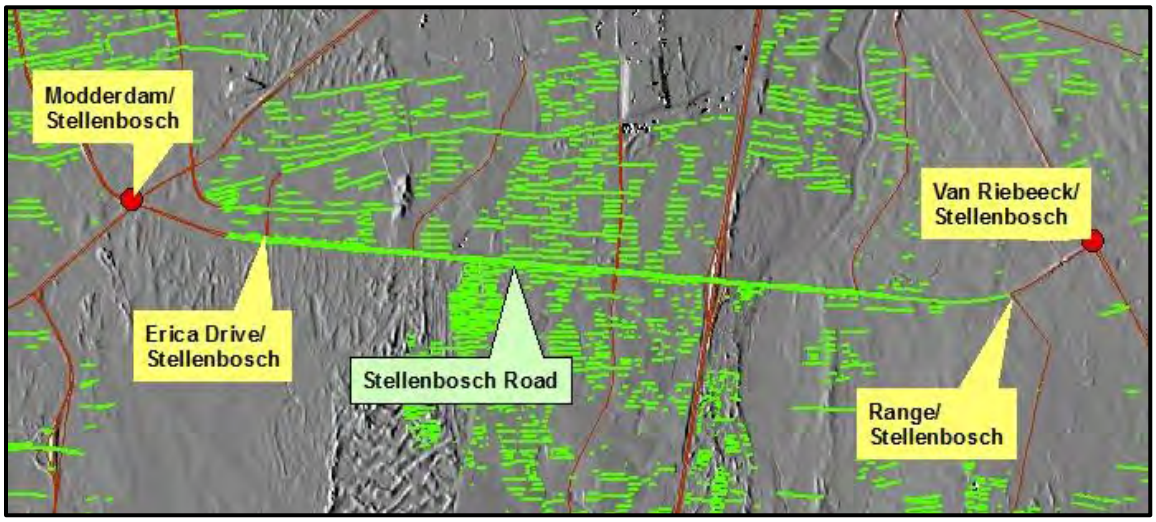

Figure 5-70: Road Segment Distribution in Plattekloof Road for the 07th of November

IV. 30 November 2013 at 06h00 (Plattekloof RD and Koeberg RD node)

The segment orientation for this snapshot is southwest, at a slope ranging between 97º and 115º. This means that vehicles moving towards the northeast would be facing the sun, thus, making them relatively more vulnerable to sun glare risk. The segments in Figure 5-71 reveal that a little over half of Plattekloof road (between the two red circles) is exposed to direct sunlight as indicated by the purple colour in the road stretching from Koeberg road. A full view of the segment distribution in Cape Town on this day is shown in Appendix E.

According to the accident data, the accident occurred around the Plattekloof and Koeberg road. In the couple of meters that it takes for the sun glare to happen, there may be a car or pedestrian not visible to the driver. In addition, overtaking into the low sunlight when the road ahead is obscured is risking disaster. Seeing as glare is the worst typically an hour or so after sunrise and before sunset, the time of this incident is well within these periods since the sunrise on this day was at 05h28. This is a further indicator of the potential involvement of the sun in this case, which could have possibly been avoided with information provision or the use of a route that opposes the sun illumination.

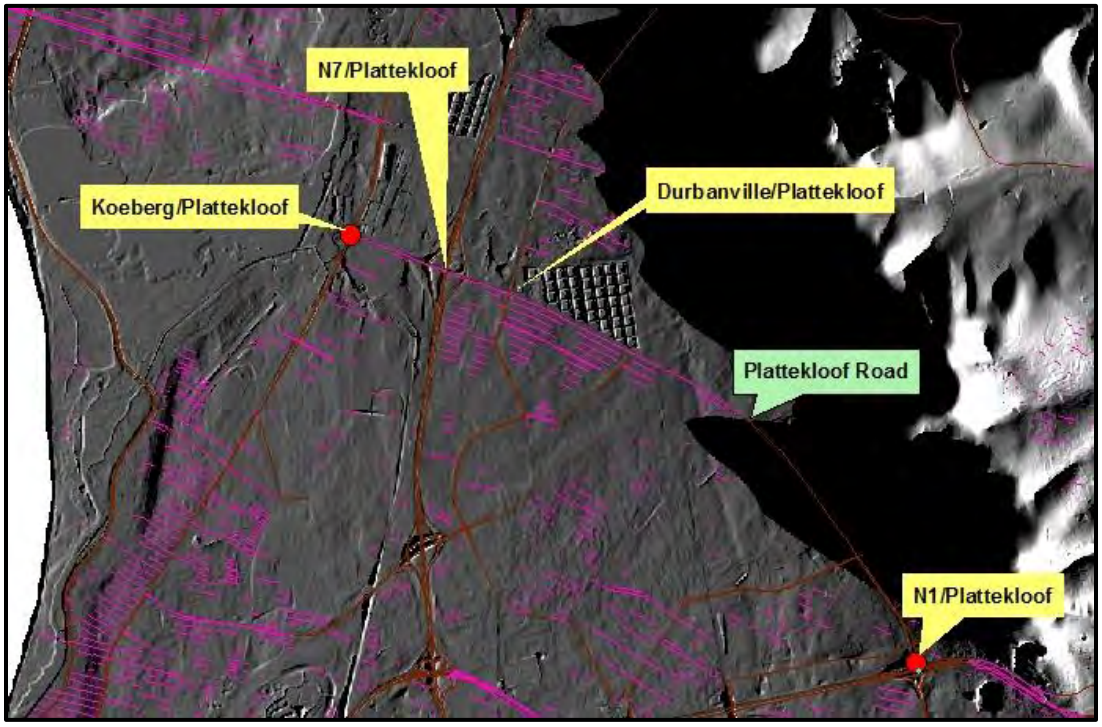

Figure 5-71: Road Segment Distribution in Plattekloof Road for the 30th of November

5.4 Résumé

Analysis of ArcGIS Results

Overall, and in agreement with the quantitative data and map analysis, statistical analysis of the four days (16 scenarios) reveals that on average the autumnal and spring equinox have more sunlight exposure compared to the summer and winter solstice – with the latter having the least of all. The output also revealed that, on average, there is less sunlight in the afternoon compared to the morning. However, looking at the individual days, this is not the case for the summer and winter solstice, whereby there is more sunlight in the afternoon compared to the morning.

The results presented in this section confirm that the occurance of sun glare is highly depandant on the position of the sun, the geometry of the road network and the terrain profile, among other factors. The intensity of the sun, however, appears to be an insignificant factor in the occurrence of sun glare. Nevertheless, it may have an influence on other traffic related matters. The degree of solar illumination on the other hand plays a key role in the occurance of sun glare conditions.

Validation of Methodology

Taking everything into account, it appears that the model outcomes are concurrent with the field investigation findings. However, because of the narrow sun cone range (19°-25°) used in this study, road segments that actually experience sun glare conditions outside this altitude range in the morning and/or afternoon period may not be represented in the ArcGIS maps. Furthermore, the results from this model do not indicate the direction of travel actually exposed to direct sunlight, but they simply indicate all the roads insulated within the identified horizontal and vertical sun cones. For that reason, roads that are actually facing away from the sun might be denoted as segments exposed to direct sunlight. Nevertheless, these roads may still be at risk as a result of veiling glare, as was apparent in Buitenkant Street and Strand Street observations for the afternoon period. In short, ArcGIS is an appropriate tool for establishing a real time database for road networks exposed to direct sunlight. Compared to the field investigation recordings, the results produced by the thesis methodology are satisfactory, although there are a few difficulties that might need to be addressed.

Sun glare is a hazard that few people anticipate. The risk is particularly high in winter when the sun sets at the busiest times on roads at around 17h40 – just as most drivers are heading for home. The glare of the setting sun during rush hour can almost certainly be blamed for a couple of accidents throughout the year. According to an article by Massey (2013), the setting sun plays a part in nearly 3 000 accidents every year with drivers at risk of being temporarily 'blinded' by the dazzle of the sun on the windscreen. Because of the absence of glare specific statistics in the accident data, it is not known how many accidents can be blamed on sun glare.

From the observations made in the preceding sections it is evident that glare is a likely contributor to these accidents, given that individuals involved attributed the accident occurrence to being "blinded". It is also apparent that the biggest danger is on minor roads. Out of the 209 'blinded' accidents in 2013, 149 happened in single carriageway roads, while a total of 52 'blinded' accidents happened in dual carriageway roads. Furthermore, seeing as the location or coordinates of each 'blinded' accident event in these sections was not specified, a couple of scenarios can be envisioned. For instance, in the 'head/rear end' accidents the most likely scenario is a case of "sudden stop" by the leading driver and a late reaction from the driver in the vehicle behind. Generally, most drivers are sensible enough to slow down when they are dazzled by the sun. However, where a dazzling sunset gets particularly hazardous is when the road turns into it or the glare appears from behind trees, buildings, or by reflection. Additionally, a City's hills can offer some shade, but when drivers crest those hills, they can be blinded by the sudden burst of sunlight.

Furthermore, glare is not only a problem when motorists are driving into the sun. There is also veiled glare, which is indirect stray sunlight that comes in at an angle, or reflects off glass towers and other cars. Like a veil, you can see through it, but not very clearly. Red light running can also be attributed to sun glare effects. According to a traffic specialist quoted in an article in the San Francisco Examiner (http://www.sfexaminer.com/), when the sun is behind motorists the light often bounces off the reflectors of the traffic lights ahead, causing them to have the same brightness – and to look like they are all the same colour. Consequently, some motorists run the red light, because it looks the same upon approach as the green light they saw moments before.

On the whole, the accident information recorded in the AR forms do not permit the solar position and vehicle travel direction to be determined, which makes it difficult to conclude whether the accidents discussed in the preceding sections could be blamed on sun glare. Nevertheless, through real time information provision and other mitigation measures it is highly likely that accidents resulting from sun glare effects could have been avoided.

6 Conclusions and Recommendations

6.1 Conclusions

There are numerous potential explanations of traffic crashes and it is not surprising that so many dimensions appear important, since driving is such a complex task (Plainis e al., 2006). Visibility conditions have been identified by various authors as being an important environmental factor. In most cases, visibility refers to night and rainy conditions, both influencing the severity and the rate of crashes (Clarke et al., 2006; Konstantopoulos et al., 2010).

Although, less frequently, sun glare is mentioned in literature as a visibility factor (Pande and Abdel-Aty, 2009; Mitra and Washington, 2012; Dozzaa and Paneda González, 2013). Glare resulting from direct sunlight exposure can be painful to the eye of the observer and potentially very distracting to the driver in terms of visibility (Auffray, 2007). Consequently, this distraction to the driver has well under-stood adverse effects, not only on the safety of the driver but on adjacent drivers as well.

The objective of this dissertation was to develop a method that will determine which parts of the City of Cape Town road network are exposed to direct sunlight, thus, making them vulnerable to road accident risk as a result of impaired vision. This chapter provides a summary of the findings with regards to the research questions asked and investigated.

Is sun glare a road safety issue?

As a basic requirement for safe driving, visibility gives drivers a preview of roadway and its information. Therefore, any obscurity in a driver's vision can impose a threat to roadway safety, due to interference with the driving task (Choi and Singh, 2005). Be it from a natural or artificial light source, glare can result in temporary visual impairment, thus, increasing the risk of an accident (Nakagawara et al., 2004). Glare from a natural light source, termed sun glare, is a hazard that few people anticipate. According to Hagita and Mori (2013), the sun is most potent to drivers during the times when it is closest to the horizon, at dawn and dusk – about an hour after sunrise and before sunset. When the sun is moderately high in the sky its effects can be mitigated by proper use of sun visors or other means. However, the position of the sun and the angle of

rays in low sun periods (dusk and dawn) may render sun visors useless, thus, interfering with a driver's ability to see features on the road and environment ahead. In the United Kingdom, the setting sun plays a part in nearly 3 000 accidents every year (Massey, 2013), with drivers at risk of being temporarily 'blinded' by the dazzle of the sun on the windscreen. In South Africa, the sun glare risk proved to be particularly high in winter when the sun sets at the busiest times on roads – just as most drivers are heading for home. Due to the absence of glare specific statistics in the accident data, it is not known how many accidents can be blamed on sun glare in South Africa.

What are the key factors that influence sun glare conditions?

A study by Jurado-Pina and Pardillo-Mayora (2010) highlighted several factors that determine the occurrence of sun glare along a roadway at a given moment in time. These include the **position of the sun** relative to the driver's line of sight, and the **configuration of the terrain**. The sun position is defined by azimuth and altitude (in degrees), relative to the Earth's surface. The line of sight varies with vehicle speed and roadway layout. The terrain profile refers to physical features of the environment under investigation, e.g. topography. Another key factor in the occurrence of invasive sun glare conditions is the **geometric design of the roadway**. Since the occurrence of glare varies according to location and times, certain combinations of the horizontal and vertical geometry of the roadway contribute directly to sun glare conditions by placing the driver's line of sight in a situation to be susceptible to glare effects (Auffray et al., 2007). As a result of the axial tilt of the Earth, the trajectory of the sun through the sky changes over the course of the year (Churchill et al. 2012). For that reason, glare conditions are highly dependent on **geographical locations**. Additionally, mountainous areas are less susceptible to sun glare conditions, since the sun may be occluded when it might be most problematic. Similarly, cloud cover potentially blocks direct sunlight exposure on drivers as well. On the whole, the wrong combination of all these factors may be detrimental to the safety of road users as a result of the blinding invasive sun.

For an arbitrary position on a roadway alignment, how can the times of the year or day be determined that drivers on that roadway could be faced with the risk of vision impairment as a result of sun glare?

Among the many factors identified as influences in the occurrence of sun glare conditions, three were identified as the key factors. These are the geometric design of the road network, the physical environment (topography and terrain profile) and the solar position (azimuth and altitude). These factors informed the formulation of the research, which included the selection of the appropriate tool to combine these factors and, thus, produce the anticipated results (direct sunlight exposure on the Cape Town road network). Considering the need for a tool, which can combine spatial data and solar position data, the ArcGIS software was identified as the most suitable tool for the study.

What tools needs to be available to develop and execute the proposed methodology for the City of Cape Town road network?

Availability was also a factor in the selection of a tool. The ArcGIS software was provided by the University of Cape Town GIS Laboratory. ArcGIS is Geographic Information System software which allows people to collect, organise, manage, analyse, communicate and distribute geographic information (www.esri.com). GIS can be used to store geographic data, make maps and analyse spatial data (Atkinson, 2012). The role of ArcGIS in applications, such as urban planning and transportation provides users, managers and decision makers, powerful tools for solving complex spatial problems.

The ArcGIS software includes a tool (hillshade), which allows for the modelling of sun illumination over the Earth's surface. Hillshade is shaded relief technique, which mimics the sun's effects – illumination, shading and shadows – on hills and canyons; thus, obtaining hypothetical illumination of a surface by determining illumination values for each cell in a raster (Hegazy and Effat, 2011). A hillshade model is a derivative of a Digital Elevation Model (DEM) that stimulates relative solar insolation for each grid cell based on its slope, aspect and the position of the sun (as defined by elevation and azimuth angle) (Bricher et al., 2008).

What data needs to be available to develop and execute the proposed methodology for the City of Cape Town road network?

A range of data was required for the execution of the proposed methodology, using the selected tools. The data was grouped into GIS data and analysis data. GIS data entails the background data collected for use in the ArcGIS software. This included a DEM (elevation data representing terrain relief) for the study area, which had a 10m spatial resolution. Similar to the DEM, the road network layer was also obtained from the UCT GIS Laboratory, and is derived from 10m topographical map. Sun position data for four representative days chosen in this study (autumnal and spring equinox; summer and winter solstice) was obtained from the Astronomical Applications Department of the U.S. Naval Observatory server (aa.usno.navy.mil/). Azimuth and altitude sun cones, which were used in the filtering of road segments, were both derived from literature sources. Overall, the methodology integrates background data (road network and DEM) and sun position data with a shadow determination algorithm in ArcGIS – as well as other advance GIS functionality for spatial analysis – to model and map the exposure of direct sunlight in the Cape Town road network; thus, identifying high risk areas and roads.

Using the chosen methodology, is it possible to identify which road networks are vulnerable to sun glare conditions in the City of Cape Town road network?

Implementation of this method to the Cape Metropolitan road network revealed that the AE and SE both have approximately 14.7% of the road network exposed to direct sunlight – sun glare conditions. The WS and SS, on the other hand, have about 12.2% and 15.2% of the road network exposed, respectively. With the exception of the WS, and in agreement with the quantitative data outcomes, statistical analysis of the results revealed that there is a significant difference in the amount of sunlight exposure between the morning and afternoon time periods in the other three days (AE, SE and SS). According to these results, the afternoon – on average – has less sunlight compared to the morning. Looking at the individual days, the afternoon period in the AE and SE does actually have less sunlight compared to the morning period. However, the WS and SS actually have more sunlight exposure in the afternoon compared to the morning. Overall, the AE and SE have the most sunlight exposure, while the WS has the least exposure. Table 6-1 gives a summary of the total lengths (out of a total of 112 661km) and percentages of road segments exposed to direct sunlight in the four days and 16 scenarios.

Table 6-1: Total Lengths and Percentages of Road Segments Exposed to Direct Sunlight

Astronomical Day	Time Period	Total Road Length Exposed to Sunlight					
		Distance in km			Percentage		
		19°	25°	Average	19°	25°	Average
Autumnal Equinox	am	24064	22452	**23258**	21.4	19.9	**20.6**
	pm	18104	16538	**17321**	16.1	14.7	**15.4**
Spring Equinox	am	24039	22605	**23322**	21.3	20.1	**20.7**
	pm	18113	16545	**17329**	16.1	14.7	**15.4**
Winter Solstice	am	15063	13748	**14406**	13.4	12.2	**12.8**
	pm	16134	17565	**16850**	14.3	15.6	**15.0**
Summer Solstice	am	17149	18110	**17629**	15.2	16.1	**15.6**
	pm	23321	24140	**23730**	20.7	21.4	**21.1**

With regards to map analysis, there was an observed uneven distribution of road segments in all the scenarios, across the Cape Metropolitan map. The northern part of the Cape Metropolitan, which is the Western Seaboard, and the top part of the Northern Suburbs have significantly less roads exposed to direct sunlight as indicated by the observed sparse distribution of road segments. The majority of road segments exposed to direct sunlight are concentrated in the southern part of the city, which includes the Southern Suburbs, Cape Flats, and parts of the Northern Suburbs and Southern Peninsula. These parts of the Cape Metropolitan are characterised by a plain topographic profile – there is a lack of mounds or raised areas of land to provide shadowing – and that is why they experience more sun radiation. These observations confirm that terrain profile does actually play a key role in the occurrence of sun glare conditions.

Does the proposed methodology produce valid results?

On the 15th of August 2014, a video footage of four Freeway and Primary arterial roads in the Cape Metropolitan Central Business District (CBD) was taped for the morning and afternoon periods during the times when the sun was considered to be at its worst – which in this case is defined by the 19º/25º sun cone. The aim was to validate the proposed model through the comparison of field investigation outcomes with the model outcomes, for the same roads. The investigation was carried out using Road Eye JS-300 camera, which is an intelligent electronic device designed to record driving parameters. Footage was recorded, while travelling at speed approximately between 40 and 60km/h. The terrain around these four roads is relatively flat.

In the morning the 19º/25º sun cone occurred between 09h15 and 09h45, while in the afternoon it occurred between 15h55 and 16h30. Considering that these times are well within an hour or so after sunrise (07h24) and before sunset (18h16), a decision was made to record sun glare footage between these periods. The clear weather condition on this day also made for a suitable recording environment. Figure 6-1 provides an example of the footage collected. While the image on the left clearly indicates a sun glare challenge, the image on the right indicates that high buildings can influence sun glare exposure in practice.

Figure 6-1: Buitenkant Street Snapshots (NE bound)

Using the ArcGIS Hillshade tool for the same day, time and area, the model calculations provide the same result, i.e. sun glare exposure in Buitenkant Street. However, the current model data for this area does not include the buildings. Even if exposure to sun glare might be reduced at times, the overall risk is, nonetheless, still prevalent. Overall, the validation of the proposed model revealed a satisfactory level of concurrence between the results. It was, therefore, concluded that the model is valid.

In the event, of accidents which occurred as a result of sun glare in the City of Cape Town, would it have been possible to warn drivers of this risk through the provision of real time information provided by the methodology?

Recorded data from the City of Cape Town was used to determine whether accidents resulting from sun glare could have been prevented had this model been applied. Given that sun glare was not one of the recorded accident causes, the closest possible description to sun glare accident

scenarios was, therefore, selected for use in the accident data analysis. The selected accidents were the ones specified to have been caused by being 'blinded'. Prior to 2013 'blinded' accident data was not recorded, ergo not available. Out of the 209 'blinded' accidents recorded in 2013, 149 happened in single carriage way roads and 52 in dual carriageways. Comparatively, this implies a bigger danger on minor roads.

Considering the insufficient amount of information to verify the 'blinded' accident data as having been caused by direct sunlight exposure, it was impossible to conclude whether the selected accidents could have been avoided with the use of the methodology. However, the formulation of accident scenarios, through the employment of sun radiation data from the modelled accidents and the assumption of vehicle travel direction, facilitated the drawing of hypothetical conclusions. For instance, in a case where the sun is facing the southwest direction, traffic in the northeast bound direction is facing the dazzling sun. In an event when the sun appears from behind trees, buildings or by reflection, drivers can be blinded by the sudden burst of sunlight, thus, resulting in 'head/rear end' accidents, because of the rapid decrease in speed or 'sideswipe' accidents. Overall, in scenarios where all the necessary aspects of sun glare are known, provision of a sun glare risk real time information system could have averted the occurrence of these accidents.

6.2 Recommendations

The assumptions and limitations of the study are informants which relate to, whether increased exposure entails increased risk of accidents. One of the key assumptions was the identification of a sun cone, ranging between 19º and 25º altitude, which according to Jurado-Piña and Pardillo-Mayora (2009) characterises vision impairment situations for drivers aged between 40 and 60 years. Because of the narrow range of the 19º-25º sun cone, road segments that actually experience sun glare conditions outside this altitude range in the morning and/or afternoon period may not be represented in the output maps – as was observed in Glynn Street in the morning period (NE bound). For that reason, future work on this research would have to further investigate the sun cone, to determine one that covers a wider range of sun glare conditions. This recommendation also applies to the ±15º threshold adopted for azimuth and slope filtering, which allows for the selection of road segments whose azimuth (bearing) was ±15º of the sun

azimuth for the scenario in question. Recommended future work on this threshold would have to focus on investigating the implications of a different threshold range, either narrower or wider than 30º.

In addition to the absence of atmospheric effects (cloud cover, rainfall etc.) assumed by the model, there was also an assumed absence of special on site conditions such as buildings, line of trees or any tall objects, affecting direct sunlight. A comparison of the field investigation and methodology outcomes in Chapter 5 (Section 5.2), made these assumptions apparent. For instance, in the morning, northeast bound traffic in the whole of Buitenkant Street is exposed to direct sunlight according to the methodology. However, the field investigation results indicated that a few parts of the street are actually free of exposure at certain times. This was attributed to the presence of tall buildings on either side of the road. Therefore, the incorporation of special on site conditions and atmospheric effects in the proposed model are among the key subjects of future extension of this methodology.

Outcomes from the proposed methodology can be applied to both existing and new road designs. With respect to the design process for new roads, it would be an informative dimension to consider, particularly when evaluating different layout and alignment alternatives. The methodology could also be used to assess overall road safety in existing networks. Apart from mitigation measures, such as visual barriers (e.g. row of trees), Intelligent Transport Systems (ITS) should be prioritised in implementing the proposed model in this dissertation. Considering that the model produces results for a specific time in the day, automated real time warning systems could be implemented for the identification of high risk conditions and road segments as a result of direct sunlight exposure. Among other things, such systems must be able to integrate and synchronise temporal traffic information from a variety of sensors (e.g. GPS, cameras from a computer vision-based system).

In a similar study, Chalkias et al. (2013) proposed incorporating a methodology like this in car navigation systems, in order to provide additional real-time information to drivers. An optimal system would be one that provides countermeasures in real-time, i.e. alternative routes. The incorporation of GIS technology with GPS could enable the development of such systems. All in

all, ITS can provide endless options for the mitigation of sun glare conditions in line with this methodology.

Bibliography

Andrey, J., Mills, B. and Vandermolen, J., 2001. *Weather Information and Road Safety*. Toronto, Ontario: Institute for Catastrophic Loss Reduction.

Andrey, J., Olley, R., 1990. *Relationships between weather and road safety, past and future directions*. Climatol. Bull. 24 (3), 123–137.

Andreescu, M. and Frost, D., 1998. *Weather and traffic accidents in Montreal, Canada*. Climate Research. 9(3): 225-230. DOI:10.3scal investigation of the impacts of sun-related glare on traffic flow. TRB 87th Annual Meeting Compendium of Papers, Transportation Research Board, Washington, DC.

ArcGIS for Desktop. Available from: <http://www.esri.com/>. [13 March 2014]

Archer, C. B.,1980. *Comments on 'Calculating the position of the sun'*. Solar Energy **25**, 91.

Atkinson, L., 2012. *What is ArcGIS?* Bodleian Libraries, University of Oxford. Available from: <www.bodleian.ox.ac.uk/>. [12 April 2014]

Auffray, B., 2007. *Effect of the Sun Glare on Traffic Flow Quality*. Terwilliger, Portland, Oregon, USA.

Auffray, B., Monsere, C. M., and Bertini, R. L., 2008. *An empirical investigation of the impacts of sun-related glare on traffic flow*. TRB 87th Annual Meeting Compendium of Papers, Transportation Research Board, Washington, DC.

Ayres, T. J., Kelkar, R., and Woodruff, W. H., 2004. *Driver Adjustment to Solar Glare*. Journal of Proceeding of the human factors and Ergonomics society annual meeting, **48**(5), pp. 2295-2299.

Babari, R., Hautiere, N., Dumont, E., Paparoditis, N., and Misener, J., 2010. *Visibility monitoring using conventional roadside cameras: Shedding light on and solving a multi-national road safety problem*. Paris, France, TRB, pp. 1-12.

Bergel-Hayat, R., Debbarh, M., Antoniou, C. and Yannis, G., 2013. *Explaining the road accident risk:Weather effects*. Accident Analysis and Prevention. 60(0): 456-465.

Blanco-Muriel, M., Alarcon-Padilla, D., Lopez-Moratalla, T. and Lara-Coira, M., 2001. *Computing the solar vector*. Solar Energy, 70(5), pp. 431-441.

Brent & Kilburn Times, 2014. *Blinding sun caused crash that killed motorcycle courier from Wembley in Paddington*. Available from: < http://www.kilburntimes.co.uk/news/>.

[26 August 2014].

Bullough, J. D. and Rea, M. S., 2001. *Driving in Snow: Effect of Headlamp Color at Mesopic and Photopic Light Levels.* Lighting Technology Developments for Automobiles , 5-8 March.

Briney, A., NA. *Geography of Cape Town*, South Africa. Available from: < http://geography.about.com/>. [26 May 2014].

Brodsky, H., Hakkert, A.S., 1988. *Risk of a road accident in rainy weather.* Crash Anal. Prev. 20 (2), 161–176.

Cavallo, V., Colomb, M. and Dore, J., 2001. *Distance Perception of Vehicle Rear Lights in Fog*. The Journal of the Human Factors and Ergonomics Society, 1 January, 43(3), pp. 442-451.

Chalkias, C., Faka, A., and Kalogeropoulos, K., 2013. *Assessment of Direct Sun-Light on Rural Road Network through Solar Radiation Analysis Using GIS*. Open Journal of Applied Sciences, Scientific Research. DOI:10.4236/ojapps.2013.32030.

Charman, W. N., 1997. *Vision and driving - a literature review and commentary*. Journal of the College of Optometrists, 17(5), pp. 371-391.

Choi, E., and Singh, S., 2005. *Statistical assessment of the glare issue—Human and Natural Elements*. Proc., 2005 FCSM Conf., Federal Committee on Statistical Methodology, Arlington, VA.

Chu, S. B., Wood, J. M. and Collins, M. J., 2010. *The Effect of Presbyopic Vision Corrections on Nighttime Driving Performance*. Investigative Opthalmology and Visual Science, 51(0).

Churchill, A.M., Tripodis, Y. and Lovell, D.J., 2012. *Sun Glare Impacts on Freeway Congestion: Geometric Model and Empirical Analysis*. Journal of Transportation Engineering-Asce, **138**(10), pp. 1196-1204.

Clarke, D. D., Ward, P., Bartle, C. and Truman, W., 2006. *Young driver accidents in the UK: The influence of age, experience, and time of day*. Accident Analysis and Prevention, Volume 38, pp. 871-878.

Codling, P. J., 1971. *Thick fog and its effect on traffic flow and accidents*. Road Research Laboratory, p. 24.

Datla, S. and Sharma, S., 2008. *Impact of cold and snow on temporal and spatial variations of highway traffic volumes*. Journal of Transport Geography. 16(5): 358-372.

Department of Health and Human Services, 2011. *Glare-related Crashes in Nebraska*.

Doherty, S. T., Andrey, J. C. and Marquis, J. C., 1993. *Driver Adjustments to Wet Weather Hazards*.Waterloo, Ontario: Climatologial Bulletin.

Dozzaa, M., and Pa˜neda Gonzáleza, N., 2013. *Recognising safety critical events: Can automatic video processing improve naturalistic data analyses?* Accident Analysis and Prevention 60 (2013) 298– 304.

Edwards, J. B., 1996. *Weather-related road accidents in England and Wales: a spatial analysis*. Journal of Transport Geography, 4(3), pp. 201-212.

Encyclopaedia Britannica, 2014. *Cape Town*. Encyclopaedia Britannica Online Academic Edition. Encyclopædia Britannica Inc., 2014. <http://www.britannica.com/EBchecked/topic/93686/Cape-Town>. [25 May 2014]

Eurostat, 2007. P*anorama of Transport.* Luxembourg.

Fridstrom, L., Ifver, J., Ingebrigtsen, S., Kulmala, R. and Thomsen, L., 1995. *Measuring the Contribution of Randomness, Exposure, Weather, and Daylight to the Variation in Road Accident Counts*. Accident Analysis and Prevention. 27(1): 1-20.

Gardner, M.J., and Altman, D.G., 1986. *Confidence interval rather than P values: estimation rather than hypothesis testing.*

General Facts. Available from: <http://www.capetown.travel/content/page/general-facts>. [26 May 214].

Grena, R., 2008. *An algorithm for the computation of the solar position.* Solar Energy, **82**(5), pp. 462-470.

Ha, Y., 2011. *New York Court Finds Driver Blinded by Sun Glare May be Liable in Accident.* East News, Insurance Journal. Available from: < http://www.insurancejournal.com/news/east/>. [13 August 2014].

Hagita, K., and Mori, K., 2013. *The Effect of Sun Glare on Traffic Accidents in Chiba Prefecture, Japan*. Proceedings of the Eastern Asia Society for Transportation Studies, Vol.9, 2013.

Hall, P., and Wilson, R.S., 1991. *Two Guidelines for Bootstrap hypothesis Testing*. Biometrics 47, 757-762.

Hargroves, R., 1983. *Road Lighting*. 130, 420 - 441.

Hastings, P., 2012. *As sun sets, risk of crashes rises*. The Columbian 14 September. Available from: <http://www.columbian.com/news/>. [10 August 2014].

Hegazy, M.N., and Effat, H., 2011. *Exploring the Egyptian Terrain Characteristics from Space for Strategic Planning*. Survival and Sustainability, Environmental Earth Sciences, Springer-Verlag Berlin Heidelberg. DOI 10.1007/978-3-540-95991-5_75.

Hermans, E., Brijs, T., Stiers, T., and Offfermans, C., 2002. *The Impact of Weather Conditions on Road Safety Investigated on an Hourly Basis*. pp. 1-17.

Hogema, J. H. and Van der Horst, A., 1994. *Driving behaviour in fog: Analysis of inductive loop data*. Soesterberg, Netherlands: TNO Human Factors Research Institute.

How Hillshade works. Avialable from: < http://webhelp.esri.com/>. [10 October 2013]

Ilyas M., 1983. *Solar position programs: refraction, sidereal time and Sunset / Sunrise*. Solar Energy **31**(4), 437–438.

Jun, M. (2010). Towards a general optimal model for minimizing nighttime road traffic accidents and road lighting power consumption.

Jungu-Omara, I and Vanderschuren, M., 2006. *Ways of Reducing Crashes on South African Roads*. Paper for the South African Transport Conference, Pretoria, South Africa, July 2006.

Jurado-Pina, R. and Pardillo-Mayora, J.M., 2010. *Methodology to Analyze Sun Glare Impact on Highway under Prolonged Exposure*. Journal of Transportation Engineering-Asce, **136**(12), pp. 1137-1144.

Jurado-Pina, R., Pardillo-Mayora, J.M. and Jimenez, R., 2010. *Methodology to Analyse Sun Glare Related Safety Problems at Highway Tunnel Exits*. Journal of Transportation Engineering-Asce, **136**(6), pp. 545-553.

Knott, R., 1983. *Proposed American National Standard Practice for Industrial Lighting*. Lighting Design and Application, **13**(7), pp. 29-68.

Konstantopoulos, P., Chapman, P. and Crundall, D., 2010. *Driver's visual attention as a function of driving experience and visibility*. Using a driving simulator to explore drivers' eye movements in day, night and rain driving. Accident Analysis and Prevention. 42(3): 827-834.

Lamm, R., Choueiri, E.M., and Mailaender, T., 1990. *Comparison of Operating Speeds on Dry and Wet Pavements of Two-Lane Rural Highways*. In Transportation Research Record 1280, Transportation Research Board, National Research Council, Washington DC, pp 199-207.

Lane, P.L., McClafferty, K.J., Green R.N. and Nowak E.S., 1995. A *study of injury-producing*

crashes of median divided highways in Southwestern Ontario. Accident Analysis and Prevention 27:175-184.

Liu, X., 2007. *Study on the Influence of Glare on Driver's Visual Works at Night*.

Lynch, S.M., 2013. *Using Statistics in Social Research: A Concise Approach*. Springer Science, Business Media, New York. DOI 10.1007/978-1-4614-8573-5_2.

Making Effective Use of Shaded Relief. Available from: < http://landtrustgis.org/technology/advanced>. [19 July 2013].

Mainster, M.A. and Turner, P.L., 2012. *Glare's Causes, Consequences, and Clinical Challenges After a Century of Ophthalmic Study*. American Journal of Ophthalmology, **153**(4), pp. 587-593.

Massey, R., 2013. *The dazzling sunsets that kill 36 drivers in 12 months: Glare contributes to 3,000 accidents and is particularly dangerous at this time of yea*r. United Kingdom Mail Online, 15 October. Available from: <http://www.dailymail.co.uk/>. [06 August 2014]

Mitra, S., 2008. *Investigating Impact of Sun Glare on Transportation Safety*. TRB 87th Annual Meeting, Transportation Research Board, Washington, DC.

Moore, R. L. and Cooper, L., 1972. *Fog and Road Traffic*. Crowthorne, Berkshire England: Transport and Road Research Laboratory.

Morris, R.S., Mounce J.M., Button J.W., and Walton N.E., 1977. *Visual performance of drivers during rainfall*. Transportation Research Record 628:19-25

Mosedale, J., Purdy, A. and Clarkson, E., 2004. *Contributory factors to road accidents.* Transport Research Labortory, p. 13p.

Nakagawara, V.B., Wood, K.J. and Montgomery, R.W., 2004. *Natural sunlight and its association to civil aviation accidents*. Optometry (St. Louis, Mo.), **75**(8), pp. 517-522.

National Highway Traffic Safety Administration (NHTSA), 1990–1999. State Data System. National Centre for Statistics and Analysis, NHTSA, Department of Transportation, Washington, DC.

National Oceanic and Atmospheric Administration (NOAA), 2007. *Hillshades for the main 8 Hawaiian Islands.* Centre for Coastal Monitoring and Assessment (CCMA), Biography Branch, Department of Commerce. Silver Spring, USA.

National Traffic Safety Board (NTSB), 1980. *Fatal Highway Accidents on Wet Pavement—The Magnitude Location and Characteristics*, HTSB-HSS-80-1. NTIS, Springfield, VA.

O'Leary, D., 1978. *Some Impacts of weather on Modern Transportation Systems: A Natural*

Hazards Approach. Warterloo, Ontario: Wilfrid Laurier University.

Otmani, S., Roge, J. and Muzet, A., 2005. *Sleepiness in professional drivers: Effect of age and time of day*. Accident Analysis and Prevention, Volume 37, pp. 930-937.

Owsley, C. and McGwin Jr, G. 1999. *Vision Impairment and Driving*. Survey of Ophthalmology. 43(6): 535-550.

Pandea, A., and Abdel-Aty, M., 2009. *A novel approach for analysing severe crash patterns on multilane highways*. Accident Analysis and Prevention 41 (2009) 985–994.

Pitman C. L. and Vant-Hull L. L., 1978. *Errors in locating the Sun and their effect on solar intensity predictions*. In: Meeting of the American Section of the International Solar Energy Society, Denver, 28 Aug 1978, pp. 701–706.

Plainis, S., Murray, I.J. and Pallikaris, I.G., 2006. *Road traffic casualties: understanding the night- time death toll*. Injury Prevention. 12(2): 125-138. DOI:10.1136/ip.2005.011056.

Pormerleau, D., 1998. *Visibility Estimation from a Moving Vehicle Using the Ralph System.* Institute of Electrical and Electronics Engineers, pp. 906-911.

Rooney, J., 1967. *The Urban Snow Hazard in the United States: An Appraisal of Disruption*. 57(4): 538-559.

Rosner, B., Glynn, R.J., and Lee, M.T., 2005. *The Wilcoxon Signed Rank Test for Paired Comparisons of Clustered Data*. Biometrics 62, 185-192.

Salama, S., 2010. *Blinding sun caused 22 car crashes in eight months.* The Gulf News 19 October. Available from: < http://gulfnews.com/news/gulf/>. [16 August 2014].

Shepard, F. D., 1996. *Reduced Visibility due to fog on the highway.* United States: Transportation Research Board.

Spencer, J.W., 1971. *Fourier series representation of the position of the Sun*. Search 2 (5).

Spencer J. W., 1989. *Comments on 'The astronomical almanac's algorithm for approximate solar position (1950–2050)'.* Solar Energy **42**(4), 353.

Statistics South Africa, 2009. *Road Traffic Accident Deaths in South Africa 2001-2006*. Report No. 03-09-07, Stats SA publications, Pretoria.

Stone, M., 2007. *The Sun's Glare and Car Accidents.* KKTV 09 October. Available from: <http://www.kktv.com/home/headlines>. [10 August 2014].

Stubbs, K., Arumugam H., and Masoud, O., 2003. *A Real-time Collision Warning System for Intersections.* Department of Computer Science and Engineering, University of Minnesota.

Suggett, J., 1999. *The Effect of Precipitation on Traffic Safety in the City of Regina.* Master of Science thesis, University of Regina, Saskatoon.

Theeuwes, J.J., Alferdinck, Johan W. A. M. and Perel, M.M., 2002. *Relation Between Glare and Driving Performance*. Human Factors: The Journal of the Human Factors and Ergonomics Society, **44**(1), pp. 95-107.

Times News Online, 2014. *One woman injured following early morning crash in West Penn Township.* Available from: < http://www.tnonline.com/2014/>. [26 August 2014].

Van Niekerk, A., 2012. *Developing a Very High Resolution DEM of South Africa.* Stellenbosch University, Position IT.

Vos, J.J., 2003. *On the cause of disability glare and its dependence on glare angle, age and ocular pigmentation.* Clinical and experimental optometry : journal of the Australian Optometrical Association, **86**(6), pp. 363-370.

Walraven, R., 1978. *Calculating the position of the sun.* Solar Energy. 20(5): 393-397.

Walraven R., 1979. *Erratum*. Solar Energy **22**, 195.

Williams, A.F., 2003. *Teenage drivers: patterns of risk*. Journal of Safety Research. 34(1): 5-15.

World Health Organisation, 2009. *Global Status Report on Road Safety: Time for Action.* WHO Library Cataloguing-in-Publication Data, Geneva.

Wood, J. M. and Owens, A. D., 2005. *Standard Measures of Visual Acuity Do Not Predict Drivers' Recognition Performance Under Day or Night Conditions*. Optemetry and Vision Science, 82(8), pp. 698-705.

Yannis, G. and Karlaftis, M. G., 2010. *Weather Effects on Daily Traffic Accidents and Fatalities: A Time Series Count Data Approach*. Washington, Transportation Research Board.

Zein, S. R. and Navin, F. P., 2007. *Improving Road Safety: A New Systems Approach.* Transportation Research Record: Journal of the Transportation Research Board, 24 January, 1830(2003 Highway Safety, Traffic Law Enforcement, and Truck Safety), pp. 1-9.

Appendices

Appendix A: Overview of ArcGIS Processes

Appendix B: Morning Period Overlay (Section 5.1)

Appendix C: Morning Period Overlay (Section 5.1)

Appendix D: Afternoon Period Overlay (Section 5.1)

Appendix E: Morning and Afternoon Period Overlay (Section 5.1)

Appendix F: Picture of Road Eye JS-30

Appendix A: Overview of ArcGIS Processes

HILLSHADE

Input raster	Output raster	Azim.	Alti.	Model shadows	Z factor
E:\Nothando_sunglare\topo_10m	C:\GIS\nothando2\New_Roads2.0.gdb\hsae0855	72.1	24.8	TRUE	1
E:\Nothando_sunglare\topo_10m	C:\GIS\nothando2\New_Roads2.0.gdb\hsae1655	287.7	24.4	TRUE	1
E:\Nothando_sunglare\topo_10m	C:\GIS\nothando2\New_Roads2.0.gdb\hsse0840	72	24.8	TRUE	1
E:\Nothando_sunglare\topo_10m	C:\GIS\nothando2\New_Roads2.0.gdb\hsse1640	287.5	24.4	TRUE	1
E:\Nothando_sunglare\topo_10m	C:\GIS\nothando2\New_Roads2.0.gdb\hsws1035	33.7	24.5	TRUE	1
E:\Nothando_sunglare\topo_10m	C:\GIS\nothando2\New_Roads2.0.gdb\hsws1500	326.8	24.7	TRUE	1
E:\Nothando_sunglare\topo_10m	C:\GIS\nothando2\New_Roads2.0.gdb\hsss0745	102.6	24.8	TRUE	1
E:\Nothando_sunglare\topo_10m	C:\GIS\nothando2\New_Roads2.0.gdb\hsss1745	257.5	24.8	TRUE	1
E:\Nothando_sunglare\topo_10m	C:\GIS\nothando2\New_Roads2.0.gdb\hsae0830	76.2	19.9	TRUE	1
E:\Nothando_sunglare\topo_10m	C:\GIS\nothando2\New_Roads2.0.gdb\hsae1720	283.6	19.4	TRUE	1
E:\Nothando_sunglare\topo_10m	C:\GIS\nothando2\New_Roads2.0.gdb\hsse0815	76.1	19.8	TRUE	1
E:\Nothando_sunglare\topo_10m	C:\GIS\nothando2\New_Roads2.0.gdb\hsse1705	283.4	19.5	TRUE	1
E:\Nothando_sunglare\topo_10m	C:\GIS\nothando2\New_Roads2.0.gdb\hsws0955	41.9	19.4	TRUE	1
E:\Nothando_sunglare\topo_10m	C:\GIS\nothando2\New_Roads2.0.gdb\hsws1540	318.5	19.7	TRUE	1
E:\Nothando_sunglare\topo_10m	C:\GIS\nothando2\New_Roads2.0.gdb\hsss0720	105.5	19.8	TRUE	1
E:\Nothando_sunglare\topo_10m	C:\GIS\nothando2\New_Roads2.0.gdb\hsss1810	254.5	19.8	TRUE	1

RECLASSIFY

Input raster	Reclass field	Reclassification	Output raster	Change missing values to NoData
hsss1745	Value	0 1 1;1 254 NODATA	C:\GIS\nothando2\New_Roads2.0.gdb\Rhsss1745	TRUE
hsss0745	Value	0 1 1;1 254 NODATA	C:\GIS\nothando2\New_Roads2.0.gdb\Rhsss0745	TRUE
hsws1500	Value	0 1 1;1 254 NODATA	C:\GIS\nothando2\New_Roads2.0.gdb\Rhsws1500	TRUE
hsws1035	Value	0 1 1;1 254 NODATA	C:\GIS\nothando2\New_Roads2.0.gdb\Rhsws1035	TRUE
hsse1640	Value	0 1 1;1 254 NODATA	C:\GIS\nothando2\New_Roads2.0.gdb\Rhsse1640	TRUE
hsse0840	Value	0 1 1;1 254 NODATA	C:\GIS\nothando2\New_Roads2.0.gdb\Rhsse0840	TRUE
hsae1655	Value	0 1 1;1 254 NODATA	C:\GIS\nothando2\New_Roads2.0.gdb\Rhsae1655	TRUE
hsae0855	Value	0 1 1;1 254 NODATA	C:\GIS\nothando2\New_Roads2.0.gdb\Rhsae0855	TRUE
hsss1810	Value	0 1 1;1 254 NODATA	C:\GIS\nothando2\New_Roads2.0.gdb\Rhsss1810	TRUE
hsss0720	Value	0 1 1;1 254 NODATA	C:\GIS\nothando2\New_Roads2.0.gdb\Rhsss0720	TRUE
hsws1540	Value	0 1 1;1 254 NODATA	C:\GIS\nothando2\New_Roads2.0.gdb\Rhsws1540	TRUE
hsws0955	Value	0 1 1;1 254 NODATA	C:\GIS\nothando2\New_Roads2.0.gdb\Rhsws0955	TRUE
hsse1705	Value	0 1 1;1 254 NODATA	C:\GIS\nothando2\New_Roads2.0.gdb\Rhsse1705	TRUE
hsse0815	Value	0 1 1;1 254 NODATA	C:\GIS\nothando2\New_Roads2.0.gdb\Rhsse0815	TRUE
hsae1720	Value	0 1 1;1 254 NODATA	C:\GIS\nothando2\New_Roads2.0.gdb\Rhsae1720	TRUE
hsae0830	Value	0 1 1;1 254 NODATA	C:\GIS\nothando2\New_Roads2.0.gdb\Rhsae0830	TRUE

CONVERT FROM RASTER TO VECTOR (POLYGON)

Input raster	Output polygon features	Simplify polygons	Field
Rhsae0855	C:\GIS\nothando2\New_Roads2.0.gdb\shade_hsae0855	TRUE	Value
Rhsae1655	C:\GIS\nothando2\New_Roads2.0.gdb\shade_hsae1655	TRUE	Value
Rhsse0840	C:\GIS\nothando2\New_Roads2.0.gdb\shade_hsse0840	TRUE	Value
Rhsse1640	C:\GIS\nothando2\New_Roads2.0.gdb\shade_hsse1640	TRUE	Value
Rhsws1035	C:\GIS\nothando2\New_Roads2.0.gdb\shade_hsws1035	TRUE	Value
Rhsws1500	C:\GIS\nothando2\New_Roads2.0.gdb\shade_hsws1500	TRUE	Value
Rhsss0745	C:\GIS\nothando2\New_Roads2.0.gdb\shade_hsss0745	TRUE	Value
Rhsss1745	C:\GIS\nothando2\New_Roads2.0.gdb\shade_hsss1745	TRUE	Value
Rhsae0830	C:\GIS\nothando2\New_Roads2.0.gdb\shade_hsae0830	TRUE	Value
Rhsae1720	C:\GIS\nothando2\New_Roads2.0.gdb\shade_hsae1720	TRUE	Value
Rhsse0815	C:\GIS\nothando2\New_Roads2.0.gdb\shade_hsse0815	TRUE	Value
Rhsse1705	C:\GIS\nothando2\New_Roads2.0.gdb\shade_hsse1705	TRUE	Value
Rhsws0955	C:\GIS\nothando2\New_Roads2.0.gdb\shade_hsws0955	TRUE	Value
Rhsws1540	C:\GIS\nothando2\New_Roads2.0.gdb\shade_hsws1540	TRUE	Value
Rhsss0720	C:\GIS\nothando2\New_Roads2.0.gdb\shade_hsss0720	TRUE	Value
Rhsss1810	C:\GIS\nothando2\New_Roads2.0.gdb\shade_hsss1810	TRUE	Value

ERASE SHADED ROADS

Input features	Erase features	Output feature class
Summer_Solstice_17h45	shade_hsss1745	C:\GIS\nothando2\New_Roads2.0.gdb\Summer_Solstice_17h45_Erase
Summer_Solstice_07h45	shade_hsss0745	C:\GIS\nothando2\New_Roads2.0.gdb\Summer_Solstice_07h45_Erase
Winter_Solstice_15h00	shade_hsws1500	C:\GIS\nothando2\New_Roads2.0.gdb\Winter_Solstice_15h00_Erase
Winter_Solstice_10h35	shade_hsws1035	C:\GIS\nothando2\New_Roads2.0.gdb\Winter_Solstice_10h35_Erase
Spring_Equinox_16h40	shade_hsse1640	C:\GIS\nothando2\New_Roads2.0.gdb\Spring_Equinox_16h40_Erase
Spring_Equinox_08h40	shade_hsse0840	C:\GIS\nothando2\New_Roads2.0.gdb\Spring_Equinox_08h40_Erase
Autumnal_Equinox_16h55	shade_hsae1655	C:\GIS\nothando2\New_Roads2.0.gdb\Autumnal_Equinox_16h55_Erase
Autumnal_Equinox_08h55	shade_hsae0855	C:\GIS\nothando2\New_Roads2.0.gdb\Autumnal_Equinox_08h55_Erase
Autumnal_Equinox_08h30	shade_hsae0830	C:\GIS\nothando2\New_Roads2.0.gdb\Autumnal_Equinox_08h30_Erase
Autumnal_Equinox_17h20	shade_hsae1720	C:\GIS\nothando2\New_Roads2.0.gdb\Autumnal_Equinox_17h20_Erase
Spring_Equinox_08h15	shade_hsse0815	C:\GIS\nothando2\New_Roads2.0.gdb\Spring_Equinox_08h15_Erase
Spring_Equinox_17h05	shade_hsse1705	C:\GIS\nothando2\New_Roads2.0.gdb\Spring_Equinox_17h05_Erase
Winter_Solstice_09h55	shade_hsws0955	C:\GIS\nothando2\New_Roads2.0.gdb\Winter_Solstice_09h55_Erase
Winter_Solstice_15h40	shade_hsws1540	C:\GIS\nothando2\New_Roads2.0.gdb\Winter_Solstice_15h40_Erase
Summer_Solstice_07h20	shade_hsss0720	C:\GIS\nothando2\New_Roads2.0.gdb\Summer_Solstice_07h20_Erase
Summer_Solstice_18h10	shade_hsss1810	C:\GIS\nothando2\New_Roads2.0.gdb\Summer_Solstice_18h10_Erase

Appendix B: Morning Period Map Overlay

I. Autumnal Equinox (08h30 and 08h55)

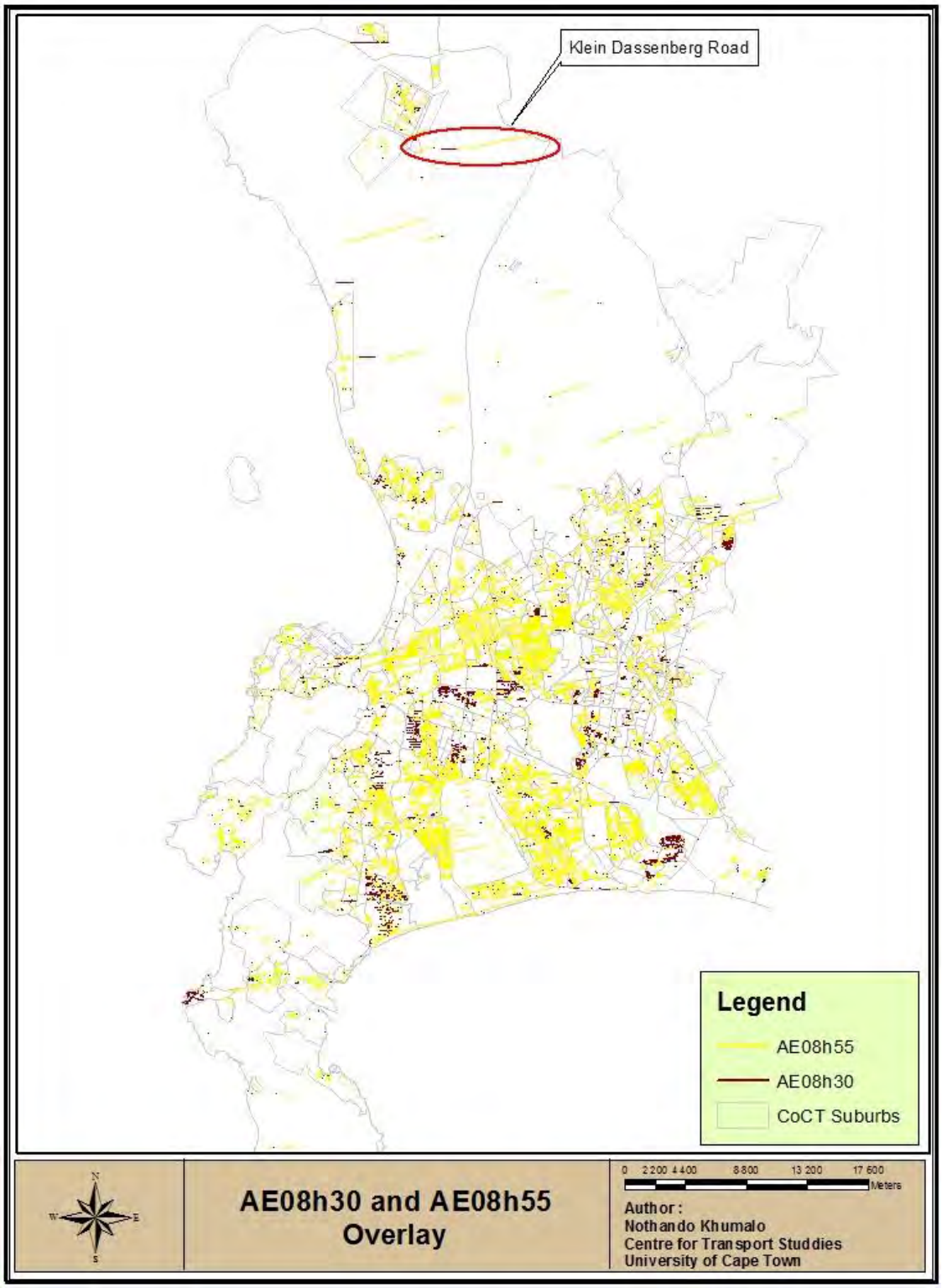

II. Spring Equinox (08h15 and 08h40)

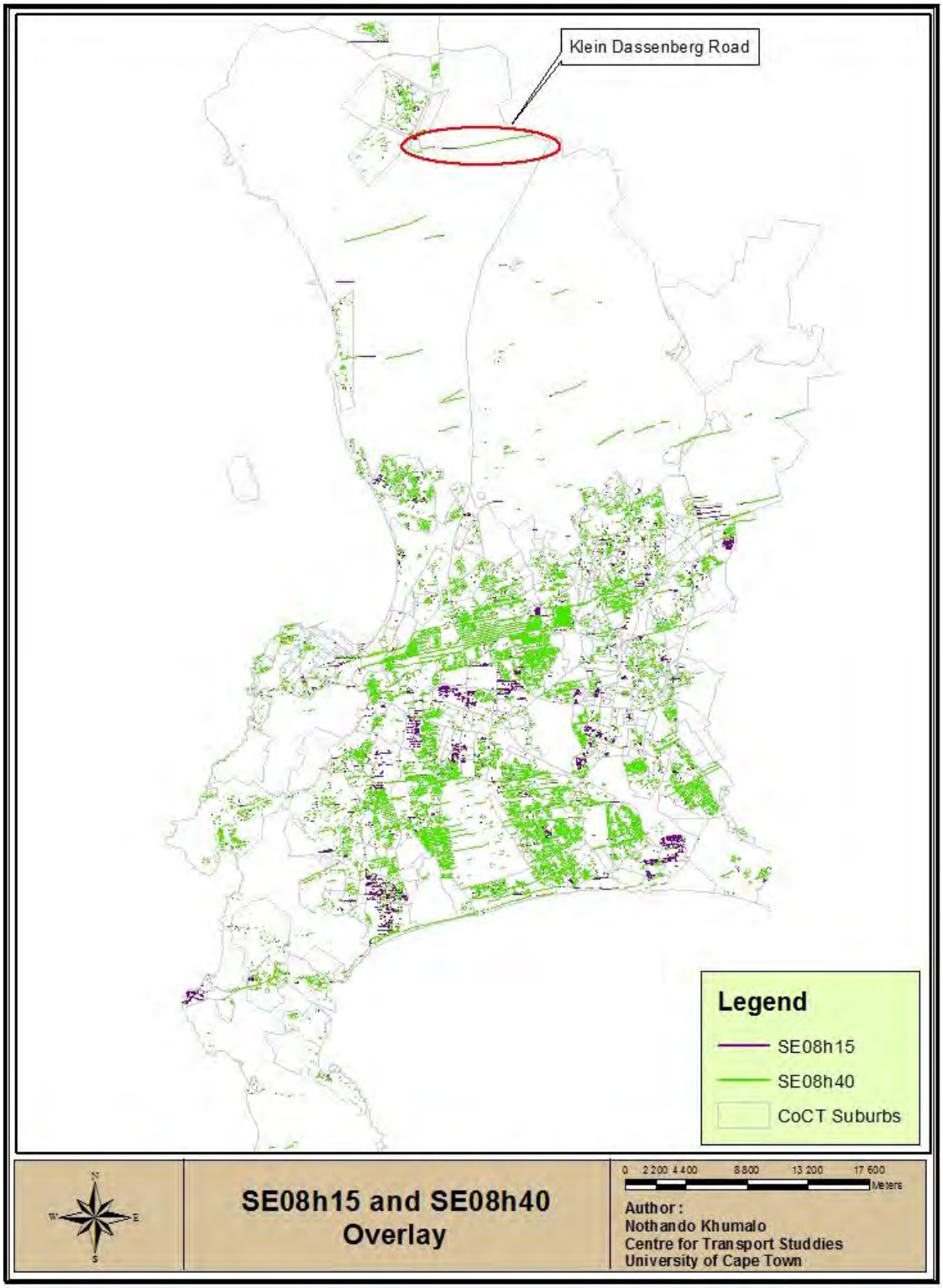

III. Winter Solstice (09h55 and 10h35)

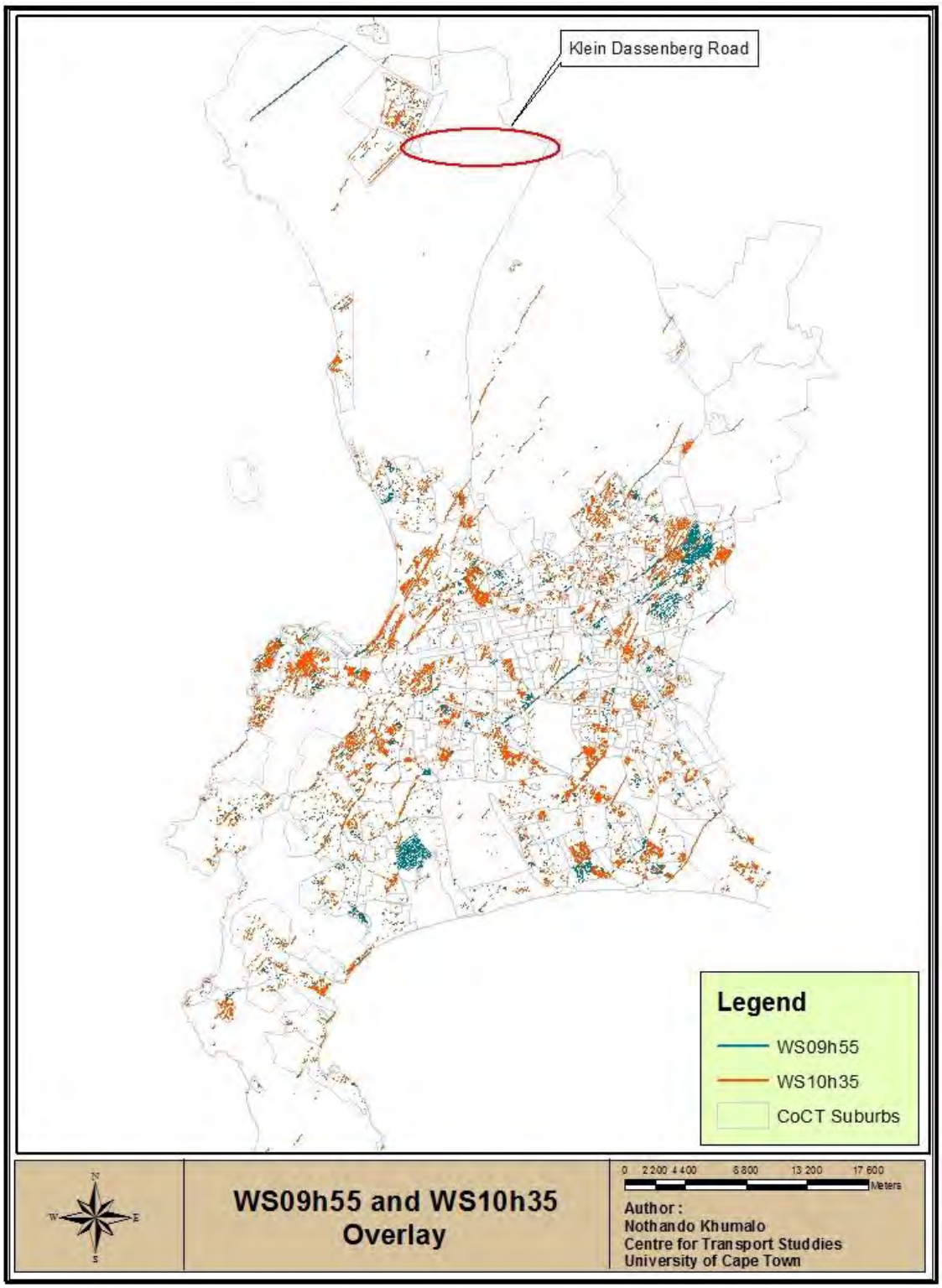

IV. Summer Solstice (07h20 and 07h45)

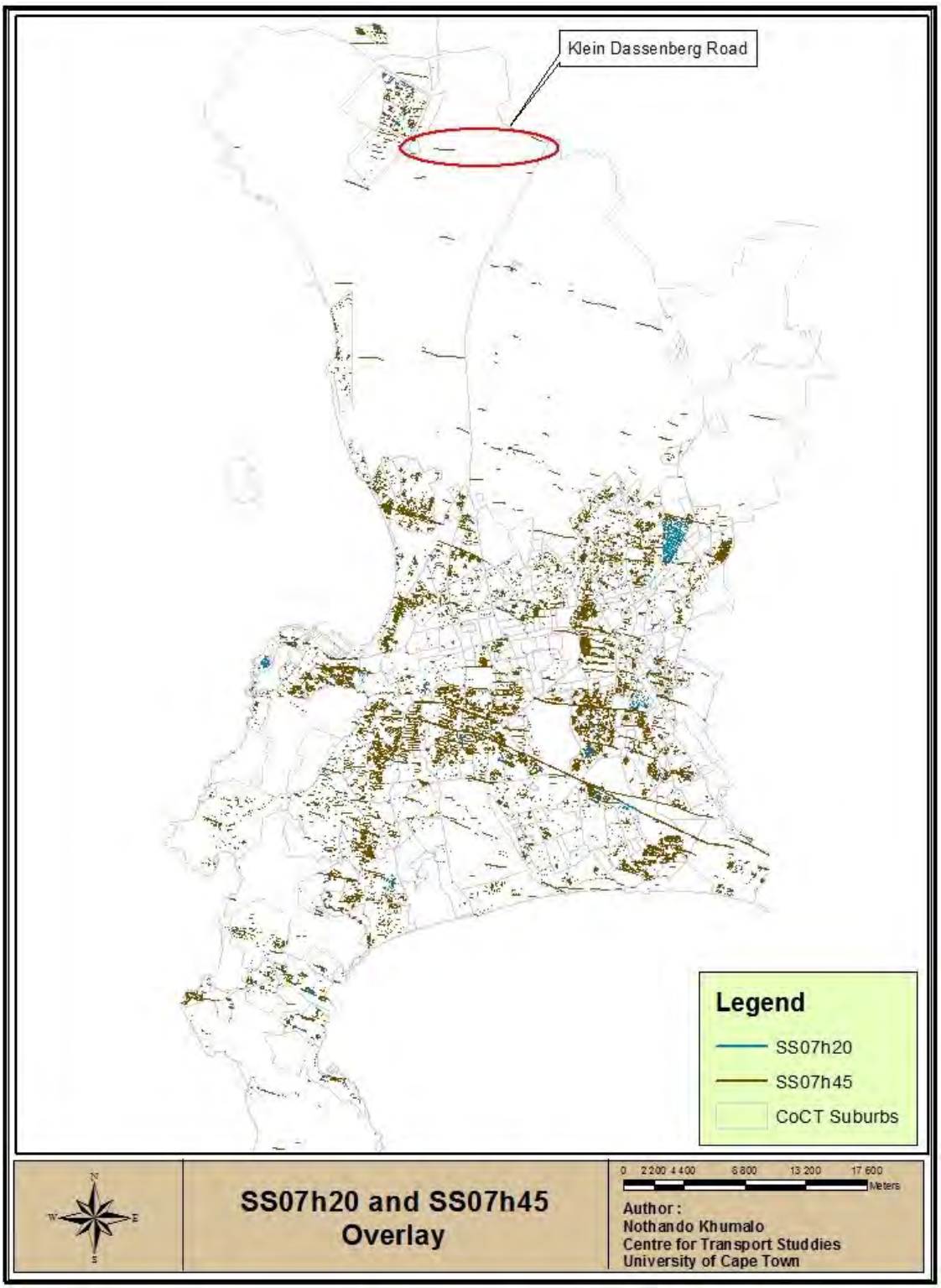

Appendix C: Afternoon Period Map Overlay

I. Autumnal Equinox (16h55 and 17h20)

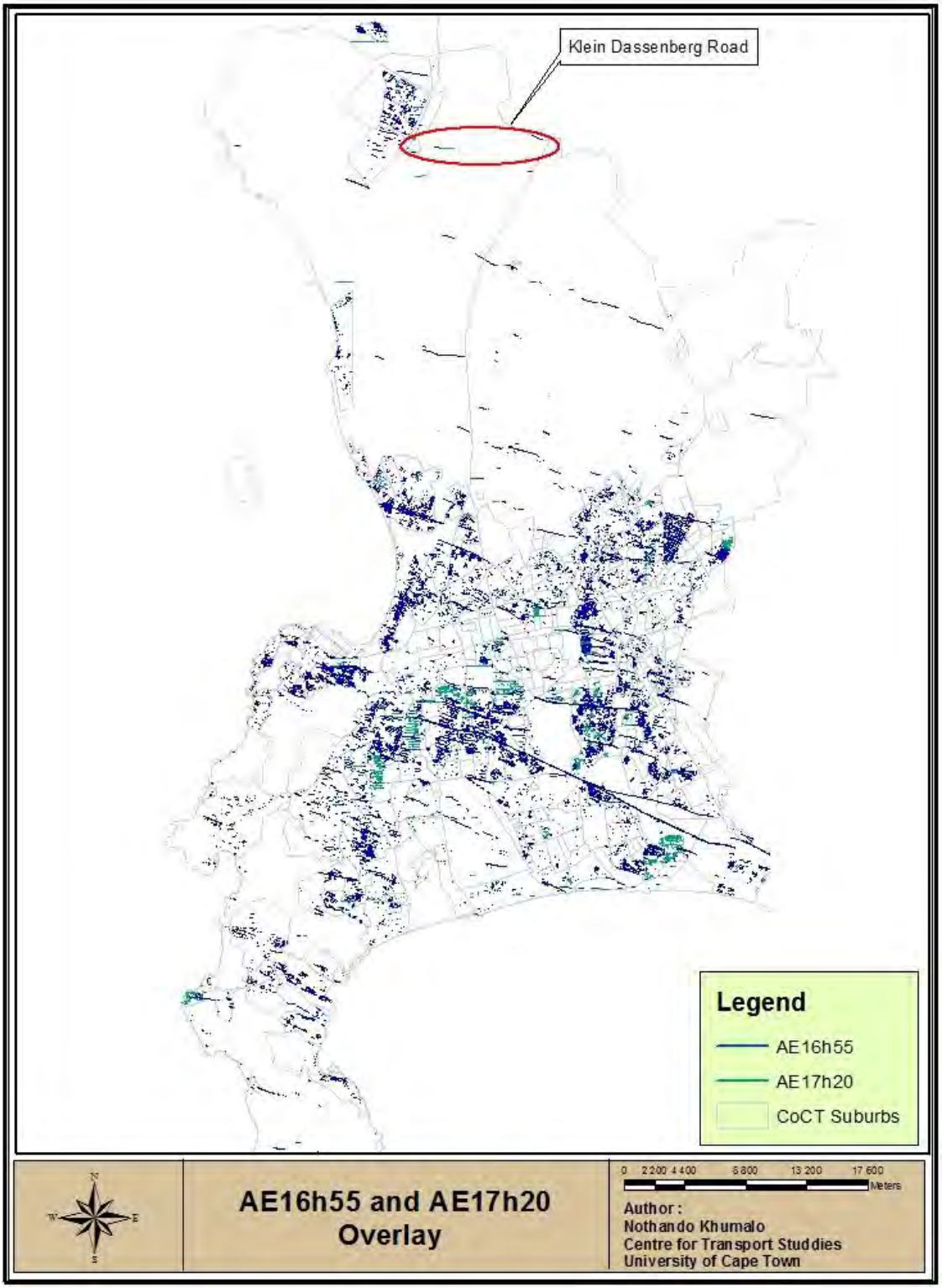

II. Spring Equinox (16h40 and 17h05)

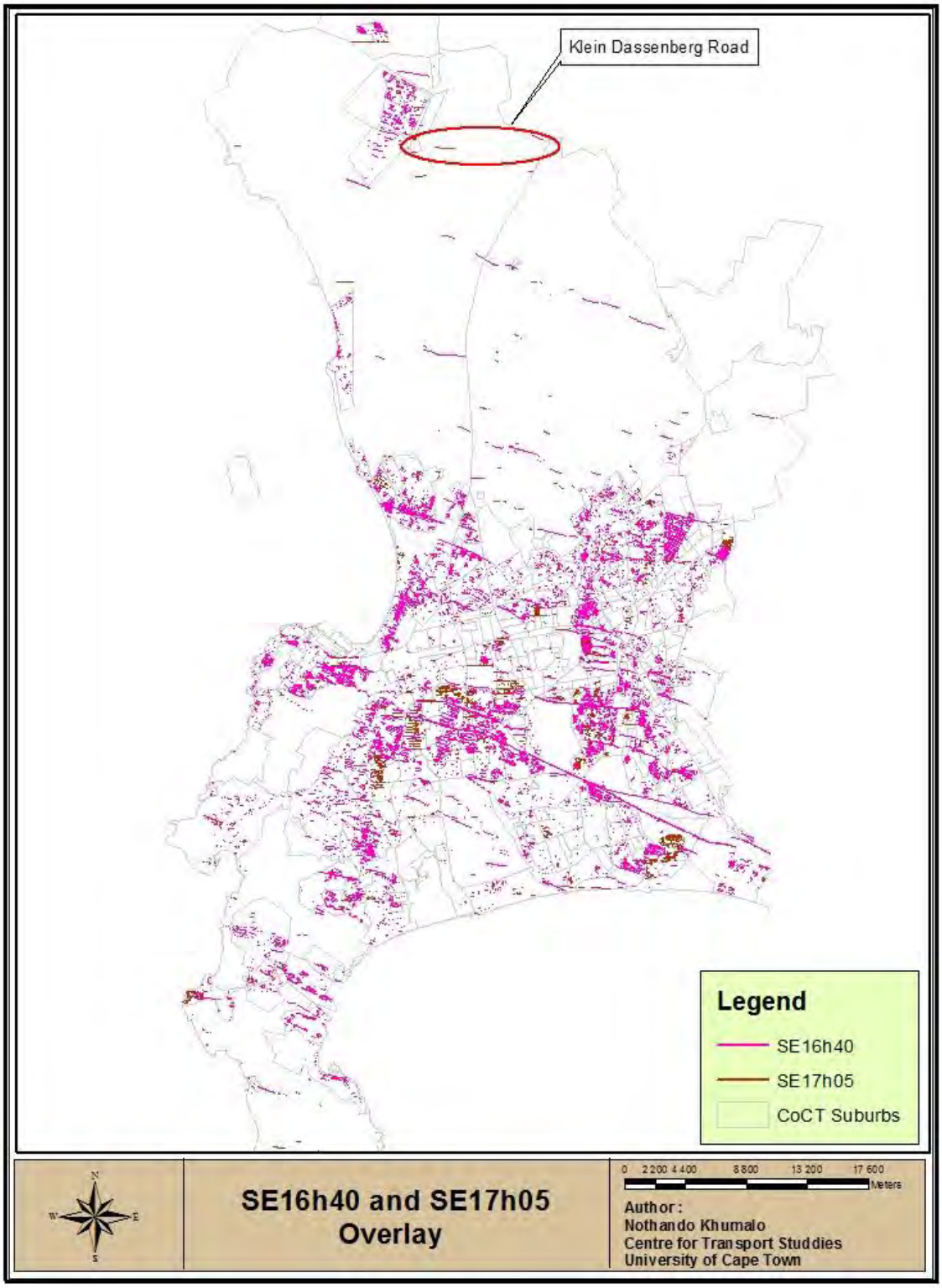

III. Winter Solstice (15h00 and 15h40)

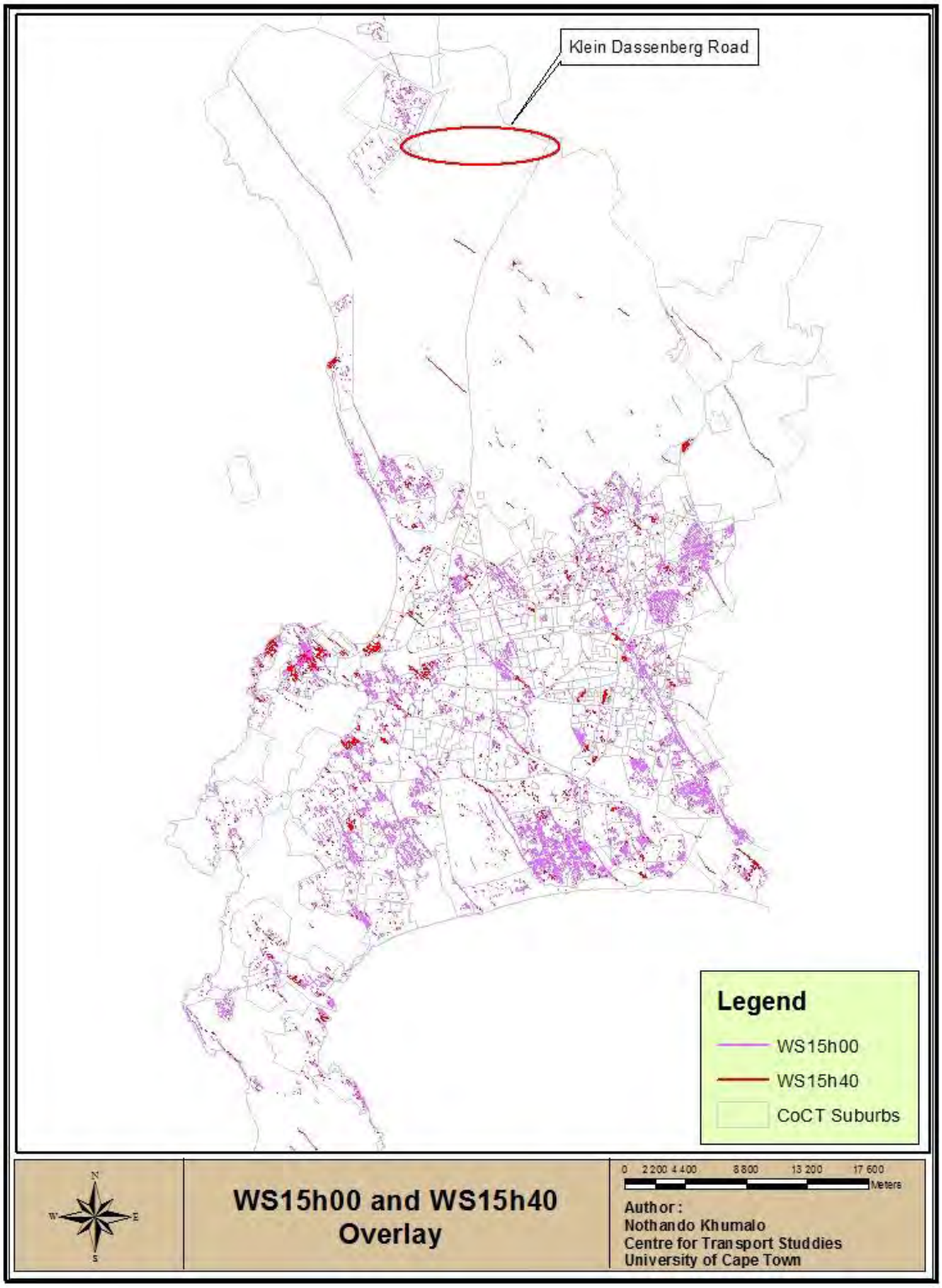

IV. Summer Solstice (17h45 and 18h10)

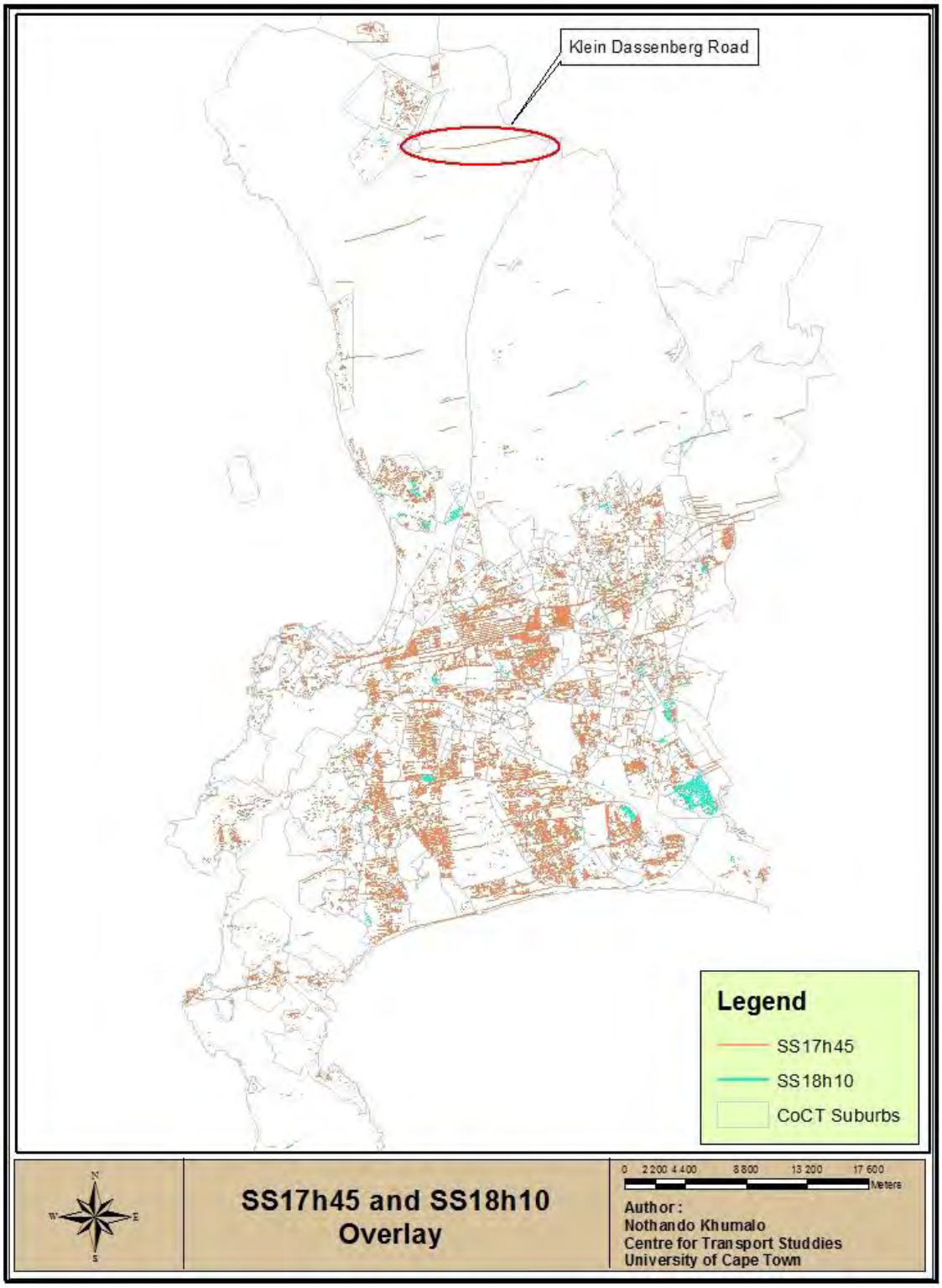

Appendix D: Morning and Afternoon Period Overlay

I. Autumnal Equinox (08h30 and 17h20) (19°)

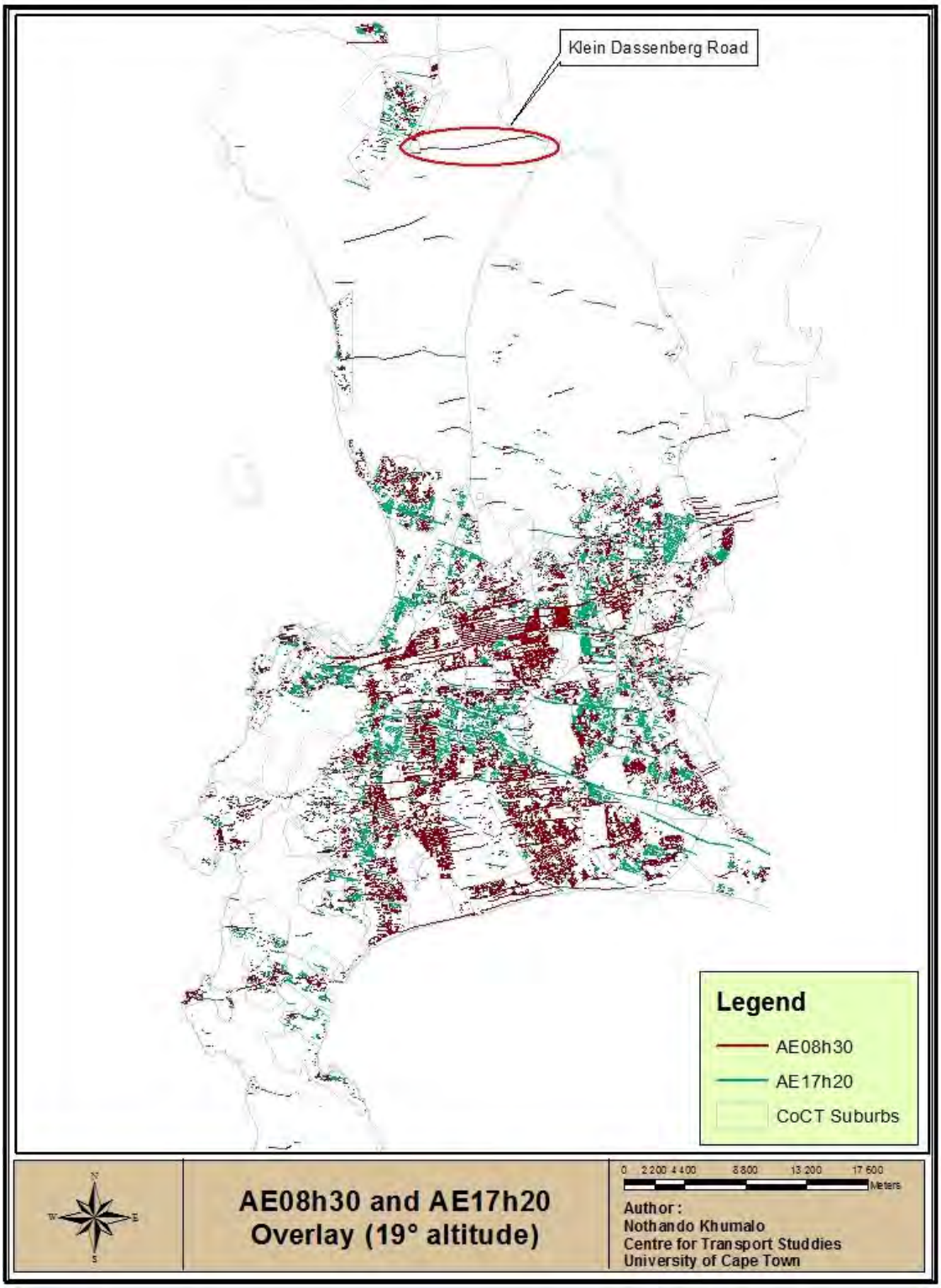

II. Autumnal Equinox (08h55 and 16h55) (25°)

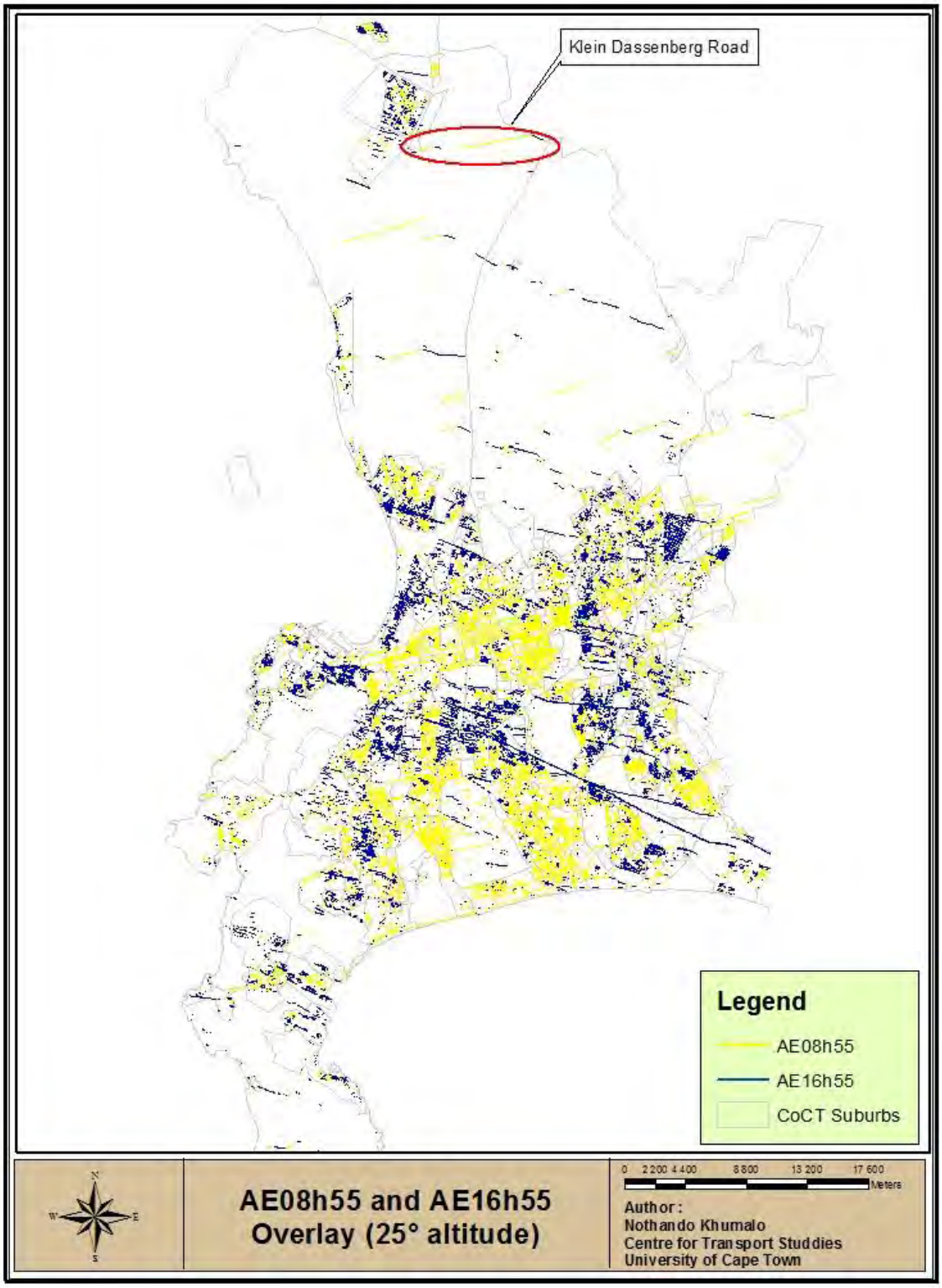

III. Spring Equinox (08h15 and 17h05) (19°)

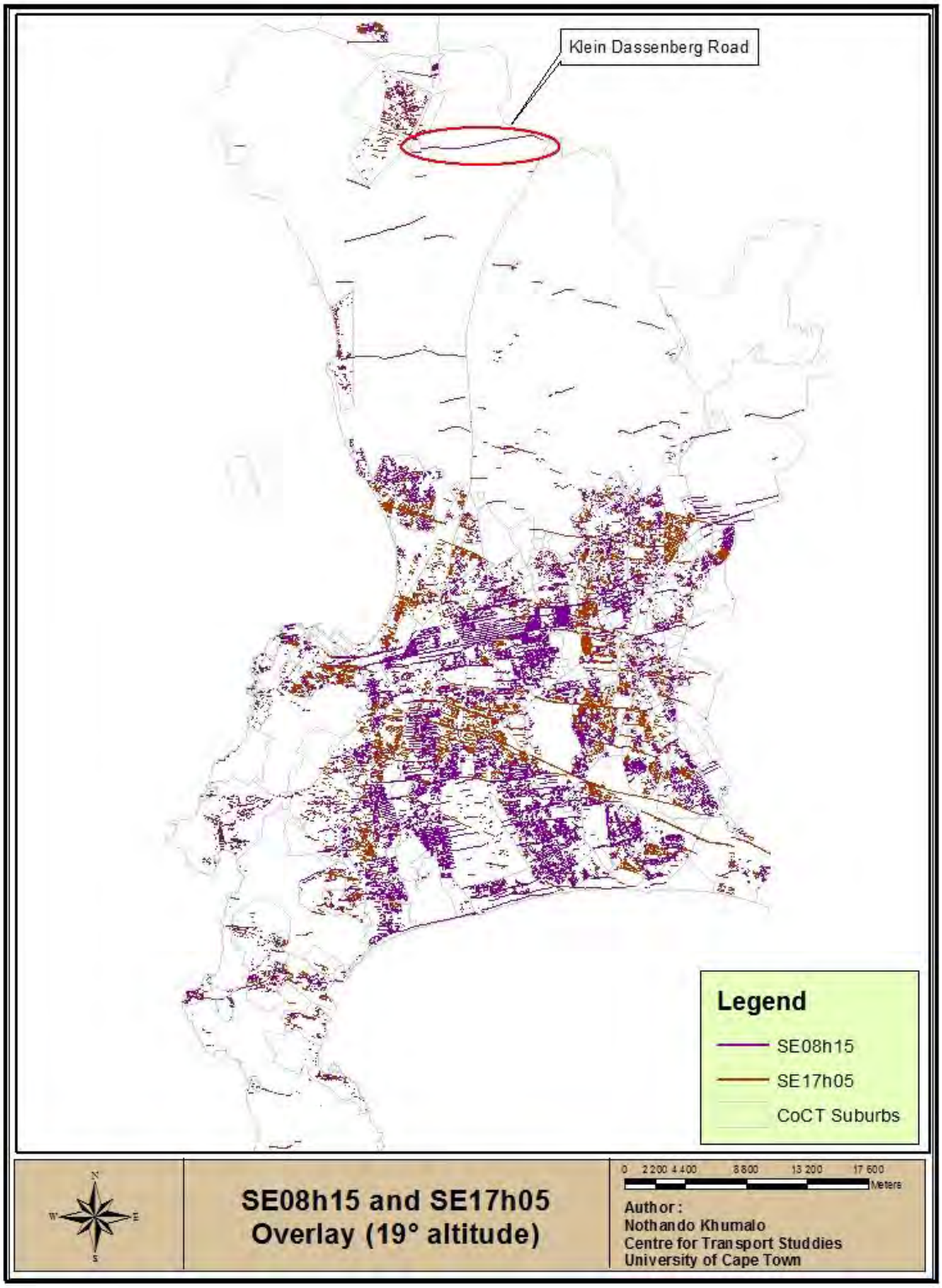

IV. Spring Equinox (08h40 and 16h40) (25°)

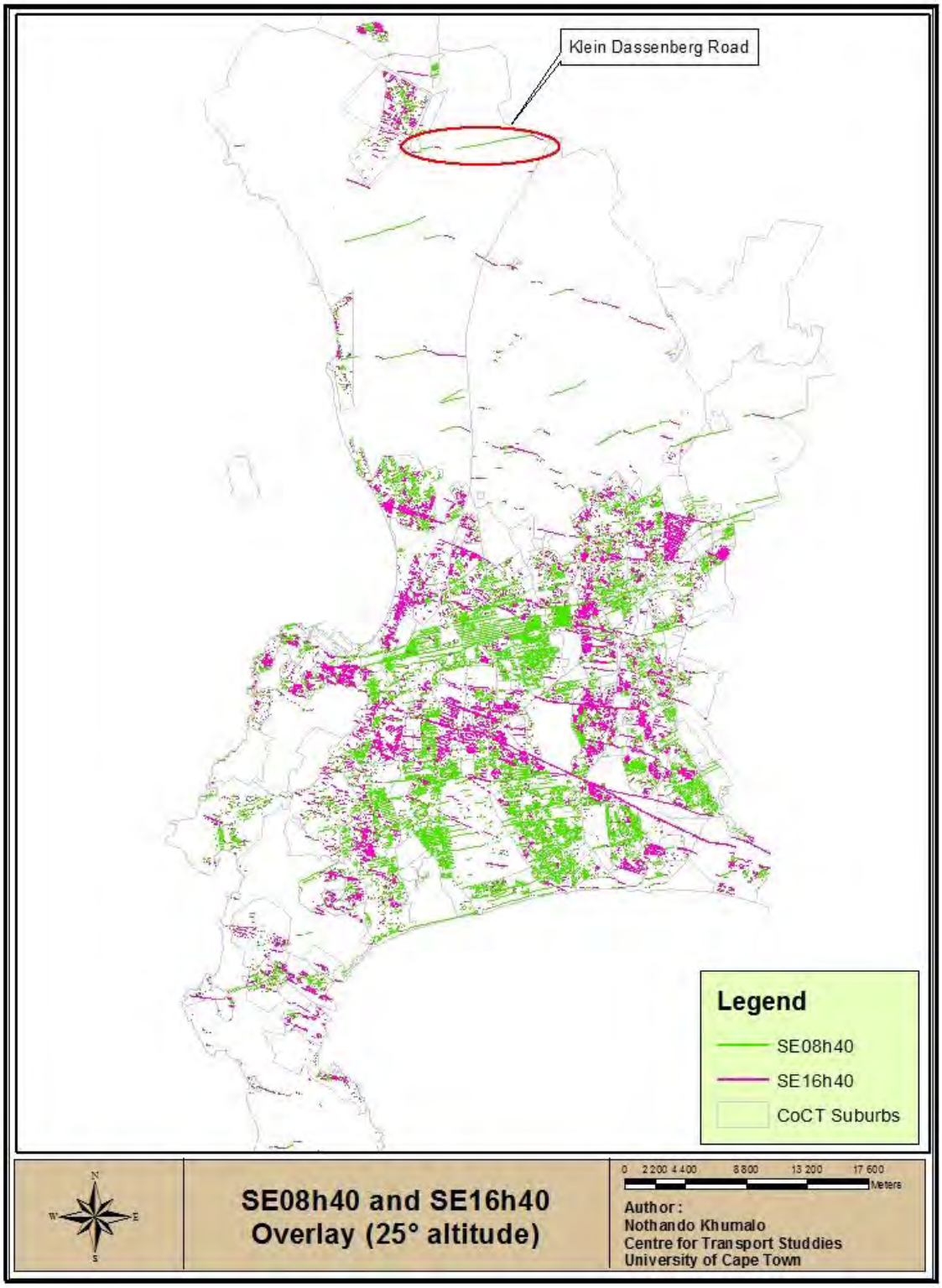

V. Winter Solstice (09h55 and 15h40) (19°)

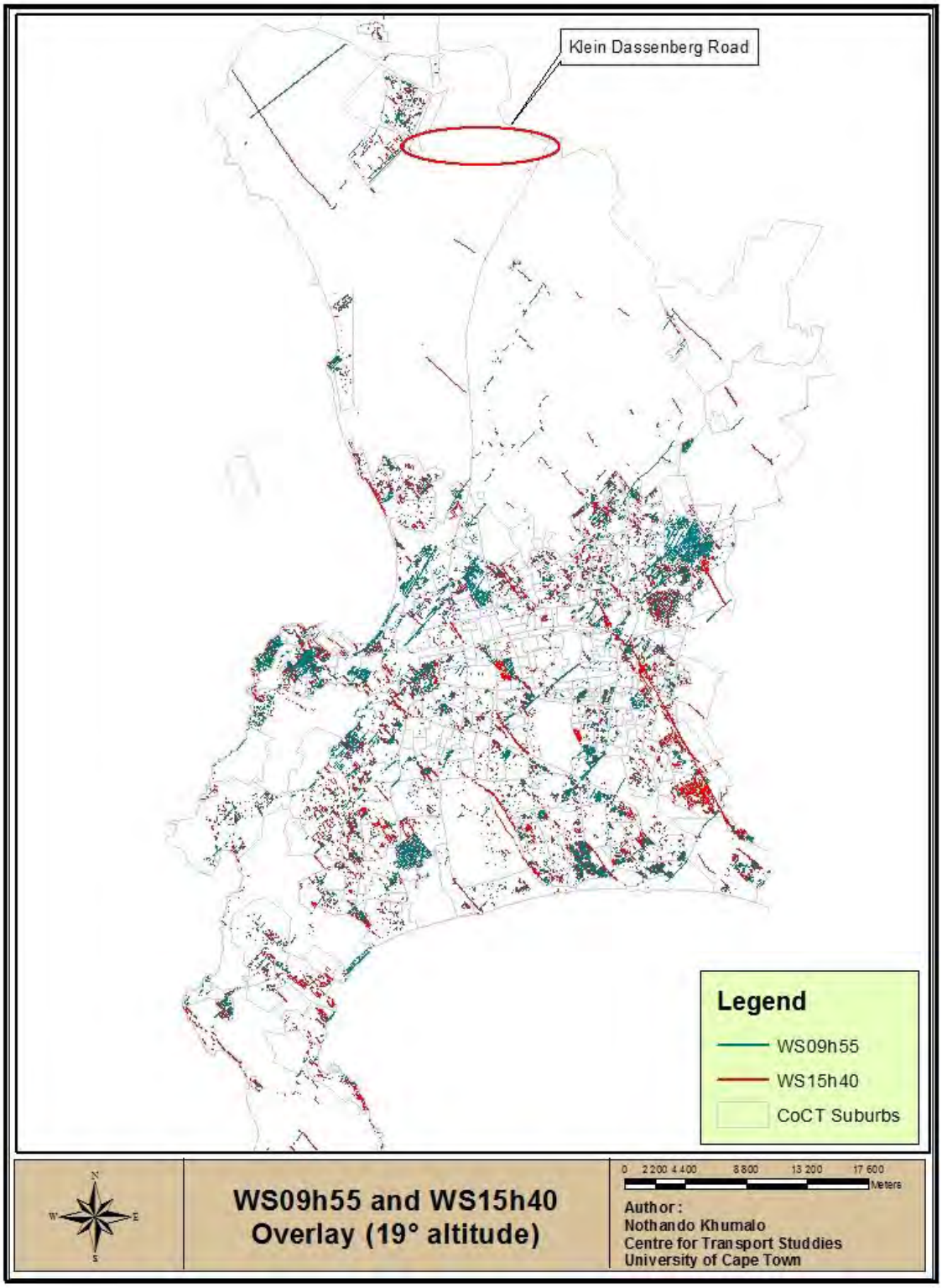

VI. Winter Solstice (10h35 and 15h00) (25°)

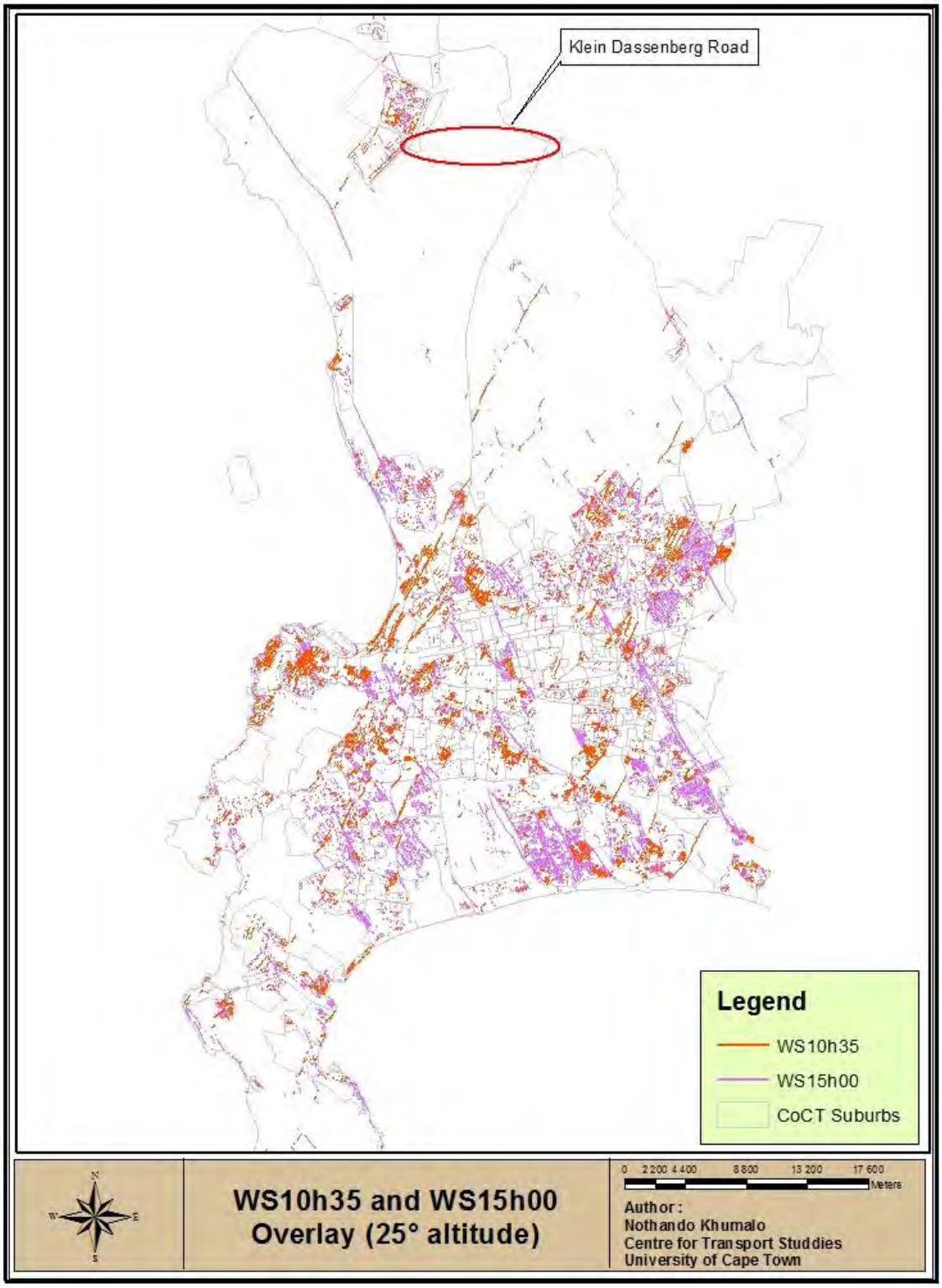

VII. Summer Solstice (07h20 and 18h10) (19°)

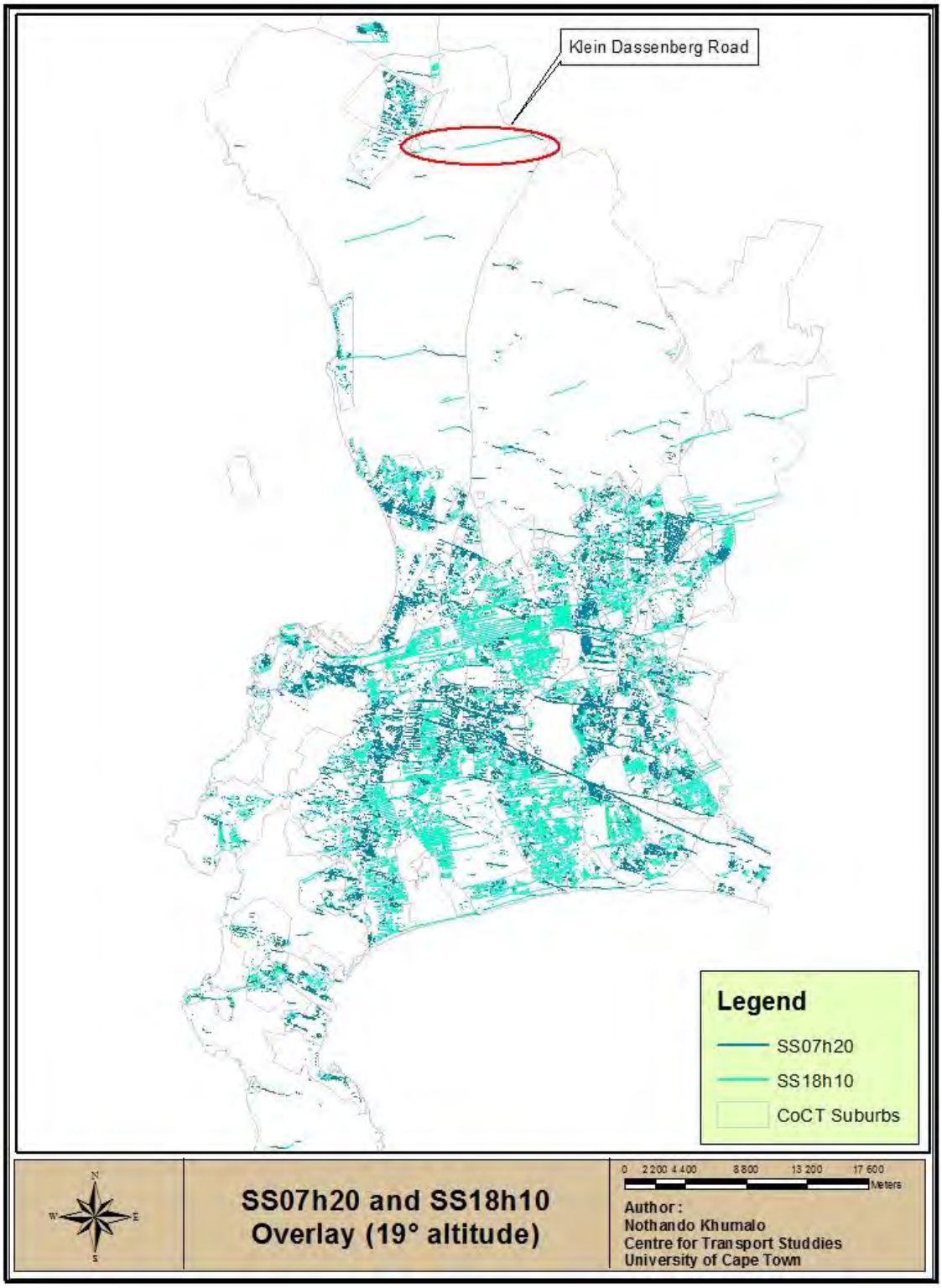

VIII. Summer Solstice (07h45 and 17h45) (25°)

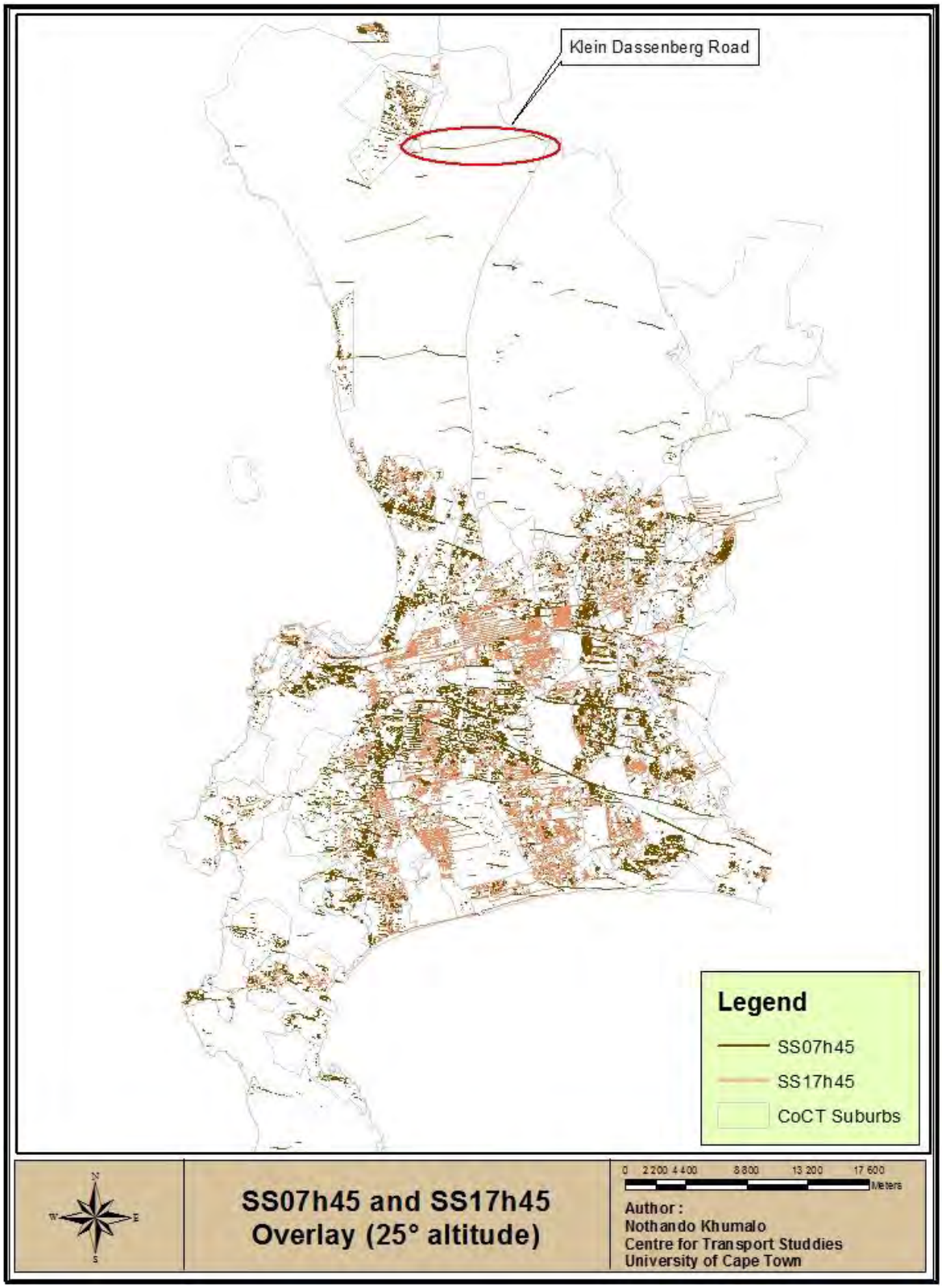

Appendix E: CoCT Accident Data Analysis

I. 25 January 2013

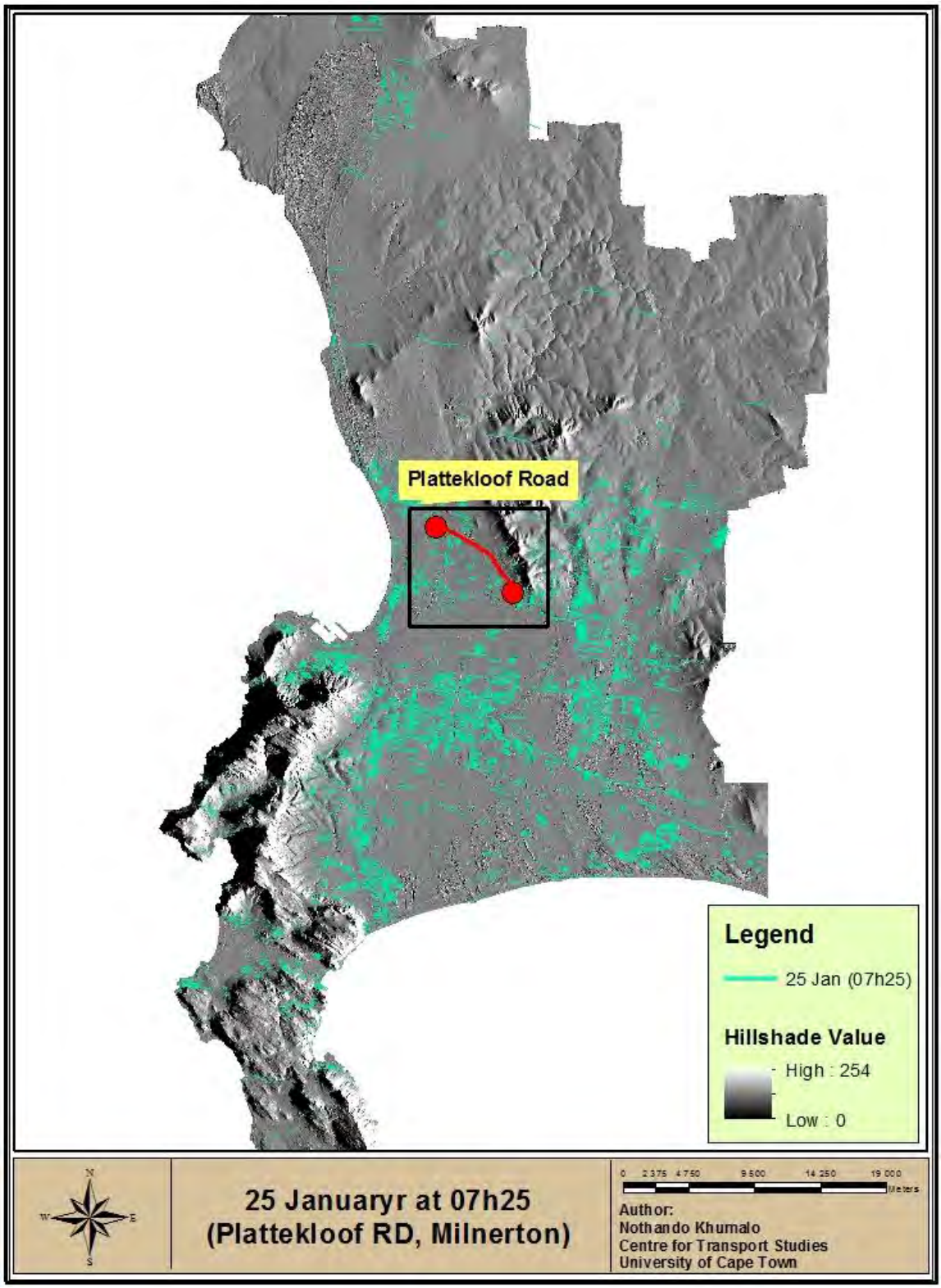

II. 20 August 2013

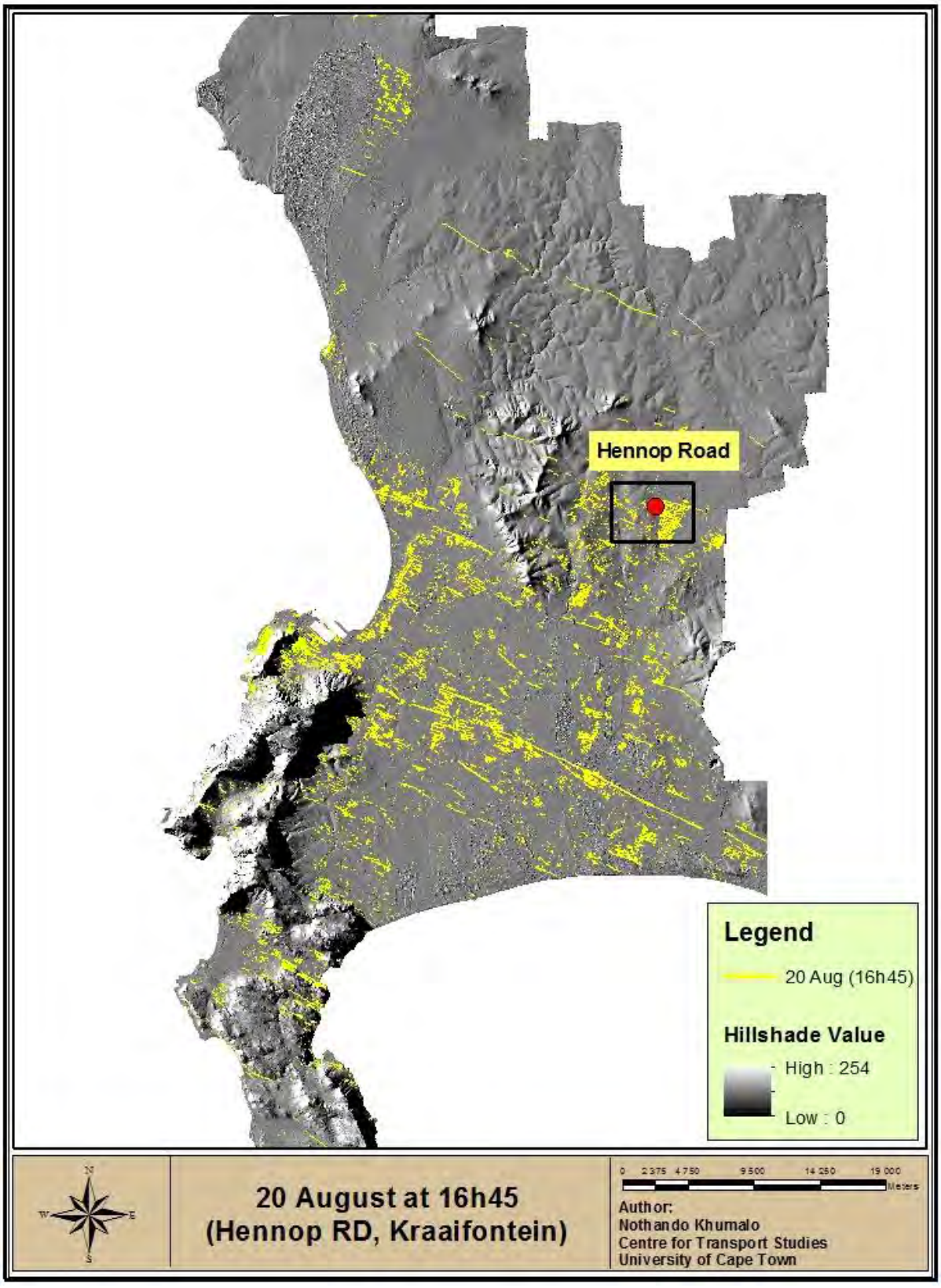

III. 07 November 2013

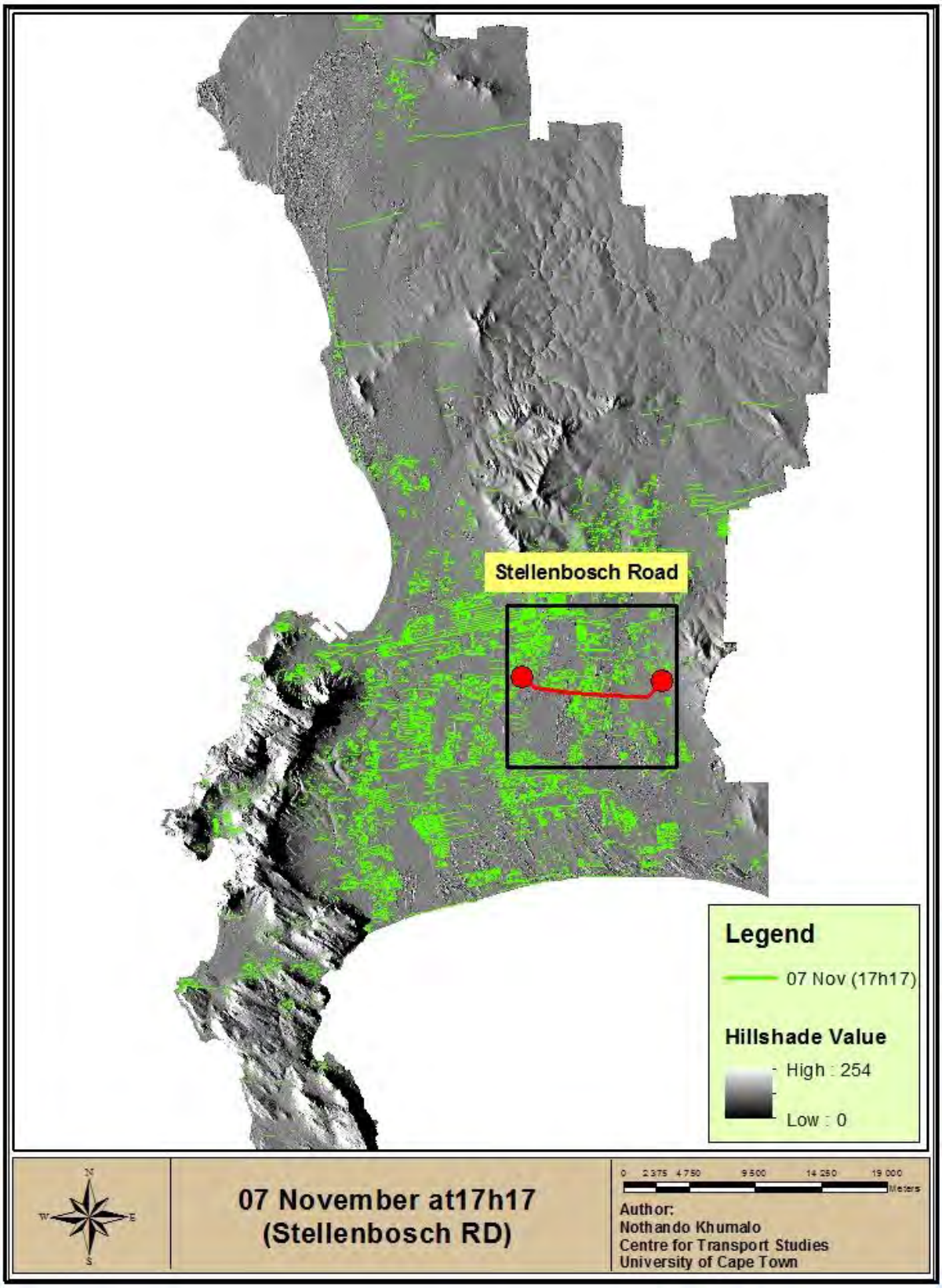

IV. 30 November 2013

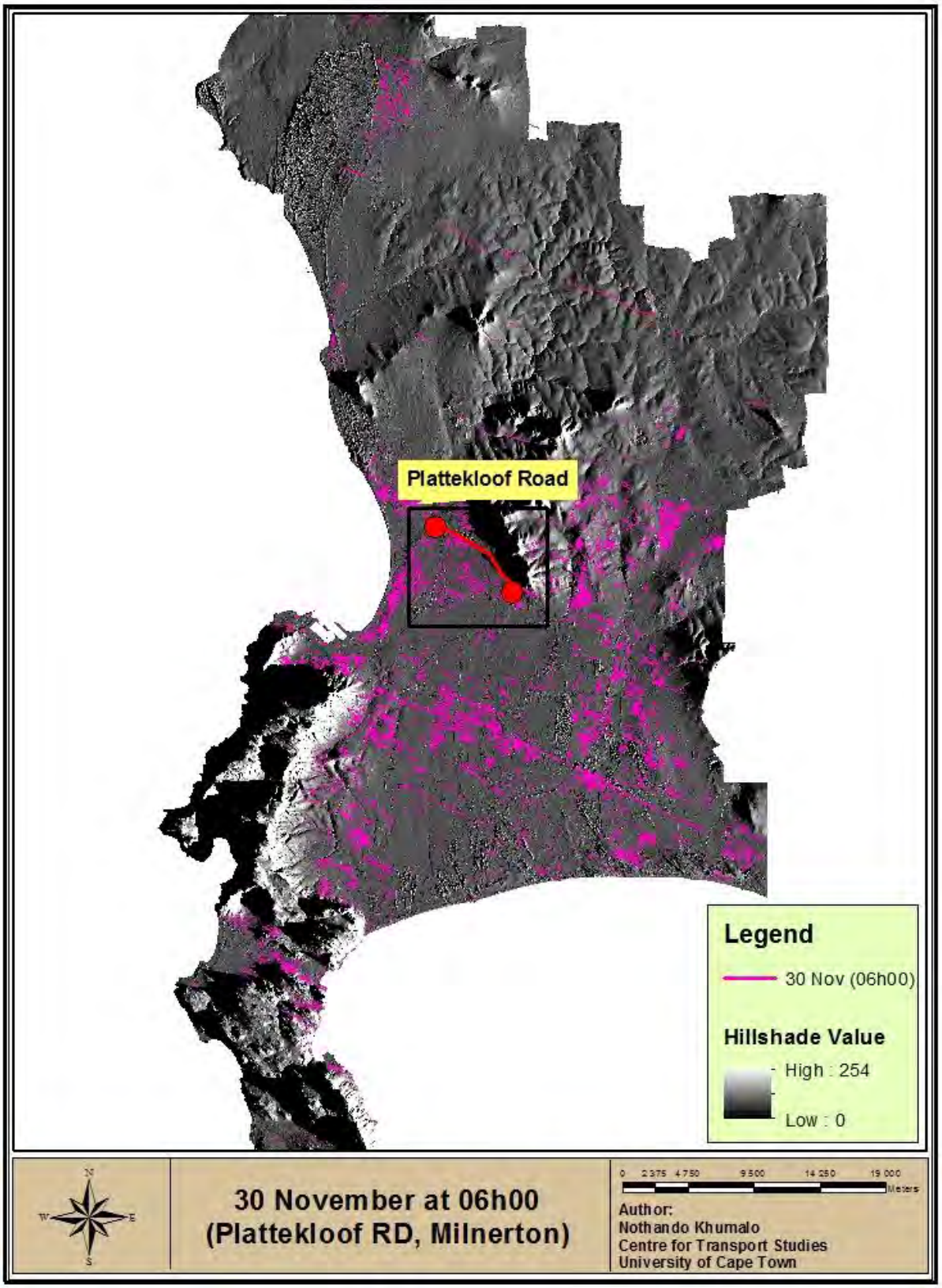

Appendix F: Picture of Road Eye JS-300C

Source: *http://www.carsonhonda.net/*